Investigating the interaction of a metallosupramolecular cylinder with nucleic acids

UNIVERSITY OF BIRMINGHAM

Siriporn Phongtongpasuk

A thesis submitted in partial fulfilment of the requirements for the degree of Doctor of Philosophy in Chemistry

School of Chemistry
College of Engineering and Physical Sciences
University of Birmingham
January 2011

Acknowledgements

I would like to express my deepest gratitude and sincere appreciation to my supervisor, Professor Mike Hannon, for his valuable advice and help throughout my PhD studies. I also would like to thank all the members of the Hannon group, past and present, for their support and help, particularly Jenna and Laura who helped me to do proofreading of this thesis. I would like to thank to Anna Leczkowska and Victoria Sadovnikova for not only all the help and support in the lab but also for sharing fun times, great trips, pain from visa applications (for Victoria) and interesting conversation topics during my time in Birmingham. Also I would like to thank the Analytical Department of the School of Chemistry for the technical support received during the last four years.

Without nice collaborations, this thesis would not have been completed. I would like to thank Professor Kevin Chipman for allowing me to use the facilities on 4th floor at School of Bioscience. I would like to thank Dr. Benjamin Willcox from Medical School, University of Birmingham for his kind help and advice for the SPR experiment. Thank you to Professor Richard E. Palmer and his PhD student, Tianluo Pan from School of Physics, University of Birmingham for teaching me how to do AFM and a valuable result discussion. I would like to thank Professor Roland K.O. Sigel from Institute of Inorganic Chemistry, University of Zurich, Switzerland for being a great host, for his help and many ideas and tips on how to do RNA gel experiment experiments. Moreover, I would like to thank the Sigel group and Freisinger group for their very warm welcome, many parties, help and support during my stay, in particular Susann Paulus who taught me how to do RNA gel experiments and for her advices and discussions for the experiments.

I would like to thank the Strategic Scholarships Fellowships Frontier Research Networks from the Commission on Higher Education, Government of Thailand for financial support during the course of the PhD. I would like to thank Thai Orchid restaurant and staffs there for giving me an opportunity to work as a part time job and COST D39 for financial support during the scientific mission in the group of Professor Sigel at Institute of Inorganic Chemistry, University of Zurich, Switzerland.

This thesis is dedicated to my loving parent and all members in my family. Without their support, I might not have become the person who I am today.

Declaration

The experimental work, observations and recommendations reported in this thesis are the author's unless specifically stated and have not previously been submitted as part of a degree at the University of Birmingham or any other institution.

Siriporn Phongtongpasuk

January 2011

List of papers published from this Thesis

1. L. Cardo, V. Sadovnikova, S. Phongtongpasuk and M.J. Hannon, Arginine residues conjugated to di-nuclear Fe(II) cylinders mediate the diastereoselectivily of the hybrids and improve their DNA binding and cytotoxicity (*manuscript to be submitted*)

2. S. Phongtongpasuk, J. Schnabl, S. Paulus, M. J. Hannon, B. Spingler, E. Freisinger and R. K. O. Sigel, RNA versus DNA: Three-way junctions induced by the same molecular cylinder, but being distinctly different (*manuscript in preparation*)

Contents

Abbreviations

2D	Two dimension
3D	Three dimension
3WJ	Three way junction
A	Adenine
AFM	Atomic Force Microscopy
Arg	Arginine
bp	base pair
bpy	2, 2-bipyridine
bpz	bipyrazine
C	Cytosine
CD	Circular dichroism
$CDCl_3$	deuterated chloroform
CD_3OD	deuterated methanol
chrysi	chrysene-5,6-quinone diimine
Ci	Curies
ct-DNA	calf thymus DNA
d	doublet
DAPI	4, 6'-diamidio-2-phenylindole
ddd	doublet of doublet of doublet
DIP	4, 7-diphenylphenanthroline
DNA	Deoxyribonucleic acid
DOS	Deoxystreptamine

dsDNA	double stranded DNA
dsDNA_L	double stranded DNA with loop
dt	double triplet
EDC	1-ethyl-3-(3-dimethylaminopropyl) carbodiimide
EDTA	Ethylenediaminetetraacetic acid
ESI	Electrospray Ionisation Mass Spectrometry
en	ethylenediamine
g	gram
G	Guanine
Gly	Glycine
HIV	Human Immunodeficiency Virus
Hz	Hertz
IC_{50}	half maximal inhibitory concentration
ICD	Induced Circular Dichroism
MHz	Mega Hertz
min	minute
MLCT	Metal to Ligand Charge Transfer
ml	millilitre
mM	millimolar
mmol	millimole
m/z	mass to charge ratio
NHS	N-hydroxysuccinimide
nm	nanometer

NMR	Nuclear Magnetic Resonance
PAGE	Polyacrylamide gel electrophoresis
PC	Parent Cylinder
Ph	Phenyl
phen	1, l0-phenanthroline
phi	9, l0-phenanthrenequinone diimine
phzi	benzo[α]phenazine-5,6-quinone diimine
PNA	Peptide Nucleic Acid
Py	Pyridine
RNA	Ribonucleic acid
RRE	Rev response element
rRNA	ribosomal ribonucleic acid
rpm	revolutions per minute
RU	Resonance Unit
s	second
s	singlet (in NMR)
S	Subunit
Ser	Serine
SPR	Surface Plasmon Resonance
ssRNA	single stranded RNA
t	triplet
T	Thymine
TAR	transactivation response region

Tat	Trans-activator of transcription protein
TB	Tris-Borate
TBE	Tris-Borate EDTA
TBN	Tris-Borate NaCl
td	triple doublet
TEM	Transmission Electron Microscopy
TEMED	Tetramethylethylenediamine
TFIIIA	transcription factor IIIA
T_m	Melting Temperature
TM	Tris-Magnesium chloride
TMP	tetramethylphenantholine
tRNA	transfer ribonucleic acid
U	Uracil
UV-Vis	Ultraviolet-Visible spectroscopy
w/v	weight / volume
µl	microlitre
µM	micromolar

Abstract

Chapter 1 reviews the background of nucleic acid structures and drug targeting to nucleic acids. The concept of molecular recognition between drugs and nucleic acids is also discussed. Besides, being a drug target, DNA can be used as material for constructing beautiful architectures. Examples of these DNA nanostructures are presented.

In Chapter 2, three way junction recognition by a metallocylinder is shown to occur not only in DNA but also in RNA. The recognition of RNA three way junctions by the metallosupramolecular cylinder, its enantiomers and its analogues are explored. It shows that the cylinders have the ability to bind preferentially to RNA three way junctions and to RNA-DNA hybrids. In addition, a competition assay of nucleic acids to the iron cylinder is examined. It indicates that the iron cylinder may prefer to bind to RNA three way junctions rather than DNA.

In Chapter 3, to elucidate the crucial features of the metallosupramolecular cylinder for recognition of the DNA three way junction, an array of cylinder derivatives are screened. The results indicate that the geometry of the cylinder is the key trait for the recognition. Moreover, the electrostatic interaction from the cylinder can enhance the affinity of the recognition.

In Chapter 4, the molecular effect of the iron cylinder on the structure of a DNA tetrahedron nanostructure is examined. Several biophysical techniques confirm that the cylinder binds strongly with the nanostructure, thus leading to the unusual style of a very rigid DNA nanostructure.

In Chapter 5, to precisely determine the binding affinity of the cylinder to DNA, the development of SPR experiments is described. The results show that the value of the binding affinity obtained from SPR is less than that obtained using the conventional method of ethidium bromide displacement. This is due to the inaccurate measuring of the latter method during the experiment.

Chapter 1

Introduction

1.1 Introduction to DNA

1.1.1 A brief history of DNA

DNA is a nucleic acid which contains the genetic information that is exploited in the development and functioning of most living cells. The two main functions of DNA are to store genetic information and pass it to offspring cells on replication and to utilise the information through transcription into complementary RNA strands which later will be translated into a precise protein which will have a functional role in cell activity.

The history of the discovery of DNA began in 1869 when Miescher, a Swiss physician, isolated leucocytes from pus. He first found an unknown substance which was fundamentally different from protein, a crude sample of DNA.[1] Later, it was termed "nuclein". In 1951, Chargaff reported that the base compositions were different depending on the species, however the ratio of total purine bases to total pyrimidine bases was always close to one. The amount of adenine and thymine and that of cytosine and guanine base were equivalent. This discovery is known as Chargaff's rules and provided a valuable clue for Watson and Crick to solve the DNA structure. In 1952, an X-ray diffraction picture of a fibrous DNA was taken by Franklin. The picture is shown in **Figure 1.1**. The diffraction pattern illustrated a number of spots aligned in an X shape. Information about the size of DNA was obtained. This indicated that the DNA structure must be simple with a regular repeating structure. The conclusion drawn from the experiment was that DNA was a helix.

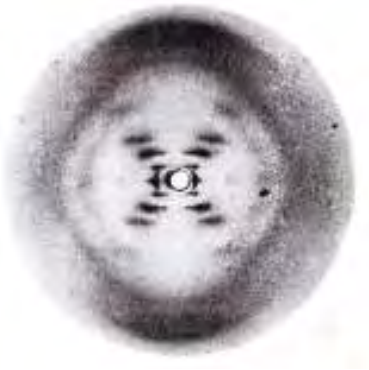

Figure 1.1 Franklin's X-ray picture of DNA.[2]

The three dimensional structure of DNA was unveiled in 1953 when Watson and Crick combined the information achieved from Chargaff's rule and Franklin's X-ray picture (**Figure 1.2**). They proposed that DNA was a double helix with a sugar-phosphate backbone on the outside and bases on the inside. Moreover, the bases must be paired with a purine in one strand always across from a pyrimidine in the other strand. This way the helix would be uniform.[3]

Figure 1.2 Francis Crick (left) and James Watson (right) elucidated that DNA has a double-helical structure.[4]

1.1.2 DNA structures

DNA is a double helical biopolymer consisting of a series of nucleotides containing a phosphate group, deoxyribose sugar and nitrogenous bases (**Figure 1.3**). The deoxyribose sugars are linked together by phosphodiester bonds and the bases are attached to the sugar unit. The nitrogenous bases are purines (adenine (A) and guanine (G)) and pyrimidines (cytosine (C) and thymine (T)). The right handed double stranded DNA helix, discovered by Watson and Crick, is defined as the B structure. The two polynucleotide chains are held together by hydrogen bonding between the bases on the different strands. All the bases are in the centre of the double helix and the sugar-phosphate backbones are on the outside. In each case, a purine is paired with a pyrimidine; adenine (A) always pairs with thymine (T) via double hydrogen bonding, and G with C by triple hydrogen bonding. The bases are perpendicular to the helix axis and are stacked in a parallel fashion upon each other via face to face π-π interactions. The attachment points of the bases to the sugar-phosphate backbone are offset with respect to the hydrogen bonds between the bases. This creates two distinct grooves in the double helix DNA, defined as minor and major. These two grooves are important in DNA recognition by synthetic and natural compounds. This topic will be discussed in **Section 1.1.4**.

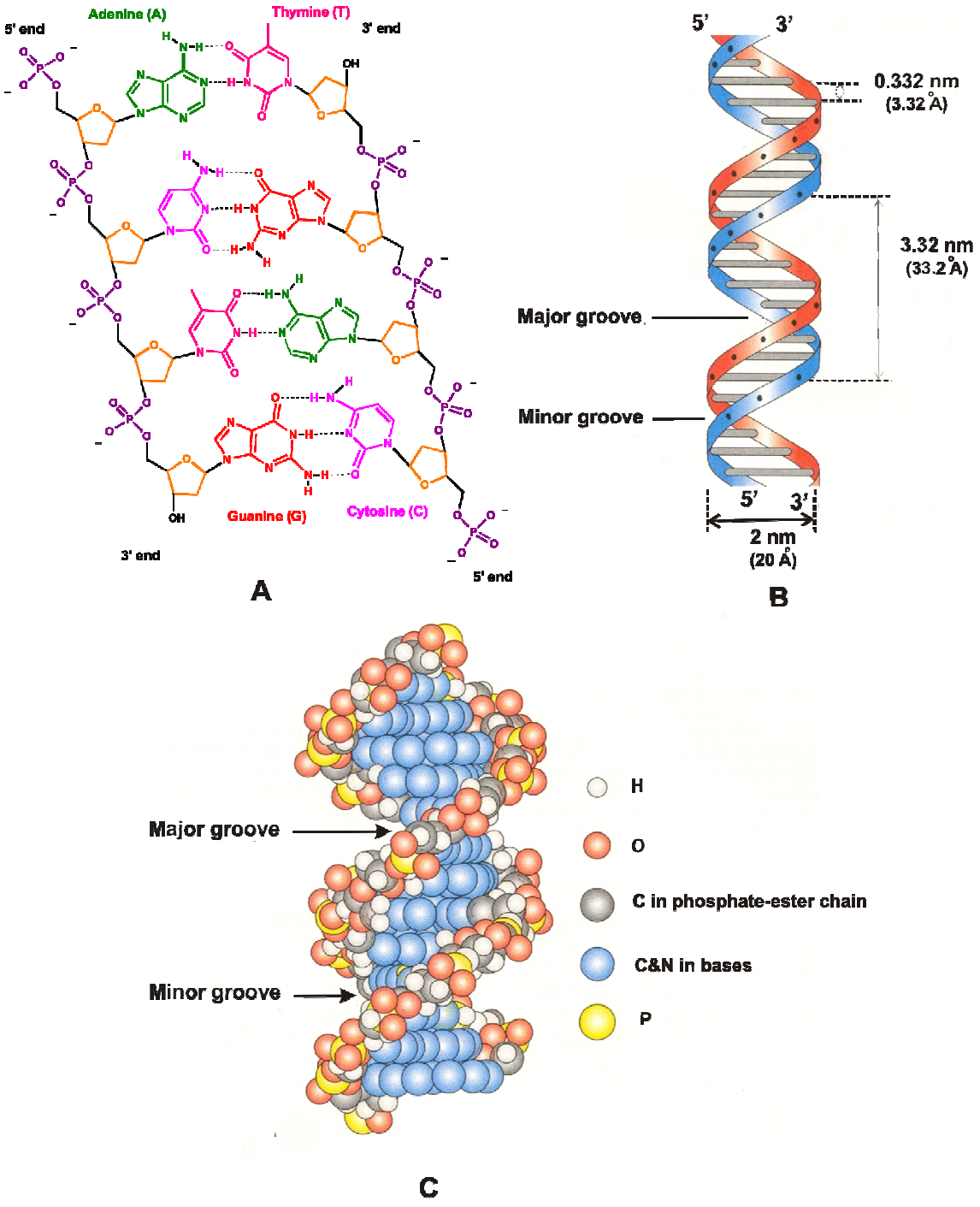

Figure 1.3 Three models of DNA structure. **A)** Schematic drawing of DNA structure illustrating Watson and Crick base pairing. **B)** The drawing of DNA double helix whose sides represent the sugar-phosphate backbones of the two strands and whose rungs represent base pairs. The width of DNA and the distance between repeated nucleotides are 2 nm and 0.332 nm, respectively. **C)** Space filling model of double helix DNA.[5]

1.1.3 A variety of DNA conformations

The B structure of DNA elucidated by Watson and Crick is the most common conformation found in the cell. However, the B form is not the only conformation available to double stranded DNA. A form DNA, a right handed helix, can be obtained when the relative humidity surrounding the fibrous DNA is reduced to 75%.[5] In 1979, Rich and his colleagues reported that DNA does not always have a right handed twist.[6] The structure of a poly CG DNA double helix was significantly different from B form DNA. It was left handed with a zigzag shaped backbone when viewed from the side. This DNA structure is therefore called Z-DNA (**Figure 1.4**).

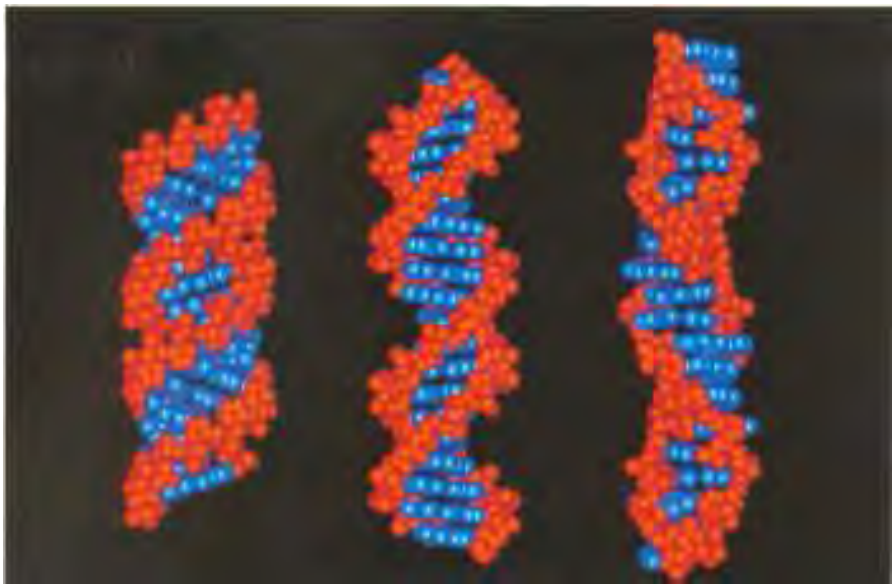

Figure 1.4 The model of A, B and Z DNA (from left to right).[5]

These three DNA structures are different in several respects. A summary of the helical parameters are shown in **Table 1.1**

Table 1.1 Geometries of DNA forms.[5]

Geometry attribute	***A form***	***B form***	***Z form***
Helix direction	Right-handed	Right-handed	Left-handed
Repeating unit (bp)	1	1	2
bp/turn	11	10.5	12
Inclination of bp to axis	+19°	-1.2°	-9°
Rise/bp along axis (nm)	0.23	0.332	0.38
Pitch/turn of helix (nm)	2.82	3.32	4.56
Diameter (nm)	2.3	2.0	1.8

Besides the double helix, DNA can form higher order structures such as DNA junctions which are a branched DNA structure consisting of double strand(s) converging at one point (**Figure 1.5A, B**). The DNA junction is an intermediate in several genetic processes in living cells. Examples include the replication fork observed during DNA replication,[7] and the four way junction (Holliday junction) presenting homologous genetic recombination.[8, 9]

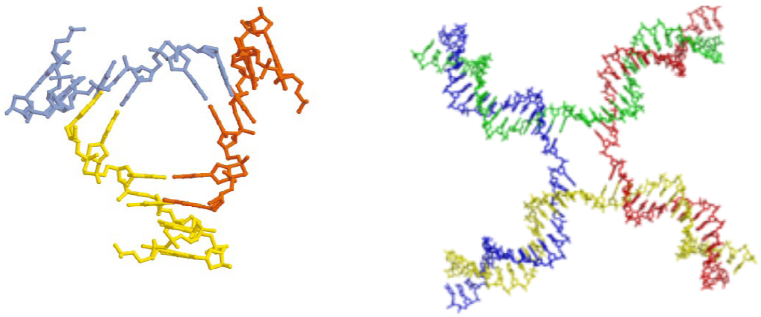

Figure 1.5 Higher order DNA structures. **A)** DNA three way junction.[10] **B)** DNA four way junction or Holliday junction.[11]

In addition to the structure of DNA four way junctions, the four way junctions can form in a number of different conformers. It has been reported that the folding of the DNA junction depends on the divalent ion such as magnesium ions. Upon addition of magnesium ions (≥ 100 μM Mg^{2+}), the four way junction folds by the pairwise coaxial stacking of helical arms and usually adopts a right handed antiparallel structure (**Figure 1.6**). A small angle of ~ 60º between helical axes is observed. This structure was probed and confirmed by several techniques such as comparative gel eletrophoresis[12], FRET analysis[13] and enzyme and chemical probing method.[14, 15]

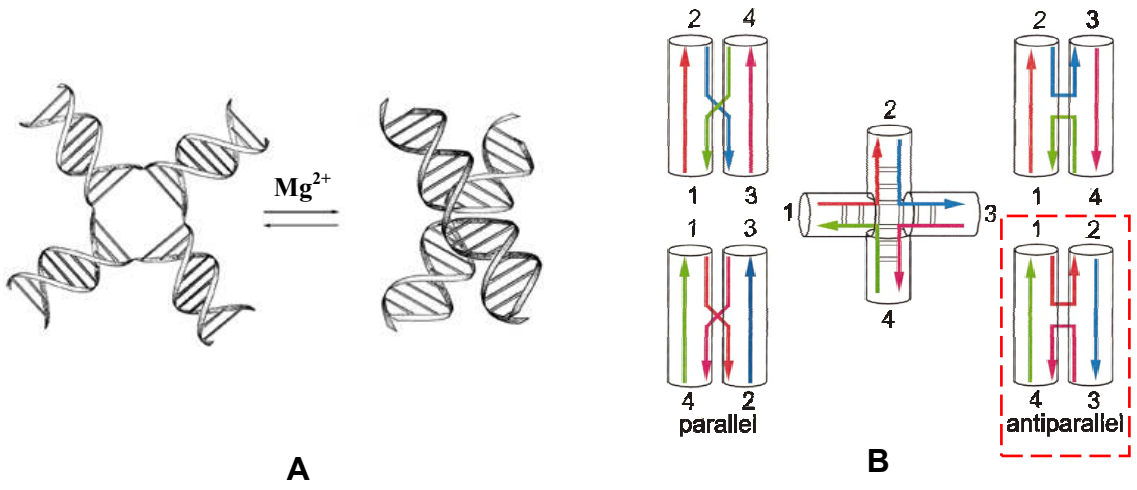

Figure 1.6 A) Changing folding of DNA four way junction from an extended conformation to a pairwise coaxial stacking structure in the presence of Mg^{2+}. **B)** Possible topology of strands and helices in the coaxial stacking structure of the four way junction. The centre shows the junction in an extended conformation with four arms pointing towards the corner of a square. The arms are labeled 1-4 in a clockwise direction. The strands can be drawn as non-crossed or crossed, illustrating a parallel (left) or antiparallel (right) structures, respectively. Each of which can generate a left handed form (top) and a right handed form (bottom). The proposed four way junction in the presence of magnesium ions is the coaxial stacking with a right handed antiparallel conformation, shown in red frame. Taken from ref.[11]

For DNA three way junction, it has been demonstrated that a perfect three way junction (3H) only adopts a fully extended structure either in the presence or absence of magnesium ions (**Figure 1.7A**).[16] This is due to the rigid framework of the fully paired DNA three way junction removes any possibility of folding by coaxial stacking of the helical arms. However, the addition of a single stranded bulge at the intersection of the helical arms, generating a $3HS_n$ junction, will provide the flexibility to the DNA three way junction structure. Therefore, in the presence of magnesium ions, coaxial stacking of the helical arms can be observed from bulged DNA three way junction.[17, 18] The intensive NMR studies of DNA three way junction containing two unpaired base ($3HS_2$ junctions) has revealed that in the presence of magnesium ions, two helical arms remained in coaxial stacking but the third helix was unstacked and pointed away from the intersectional point.[19-21] Two alternative stacking conformers shown in **Figure 1.7B** can be generated from this bulged DNA three way junction. Surprisingly, both forms of DNA three way junction can exist and the stability of each forms depends on the sequences.[22]

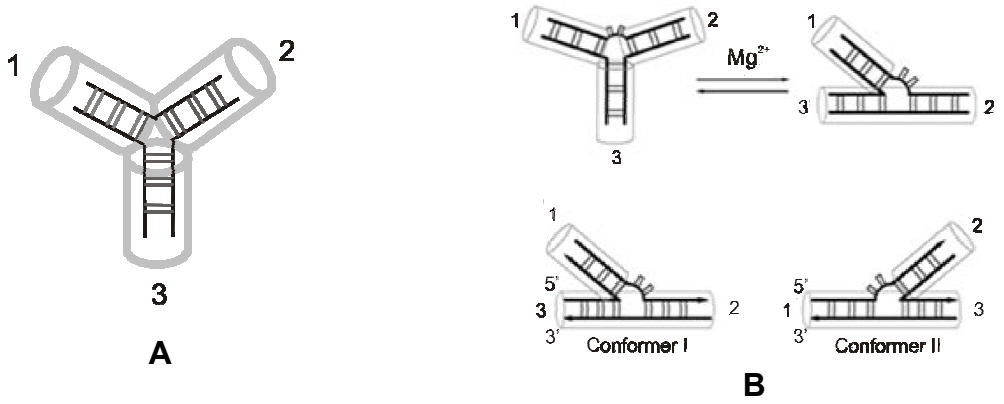

Figure 1.7 A) Perfect three way junction with extended structure. **B) Top:** Transition folding of bulged three way DNA junctions from extended structure to coaxial stacking structure in the presence of magnesium ions. **Bottom:** Two alternative conformers achieved from coaxial stacking of bulged DNA three way junction ($3HS_2$). Taken from ref.[11]

It is noteworthy that metal ions play important role in folding of DNA helical junctions due to the polyelectrolyte feature from phosphate backbone of nucleic acids. Besides, magnesium ions, other divalent ions such as calcium ions can be used instead of magnesium ions however monovalent metal ions are ineffective in promoting transitions of folding.[23]

In addition to double helical DNAs and DNA junction structures, quadruplex DNA is another "unusual" DNA structure. It is an array of G-quartets, each of which comprises four guanine bases, aligned with a four-fold rotational symmetry. Hydrogen bonds are formed along each edge, as shown in **Figure 1.8A, B.**. The G-quartets stack on each other in a helical fashion, producing a G-quadruplex structure in the centre of which is often found a metal cation.[24] This structure was found to be involved in the structure and stability of telomeres in organisms.[25, 26]

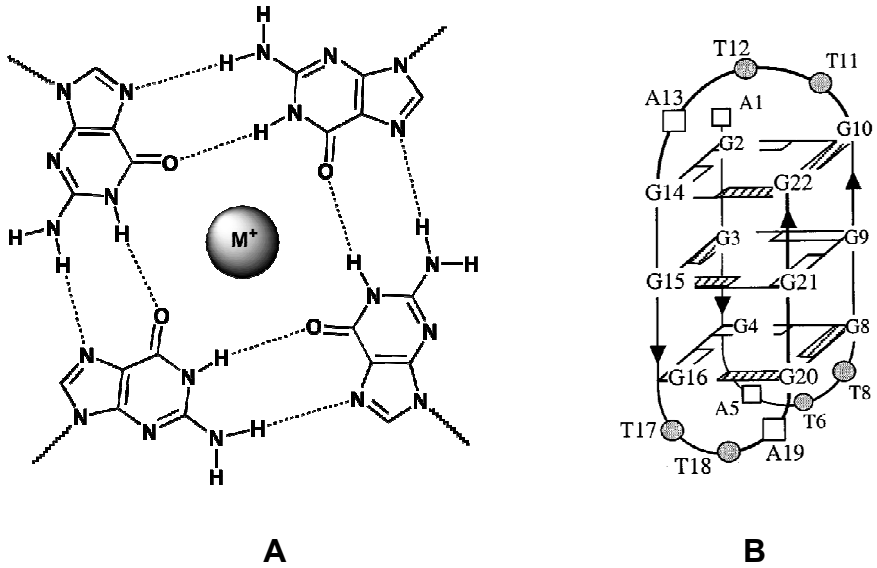

Figure 1.8 A) G-quartet with the metal ion. **B)** Human telomeric quadruplex DNA. Taken from ref.[27]

1.1.4 Mode of DNA recognition

DNA contains all the genetic information which is responsible for the physical traits and functions of the organism. The genetic data is transcribed into RNA which is used as a template for synthesising protein via the translation process. Changes in DNA sequences may result in deficiencies in the protein function and misregulation of its information, leading to over- or under- stimulation of cell processes. These are the origins of many diseases e.g. cancer. Therefore, DNA is an attractive medical target for design of drugs that control gene expression.

There are five distinct traditional DNA binding modes for drugs: intercalation between DNA base pairs, covalent binding or metal coordination to bases, sugar phosphate backbone binding, minor groove recognition and major groove recognition. These DNA binding modes were discovered in 1960s. Two additional new binding modes, junction recognition and quadruplex recognition, have been reported recently. These drug DNA recognition modes and their examples are presented in the following section.

1.1.4.1 DNA intercalation

Intercalation was first reported by Lerman in 1961 when the binding of planar aromatic chromophores to DNA was explored.[28] Research focused on this concept has been ongoing ever since. In technical terms, intercalation is the insertion of planar aromatic ring(s) into the gap between the base pairs of DNA. This interaction can be full insertion or partial insertion depending on the size of the DNA intercalators. DNA-drug intercalation is stabilised by several interaction forces: π electron overlap, hydrophobic

and polar interactions and electrostatic force from positive charges on the intercalators to the negative charge of the DNA phosphate backbone. The insertion of intercalators can occur from either the major or minor groove. However, the backbone is not flexible enough to permit all intercalators to insert into every single gap. The maximum number of DNA intercalators, that can insert, is one molecule per two DNA base pairs according to the neighbour-exclusion principle.[29] The result of intercalation is the alteration of DNA structure by lengthening, stiffening, and unwinding the DNA helix. These changes in the DNA structure are believed to prevent DNA replication, thus inhibiting the growth of cancers or causing cell death.

A well known DNA intercalator, mainly used in molecular biology and biochemistry for DNA staining, is ethidium bromide (**Figure 1.9**).

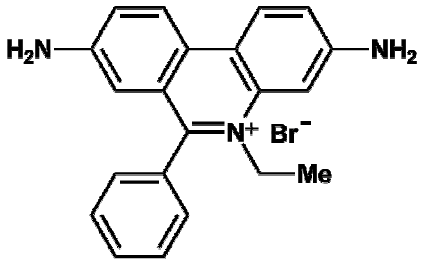

Figure 1.9 Chemical structure of ethidium bromide.

An example of a DNA intercalator used in medical treatment is doxorubicin (**Figure 1.10**). It has been used in the clinic as an anticancer drug since the 1960s, categorised as an "anthracycline antiobiotic".[30]

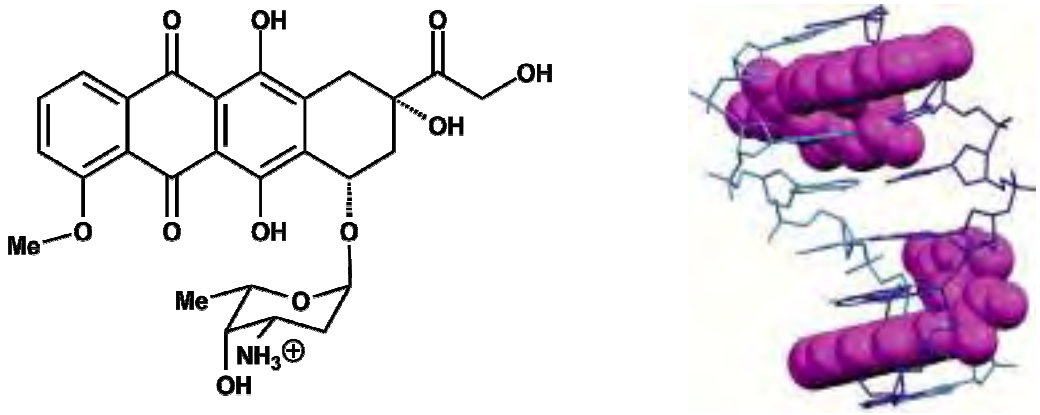

Figure 1.10 Left: Chemical structure of doxorubicin. **Right:** Two doxorubicins (purple spheres) inserted in between DNA base pairs. Taken from ref.[22]

Besides these organic molecules, scientists have synthesised intercalators containing metals, termed metallo-intercalators. An increase of positive charge is not the only benefit from incorporating metal into the design of intercalators: other features such as shape of the complex may be also controlled by changing the metal used.

An early example of a metallo-intercalator was Lippard's use of platinum metal to create a planar platinum (II) terpyridine intercalator (**Figure 1.11**).[31]

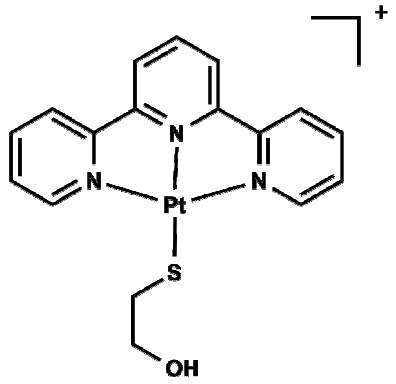

Figure 1.11 Chemical structure of Lippard's metallo-intercalator.

Building on this basic concept, Barton *et al.* synthesised rhodium based metal intercalators with large chrysi and phyzi ligands (**Figure 1.12**). These intercalators are too big to insert into normal Watson and Crick base pairing but are able to insert into a mismatch base pair. The application of these intercalators is to detect the mismatches of DNA base pairs by fluorescence.[32, 33]

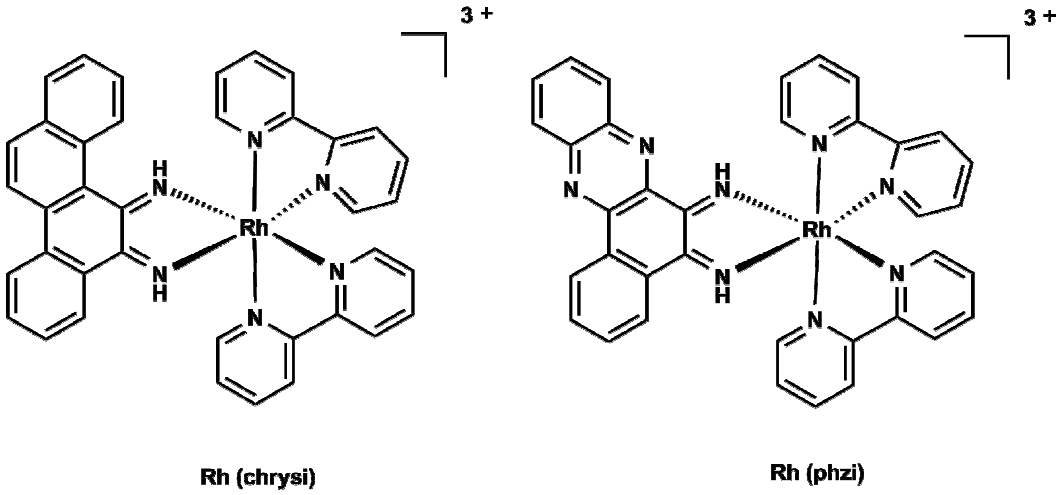

Figure 1.12 Chemical structures of Barton's rhodium (II) intercalators.

Besides mononuclear metallo-interacalators, bis-intercalators containing molecules with two interacalators linked together have been prepared. The flexibility and length of linking chain is important to allow the molecule to wrap and intercalate into the two sites on the same DNA duplex. However, using a rigid linking chain creates agents that might bind to targets where two duplex are in close proximity (**Figure 1.13A**).[34] This approach was exemplified by Lowe's platinum terpyridyl intercalators[35] (**Figure 1.13D**) or two acridine intercalators, used to probe the spatial organisation of DNA.[36] Pikramenou *et al*. reported a hairpin style of bis-intercalator.[37] In this molecule, two

platinum-terpyridyl moieties are attached onto aromatic thiolates, attached to a neodinium aminocarboxylate complex (**Figure 1.13B**). With the design of this hairpin intercalator, it binds to the same double stranded DNA with the intercalation about 10.5Å (i.e. a two bp gap between the intercalation sites).

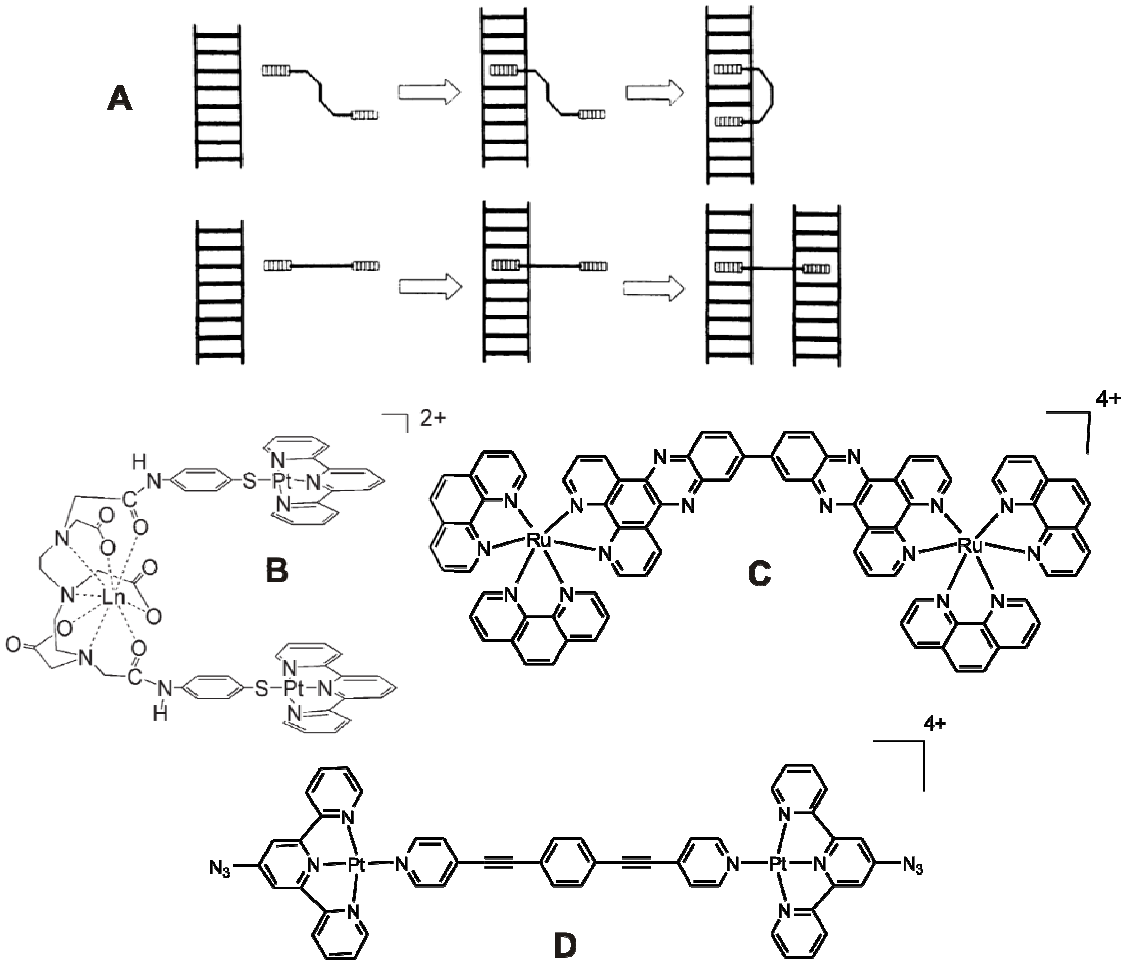

Figure 1.13 A) Intercalating fashions of bis-intercalators with flexible linkers (top) and rigid linkers (bottom). **B)** Pikramenou's bisintercalator. **C)** Threading intercalator. **D)** Lowe's platinum terpyridyl intercalators.

Interestingly, this luminescent compound binds strongly to ct-DNA and is capable of harvesting light energy which is used to drive the NIR emission of the neodinium by the

platinum-terpyridyl units. Another bis-intercalator $[D,D\text{-}\mu\text{-}(bidppz)\text{-}(phen)_4Ru_2]^{4+}$ (**Figure 1.13C**), known as threading intercalator, was synthesised by Lincoln and Norden.[38] In this complex, two $[Ru(phen)_2(dppz)]^{2+}$ units are linked together to form the semirigid binuclear ruthenium complex. DNA binding studies revealed that this complex slowly rearranges from an initial groove-bound, non-luminescent state to form a final intercalated emissive state by threading one of its $Ru(phen)_2$ units through the DNA base stack.

1.1.4.2 Alkylation or covalent binding

Another DNA binding mode is observed when drugs bind directly to the DNA bases, usually to the N7 position of G or A bases in the DNA major groove. The nitrogen mustards such as chlorambucil (**Figure 1.14**), are the example of this DNA binding mode.[39, 40] This organic compound covalently binds to DNA bases by alkylation of the nitrogen via substitution of the chlorine, and is used in the clinic for the treatment of lymphocytic leukemia, ovarian and breast carcinomas and Hodgkin's disease.[41]

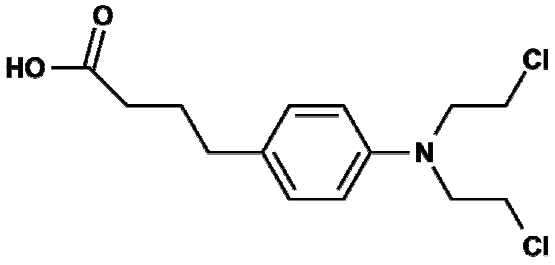

Figure 1.14 Chemical structure of the nitrogen mustard, chlorambucil.

One of the most successful of the clinical "alkylating" agents for cancer treatment is cis-platin, a platinum-based drug. It binds to DNA with displacement of two chlorides ligands and formation of two metal-coordination bonds to the N7 of two adjacent purine DNA bases on the same strand (**Figure 1.15**) This type of DNA binding causes a kink in the DNA of around 45 degrees at the platination site.[42] This kink is recognised by HMG proteins and this is believed to protect the lesion from DNA repair.[43]

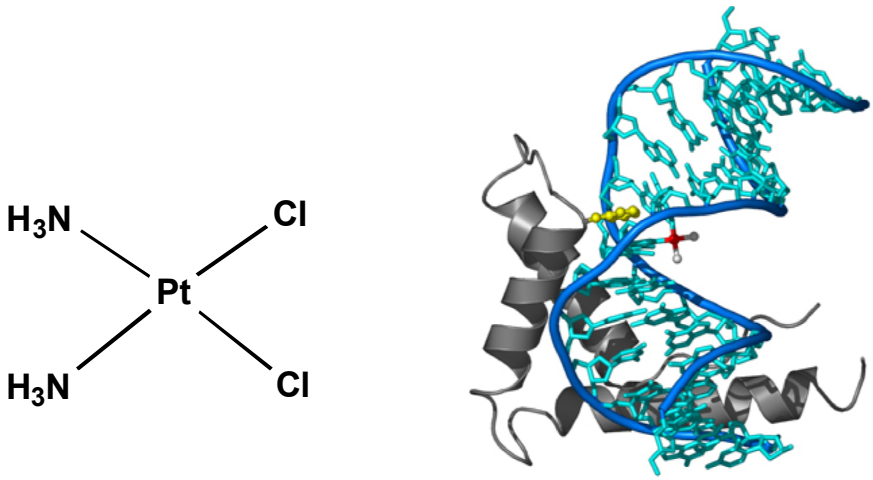

Figure 1.15 Left: Chemical structure of cis-platin. **Right:** Cisplatin-DNA adduct bound to HMGB1. Cisplatin is shown as red and white spheres. DNA is shown in blue, HMGB1 shown as grey cartoon with intercalated phenylalanine shown as yellow spheres. Taken from ref.[44]

Although cisplatin is an effective antineoplastic agent, its clinical use is limited because of its severe side effects including nephrotoxicity, gastrointestinal toxicity, neurotoxicity, ototoxicity, hematologic and hyperuricemia. To overcome these problems, scientists designed and developed a range of cisplatin derivatives, which are more effective and less toxic (**Figure 1.16**). These are carboplatin and oxaliplatin which have been approved for worldwide use. Other cisplatin derivatives have been clinically approved for some countries such as nedaplatin (Japan), lobaplatin (China) and heptaplatin (South Korea).

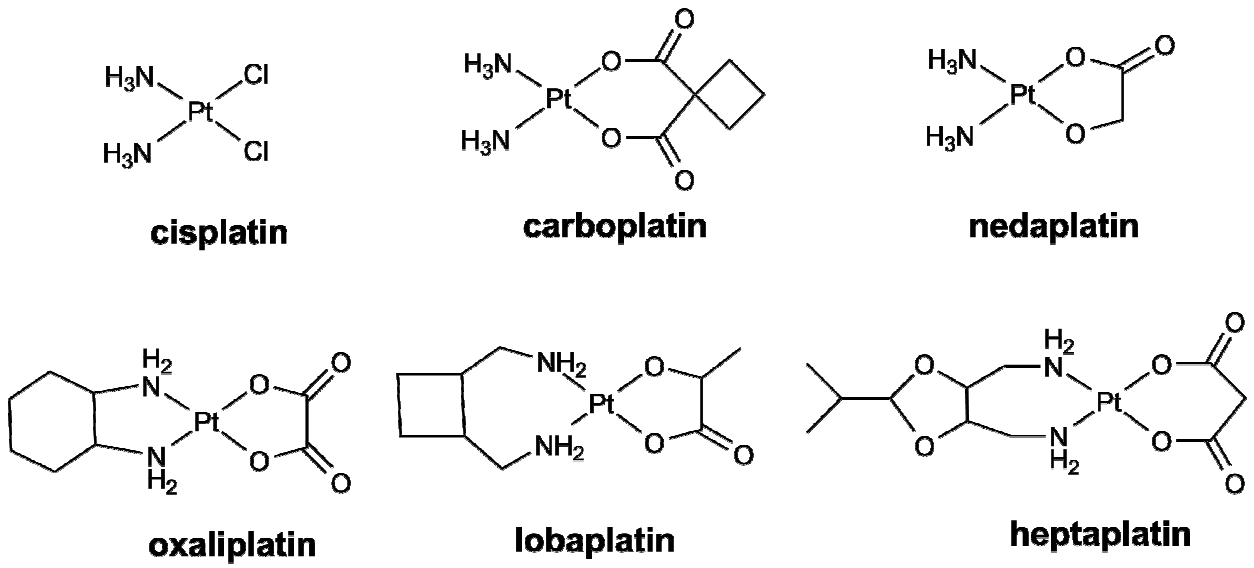

Figure 1.16 Cisplatin and its derivatives

The toxicity of platinum drugs is directly related to how easily the leaving groups leave and the complex is aquated. Platinum complexes with highly labile ligands are very toxic whereas ligands which aquate very slowly are much less toxic.[45] In carboplatin, the dichloride ligands of cisplatin were substituted by a bidentate 1, 1-cyclobutanedicar boxylic acid ligand (**Figure 1.16**). It was found that the side effects associated with cisplatin treatment were reduced with no significant renal or neural toxicity. In addition, carboplatin is believed to form the same DNA adduct as cisplatin due to the presence of the same carrier ligand (NH_3). Nedaplatin is a square planar platinum (II) complex with a glycolic acid bidentate ligand with one carboxyl and one hydroxyl donor (**Figure 1.16**). Its solubility is ten times greater than that of cisplatin. It has shown higher antitumor activity than carboplatin but equivalent to that of cisplatin with less nephrotoxicity, neurotoxicity and gastrointestinal toxicity than cisplatin.[46-48] Oxaliplatin is a squar planar platinum (II) complex containing 1,2 diaminocyclohexane (DACH) and oxalic acid as a

carrying group and leaving group, repectively (**Figure 1.16**). This oxalate ligand dramatically reduces the severe side effects of the drug compared with cisplatin.[49] Oxaliplatin was the first drug approved that was capable to overcome cisplatin resistance due to the different adducts forming with DNA. In combination with the other anticancer agents including 5-fluorouracil (5-FU) and folinic acid, oxaliplatin is used to treat colorectal cancer.[50] Lobaplatin is a disastereomeric mixture (50:50) of the carrier ligand, 1,2- diaminomethylcyclobutane (**Figure 1.16**). The leaving group of this drug is lactic acid. Lobaplatin is currently approved for the treatment of leukaemia, breast cancer and small cell lung cancer.[45] Heptaplatin was approved to use in Korea (**Figure 1.16**). Its cytotoxicity can be equal to or greater than cisplatin in various cell lines.[51, 52] It had a high stability in solution, no remarkable toxicity and ability to overcome cisplatin-resistant cells. It is currently used in clinic for the treatment of gastric cancer.[45]

1.1.4.3 Sugar phosphate backbone binding

Farrell synthesised a cationic trinuclear Pt(II) complex (TriplatinNC, **Figure 1.17B**) which can bind to the DNA phosphate backbone.[53] This agent is related to the trinuclear trans-platinum drug BBR3464 (**Figure 1.17A**) but lacks the reactive Pt-Cl groups. It can non-covalently bind to DNA through hydrogen bonding and electrostatic interactions. Recently the crystal structure of a double-stranded B-DNA dodecamer with TriplatinNC has indicated that this compound can form multiple hydrogen bonds with the phosphate oxygen and can track along the phosphate backbone, described as "Backbone tracking".[54] It can also span the minor groove making a bridge between the phosphate

backbones on each strand. TriplatinNC shows micromolar activity against human ovarian cancer cell lines.[55]

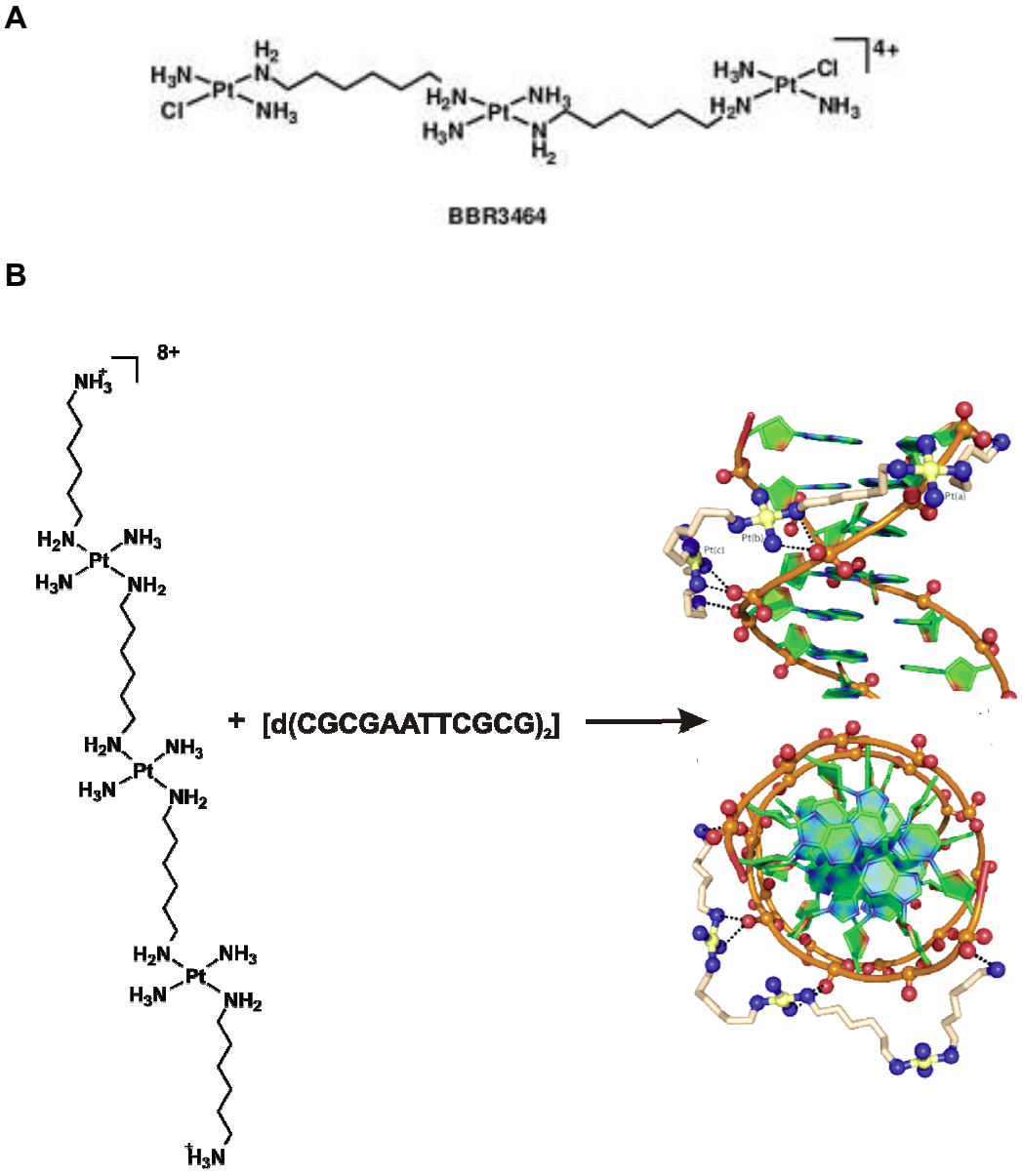

Figure 1.17 A) BBR3464. **B)** Crystal structure of backbone tracking of the trinuclear platinum(II) compound, TriplatinNC which was cocrystallised with DNA.[54]

1.1.4.4 Minor groove recognition

Several organic agents such as diarylamides (DAPI, berenil and pentamidine) and bis-benzimidazoles (Hoechst 33258 and their derivatives) target the DNA minor groove (**Figure 1.18**). These are used as anticancer, antiparasite, antiviral and antibacterial agents. Some, such as DAPI and Hoechst, show attractive fluorescent properties when bound to DNA, and are therefore widely used as DNA stains for biological imaging.[56, 57] The common structural features shared by most minor groove binders are a positive charge, linked aromatic or heteroaromatic rings and a crescent shape.[58] Most minor groove binders have a preference for AT sequences over CG sequences as the AT sequence has a narrower and more flexible minor groove, resulting in a snug fit.[34]

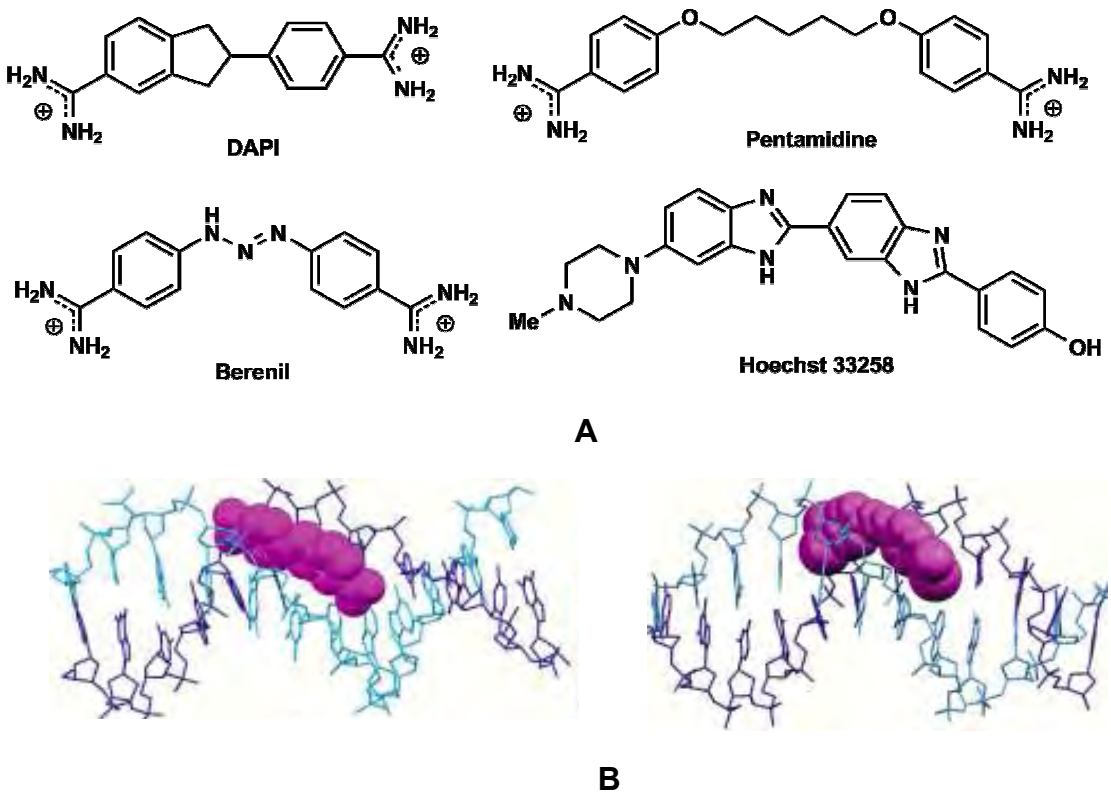

Figure 1.18 A) Chemical structures of DNA minor groove binders. **B)** Binding of DAPI (left) and berenil (right) in the minor groove of DNA.[34]

Another well known example of minor groove binder is an array of polyamides which are known as sequence specific DNA binding agents. Dervan *et al*. have established a combination of code, by which synthetic agents relied on modified distamycin-type structures, can recognise the DNA sequence via the minor groove (**Table 1.2**).

Table 1.2 Pairing code for minor groove recognition. Taken from ref.[59]

	C•G	G•C	A•T	T•A
Py/Im	+	-	-	-
Im/Py	-	+	-	-
Py/Hp	-	-	+	-
Hp/Py	-	-	-	+

Note: Py = pyrrole, Im = imidazole, Hp = hydroxypyrrole. (+) = favored, (-) = disfavoured.

At the first step of Dervan's study, a methylpyrrole of distamycin was substituted by a methylimidazole group (**Figure 1.19A, B**).[34] As expected, the formation of hydrogen bonding was observed between the new nitrogen in the ring system and the NH_2 of the guanine base in the minor groove (**Figure 1.19C**). At high drug loading, it is interesting that two strands of two pyrrole/imidazole peptide could bind side by side in the minor groove (**Figure 1.19D**). This is different from the other minor groove binders such as DAPI and berenil which are formed 1:1 ratio of drug to DNA strand. The two polyamide strands align head-to-tail in the groove therefore the cationic guanadinium ends are placed away from each other (**Figure 1.19E**).

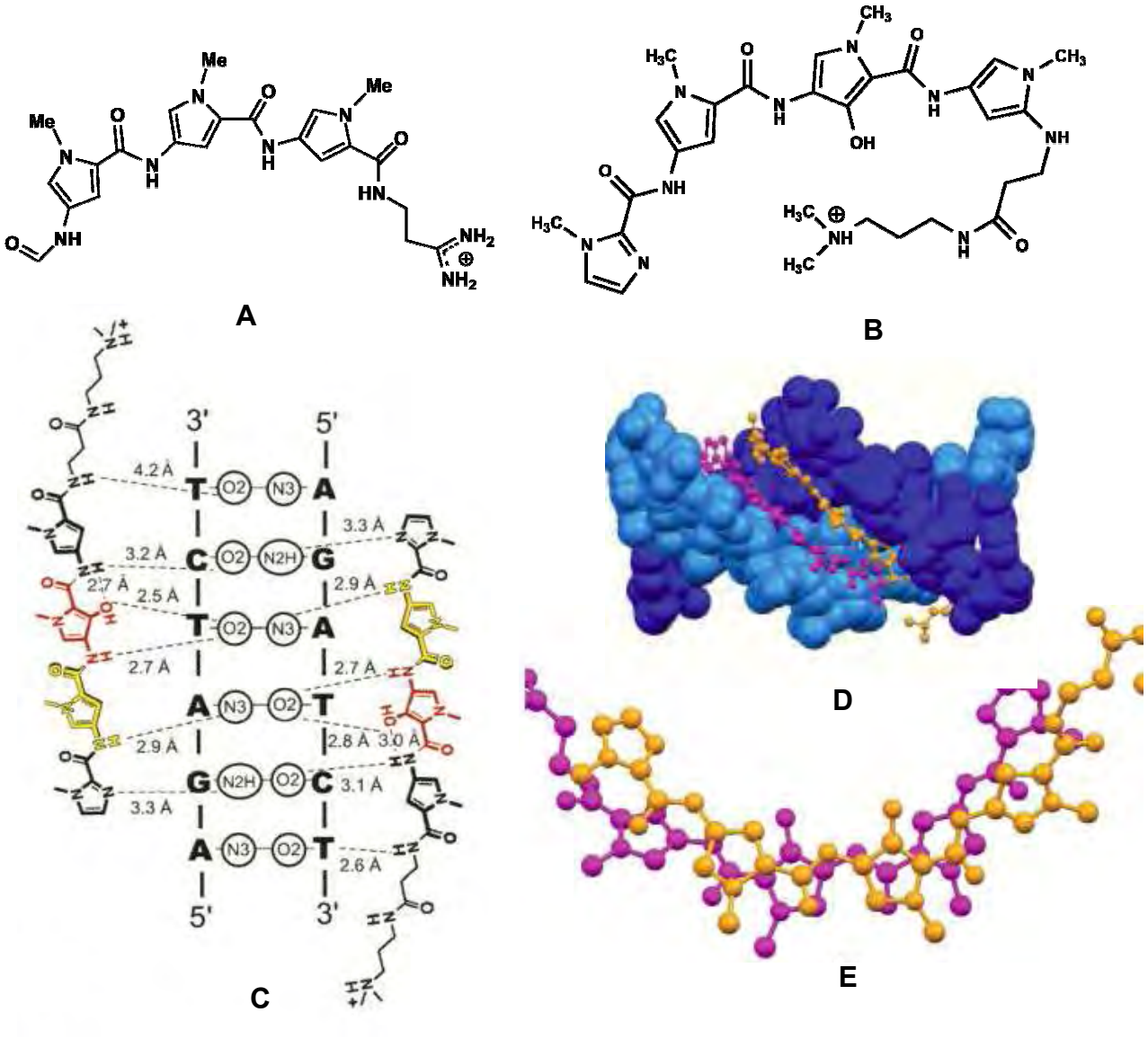

Figure 1.19 A) Chemical structure of distamycin A. **B)** Structure of polyamide strand (ImPyHpPy). **C)** Schematic diagram of hydrogen bonding interaction of polyamide strand (ImPyHpPy) with the 5′-AGATCT-3′. Hydrogen bonds are shown in dash line and numbers indicate distance between non hydrogen atoms. **D)** Two polyamide strands (pink and orange) aligning side by side in the DNA minor groove (blue and cyan) **E)** Relative orientations of two polyamide strands. Taken from ref.[34, 60]

In addition, each polyamide strand interacts with the bases of one strand of the DNA. Subsequently, two polyamide strands forming π-π stacking between the pyrrole/imidazole rings of one strand and the amide carbonyls of the other strand can recognise a base pair of DNA in the minor groove. Based on this concept, a hairpin linker

was introduced to incorporate two antiparallel polyamide strands into one molecule. The biological studies demonstrate that these polyamides can inhibit the transcription of specific genes.[61] Furthermore, a series of conjugated hairpin polyamides with DNA binding agents was synthesised. It was reported that the polyamide with DNA alkylator (chlorambucil) conjugate is able to cause cell arrest in the G2/M stage in the cell cycle. The conjugate is also active against a wide range of cancer cells without animal toxicity.[62] Moreover, hairpin polyamide-fluorescent dye conjugate was created.[63] The aim of synthesising this compound is to probe and quantify the uptake of the polyamide to nucleus of live cells.

1.1.4.5 Major groove recognition

The DNA major groove provides a large variety in size and shape and a greater variety in pattern of hydrogen bond donor and acceptor units than the minor groove. Therefore, it is a common target for proteins.[34] Major groove recognition by proteins usually involves cylindrical binding units based on alpha helices. This unit has the perfect size and shape to fit tightly into the major groove but is too large for the minor groove. The principle recognition motifs found in DNA binding proteins are α-helix-turn-α-helix, zinc-finger and leucine zippers.[58] Besides proteins, oligonucleotides can recognise the DNA major groove by forming triplex DNA via Hoogsteen or reverse Hoogsteen base pairing (**Figure 1.20**). This sequence specific binding has been used in an application for genetic manipulations.[64, 65]

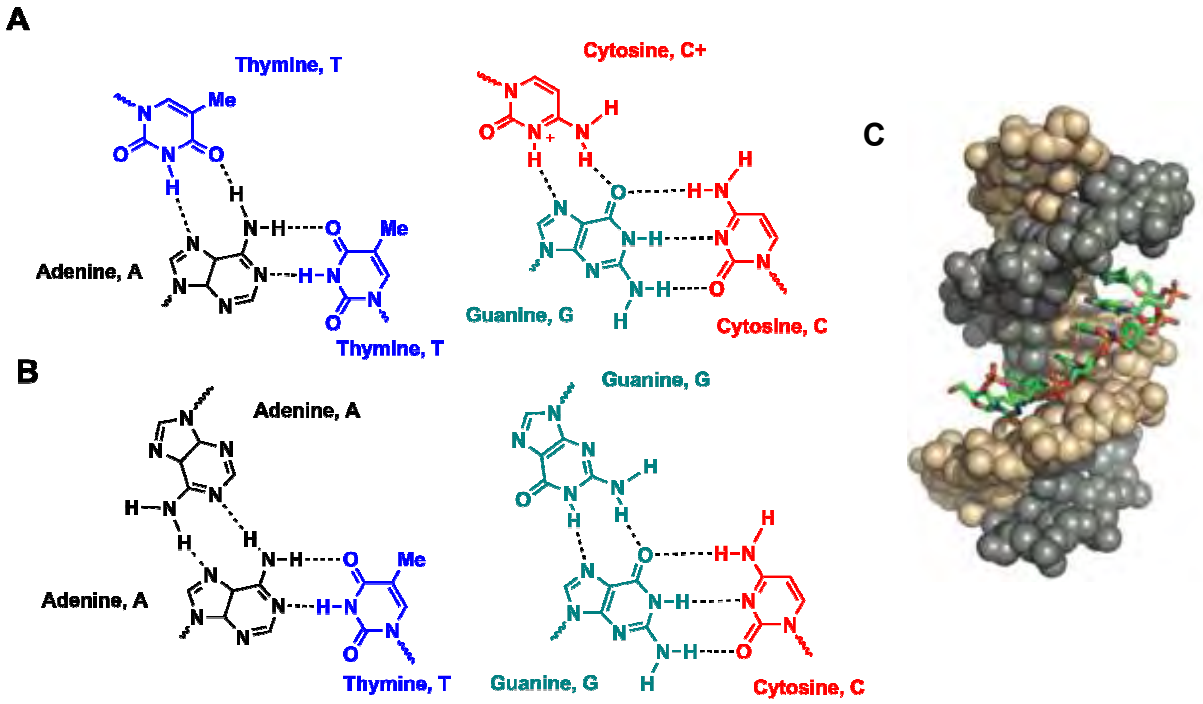

Figure 1.20 Hydrogen bonding in the major groove involving triplex formation. **A)** Hoogsten base pairing. **B)** Reverse-Hoogsteen base pairing. **C)** Structural representation of triple helix forming oligonucleotide (TFO, green) bond in the major groove of double stranded DNA.[66]

Based on this triplex DNA formed from oligonucleotides, Nielsen *et al.* invented peptide nucleic acid (PNA) in which the sugar backbone of conventional DNA was replaced by a polyamide (**Figure 1.21**).[67] The benefit from this replacement is the reduced negative charge resulting in greater binding of PNA to DNA than oligonucleotide to DNA. Thus, PNAs are capable to form $(DNA)_2(PNA)$ triplex with double stranded DNA. However in practice, these agents frequently displace one of the DNA strands forming a $(PNA)_2(DNA)_1$ triplex. This occurs when the DNA double helix is opened up and two PNA strands invade. One of those PNAs binds to one of the DNA strands with respect to Watson and Crick base pairing and another strand binds to the major groove of that PNA-DNA double helix.

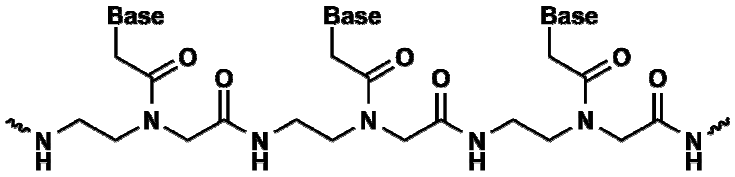

Figure 1.21 Chemical structure of PNA.

Not only proteins, oligonucleotides and PNA can target the major groove DNA but also a synthetic agent, called a metallosupramolecular cylinder (**Figure 1.22**). This compound was initially synthesised by Hannon *et al*.[68] It was first reported as a synthetic agent that targets the major groove by fitting snugly into the DNA major groove across five base pairs.[69, 70] The nucleic acid binding is more complex than this though and this cylinder and its derivatives are the subject of detailed studies herein. The review of the cylinder and its derivatives will be shown in **Section 1.1.4.5.1**.

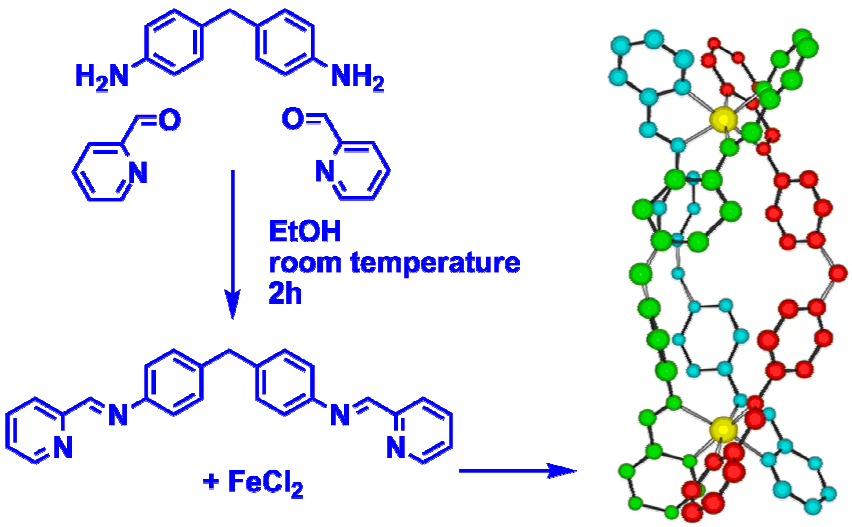

Figure 1.22 Synthetic scheme of the iron metallosupramolecular cylinder.[69]

1.1.4.5.1 Metallosupramolecular iron (II) cylinders

The first metallosupramolecular iron cylinder was synthesised by Hannon *et al.*[68] This complex contains two metal iron (II) centres wrapped by three pyridylimine ligand forming triple stranded helicate (**Figure 1.23**).

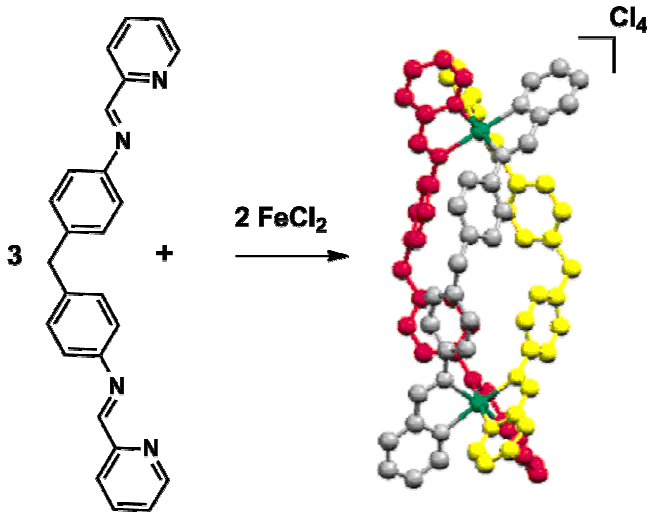

Figure 1.23 Synthetic scheme of a metallosupramolecular iron (II) cylinder ($Fe_2(C_{25}H_{20}N_4)_3Cl_4$).

This tetracationic iron helicate compound ($[Fe_2L_3]^{4+}$) has a cylindrical shape with ~2 nm in length and ~1 nm in width therefore sometimes it is called a iron cylinder. The synthetic approach of this iron cylinder is inexpensive and easy. The iron cylinder is a helical molecule containing two enantiomers: left handed helicate (M enantiomer) and right handed helicate (P enantiomer) (**Figure 1.24**). These enantiomers are easily separated by using cellulose as a stationary phase and 20 mM NaCl solution as eluent.[71, 72] Interestingly, the dimensions of the iron cylinder are similar to protein DNA-recognition motif therefore this cylinder should have the same target as DNA recognition proteins which are mainly at the major groove.

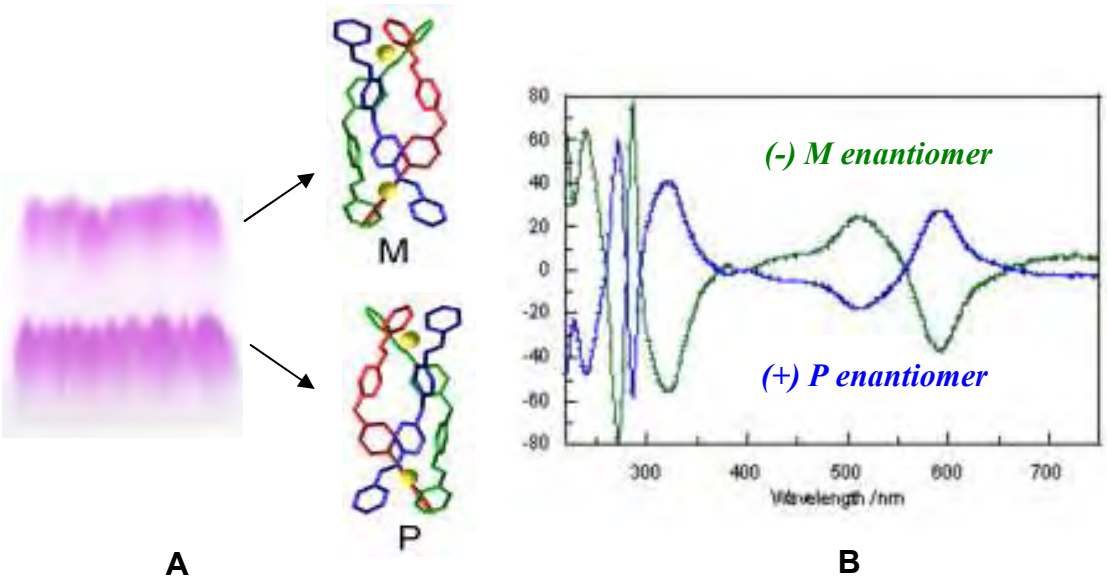

Figure 1.24 Enantiomers of the iron cylinder. **A)** Separation of the iron cylinder by cellulose paper and NaCl solution. **B)** CD spectrum of enantiomerically pure M and P of the iron cylinder. Taken from ref.[71]

DNA binding studies of the iron cylinder to DNA were probed by several biophysical techniques such as CD, LD and AFM (**Figure 1.25**). The results show that the iron cylinder targets the major groove of B-DNA by binding across five base pairs[70] and induces intramolecular DNA coiling.[69] It has been shown that two enantiomers of the iron cylinder bind differently to the major groove. The M enantiomer dramatically induces the intramolecular ct-DNA coiling, bending more than that of the P enantiomer. It has been also reported that the two enantiomers of the iron cylinder clearly show a different in DNA binding modes. The M enantiomer preferentially binds to the major groove while the P enantiomer is believed to bind along the minor groove spanning the two phosphate backbones.[73]

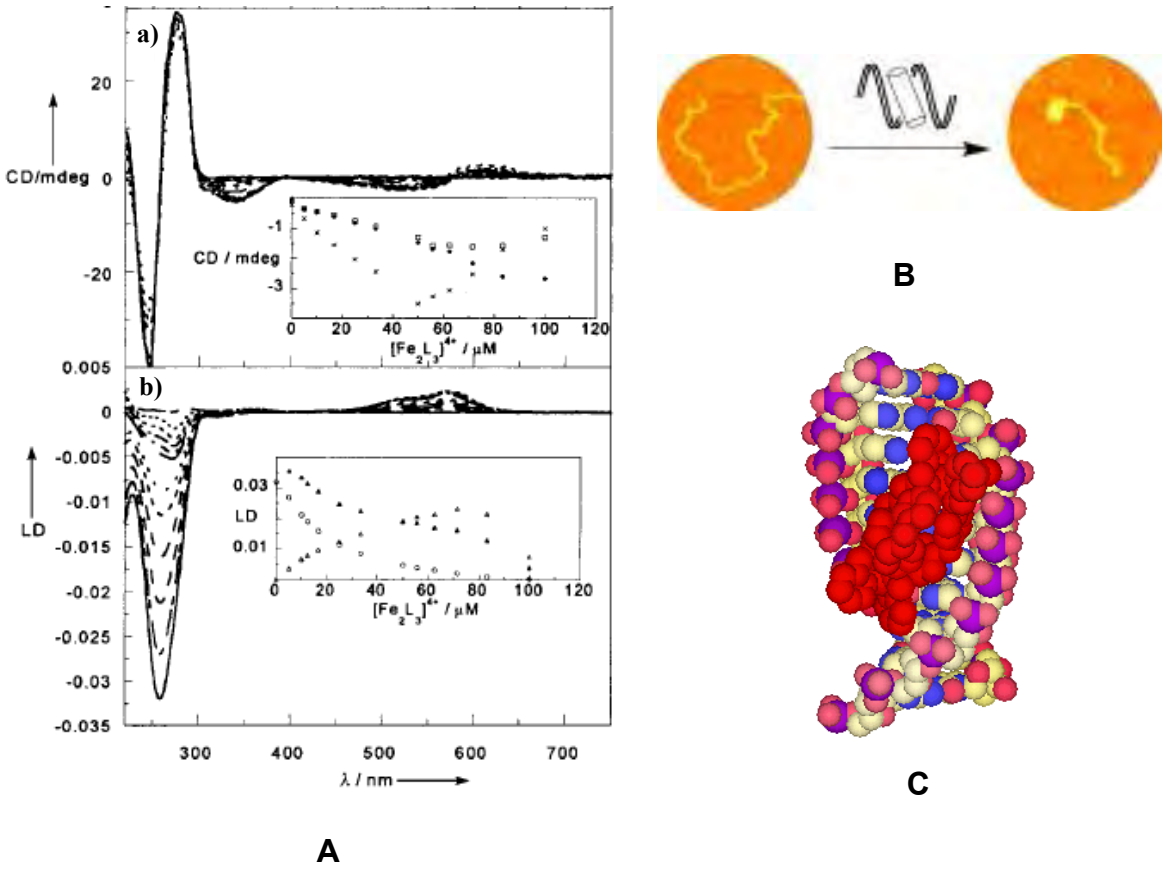

Figure 1.25 DNA binding studies of the iron cylinder to DNA. **A)** CD and LD showing that the iron cylinder binds to B-DNA and it does not change the conformation of B-DNA. **B)** AFM image representing intramolecular coiling of the iron cylinder to ct-DNA. **C)** X-ray structure of the iron cylinder locating at the core cavity of DNA three way junction. Taken from ref.[69]

One interesting biophysical parameter for evaluating the ability of the compound to interact with DNA is unwinding angle. It is the number representing the degrees by which the DNA is unwound about its helical axis per the molecule bound.[74] The result shows that the M enantiomer is more effective than the P enantiomer at unwinding DNA (**Table 1.3**).[75] The high efficacy of the iron cylinder at unwinding DNA, compared to the other synthetically non-covalent DNA binding agents, may reveal a potential to affect cellular processes involving DNA strand separation, such as DNA replication, transcription or repair. Moreover, both enantiomers exhibited the lower binding affinity

of ct-DNA than poly(dA-dT)$_2$ and poly(dG-dC)$_2$ (**Table 1.3**). This suggests that the enantiomers has a preferential binding for regular purine-pyrimidine tracts rather than a random DNA sequence. The result also demonstrates that repetitive AT sequences is preferred by both enantiomers over GC sequences.

Table 1.3 Summary of value achieved from biochemical and molecular biological studies of DNA-complex interaction. Taken from ref.[75, 76]

Compound	**Unwinding angle (degree)**	**Kapp (x 10^6 M^{-1})**		
		ct-DNA	**poly (dA-dT)$_2$**	**poly (dG-dC)$_2$**
rac-$[Fe_2L_3]^{4+}$	27±3º	60	ND	ND
M-$[Fe_2L_3]^{4+}$	32±3º	46	106	77
P-$[Fe_2L_3]^{4+}$	22±3º	76	142	89

ND = not determined

Besides the major groove recognition, the iron cylinder has an additional unprecedented DNA binding mode which is three way junction recognition. An X-ray crystal structure, which was obtained from a solution containing a palindromic hexanucleotide DNA and the iron cylinder, shows that the iron cylinder is perfectly located at the heart cavity of the DNA three way junction.[77] This is interesting because a palindromic oligonucleotide used for preparing crystal structure can usually form a double stranded DNA rather the other possible structures such as three way junction, four way junction, etc. In the presence of the iron cylinder, the helicate has chosen three way junction to which it binds most effectively, therefore the crystal structure in the form of

the cylinder locating at the core cavity of three way junction is obtained (**Figure 1.26**). The binding of the iron cylinder to three way junction were confirmed again by other techniques including NMR and gel electrophoresis to ensure that the obtained X-ray structure is not solely the artefact from the crystallisation. The X-ray study suggests that several non-covalent interactions are contributed in this stabilisation including electrostatic interactions, face to face π-π stacking interactions, sandwiching interactions in the minor groove, hydrogen bonding interactions and hydrophobic interactions.[77]

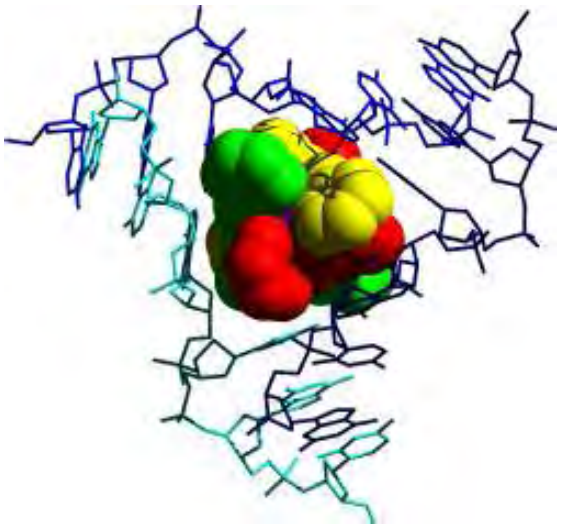

Figure 1.26 DNA junction recognition by a metallosupramolecular tetracationic cylinder. The stick represents hexanucleotide DNA and space filling demonstrates the cylinder. Taken from ref.[77]

Three way junctions can be found in DNA and RNA. In RNA, they are involved in splicing[78] and translation processes.[79] In DNA, they are known as replication fork, forming transiently during DNA replication.[7] They also form as intermediated structures during triplet repeat expansions which are associated with several human genetic diseases such as myotonic dystrophy type1 and Huntington's diseases.[80] A drug designed to recognise DNA three way junction could be a promising strategy for a potential

anticancer drug as it could selectively bind to the DNA target. This could possibly overcome the unpleasant side effect of current anticancer drug used in clinic such as cisplatin.

Recently, it is reported that the iron cylinder can stabilise G-quadruplex structure and its chiral cylinders can distinguish G-quadruplex DNA. The P enantiomer has a stronger selectivity to G-quadruplex than the M enantiomer. Moreover, only the P enantiomer can convert antiparallel G-quadruplex to hybrid structure.[81] The conversion of G-quadruplex structure by the P enantiomer was probed by several techniques such as CD, UV melting curve and gel electrophoresis.[81] Due to a hydrophobic surface, compatible size of the cylinder (length ~ 18 Å, diameter ~ 8 Å)[68] to the G-quartet (length ~ 14 Å, diameter ~ 11 Å)[82] and electrostatic interactions between positive charge of the complex (4+) and negative charge from phosphate backbone of the DNA, the cylinder has a potential to interact with the two lateral loops and grooves of G-quadruplex via external stacking.

Biological studies demonstrate that the supramolecular cylinder inhibits the proliferation in a number of cancer cell lines and induces cytostasis at the G_0/G_1 phase and apoptosis in myeloid leukaemia cell line HL-60.[83] Moreover, this anticancer activity is not associated with genotoxicity or mutagenicity confirming by COMET assays and AMES tests, respectively. This is important because those are the major drawbacks of cisplatin which can lead to an increased risk of secondary cancers such as leukaemias. Recently, it has been reported that the enantiomers of the cylinder can inhibit a telomerase activity and influence telomere shortening, β-galactosidase activity which are associated with cell senescence and upregulation of cyclin-dependent kinase (CDK)

inhibitors p16 and p21 in chronic myelogenous leukemia known as K562 cell lines. In addition, the P enantiomer is more effective than the M enantiomer.[81] This work provides new insights into elucidating chiral complex and G-quadruplex.

Furthermore, the cylinder also exhibits antimicrobial activity against *B. subtilis* and *E. coli* representing of gram positive and gram negative bacteria through a bactericidal manner.[84] Due to the extremely fast rate of killing, it is believed that DNA binding may not the only mechanism of bactericidal activity. Interestingly, the structure and the mode of action of the cylinder are different from all known antimicrobial agents. Consequently, it may effectively act against bacterial resistant strains to other antibiotics.

Since the metallosupramolecular cylinder was synthesised, much effort has been put on the modification of the parent cylinder in order to enhance its selectivity to DNA and improve a physical feature of the modified compound such as fluorescent property. All modified cylinders which were synthesized in Hannon group, will be reviewed herein. Firstly, Uerpmann *et al*. synthesised an extended triple stranded metallosupramolecular cylinder.[85] The modified iron cylinder is longer and slightly wider than the parent iron cylinder. The DNA binding studies showed that the compound binds in the same fashion as the parent cylinder does however a DNA coiling effect of the modified cylinder is much less than the parent cylinder. Later, Peberdy and co-workers showed that increasing the width of the parent cylinder by adding methyl group (CH_3) on the parent ligand at the 3 position of the pyridyl ring adjacent to the metal binding site unit (**Figure 3.3C, F** in **Chapter 3**) weakens the DNA binding strength, reduces the bending and coiling effect.[76] Interestingly, lengthening the cylinder by introducing methyl group on the parent ligand at the 5 position of the pyridyl ring shows a similar

DNA interaction to those of the parent cylinder.[76] This indicates that the dimensions of the cylinder are crucial for its binding ability to DNA. Furthermore, Pascu *et al*. combined the DNA binding features of the parent cylinder with the photoactive properties of ruthenium by synthesising a metallosurpramolecular triple stranded ruthenium cylinder ($[Ru_2L_3]^{4+}$).[86] Using ruthenium instead of iron metal will increase the stability of the compound as well as the fluorescent property. DNA binding studies of the ruthenium cylinder show that the ruthenium cylinder binds and coils ct-DNA in a similar fashion as the parent cylinder does. It is because both cylinders have the same size, shape and charge. Surprisingly, the unwinding angel of the ruthenium cylinder, shown in **Table 1.4**, was noticeably less than the parent cylinder ($[Fe_2L_3]^{4+}$).

Table 1.4 Comparison of bending angel and binding constant of the iron and ruthenium cylinder. Taken from ref.[74-76]

Compound	Unwinding angel (degree)	K_{app} (x 10^6 M^{-1})
$[Fe_2L_3]^{4+}$	27±3º	60
$[Ru_2L_3]^{4+}$	13±2º	58

This may be the effects emerging from differences in the extent of polarization of the protons on the exterior of $[Ru_2L_3]^{4+}$.[74] Moreover, $[Ru_2L_3]^{4+}$ exhibits a highly effective DNA-photocleavage ability via singlet oxygen ($^1O_2$) mechanism. Therefore, this compound could be used as specific photoreagents in photodynamic therapy due to a low toxicity of the compound in the absence of light and its localized effects.[74] Furthermore, the cytotoxicity of $[Ru_2L_3]^{4+}$ is drastically different from that of $[Fe_2L_3]^{4+}$. $[Fe_2L_3]^{4+}$ is active against an ovarian cancer cell line but $[Ru_2L_3]^{4+}$ is not. This indicates that the

mechanism of action of $[Ru_2L_3]^{4+}$and DNA interaction could be different from that of $[Fe_2L_3]^{4+}$.[83, 86] Another promising strategy for enhancing the specificity of the parent cylinder is to attach short amino acids to the end of $[Fe_2L_3]^{4+}$. By this approach, the conjugated cylinder will combine the DNA binding properties of the parent cylinder and a selectivity property from attached amino acids. The first conjugated cylinder was synthesised by Cardo *et al*.[87] Several biophysical experiments were carried out to probe DNA-complex interactions. It is shown that the conjugated cylinders are able to coil DNA but less effective than that of the parent cylinder (see **Section 3.5.2.3** in **Chapter 3**). In addition, the stability of conjugated complexes is less stable than that of the parent cylinder. The instability of the conjugate complex increases when a long peptide is anchored to the parent cylinder. Interestingly, the conjugated compounds also show the cytotoxicity to cancer cell lines.[88]

1.1.4.6 Recognition of DNA junction structure

Nucleic acid junctions, in RNA and DNA, are unique branched structure containing double strand(s) emerging at one point. They can be a perfect junction which has Watson and Crick base pairing or with mismatched base pairs.[89] Recently, a new DNA binding mode defined as DNA junction recognition was reported by Hannon *et al*. Crystallographic studies of a palindromic hexanucleotide DNA and a dinuclear tetracationic triple stranded helicate, the iron cylinder, were performed.[69] Surprisingly the cylinder was found to be located in the hollow cavity of a DNA Y-shaped junction rather than simply binding to duplex DNA (**Figure 1.27**).[77] This new binding mode does not

cause any changes in the structure of the DNA three way junction or the cylinder, rather they seem to be a perfect fit.

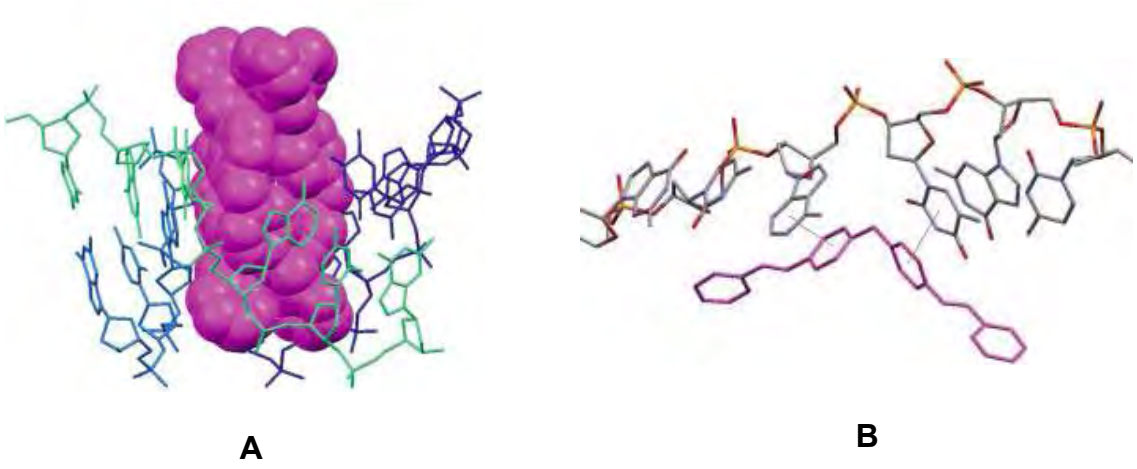

Figure 1.27 A) Recognition of DNA three way junction by iron cylinder. **B)** Face to Face π stacking of phenyl rings of the ligand of complex and DNA bases. Taken from ref.[34]

Several interactions contribute to this recognition:[77] electrostatic forces from the positive charge of the cylinder to the negative charge of phosphate backbone, and face-face π stacking interaction from the aromatic surfaces of the cylinder to DNA bases. In addition, a hydrogen bond, CH···X formation, between the imine hydrogen and N3 of an adenine base occurred. Moreover, the pyrimidine rings are sandwiched in the minor groove as seen with minor groove binders. This unprecedented binding mode is of particular interest for gene regulation as the replication fork, occurring during the DNA replication process, is a Y-shaped junction and the cylinders might therefore be used to stop the growth of cancer cells. Indeed, experiments have confirmed that they are active against cancer cell lines.[83]

1.1.4.7 Recognition of quadruplex DNA structure

Quadruplex DNAs are secondary DNA structures which are assembled from guanine-rich sequences usually presented in telomeres.[90] Telomeres usually contain tandem repeated guanine rich sequences at the 3′ overhang of single stranded DNA, present at the end of chromosomes. Telomeres shorten in every cell cycle due to incomplete DNA replication of telomeric termini, thus resulting in cell senescence. Several studies reveal that a large number of human cancers maintain the elongation of telomeres by exploiting the enzyme telomerase, a kind of reverse transcriptase, so the cancer cells become immortal. Aside from telomeres, G-rich sequences that have the potential to form quadruplex structures also exist in promoter regions of certain oncogenes. This suggests that quadruplex structures may be involved in the regulation of gene expression.[91] For these reasons, quadruplex structures have been proposed as potential new targets for anticancer agents.[92, 93] The conventional agents targeted to quadruplex structures are mostly organic based compounds. Recently, metal based complexes have been considered as synthetic agents due to the fulfillment of the basic requirements of designing quadruplex DNA binders. Several advantages can be obtained from using metal complexes.[94] The quadruplex binding affinity and specificity can be easily optimised by changing the geometries and orientation of the complex by changing the metal used. The π interaction of the metal to the G-quartet can be increased via the electron withdrawing properties of the metal. The presence of positive charge on the metal facilitates the stablilisation of a G-quartet by substituting the alkali cation. An example of the metal based complex as quadruplex DNA binder is shown **Figure 1.28**.

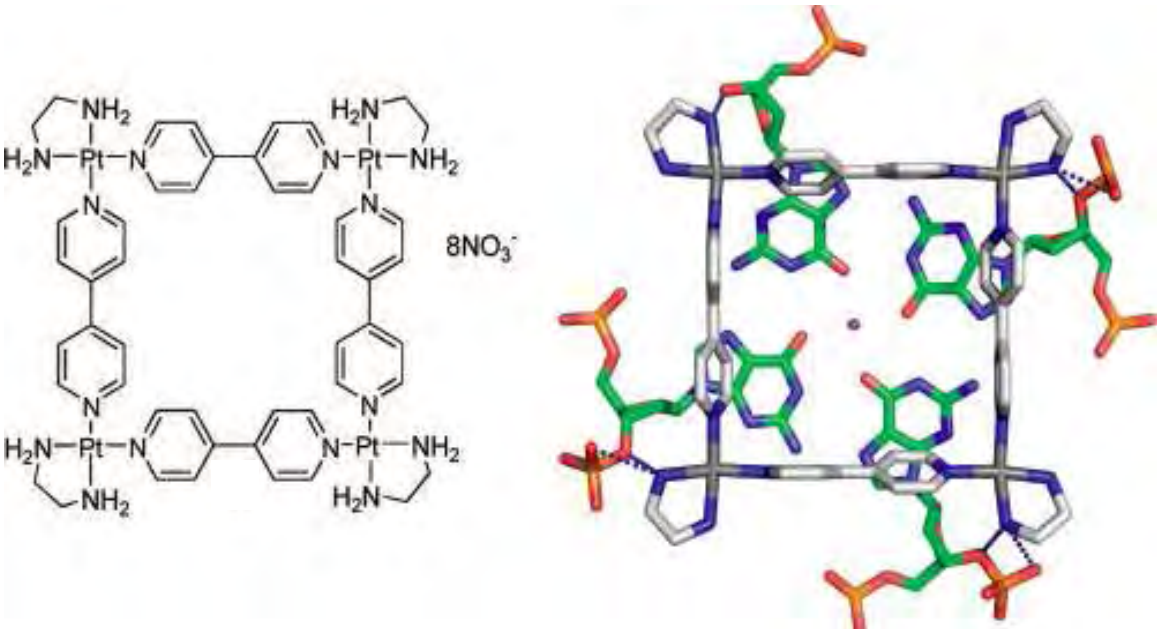

Figure 1.28 Left: Chemical structure of platinum molecular square. **Right:** Model of the platinum square binding to quadruplex DNA. Platinum complex is shown in blue and grey. Hydrogen bonding to phosphate backbone is illustrated as blue dotted line. Taken from ref.[95]

1.2 Introduction to RNA

1.2.1 The fundamental structure of RNA

Ribonucleic acid (RNA) is an important biological molecule, consisting of a long chain of nucleotides. As mentioned in the previous section, deoxyribonucleic acid (DNA) is also made up of nucleotides however RNA is different from DNA in two key chemical aspects. The first chemical aspect that renders RNA different from DNA is the bases present. Thymine bases (T), present in DNA, are replaced by uracils (U), which have the same hydrogen bonding but do not have a methyl group at the 5′ position (**Figure 1.29A**). Secondly, the sugar of RNA has a hydroxyl group (OH) attached at the 2′ position, known as ribose sugar while in DNA, it is deoxyribose sugar. The effect of an additional

hydroxyl group on the sugar has an effect on the conformation and stability of RNA. RNA sugars are much more rigid than DNA sugars, and only adopt the C3′-endo pucker conformation as the hydroxyl group at the 2′ position would clash with C8 of purine or C6 of pyrimidine attached (**Figure 1.29B**). Therefore, RNA adopts an A-form geometry rather than the B-form which is usually observed in DNA. The A-RNA conformation has a narrow and deep major groove and a wide, shallow minor groove (**Figure 1.29C**).

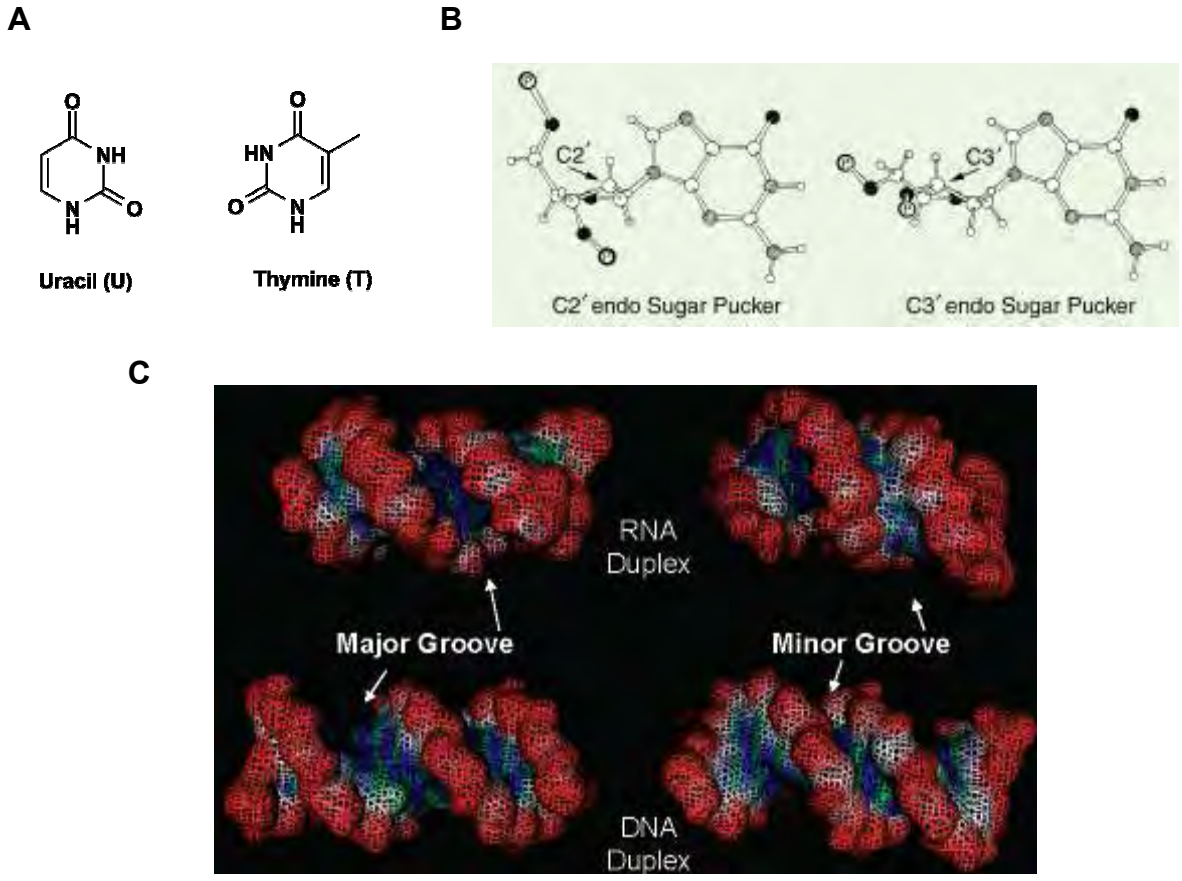

Figure 1.29 A) Uracil base (U) found only in RNA while Thymine (T) is present only in DNA. **B)** Sugar conformation of nucleic acid: C2 endo Sugar pucker is usually found in DNA while C3 endo sugar pucker is found in RNA.[96] **C)** Comparison of the groove of nucleic acids.[97]

The presence of an extra hydroxyl group on the ribose sugar also affects to the stability of RNA. RNA is much more susceptible to nucleophilic attack in the presence of OH^- on the 5'-phosphorous atom, thus resulting in breakage of the phosphodiester bond on the backbone.

1.2.2 Secondary structures of RNA

While DNA usually dimerises to form a double stranded structure, RNA frequently (but not exclusively) folds up , like a protein, to form a folded but single stranded structure. The examples of the secondary structures of RNA that have been elucidated are RNA duplexes, hairpins, bulges, loops, mismatches, and RNA junctions such as three way junctions and four way junctions.[98] These structures are defined with respect to the specific hydrogen bonding interaction located in the strands as shown in **Figure 1.30.** In addition some of these secondary structures, partially found in tertiary RNA structures, are crucial sites for ligand recognition.

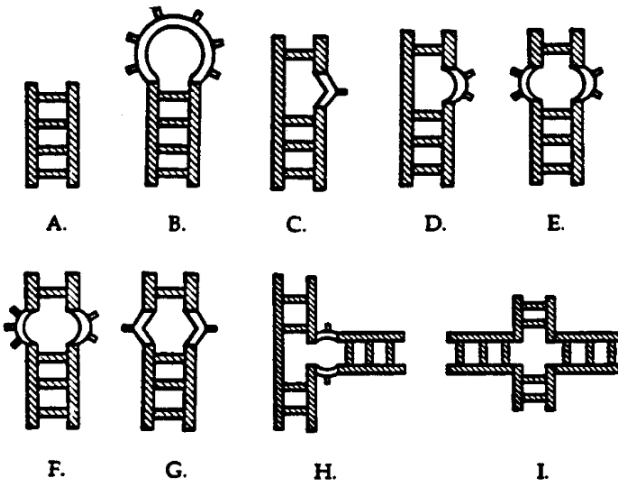

Figure 1.30 RNA secondary structures: **A)** Duplex. **B)** Hairpin loop. **C)** Single-base bulge. **D)** Multiple base bulge. **E)** Symmetric internal loop (2:2). **F)** Asymmetric internal loop (3:2). **G)** Mismatch loop. **H)** Three way junction. **I)** Four way junction. Taken from ref.[98]

1.2.2.1 Hairpin loop

Big hairpin loops (more than four bases) (**Figure 1.30B**) are found as a composition of tRNA while smaller hairpins with four-base loops, termed as tetraloops, are usually observed in ribosomal RNAs (rRNAs). Interestingly, unusual base pairing and hydrogen bonding can be observed in some tetraloops. For example, the GAAA loop has a G-A base pair [99] and the UUYG loop (Y = pyrimidine) has a U-G base pair.[100, 101] Notably, the different tetraloops will provide different structures, therefore offering significant unique binding site for targeting by small molecules.

1.2.2.2 Bulges

The formation of bulges occurs when there is one or more consecutive unopposed nucleotide on a strand of a duplex.[23] Bulges can have one unpaired nucleotides, called single base bulges (**Figure 1.30C**), or more than one unpaired nucleotide, termed as multiple-base bulges (**Figure 1.30D**). The unpaired bases of the bulge can either point into the duplex or out towards the solution, depending on the base category. Furthermore, the effect of unpaired nucleotides on RNA structures, for instance a distortion of base stacking in the duplex, bending of the helix or the reduction of the duplex's stability, can also differ. This depends on having the appropriate number and composition of bases in the bulge.[102, 103] Such bulges can open the major groove leading to an easily accessible binding site for proteins or small molecules.[104]

1.2.2.3 Internal loops

An internal loop differs from a bulge by the presence of opposing noncomplementary bases. These internal loops can have either symmetric or asymmetric loops (defined as X:Y, where X and Y correspond to the number of nucleotides on each side of the loop) within the duplex. It may have one or more mismatched loops (**Figure 1.30G**, **E**, respectively) or more unpaired loops (**Figure 1.30F**) on each strand of duplex RNA compared to a bulge. The presence of internal loops enhances the accessibility of the major groove of the RNA. It also induces conformational adaptation when a ligand is bound.[105]

1.2.2.4 RNA junctions

RNA junctions (**Figure 1.30H, I**) are found when double strand(s) are connected together. Three and four way junctions are commonly found however the higher order junctions are only observed with low frequency. The junctions can be either perfectly paired (rarely found) or most commonly interrupted by mismatched bulges at the point of strand exchange. The global structure of RNA four way junctions is different from DNA four way junction as well as changes of the structure due to metal ions.[106] It demonstrates that the RNA junction adopted a 90º cross of helical stacks in the presence of 1 mM Mg^{2+}. In the absence of metal ions, a parallel form was observed from the rotation of the RNA junctions. Increasing concentration of Mg^{2+} or using 0.5 mM Ca^{2+} can change the structure of RNA junction into an antiparallel form (**Figure 1.31**).

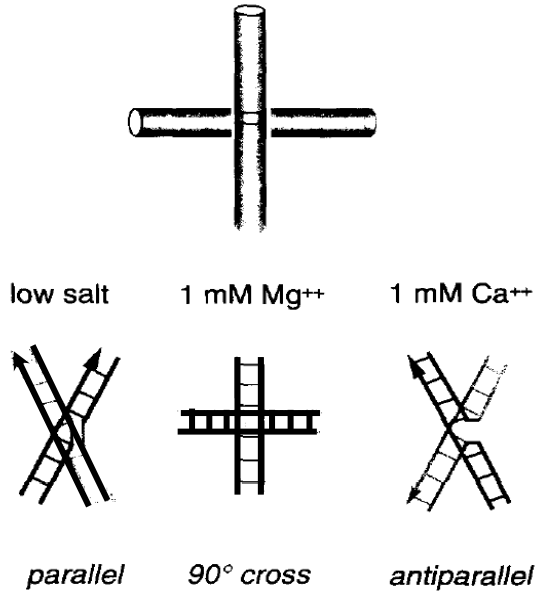

Figure 1.31 The global structures of RNA four way junction in the presence of different concentrations of metal ions. Taken from ref.[89]

Obviously, the conversion of nucleic acids from DNA to RNA has a significant impact to the global folding of four way junction. It is believed that some differences could be from the A-form helix of RNA. The most interesting difference is the structure of RNA four way junction in the absence of metal ion. In contrast to the DNA junctions, the RNA junctions tended to rotate into a parallel form instead of turning to extended form. This suggests that overall electrostatic repulsion in the RNA junction is lower than the DNA. The four way junction can be found in U1 snRNA involved in splicing of mRNA, hairpin ribozyme[23] and tRNA.[107, 108]

For RNA three way junctions, its global structure has remained unknown. The structures are restricted to specific examples, chosen for a particular study. Regarding to the basic stereochemical principle, it would suggest that the folding of RNA three way junctions should be similar to that of DNA three way junctions.[23] The folding of the

perfect RNA three way junction to coaxial stacking would be difficult unless an additional bases are added to the point of exchange to increase the flexibility of the structure. In addition, most of RNA three way junctions found in 16S and 23S rRNA usually have an additional bases in the middle of the junction and it rarely found a perfect RNA three way junction. The folding of these junctions would expect to depend on divalent metal ions. Examples of RNA three way junction include 5S rRNA[109] a ribosomal protein binding site in 16S rRNA[110] and hammerhead ribozyme.[111, 112]

1.2.3 Targeting of RNA by a small molecule

The cellular function of RNA has been elucidated for nearly two decades showing that this biomolecule is not simply working as an intermidate between the transcription[113, 114] and translation process.[115] It has been reported that RNAs are involved in many vital biological processes such as the replication of DNA,[90, 116] genetically catalytic activity.[117] The scenario of RNA dependent gene expression process is shown in **Figure 1.32**.

RNA is a promising drug target as it has a diverse array of three dimensional structures,[118] no repair mechanism and easy to access compared to extensively packed chromosomal DNA.[98]

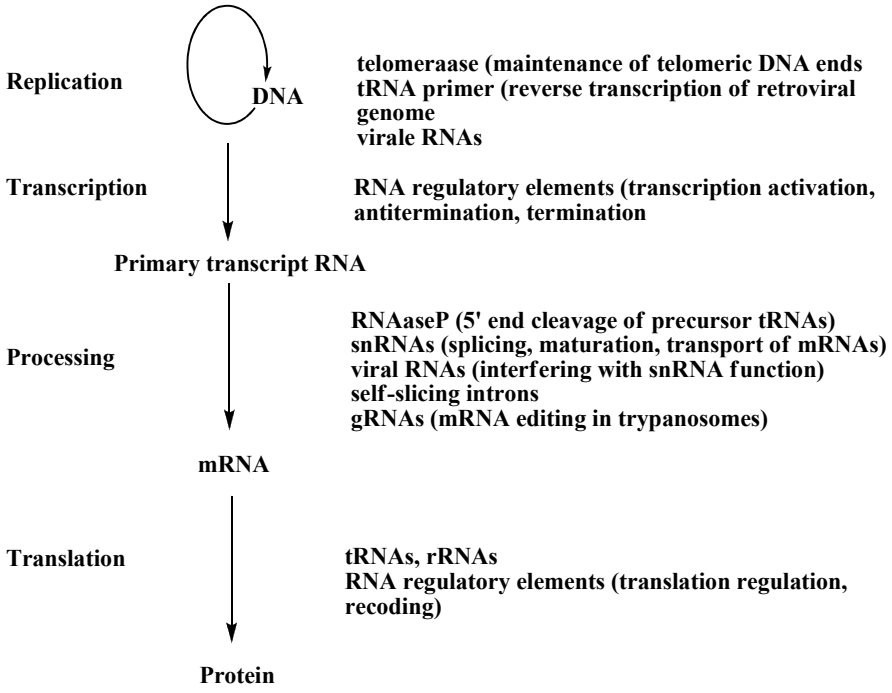

Figure 1.32 Overview of RNA participating in the important processes of gene expression.[119]

1.2.3.1 Understanding the design of RNA binding molecules

The concept of molecular recognition, used for DNA binding complexes, was initially applied to the study of RNA-small molecule interactions. Intercalators and groove binders were among the first compounds analyzed for their RNA binding ability.[120] However, to achieve the specific RNA recognition, proteins rather than DNA need to be examined as it is the three dimensional structure that is the key feature of RNA rather than the base sequences as in DNA.[119] To understand the specific association between small molecules and RNA, a general knowledge of how they interact with RNA and which interactions play an important role in the binding specificity is required. The major interactions facilitating small molecules and RNA binding will be described herein.

The first common interaction is electrostatic forces. The molecules that interact with nucleic acid, DNA and RNA usually have a positive charge in order to increase the binding affinity to nucleic acids which have a negatively charged phosphate backbone. Electrostatic forces can facilitate small molecules to tightly interact with RNA.[119] It should be noted that the increase of positive charge results in the enhancement of the binding affinity but may not enhance the specificity. Therefore electrostatic forces are considered as a non-specific interaction.

The second interaction between small molecules and RNA is hydrogen bonding. It has been demonstrated that the hydrogen bonding, observed between the phosphate group of the RNA backbone and hydrogen atoms of the small molecule, can contribute significantly to RNA-drug binding.[119] This interaction was established from intensive studies on the complex aminoglycoside, an antibacterial drug used in the clinic, and several kinds of RNA such as aptamer RNAs and oligonucleotides derived from the rRNA of bacteria.[121-123] From the three dimensional structure of the RNA and aminoglycoside complex (**Figure 1.33**), it can be seen that the ammonium and hydroxyl group of the drugs behave as hydrogen donors which interact with the oxygen of the phosphate backbone of RNA and with N7 and O4 atom of purine and uridine, repectively.[124, 125] In addition, the hydrogen bonding of a variety of substitution sites on the ammonium and hydroxyl groups in aminoglycosides and RNA are distinct in terms of strength of interactions. This shows that the hydrogen bonding is a specific interaction which can enhance or regulate the binding of the drug to DNA.

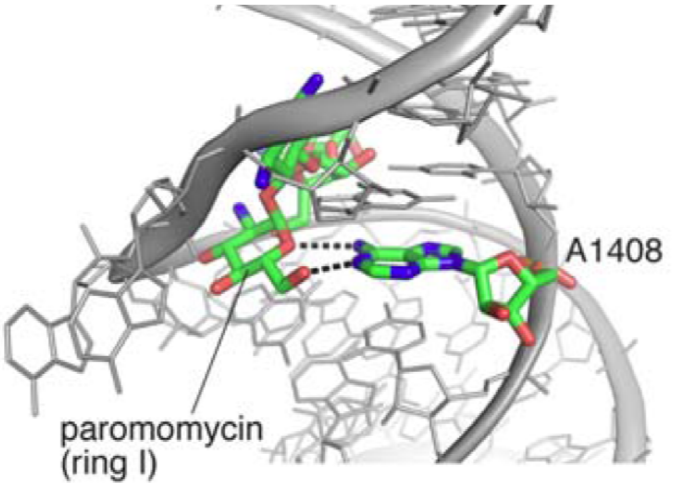

Figure 1.33 The formation of a hydrogen bond, shown by a dashed line, between donor and acceptor group in 16S A site RNA-paromomycin complex. Taken from ref.[123, 126]

Another interaction to be considered is shape complementarity and conformational adaptation. Shape complementarity, how well a ligand and receptor electrostatically and sterically fit together, provides a high binding affinity and high specificity for the formation of RNA and small molecule complexes. An example of this is the three dimensional structures of RNA aptamer complexes.[127, 128]

Conformational adaptation is the changes induced from the binding of small molecules to RNA. The changes in conformation of RNA when bound to small molecules can be small, such as the binding of A site in rRNA and aminoglycoside, [124] or larger for the interaction of HIV TAR RNA and argininamide.[129] Once this molecular interaction is understood a small molecule that can prevent the folding of RNA can be designed, in which the conformational change is crucial for the biological function of the RNA target.[130] This is an intriguing strategy for a therapeutic agent.

1.2.3.2 RNA binding molecules

By combining the known functions of RNA and the knowledge of molecular interactions between small molecules and RNA, a small molecule that specifically targets RNA can be developed. In this section aminoglycosides, well known clinically used antibiotics that target RNA, will be reviewed along with examples of RNA binding metal complexes.

1.2.3.2.1 Aminoglycoside

Aminoglycoside antibiotics consist of amino sugars linked at the 4,5 and 4,6 position of a non-sugar, 2-deoxystreptamine ring (DOS).[131] The structures of these aminoglycosides are illustrated in **Figure 1.34**.

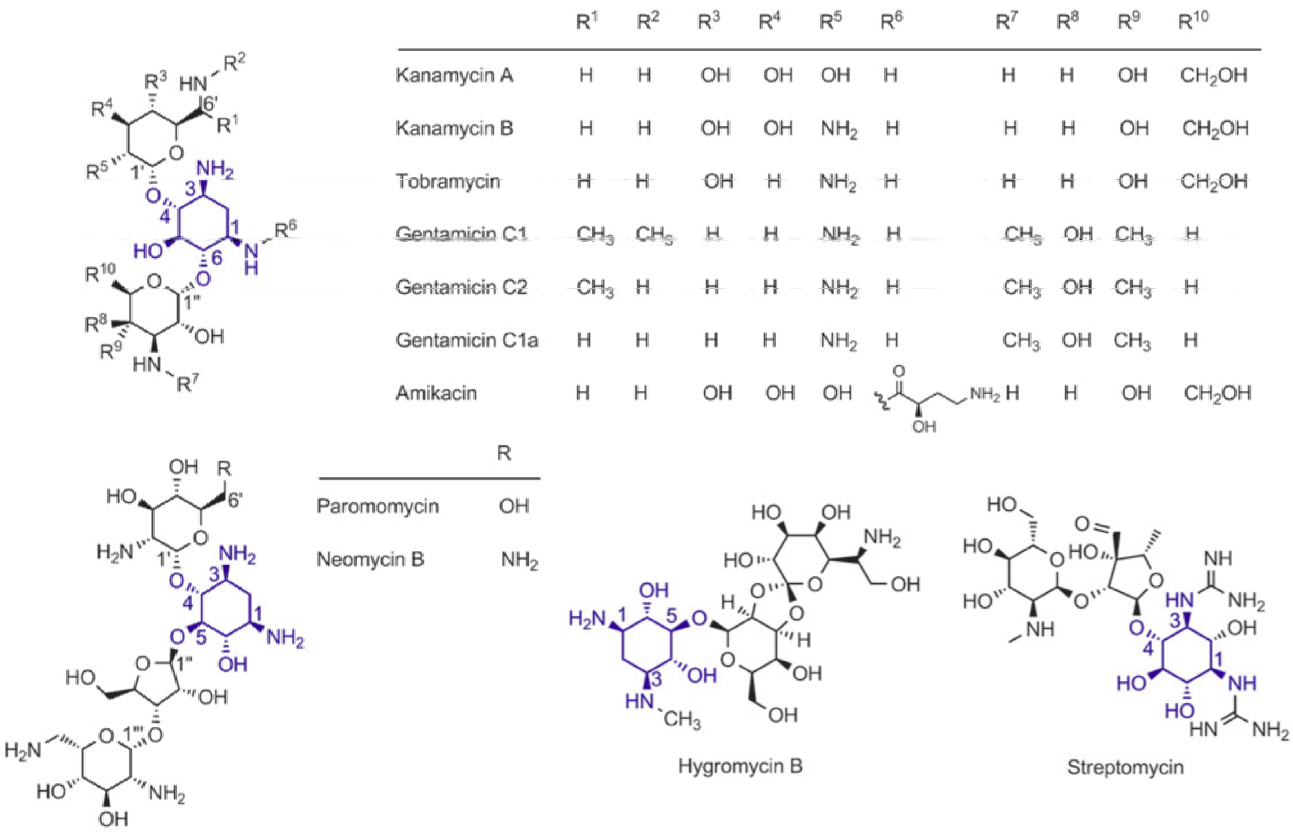

Figure 1.34 Chemical structures of aminoglycoside antibiotics. The 2-deoxystreptamine ring (DOS) is represented in blue. Modified from ref.[132]

The mechanism of action of aminoglycoside antibiotics involves binding to the 16S rRNA of a bacterial ribosome and interfering with its translational fidelity. This was discovered almost three decades ago.[133] The prokaryotic ribosome, consisting of ribosomal RNA and ribosomal proteins, has two subunits which are 30S (small)[79] and 50S (large). The responsibility of the 30S in translation is to ensure that the right amino acid from tRNA is incorporated into the peptide chain while the peptide bond formation is controlled by the 50S subunit.[5] The binding of a cognate tRNA to 16S rRNA, part of 30S rRNA subuit, induces two residues of adenine, A1492 and A1493 to adopt a conformational change while no conformational change is induced by miscognate tRNA

(**Figure 1.35**).[134] However, binding of aminoglycoside, the 4, 5 and 4, 6 substituted to 2 DOS to 16s rRNA i.e. neomycin and paranomycin for 4, 5 substituted and gentamycin, tobramycin, amikacin and kanamycin for 4,6 substituted, induces a conformational change in the same fashion as cognate tRNA, thus resulting in incorporating the noncognate tRNA to the peptide chain.[135, 136] The accumulations of error proteins, that may not correctly function, leads ultimately to bacteria cell death.

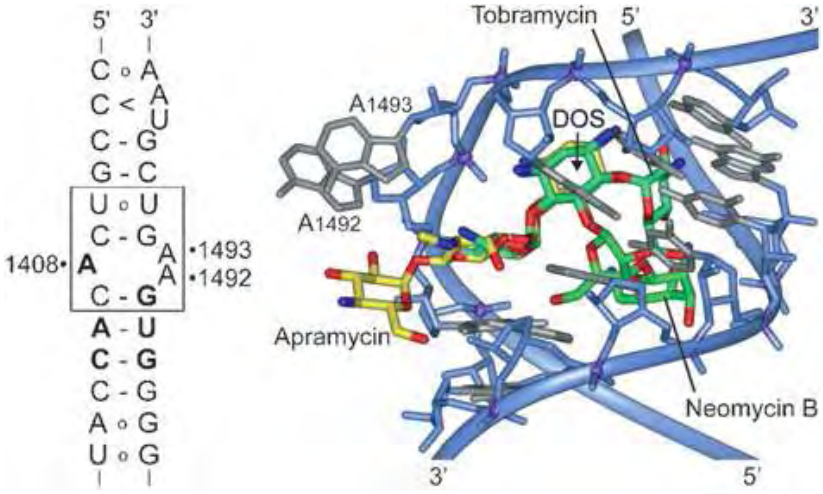

Figure 1.35 Left: Bacterial decoding site in 16S rRNA. The box shows the aminoglycoside binding site. **Right:** Overlay of the crystal structures of three aminoglycosides with the decoding site RNA. The conformational change of 16S rRNA induced by binding of the 2-DOS in aminoglycosides, is depicted. Taken from ref.[132]

Besides ribosomal RNA, aminoglycosides also bind to non-ribosomal RNA.[97, 137] It has been reported that aminoglycoside antibiotics bind to tRNA by displacing the divalent metal ion thus resulting in conformational change and inhibition of amino acylation.[138, 139] Ribozymes including the self-splicing group I intron[140], hammer head motif[141] and ribonuclease P (RNase P)[142, 143] are also the target of aminoglycoside antibiotics in addition to 16S rRNA. Interestingly, aminoglycoside antibiotics also exhibit anti-HIV activity by inhibiting the binding of the HIV-1 Tat protein, essential for

promoting transcriptional efficiency, to the bulged region, known as TAR (trans-activating response element) in RNA.[144] Neomycin, one of the aminoglycoside antibiotics, has the most potential to prevent the Tat-TAR interaction with an IC_{50} of 0.92 μM.[145] Moreover, the studies from Green and co-workers in 1993 shows that aminoglycoside antibiotics, especially neomycin, has the ability to interrupt the interaction of RRE-Rev by binding to RRE with a K_D = 100 nM.[146] The inhibition of RRE-Rev binding is believed to be one strategy to prevent the viral replication and maturation.[147]

1.2.3.2.2 Metal complexes

The use of inorganic metal complexes to target RNA has several advantages. They are relatively easy to synthesise and the ligands or metal can be altered allowing control of the shape, RNA recognition properties and reactivity of the complex.[98] Due to the benefits that can be attained from metal complexes, many researchers have currently been focused on synthesising metal complexes that target RNA. Some of these metal complexes will be exemplified.

A metal complex binding to naturally structured RNA was initially synthesised by Barton *et al.* in 1990. In this study, tris (1,10-phenantroline)ruthenium (II) $[Ru(phen)_3]^{2+}$ and tris (3,4,7,8-tetramethylphenantholine)ruthenium (II) $[Ru(TMP)_3]^{2+}$ (**Figure 1.36**) were exploited for the recognition of $tRNA^{Phe}$ as photocleavagers. $[Ru(phen)_3]^{2+}$ and $[Ru(TMP)_3]^{2+}$ were shown to cleave tRNA preferentially at guanine residues. In addition, two different patterns of cleavage were observed for the two ruthenium complexes. This shows that different selectivities for a different site can be obtained by the different

binding characteristics resulting from different molecular shapes.[148] In addition, these complex also bind to DNA.

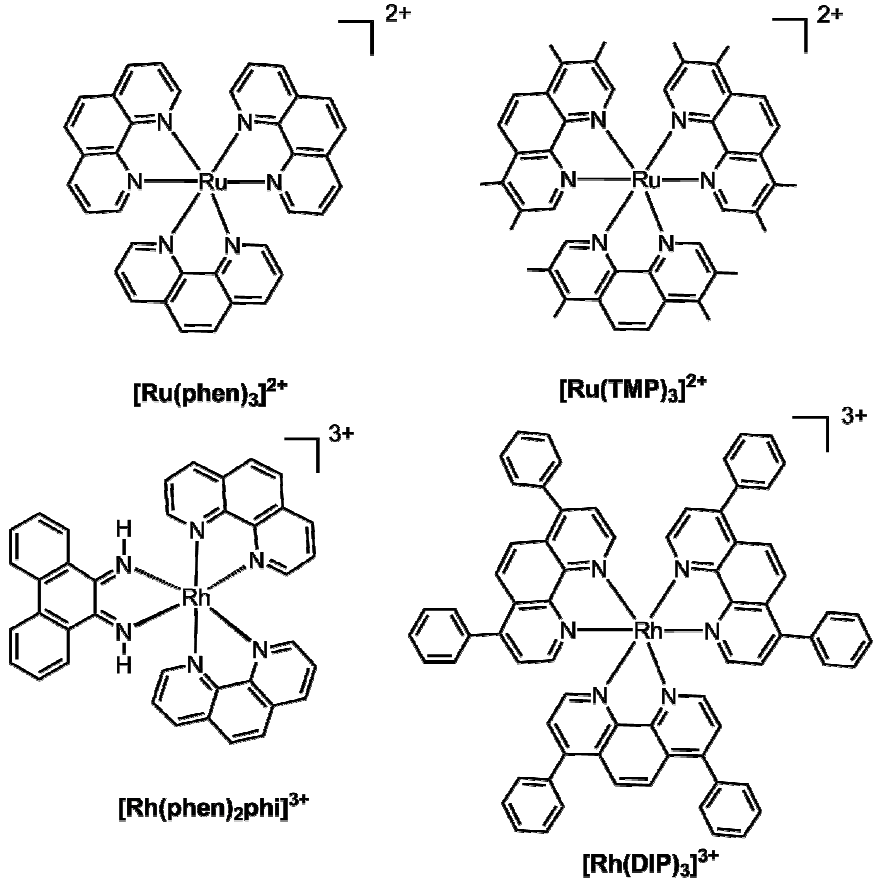

Figure 1.36 Chemical structures of rhodium and ruthenium polypyridal complexes.

Utilising rhodium metal instead of ruthenium provides the ability of direct strand scission by the complex rather than cleavage by diffusible reactive species. Additionally, Barton and co-workers studied photocleavage of yeast $tRNA^{Phe}$ by the rhodium complexes ($[Rh(DIP)_3]^{3+}$ and $[Rh(phen)_2phi]^{3+}$ (**Figure 1.36**). The studies of $[Rh(DIP)_3]^{3+}$ and $tRNA^{phe}$ show that the addition of the phenyl group substituents to the phenanthroline ring of the rhodium complex enhances the specificity of RNA binding. Also it has two major recognition sites which are pseudouracil 55 residue (ψ55) in the

pocket between two loop areas of the tRNA. This is similar to the cleavage site of this compound on DNA cruciforms.[149] The second site is 3'side of a wobble-paired U residue (G-U mismatch) within the double helix region of RNA (**Figure 1.37**).

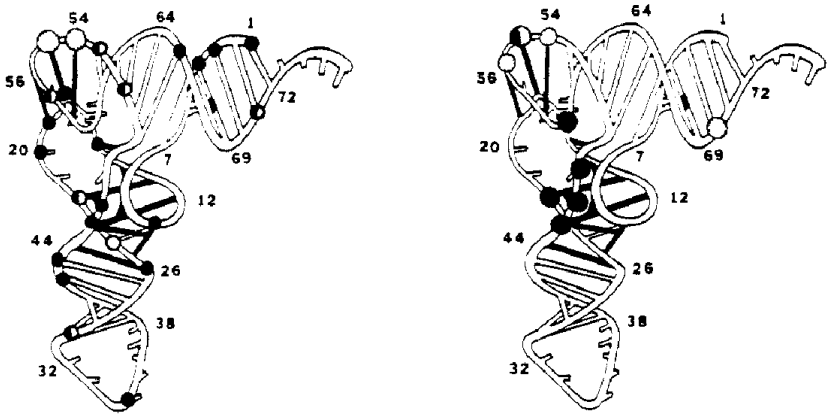

Figure 1.37 Map of cleavage sites of ruthenium and rhodium complexes on the three dimensional structure of $tRNA^{phe}$. **Left**: Cleavage by $[Ru(phen)_3]^{2+}$ and $[Ru(TMP)_3]^{2+}$. Black circles represent guanine residue cut by both complexes. Half black and white circles depict the guanine residue cut by $[Ru(phen)_3]^{2+}$. White circles illustrate the guanine residue which is not cleaved by both complexes. **Right**: Cleavage by $[Rh(phen)_2phi]^{3+}$ (black circles) and $[Rh(DIP)_3]^{3+}$ (white circles). Taken from ref.[148]

For $[Rh(phen)_2phi]^{3+}$, the interesting results show that in the presence of a denaturing agent no cleavage is observed at the specific site. This indicates that the natural structure of RNA is required for the recognition of the complex and RNA. Moreover, $[Rh(phen)_2phi]^{3+}$ demonstrates that it can target a unique region, the triple bonded sites in tRNA. It can also recognise 5S rRNA of *Xenopus* oocyte which is crucial for binding by the transcription factor IIIA (TFIIIA).[150] This might lead to a gene regulation application. Moreover, another example of an octahedral metal complex, believed to be the first example with sequence specificity for simple duplex RNAs due to the chirality of complexes, is the eilatin-containing Ru (II) complex ($[Ru(bpy)_2Eilatin]^{2+}$) (**Figure 1.38**).[151] Eilatin is a bifacial metal chelator, consisting of a fused heptacyclic. *In*

vitro studies show that $[Ru(bpy)_2Eilatin]^{2+}$ has remarkable anti-HIV activity by inhibiting Rev-RRE activity, which is an important mechanism for viral replication.

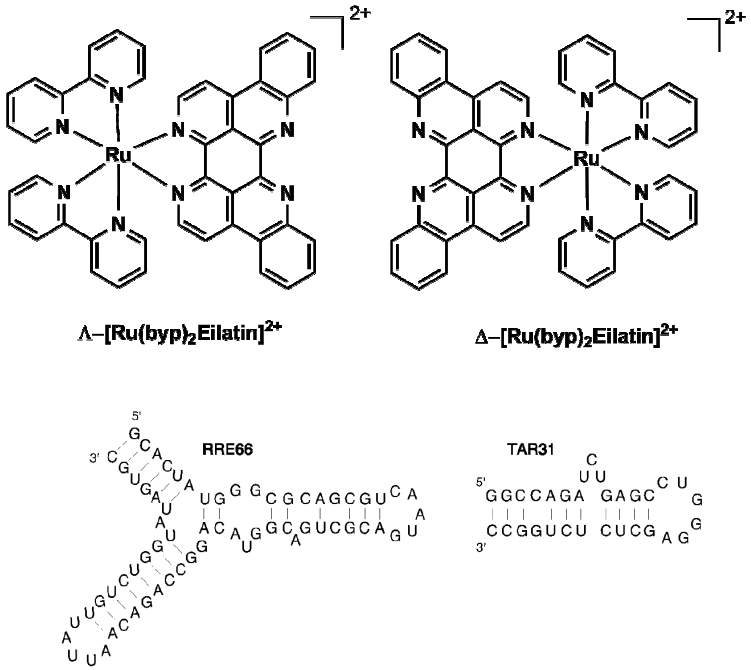

Figure 1.38 Top: Chemical structure of Λ-$[Ru(bpy)_2Eilatin]^{2+}$ and Δ-$[Ru(bpy)_2Eilatin]^{2+}$. **Bottom**: RNA target of both complexes: RRE and TAR. Modified from ref.[151]

Interestingly, $[Ru(bpy)_2Eilatin]^{2+}$ shows enantiomeric selectivity to its RNA target, RRE and TAR, providing a promising strategy for antiviral activity. It has been demonstrated that Λ-$[Ru(bpy)_2Eilatin]^{2+}$ prefers to bind to RRE (Rev Response Element) while TAR (Transactivation response Region) is the target for Δ-$[Ru(bpy)_2Eilatin]^{2+}$ (**Figure 1.38**). The planarity of the eilatin moiety is crucial for the recognition of anti-HIV activity and affinity of these complexes.

Besides therapeutic agent, metal complex can be used as a probe to detect the localisation of RNA in cells. Turro *et al*. reported a RNA imaging probe, RuEth.[152] It consists of a phenanthridine moiety covalently linked to a ruthenium(II) isothiocyanate

modified complex, RuITC (**Figure 1.39**). RuEth was obtained by the reaction of RuITC with an amine functionalised ethidium derivative. This compound combines several attractive advantages including RNA binding property, the ability to enhance fluorescence intensity and lifetimes from phenanthridine unit and ruthenium bipyridine complexes, repectively.

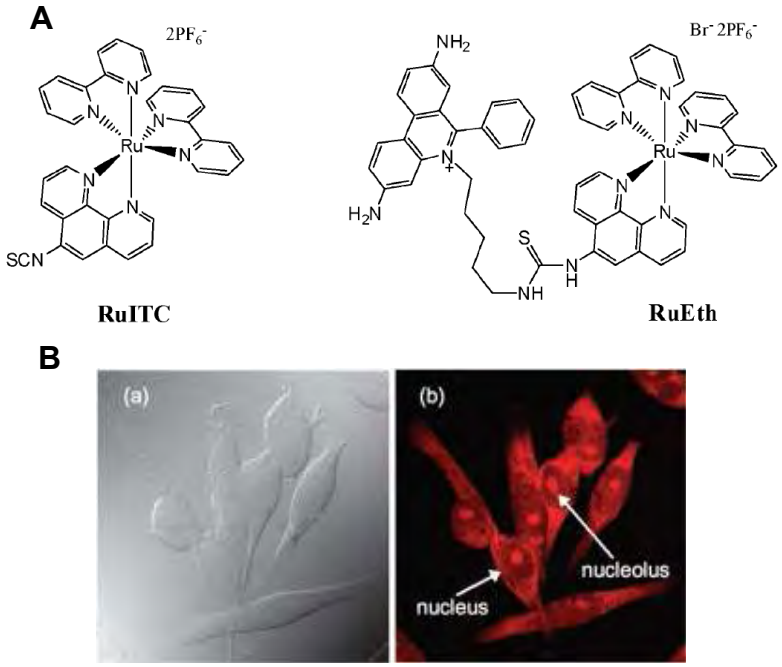

Figure 1.39 A) Chemical structures of ruthenium isothiocyanate (RuITC; left) and the RNA probe RuEth (right). **B)** Optical (a) and fluorescence (b) microscope images of RuEth uptake into mammalian cells. Taken from ref. [152]

In addition, uptake experiment of this compound into mammalian cells showed that the compound give a great signal in regions of cells where RNA localise. An image from a fluorescence microscope indicated that a maximum fluorescence intensity of the compound was detected in the nucleous, a dense region of RNA, and cytoplasm where mRNA is present but less detected in the nucleus where DNA is located.

Cisplatin (cis-diammine-dichloroplatinum (II), cis-[$Pt(NH_3)_2Cl_2$]) is a well known metal complex, used in the clinic as an anticancer drug against a variety of tumors such as testicular, ovarian, esophageal, head and neck and lung cancer, see **Section 1.1.4.2**.[153] It is known to bind to the N7 position of adjacent purine (guanine and adenine) bases of genomic DNA, causing intrastrand crosslinking on the DNA.[154] This binding fashion has been significantly linked to the induction of apoptosis and antitumor activity. Several studies have intensively focused on the interaction of cisplatin and DNA however studies with RNA have been only recently been considered. These investigations show that cisplatin has the ability to interfere with the transcription process of RNA by blocking RNA polymerase.[155, 156] Cisplatin can also inhibit splicing[157] and translation at the initial step by preventing the association of the 60S ribosomal to the 48 S preinitiation subunit.[158] Moreover, Elmroth and co-workers demonstrated that cisplatin is able to bind to the site near a G-U wobble pair at the stem of $tRNA^{Ala}$.[159, 160] Cisplatin also has the ability to inhibit the self splicing activity of ribozyme.[161] Recently, Chow *et al.* revealed that cisplatin can be used as a structural probe to identify accessible purine bases in 16S rRNA of bacteria both *in vitro* and *in vivo*.[162] The accessibility of ribosomes may provide a new target sites for novel antibacterial agents.[162] Furthermore, the studies from Hostetter and co-workers indicated that cisplatin is capable of crosslinking at internal loop of complex RNA.[163] Very recently, Chapman and colleagues showed that the platination of RNA can alter the function of RNA processing enzymes including exonuclease, endoribonuclease (RNase) and reverse transcriptase, in a sequence specific pattern. It is assumed that this *in vitro* investigation may also occur *in vivo* which may explain the antitumor activity of the platinum drug at the cellular level.[164]

1.3 DNA nanotechnology

1.3.1 Background

Technology to manipulate and control a substance at nanometer (nm) level (1 nm = one billionth of a meter) using atoms and molecules to create new materials and devices with intriguing functions is known as "Nanotechnology".[165] This topic is a highly multidisciplinary field involving areas such as biology, chemistry, physics and computer science.

There are two main approaches employed in nanotechnology[165]: one is the "top-down" approach where nano-devices are built from larger entities without atomic-level control. Nano-lithography is a good example of this approach. Another is the "bottom-up" approach where materials and objects are constructed from molecular components which assemble themselves by using principles of molecular recognition. One interesting example of this second approach is DNA nanotechnology, in which DNA is utilised as a component to precisely construct desired objects. This shows that DNA is not only considered as a genetic material for storing and transmitting the blue prints of life but also a tool for programmable architectures due to its reliable base pairing. In this section, structural DNA nanostructures will be presented.

1.3.2 Considering DNA as a material for construction

DNA has several attractive properties for use as a material for nanotechnological construction.[166-169] Firstly, it provides a programmable and reliable construction from the recognition of purine and pyrimidine, known as Watson and Crick base pairing. A binds to T while C binds to G with double and triple hydrogen bonding, respectively. Secondly,

with phosphoramidite chemistry, any arbitrary sequence of DNA can be synthesised and modified by attaching biotin or a fluorescent dye to the DNA. Thirdly, since the geometries and properties of DNA have been intensively studied, the stiffness and flexibility of the DNA can be easily adjusted by controlling the number of bases. This property of DNA is one of the key successes in controlling the DNA nanostructure to achieve a desired architecture. As mentioned in the literature, double stranded DNA can behave as a rigid rod with a persistence length of 50 nm (approximately 150 bps) while the flexibility of the desired structure can be increased by the single stranded DNA with a persistence length of 1-2 nm. Therefore, the flexibility and rigidity of the nanostructure can be adapted by changing the length of the DNA. Finally, the commercial availability of a number of enzymes used in biotechnology such as restriction enzyme, DNA ligase and kinase can be used as a tool for either probing and confirming the formation of the desired DNA construction or modifying the structure.

1.3.3 DNA nanotechnology architectures

1.3.3.1 Two dimensional DNA structures.

The initial work of structural DNA nanotechnology was firstly carried out by Seeman and co workers in the early 1980s. Inspired by nature, Seeman *et al.* exploited the branched junction motif, found as intermediates in DNA replication and recombination, i.e., four way junction or Holliday junction, as a building block to construct a DNA structure.[170] The junction was well designed to avoid the migration of the branched point, which can cause instability of the junction, by eliminating the symmetry which can occur in the sequences.[171] The first study for constructing higher

order DNA nanostructures was begun by ligating the sticky end of a four way junction to achieve quadrilateral lattices (**Figure 1.40**). However it was not possible to assemble this branched junction into defined 2D and 3D structures due to the flexibility of the junction arm. Later, the same group created a well defined double cross over motif (DX), considered as the first DNA building block for self assembly of 2D structures (**Figure 1.40**). This motif contains two double DNA strands connected at two crossover points by sticky end ligation in a parallel and antiparallel arrangement.[172] This approach subsequently generated three and four double helix cross overs.[173] The benefit obtained from this motif is the increase of the double stranded DNA rigidity in the structure.

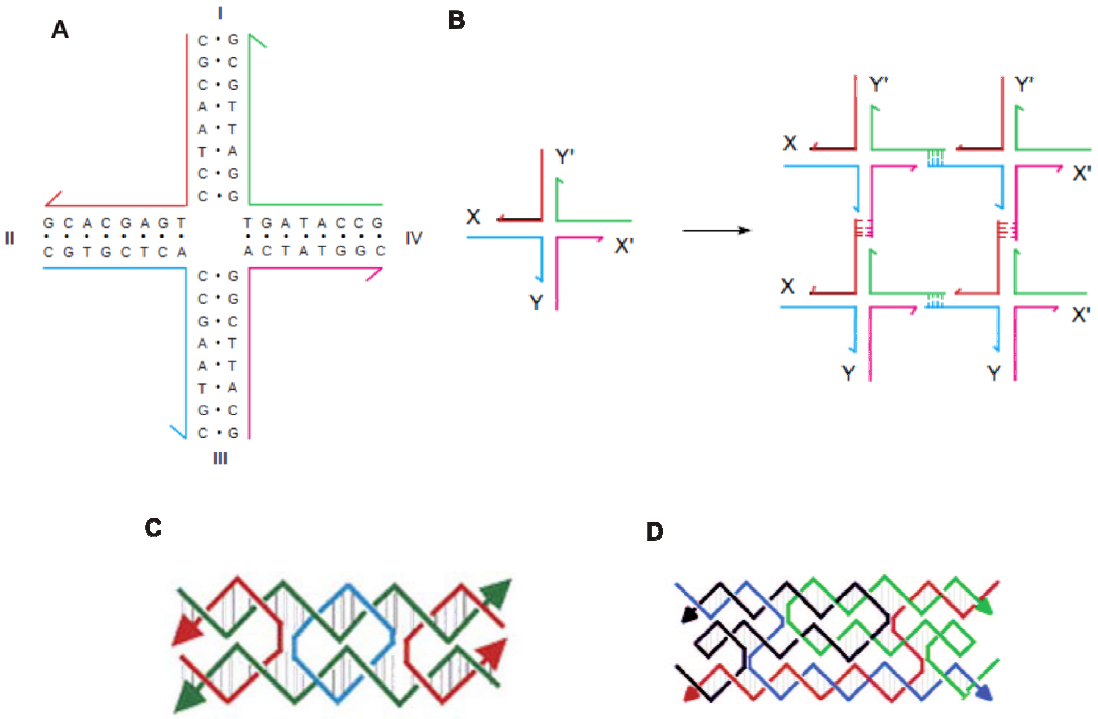

Figure 1.40 Primary DNA building blocks for DNA nanostructure constructions. **A)** Branched point DNA with four helical arms, four way junction. **B)** The formation of 2D lattice from four way junction with sticky end cohesion approach. **C)** Double cross over tile. **D)** Triple cross over tile. Taken from ref.[172, 174]

These simple foundations have been amended and developed to generate other building blocks, providing various highly controllable 2D structures such as hexagonal,[175] square[176, 177] and triangular-shaped DNA lattice[178] and helix bundle (**Figure 1.41**).[179]

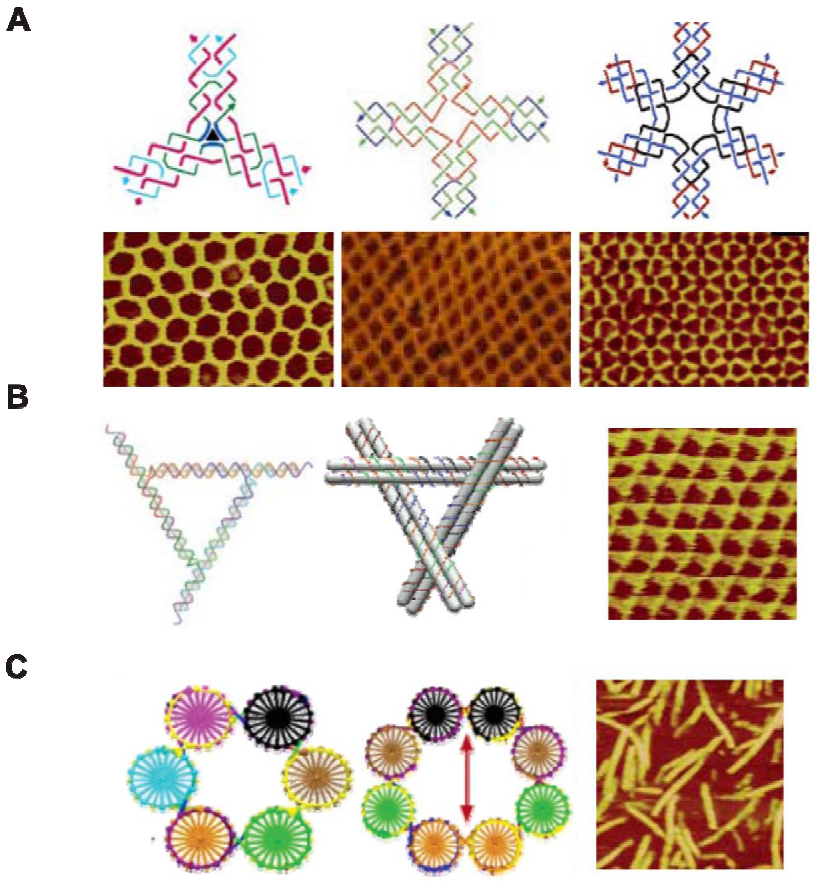

Figure 1.41 Building block units and their 2D DNA nanostructure. **A)** 3, 4 and 6 arm junctions, assembling from cross over tile, as a unit for generating 2D hexagonal, square and compound lattice. **B)** Triangular DNA building block flanked with sticky end to build triangular shaped DNA lattice. **C)** 6 and 8 membered helix bundle for helical tube assembly. Modified from ref.[180]

Recently, Rethemund *et al.* presented a novel approach to generate a defined DNA nanostructure, known as DNA origami (**Figure 1.42**). In this strategy, a long single strand of DNA is folded into a large number of different desirable shapes facilitated by short

complementary DNA strands termed staple strands. These short strands hold the DNA assembly via strand exchange crossover. Examples of 2D DNA nanostructures made using this method are squares, rectangles, stars, smiley faces, and triangles with rectangular domains.

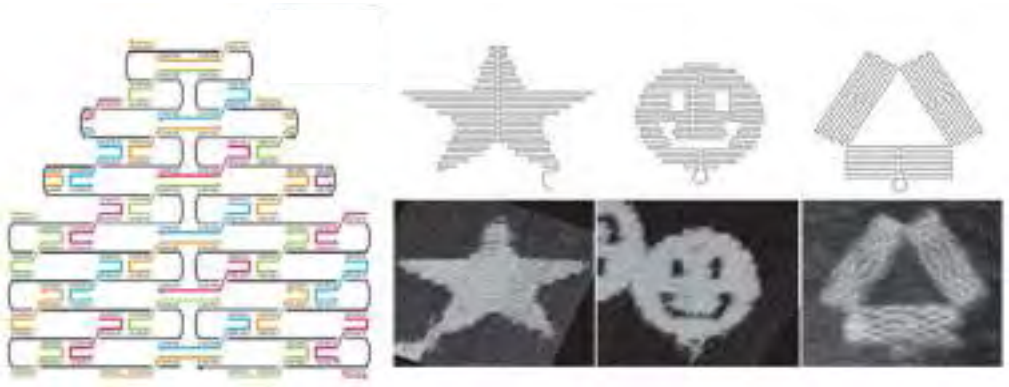

Figure 1.42 DNA origami. **Left:** The folding of DNA origami from a continuous single strand of DNA (black line) to a desired structure. Shape of DNA was maintained by a stappling strands (shown in several colours). **Right:** 2D architectures generated from DNA origami approach including a star, a smiling face and a triangle. Taken from ref.[180]

1.3.3.2 Three dimensional DNA objects

The first three dimensional DNA nanostructure was a cube-like object, constructed by Seeman *et al*. This structure was assembled from 6 interconnected cylic DNA strands by ligation strategy, however with a yield lower than 1%.[181] Consequently, the same group used a stepwise solid phase synthesis for constructing a truncated DNA octahedron, to avoid the difficult purification step in the synthetic procedure.[182] Recently, Turberfield and co-workers synthesised tetrahedral and bipyramid shaped DNA nanostructures by hybridising multiple strands of DNA in one step.[183-185] This DNA nanostructure was later used as a cage to encapsulate a protein molecule.[186] Sleiman and co-workers introduced a new strategy in which the rigid organic molecules used as the

vertices can modulate the discrete formation of 3D DNA objects such as a triangular prism, cube, pentameric prism, hexameric prism, heteroprism and biprism in a reasonable yield.[187, 188] Very recently, Andersen *et al.* generated a nanobox from the DNA origami strategy. This nanobox has a controllable lid responding to a specific key. This nanobox can be a promising vehicle for drug delivery due to its internal cavity, and the lid for loading and releasing a drug at the target.[189] All three dimensional DNA nanostructures are shown in **Figure 1.43**

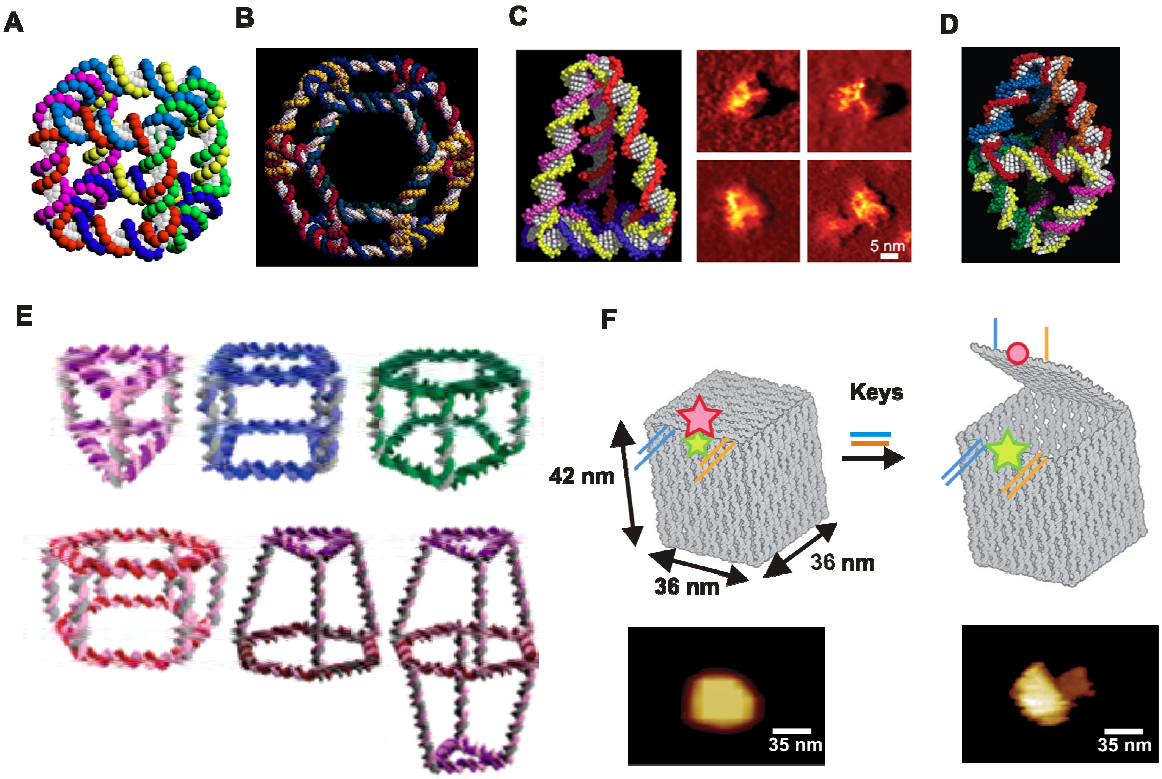

Figure 1.43 3D DNA nanostructures. **A)** DNA cube.[169] **B)** DNA truncated octahedron.[182] **C)** DNA tetrahedron and their AFM images.[185] **D)** DNA bipyramid.[183] **E)** 3D DNA constructions of triangular prism, cube, pentaprism, heptaprism, heteroprism and biprism.[188] **F)** DNA nanobox with their AFM images.[189]

1.4 Overview of thesis

The goal of this thesis is to explore how the metallosupramolecular cylinders interact with a range of different nucleic acid structures including DNAs, RNAs, DNA-RNA hybrids and DNA nanostructure. This PhD thesis will be divided into four experimental chapters as described below.

In Chapter 2, the recognition by the metallosupramolecular cylinder and its enantiomers and the stabilisation of RNA three way junctions will be investigated. As previously mentioned in Chapter 1 (**Section 1.1.4.6**) that the cylinder can also bind to the core cavity of DNA three way junctions, the competition assay of nucleic acid to the cylinder is also carried out.

In Chapter 3, exploring the appropriate size and shape of the cylinder for the enhancement of the recognition to a DNA three way junction will be discussed.

In Chapter 4, the effect of the cylinder on the structural alteration of a very rigid DNA tetrahedron will be shown.

In Chapter 5, the establishment of using SPR technique for precisely determining the binding affinity of the cylinder to DNA will be presented.

1.5 References

1. R. Dahm, *Dev. Biol.*, 2005, **278**, 274-288.
2. R. E. Franklin and R. G. Gosling, *Nature*, 1953, **171**, 740-741.
3. J. D. Watson and F. H. C. Crick, *Nature*, 1953, **171**, 737-738.
4. http://www.nature.com/scitable/topicpage/discovery-of-dna-structure-and-function-watson-397.
5. R. F. Weaver, *Molecular biology*, McGraw-Hill, New York, 2008.
6. A. H. J. Wang, G. J. Quigley, F. J. Kolpak, J. L. Crawford, J. H. Vanboom, G. Vandermarel and A. Rich, *Nature*, 1979, **282**, 680-686.
7. M. R. Singleton, S. Scaife and D. B. Wigley, *Cell*, 2001, **107**, 79-89.
8. G. Liberi and M. Foiani, *Cell Res.*, **20**, 611-613.
9. W. D. Heyer, *Curr. Biol.*, 2004, **14**, R56-R58.
10. K. C. Woods, S. S. Martin, V. C. Chu and E. P. Baldwin, *J. Mol. Biol.*, 2001, **313**, 49-69.
11. D. M. J. Lilley, *Q. Rev. Biophys.*, 2000, **33**, 109-159.
12. D. R. Duckett, A. I. H. Murchie, S. Diekmann, E. von Kitzing, B. Kemper and D. M. J. Lilley, *Cell*, 1988, **55**, 79-89.
13. A. I. H. Murchie, R. M. Clegg, E. v. Krtzing, D. R. Duckett, S. Diekmann and D. M. J. Lilley, *Nature*, 1989, **341**, 763-766.
14. A. I. H. Murchie, J. Portugal and D. M. J. Lilley, *EMBO J.*, 1991, **10**, 713-718.
15. M. Lu, Q. Guo, N. C. Seeman and N. R. Kallenbach, *J. Biol. Chem.*, 1989, **264**, 20851-20854.
16. D. R. Duckett and D. M. J. Lilley, *EMBO J.*, 1990, **9**, 1659-1664.

17. J. B. Welch, D. R. Duckett and D. M. J. Lilley, *Nucleic Acids Res.*, 1993, **21**, 4548-4555.

18. F. Stuhmeier, J. B. Welch, A. I. H. Murchie, D. M. J. Lilley and R. M. Clegg, *Biochemistry*, 1997, **36**, 13530-13538.

19. N. B. Leontis, M. T. Hills, M. Piotto, A. Malhotra, J. Nussbaum and D. G. Gorenstein, *J. Biomol. Struct. Dyn.*, 1993, **11**, 215-&.

20. M. A. Rosen and D. J. Patel, *Biochemistry*, 1993, **32**, 6576-6587.

21. I. V. Ouporov and N. B. Leontis, *Biophys. J.*, 1995, **68**, 266-274.

22. J. B. Welch, F. Walter and D. M. J. Lilley, *J. Mol. Biol.*, 1995, **251**, 507-519.

23. D. M. J. Lilley, *Biopolymers*, 1998, **48**, 101-112.

24. J. L. Huppert, *Biochimie*, 2008, **90**, 1140-1148.

25. K. Paeschke, T. Simonsson, J. Postberg, D. Rhodes and H. J. Lipps, *Nat. Struct. Mol. Biol.*, 2005, **12**, 847-854.

26. D. Gomez, T. Wenner, B. Brassart, C. Douarre, M. F. O'Donohue, V. El Khoury, K. Shin-Ya, H. Morjani, C. Trentesaux and J. F. Riou, *J. Biol. Chem.*, 2006, **281**, 38721-38729.

27. A. T. Phan and J. L. Mergny, *Nucleic Acids Res.*, 2002, **30**, 4618-4625.

28. L. S. Lerman, *J. Mol. Biol.*, 1961, **3**, 18-30.

29. S. N. Rao and P. A. Kollman, *Proc. Natl. Acad. Sci. U. S. A.*, 1987, **84**, 5735-5739.

30. R. Martinez and L. Chacon-Garcia, *Curr. Med. Chem.*, 2005, **12**, 127-151.

31. K. W. Jennette, S. J. Lippard, G. Vassilia and W. R. Bauer, *Proc. Natl. Acad. Sci. U. S. A.*, 1974, **71**, 3839-3843.

32. J. R. Hart, M. D. Johnson and J. K. Barton, *Proc. Natl. Acad. Sci. U. S. A.*, 2004, **101**, 14040-14044.

33. E. Ruba, J. R. Hart and J. K. Barton, *Inorg. Chem.*, 2004, **43**, 4570-4578.

34. M. J. Hannon, *Chem. Soc. Rev.*, 2007, **36**, 280-295.

35. G. Lowe, A. S. Droz, J. J. Park and G. W. Weaver, *Bioorg. Chem.*, 1999, **27**, 477-486.

36. N. K. Annan, P. R. Cook, S. T. Mullins and G. Lowe, *Nucleic Acids Res.*, 1992, **20**, 983-990.

37. P. B. Glover, P. R. Ashton, L. J. Childs, A. Rodger, M. Kercher, R. M. Williams, L. De Cola and Z. Pikramenou, *J. Am. Chem. Soc.*, 2003, **125**, 9918-9919.

38. F. Westerlund, L. M. Wilhelmsson, B. Norden and P. Lincoln, *J. Phys. Chem. B*, 2005, **109**, 21140-21144.

39. W. A. Denny, *Curr. Med. Chem.*, 2001, **8**, 533-544.

40. D. Mohamed, S. Mowaka, J. Thomale and M. W. Linscheid, *Chem. Res. Toxicol.*, 2009, **22**, 1435-1446.

41. G. B. Bauer and L. F. Povirk, *Nucleic Acids Res.*, 1997, **25**, 1211-1218.

42. B. Lippert, *Cisplatin, Chemistry and biochemistry of a leading anticancer drug*, Wiley-VCH, Weinheim, 1999.

43. E. R. Jamieson and S. J. Lippard, *Chem. Rev.*, 1999, **99**, 2467-2498.

44. http://openwetware.org/wiki/Image:Lippard_4.jpg.

45. N. J. Wheate, W. Shonagh, G. E. a. Craig and R. Oun, *Dalton Trans.*, 2010, **39**, 8113-8127.

46. A. Kuwahara, M. Yamamori, K. Nishiguchi, T. Okuno, N. Chayahara, I. Miki, T. Tamura, T. Inokuma, Y. Takemoto, T. Nakamura, K. Kataoka and T. Sakaeda, *Int. J. Med. Sci.*, 2009, **6**, 305-311.

47. Y. Kawai, S. Taniuchi, S. Okahara, M. Nakamura and M. Gemba, *Biol. Pharm. Bull.*, 2005, **28**, 1385-1388.

48. T. Boulikas, A. Pantos, E. Bellis and P. Christofis, *Cancer Ther.*, 2007, **5**, 537-583.

49. T. Boulikas and M. Vougiouka, *Oncol. Rep.*, 2003, **10**, 1663-1682.

50. D. Simpson, C. Dunn, M. Curran and K. L. Goa, *Drugs*, 2003, **63**, 2127-2156.

51. D. K. Kim, H. T. Kim, Y. B. Cho, J. H. Tai, J. S. Ahn, T. S. Kim, K. H. Kim and W. S. Hong, *Cancer Chemother. Pharmacol.*, 1995, **35**, 441-445.

52. D. K. Kim, H. T. Kim, J. H. Tai, Y. B. Cho, T. S. Kim, K. H. Kim, J. G. Park and W. S. Hong, *Cancer Chemother. Pharmacol.*, 1995, **37**, 1-6.

53. A. Harris, Y. Qu and N. Farrell, *Inorg. Chem.*, 2005, **44**, 1196-1198.

54. S. Komeda, T. Moulaei, K. K. Woods, M. Chikuma, N. P. Farrell and L. D. Williams, *J. Am. Chem. Soc.*, 2006, **128**, 16092-16103.

55. A. L. Harris, X. H. Yang, A. Hegmans, L. Povirk, J. J. Ryan, L. Kelland and N. P. Farrell, *Inorg. Chem.*, 2005, **44**, 9598-9600.

56. T. N. Siegel, D. R. Hekstra and G. A. M. Cross, *Mol. Biochem. Parasitol.*, 2008, **160**, 171-174.

57. R. M. Martin, H. Leonhardt and M. C. Cardoso, *Cytom. Part A*, 2005, **67A**, 45-52.

58. S. Neidle, *Principle of nucleic acid structure*, Elsevier Inc., London, 2008.

59. P. B. Dervan, *Bioorg. Med. Chem.*, 2001, **9**, 2215-2235.

60. C. L. Kielkopf, R. E. Bremer, S. White, J. W. Szewczyk, J. M. Turner, E. E. Baird, P. B. Dervan and D. C. Rees, *J. Mol. Biol.*, 2000, **295**, 557-567.

61. J. M. Gottesfeld, L. Neely, J. W. Trauger, E. E. Baird and P. B. Dervan, *Nature*, 1997, **387**, 202-205.

62. L. A. Dickinson, R. Burnett, C. Melander, B. S. Edelson, P. S. Arora, P. B. Dervan and J. M. Gottesfeld, *Chem. Biol.*, 2004, **11**, 1583-1594.

63. C. F. Hsu and P. B. Dervan, *Bioorg. Med. Chem. Lett.*, 2008, **18**, 5851-5855.

64. K. M. Vasquez, L. Narayanan and P. M. Glazer, *Science*, 2000, **290**, 530-533.

65. K. M. Vasquez, G. Wang, P. A. Havre and P. M. Glazer, *Nucleic Acids Res.*, 1999, **27**, 1176-1181.

66. I. Ghosh, C. I. Stains, A. T. Ooi and D. J. Segal, *Mol. Biosyst.*, 2006, **2**, 551-560.

67. P. E. Nielsen, *Curr. Med. Chem.*, 2001, **8**, 545-550.

68. M. J. Hannon, C. L. Painting, A. Jackson, J. Hamblin and W. Errington, *Chem. Commun.*, 1997, 1807-1808.

69. M. J. Hannon, V. Moreno, M. J. Prieto, E. Moldrheim, E. Sletten, I. Meistermann, C. J. Isaac, K. J. Sanders and A. Rodger, *Angew. Chem. Int. Ed.*, 2001, **40**, 880-884.

70. S. Khalid, M. J. Hannon, A. Rodger and P. M. Rodger, *Chem. Eur. J.*, 2006, **12**, 3493-3506.

71. M. J. Hannon, I. Meistermann, C. J. Isaac, C. Blomme, J. R. Aldrich-Wright and A. Rodger, *Chem. Commun.*, 2001, 1078-1079.

72. J. M. C. A. Kerckhoffs, J. C. Peberdy, I. Meistermann, L. J. Childs, C. J. Isaac, C. R. Pearmund, V. Reudegger, S. Khalid, N. W. Alcock, M. J. Hannon and A. Rodger, *Dalton Trans.* , 2007, 734-742.

73. I. Meistermann, V. Moreno, M. J. Prieto, E. Moldrheim, E. Sletten, S. Khalid, P. M. Rodger, J. C. Peberdy, C. J. Isaac, A. Rodger and M. J. Hannon, *Proc. Natl. Acad. Sci. U. S. A.*, 2002, **99**, 5069-5074.

74. J. Malina, M. J. Hannon and V. Brabec, *Chem. Eur. J.*, 2008, **14**, 10408-10414.

75. J. Malina, M. J. Hannon and V. Brabec, *Nucleic Acids Res.*, 2008, **36**, 3630-3638.

76. J. C. Peberdy, J. Malina, S. Khalid, M. J. Hannon and A. Rodger, *J. Inorg. Biochem.*, 2007, **101**, 1937-1945.

77. A. Oleksi, A. G. Blanco, R. Boer, I. Uson, J. Aymami, A. Rodger, M. J. Hannon and M. Coll, *Angew. Chem. Int. Ed.*, 2006, **45**, 1227-1231.

78. C. Guthrie and B. Patterson, *Annu. Rev. Genet.*, 1988, **22**, 387-419.

79. B. T. Wimberly, D. E. Brodersen, W. M. Clemons, R. J. Morgan-Warren, A. P. Carter, C. Vonrhein, T. Hartsch and V. Ramakrishnan, *Nature*, 2000, **407**, 327-339.

80. R. R. Sinden, *Nature*, 2001, **411**, 757-758.

81. H. J. Yu, X. H. Wang, M. L. Fu, J. S. Ren and X. G. Qu, *Nucleic Acids Res.*, 2008, **36**, 5695-5703.

82. A. De Cian, E. DeLemos, J.-L. Mergny, M.-P. Teulade-Fichou and D. Monchaud, *J. Am. Chem. Soc.*, 2007, **129**, 1856-1857.

83. A. C. G. Hotze, N. J. Hodges, R. E. Hayden, C. Sanchez-Cano, C. Paines, N. Male, M. K. Tse, C. M. Bunce, J. K. Chipman and M. J. Hannon, *Chem. Biol.*, 2008, **15**, 1258-1267.

84. A. D. Richards, A. Rodger, M. J. Hannon and A. Bolhuis, *Int. J. Antimicrob. Agents*, 2009, **33**, 469-472.

85. C. Uerpmann, J. Malina, M. Pascu, G. J. Clarkson, V. Moreno, A. Rodger, A. Grandas and M. J. Hannon, *Chem. Eur. J.*, 2005, **11**, 1750-1756.

86. G. I. Pascu, A. C. G. Hotze, C. Sanchez-Cano, B. M. Kariuki and M. J. Hannon, *Angew. Chem. Int. Ed.*, 2007, **46**, 4374-4378.

87. L. Cardo and M. J. Hannon, *Inorg. Chim Acta*, 2009, **362**, 784-792.

88. L. Cardo, PhD thesis, University of Birmingham, 2010.

89. D. R. Duckett, A. I. H. Murchie, R. M. Clegg, G. S. Bassi, M. J. E. Giraud-Panis and D. M. J. Lilley, *Biophys. Chem.*, 1997, **68**, 53-62.

90. M. J. McEachern, A. Krauskopf and E. H. Blackburn, *Annu. Rev. Genet.*, 2000, **34**, 331-358.

91. A. K. Todd, S. M. Haider, G. N. Parkinson and S. Neidle, *Nucleic Acids Res.*, 2007, **35**, 5799-5808.

92. E. M. Rezler, D. J. Bearss and L. H. Hurley, *Annu. Rev. Pharmacol. Toxicol.*, 2003, **43**, 359-379.

93. S. Balasubramanian and S. Neidle, *Curr. Opin. Chem. Biol.*, 2009, **13**, 345-353.

94. S. N. Georgiades, N. H. Abd Karim, K. Suntharalingam and R. Vilar, *Angew. Chem. Int. Ed.*, 2010, **49**, 4020-4034.

95. R. Kieltyka, P. Englebienne, J. Fakhoury, C. Autexier, N. Moitessier and H. F. Sleiman, *J. Am. Chem. Soc.*, 2008, **130**, 10040-10041.

96. A. Rich, *Nat. Struct. Biol.*, 2003, **10**, 247-249.

97. J. R. Thomas and P. J. Hergenrother, *Chem. Rev.*, 2008, **108**, 1171-1224.

98. C. S. Chow and F. M. Bogdan, *Chem. Rev.*, 1997, **97**, 1489-1513.

99. H. A. Heus and A. Pardi, *Science*, 1991, **253**, 191-194.

100. C. J. Cheong, G. Varani and I. Tinoco, *Nature*, 1990, **346**, 680-682.

101. G. Varani, C. J. Cheong and I. Tinoco, *Biochemistry*, 1991, **30**, 3280-3289.

102. A. Bhattacharyya, A. I. H. Murchie and D. M. J. Lilley, *Nature*, 1990, **343**, 484-487.

103. M. Zacharias and P. J. Hagerman, *J. Mol. Biol.*, 1995, **247**, 486-500.

104. K. M. Weeks and D. M. Crothers, *Cell*, 1991, **66**, 577-588.

105. K. M. Weeks and D. M. Crothers, *Science*, 1993, **261**, 1574-1577.

106. D. R. Duckett, A. I. H. Murchie and D. M. J. Lilley, *Cell*, 1995, **83**, 1027-1036.

107. J. E. Ladner, A. Jack, J. D. Robertus, R. S. Brown, D. Rhodes, B. F. C. Clark and A. Klug, *Proc. Natl. Acad. Sci. U. S. A.*, 1975, **72**, 4414-4418.

108. J. L. Sussman, S. R. Holbrook, R. W. Warrant, G. M. Church and S.-H. Kim, *J. Mol. Biol.*, 1978, **123**, 607-630.

109. Z. Shen and P. J. Hagerman, *J. Mol. Biol.*, 1994, **241**, 415-430.

110. J. W. Orr, P. J. Hagerman and J. R. Williamson, *J. Mol. Biol.*, 1998, **275**, 453-464.

111. M. Wieland, M. Gfell and J. S. Hartig, *RNA*, 2009, **15**, 968-976.

112. H. W. Pley, K. M. Flaherty and D. B. McKay, *Nature*, 1994, **372**, 68-74.

113. S. M. Uptain, C. M. Kane and M. J. Chamberlin, *Annu. Rev. Biochem.*, 1997, **66**, 117-172.

114. J. Greenblatt, *Curr. Opin. Cell Biol.*, 1997, **9**, 310-319.

115. L. Manche, S. R. Green, C. Schmedt and M. B. Mathews, *Mol. Cell. Biol.*, 1992, **12**, 5238-5248.

116. V. A. Zakian, *Science*, 1995, **270**, 1601-1607.

117. M. J. Fedor and J. R. Williamson, *Nat. Rev. Mol. Cell Biol.*, 2005, **6**, 399-412.

118. A. R. Ferre-d'Amare and J. A. Doudna, *Annu. Rev. Biophys. Biomolec. Struct.*, 1999, **28**, 57-73.

119. T. Hermann, *Angew. Chem. Int. Ed.*, 2000, **39**, 1891-1905.

120. W. D. Wilson, L. Ratmeyer, M. Zhao, L. Strekowski and D. Boykin, *Biochemistry*, 1993, **32**, 4098-4104.

121. L. C. Jiang and D. J. Patel, *Nat. Struct. Biol.*, 1998, **5**, 769-774.

122. F. Walter, Q. Vicens and E. Westhof, *Curr. Opin. Chem. Biol.*, 1999, **3**, 694-704.

123. D. Fourmy, M. I. Recht, S. C. Blanchard and J. D. Puglisi, *Science*, 1996, **274**, 1367-1371.

124. D. Fourmy, M. I. Recht and J. D. Puglisi, *J. Mol. Biol.*, 1998, **277**, 347-362.

125. D. Fourmy, S. Yoshizawa and J. D. Puglisi, *J. Mol. Biol.*, 1998, **277**, 333-345.

126. Q. Vicens, *J. Incl. Phenom. Macrocycl. Chem.*, 2009, **65**, 171-188.

127. T. Hermann and D. J. Patel, *Science*, 2000, **287**, 820-825.

128. D. J. Patel, *Curr. Opin. Chem. Biol.*, 1997, **1**, 32-46.

129. C. Wilson, J. Nix and J. Szostak, *Biochemistry*, 1998, **37**, 14410-14419.

130. M. A. Borovinskaya, S. Shoji, K. Fredrick and J. H. D. Cate, *RNA*, 2008, **14**, 1590-1599.

131. G. F. Busscher, F. Rutjes and F. L. van Delft, *Chem. Rev.*, 2005, **105**, 775-791.

132. T. Hermann, *Cell. Mol. Life Sci.*, 2007, **64**, 1841-1852.

133. D. Moazed and H. F. Noller, *Nature*, 1987, **327**, 389-394.

134. S. Yoshizawa, D. Fourmy and J. D. Puglisi, *Science*, 1999, **285**, 1722-1725.

135. A. P. Carter, W. M. Clemons, D. E. Brodersen, R. J. Morgan-Warren, B. T. Wimberly and V. Ramakrishnan, *Nature*, 2000, **407**, 340-348.

136. B. Francois, R. J. M. Russell, J. B. Murray, F. Aboul-ela, B. Masquida, Q. Vicens and E. Westhof, *Nucleic Acids Res.*, 2005, **33**, 5677-5690.

137. G. J. R. Zaman, P. J. A. Michiels and C. A. A. van Boeckel, *Drug Discov. Today*, 2003, **8**, 297-306.

138. N. E. Mikkelsen, K. Johansson, A. Virtanen and L. A. Kirsebom, *Nat. Struct. Biol.*, 2001, **8**, 510-514.

139. F. Walter, J. Putz, R. Giege and E. Westhof, *EMBO J.*, 2002, **21**, 760-768.

140. U. Vonahsen and H. F. Noller, *Science*, 1993, **260**, 1500-1503.

141. T. K. Stage, K. J. Hertel and O. C. Uhlenbeck, *RNA*, 1995, **1**, 95-101.

142. S. A. Kawamoto, C. G. Sudhahar, C. L. Hatfield, J. Sun, E. J. Behrman and V. Gopalan, *Nucleic Acids Res.*, 2008, **36**, 697-704.

143. N. E. Mikkelsen, M. Brannvall, A. Virtanen and L. A. Kirsebom, *Proc. Natl. Acad. Sci. U. S. A.*, 1999, **96**, 6155-6160.

144. A. D. Frankel and J. A. T. Young, *Annu. Rev. Biochem.*, 1998, **67**, 1-25.

145. H. Y. Mei, D. P. Mack, A. A. Galan, N. S. Halim, A. Heldsinger, J. A. Loo, D. W. Moreland, K. A. SannesLowery, L. Sharmeen, H. N. Truong and A. W. Czarnik, *Bioorg. Med. Chem.*, 1997, **5**, 1173-1184.

146. M. L. Zapp, S. Stern and M. R. Green, *Cell*, 1993, **74**, 969-978.

147. N. W. Luedtke and Y. Tor, *Biopolymers*, 2003, **70**, 103-119.

148. C. S. Chow and J. K. Barton, *J. Am. Chem. Soc.*, 1990, **112**, 2839-2841.

149. M. R. Kirshenbaum, R. Tribolet and J. K. Barton, *Nucleic Acids Res.*, 1988, **16**, 7943-7960.

150. C. S. Chow, K. M. Hartmann, S. L. Rawlings, P. W. Huber and J. K. Barton, *Biochemistry*, 1992, **31**, 3534-3542.

151. N. W. Leudtke, J. S. Hwang, E. C. Glazer, D. Gut, M. Kol and Y. Tor, *ChemBioChem*, 2002, **3**, 766-771.

152. N. A. O'Connor, N. Stevens, D. Samaroo, M. R. Solomon, A. A. Marti, J. Dyer, H. Vishwasrao, D. L. Akins, E. R. Kandel and N. J. Turro, *Chem. Commun.*, 2009, 2640-2642.

153. M. Crul, R. C. A. M. van Waardenburg, J. H. Beijnen and J. H. M. Schellens, *Cancer Treat. Rev.*, 2002, **28**, 291-303.

154. E. E. Trimmer and J. M. Essigmann, in *Essays in Biochemistry, Vol. 34, 1999*, Portland Press Ltd, London, Edn., 1999, vol. 34, pp. 191-211.

155. Y. Jung and S. J. Lippard, *J. Biol. Chem.*, 2006, **281**, 1361-1370.

156. G. E. Damsma, A. Alt, F. Brueckner, T. Carell and P. Cramer, *Nat. Struct. Mol. Biol.*, 2007, **14**, 1127-1133.

157. T. D. Schmittgen, J. F. Ju, K. D. Danenberg and P. V. Danenberg, *Int. J. Oncol.*, 2003, **23**, 785-789.

158. J. M. Rosenberg and P. H. Sato, *Mol. Pharmacol.*, 1993, **43**, 491-497.

159. P. Papsai, J. Aldag, T. Persson and S. K. C. Elmroth, *Dalton Trans.*, 2006, 3515-3517.

160. P. Papsai, A. S. Snygg, J. Aldag and S. K. C. Elmroth, *Dalton Trans.*, 2008, 5225-5234.

161. P. V. Danenberg, L. C. C. Shea, K. D. Danenberg and T. Horikoshi, *Nucleic Acids Res.*, 1991, **19**, 3123-3128.

162. K. Rijal and C. S. Chow, *Chem. Commun.*, 2009, 107-109.

163. A. A. Hostetter, E. G. Chapman and V. J. DeRose, *J. Am. Chem. Soc.*, 2009, **131**, 9250-9257.

164. E. G. Chapman and V. J. DeRose, *J. Am. Chem. Soc.*, 2010, **132**, 1946-1952.

165. H. G. Rubahn, *Basics of nanotechnology*, Wiley-VCH, Weinheim, 2008.

166. N. C. Seeman, *Annu. Rev. Biophys. Biomol. Struct.*, 1998, **27**, 225-248.

167. N. C. Seeman, *Nature*, 2003, **421**, 427-431.

168. N. C. Seeman, *Trends Biochem. Sci.*, 2005, **30**, 119-125.

169. N. C. Seeman, H. Wang, X. P. Yang, F. R. Liu, C. D. Mao, W. Q. Sun, L. Wenzler, Z. Y. Shen, R. J. Sha, H. Yan, M. H. Wong, P. Sa-Ardyen, B. Liu, H. X. Qiu, X. J. Li, J. Qi, S. M. Du, Y. W. Zhang, J. E. Mueller, T. J. Fu, Y. L. Wang and J. H. Chen, *Nanotechnology*, 1998, **9**, 257-273.

170. R.-I. Ma, N. R. Kallenbach, R. D. Sheardy, M. Petrillo, L. and N. C. Seeman, *Nucleic Acids Res.*, 1986, **14**, 9745-9753.

171. N. C. Seeman and N. R. Kallenbach, *Biophys. J.*, 1983, **44**, 201-209.

172. M. Endo and H. Sugiyama, *ChemBioChem*, 2009, **10**, 2420-2443.

173. D. Reishus, B. Shaw, Y. Brun, N. Chelyapov and L. Adleman, *J. Am. Chem. Soc.*, 2005, **127**, 17590-17591.

174. N. C. Seeman, *Trends Biotechnol.*, 1999, **17**, 437-443.

175. Y. He, Y. Chen, H. P. Liu, A. E. Ribbe and C. D. Mao, *J. Am. Chem. Soc.*, 2005, **127**, 12202-12203.

176. K. Lund, Y. Liu, S. Lindsay and H. Yan, *J. Am. Chem. Soc.*, 2005, **127**, 17606-17607.

177. H. Yan, S. H. Park, G. Finkelstein, J. H. Reif and T. H. LaBean, *Science*, 2003, **301**, 1882-1884.

178. B. Ding, R. Sha and N. C. Seeman, *J. Am. Chem. Soc.*, 2004, **126**, 10230-10231.

179. F. Mathieu, S. P. Liao, J. Kopatscht, T. Wang, C. D. Mao and N. C. Seeman, *Nano Lett.*, 2005, **5**, 661-665.

180. F. A. Aldaye and H. F. Sleiman, *Pure Appl. Chem.*, 2009, **81**, 2157-2181.

181. J. H. Chen and N. C. Seeman, *Nature*, 1991, **350**, 631-633.

182. Y. W. Zhang and N. C. Seeman, *J. Am. Chem. Soc.*, 1994, **116**, 1661-1669.

183. C. M. Erben, R. P. Goodman and A. J. Turberfield, *J. Am. Chem. Soc.*, 2007, **129**, 6992-6993.

184. R. P. Goodman, R. M. Berry and A. J. Turberfield, *Chem. Commun.*, 2004, 1372-1373.

185. R. P. Goodman, I. A. T. Schaap, C. F. Tardin, C. M. Erben, R. M. Berry, C. F. Schmidt and A. J. Turberfield, *Science*, 2005, **310**, 1661-1665.

186. C. M. Erben, R. P. Goodman and A. J. Turberfield, *Angew. Chem. Int. Ed.*, 2006, **45**, 7414-7417.

187. F. A. Aldaye, P. K. Lo, P. Karam, C. K. McLaughlin, G. Cosa and H. F. Sleiman, *Nat. Nanotechnol.*, 2009, **4**, 349-352.

188. F. A. Aldaye and H. F. Sleiman, *J. Am. Chem. Soc.*, 2007, **129**, 13376-13377.

189. E. S. Andersen, M. Dong, M. M. Nielsen, K. Jahn, R. Subramani, W. Mamdouh, M. M. Golas, B. Sander, H. Stark, C. L. P. Oliveira, J. S. Pedersen, V. Birkedal, F. Besenbacher, K. V. Gothelf and J. Kjems, *Nature*, 2009, **459**, 73-75.

Chapter 2

Recognition of RNA three way junctions by metallosupramolecular cylinders: Gel electrophoresis

2.1 Introduction

The recognition of DNA three way junctions by the metallosupramolecular cylinder has been demonstrated and confirmed by several experiments such as X-ray crystal structure[1], NMR study[2] and gel electrophoresis.[3] However, a three way junction can occur not only in DNA but also in RNA (see **Section 1.2.2.4**).

RNA is involved in many steps of gene replication and expression[4] however it has been focused on as a drug target only recently.[5-7] RNA is an attractive drug target and has intriguing features such as offering a high accessibility compared to extensively compact chromosomal DNA, no RNA repair mechanisms and the diversity of three dimensional folds.[8] The latter plays a crucial role in RNA's biological functions and allows rational design of therapeutic compounds which bind specially to RNA folds. To achieve specific RNA recognition, there are several molecular interactions that can contribute and need to be considered, such as electrostatic forces[9], H-bond formation[10] and interactions such as π-π stacking.[11] The shape complementarity (how well a ligand and receptor fit together) and conformational changes (binding induced changes in both the ligand and effector) in RNA also provide a key driving force for specific binding. The complexes should ideally bind only in a specific site rather than unspecific sites. In addition, design of a therapeutic agent that inhibits the conformational change required for the biological functions of the target, is a promising strategy in the search for therapeutic compounds.[12]

In this chapter the recognition between the supramolecular cylinder, $[Fe_2L_3]Cl_4$, and the RNA three way junction mainly by gel electrophoresis is investigated. Initially, the binding of the cylinder to the RNA three way junction is confirmed by circular dichroism. Then the stabilisations of the RNA three way

junction, bulged RNA three way junction and RNA-DNA hybrid by the iron cylinder, are probed by gel electrophoresis. Furthermore, a competition assay is established to investigate the preferential binding of the iron cylinder to nucleic acid, the DNA and RNA three way junction.

2.2 Results and discussion

2.2.1 Circular dichroism

To initially confirm the binding of the iron triple stranded helicate to an RNA three way junction, a CD experiment was carried out. The sequences used in this chapter were adapted from the DNA three way junction.[3] The same length and sequences are used however uracil is used instead of thymine as shown below (**Figure 2.1**).

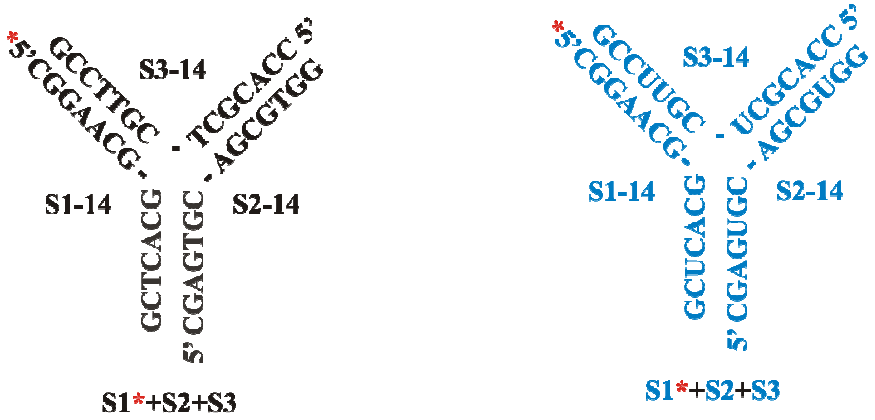

Figure 2.1 The schematic drawing of the oligonucleotide sequences used to assemble a three way junction. **Left**: DNA three way junction. **Right**: RNA three way junction. The numbers shown are the bases in each nucleic acid strand. A asterisk is the position where ^{32}P is incorporated for labelling.

Circular dichroism (CD) is a well known spectroscopic technique for detecting the change in structural conformation of nucleic acids induced by a synthetic agent.[13] A stock solution (700 μM) of the racemic mixture of the cylinder was titrated into a

preformed S1, S2 and S3 of RNA three way junction solution (10 μM) in which the RNA concentration was kept constant during the titration. It should be noted that the racemic mixture of the cylinder has no CD signal in the MLCT region due to the symmetry of the components.

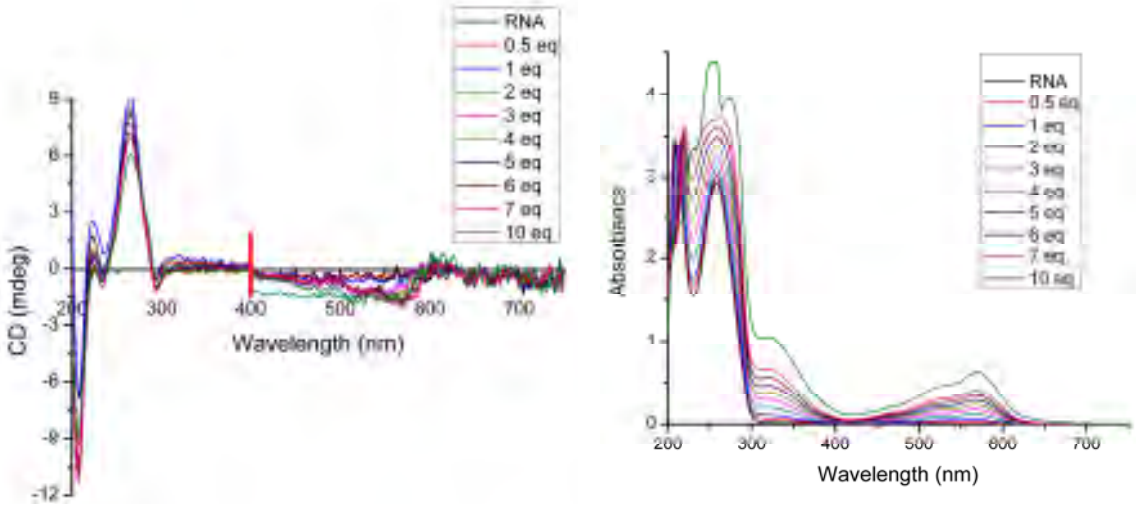

Figure 2.2 CD and UV spectra (**left** and **right**, respectively) of 10 μM RNA three way junction in buffers of 0.89 mM Na-cacodylate (pH 7.0) and 20 mM NaCl with increasing concentration of the iron cylinder (legends show increasing ratio of complex and RNA three-way junction).

The CD spectra show that in the absence of the iron cylinder, an A-form RNA was obtained confirmed by the characteristic pattern from 220-300 nm and the maximum signal at 260 nm. During the titration, the CD spectra (**Figure 2.2**, **Left**) show that in the presence of the cylinder, the spectroscopic signature of the RNA (below 300 nm) is not dramatically altered demonstrating that the RNA arms have retained their A-conformation. The appearance of induced CD signals (ICD) in the region 450-650 nm corresponding to the MLCT of cylinder indicates a binding event of the cylinder to the RNA three way junction. The corresponding UV-Vis spectra (**Figure 2.2**, **Right**) show no effect on the MLCT region of the cylinder (450-650 nm) confirming that the cylinder retains its structure.

2.2.2 The RNA three way junction induced by the iron cylinder $[Fe_2L_3]^{4+}$ ($L=C_{25}H_{20}N_4$)

The first *crystallographic study* that demonstrated the recognition of the iron cylinder and a DNA three-way junction, used a palindromic hexamer; a junction with short arms [three base pairs (bps)].[1] Initial gel electrophoresis studies used a DNA three way junction that was formed from three distinct DNA strands, each of which is a 14-mer non palindromic oligonucleotide.[3] The minimum length of DNA required for a three way junction lacking unpaired bases to stay stable during electrophoresis on a native gel at 5°C is seven base pairs per arm as shown previously.[14] Therefore, to begin probing recognition and stabilisation of the iron cylinder to the RNA three way junction by gel electrophoresis, the sequences shown in **Figure 2.1, Right** were employed. These ribonucleotides have the same length as used in DNA three way junction experiments.

The autoradiogram of the electrophoresis gel run at 4 °C (**Figure 2.3**) shows the formation of the RNA three way junction from 14-mers ribonucleotide in the presence and absence of magnesium chloride (10 μM), which is known to stabilise three way junctions at low to intermediate ionic strengths.[14, 15] This implies that the oligoribonucleotides have the ability to form the RNA three way junction regardless of whether magnesium chloride is present or not. Increasing the concentration of the tetracationic iron cylinders, the bands corresponding to the RNA three way junction became stronger. This indicates that the tetracationic iron cylinder has the ability to induce as well as stabilise the three way junction.

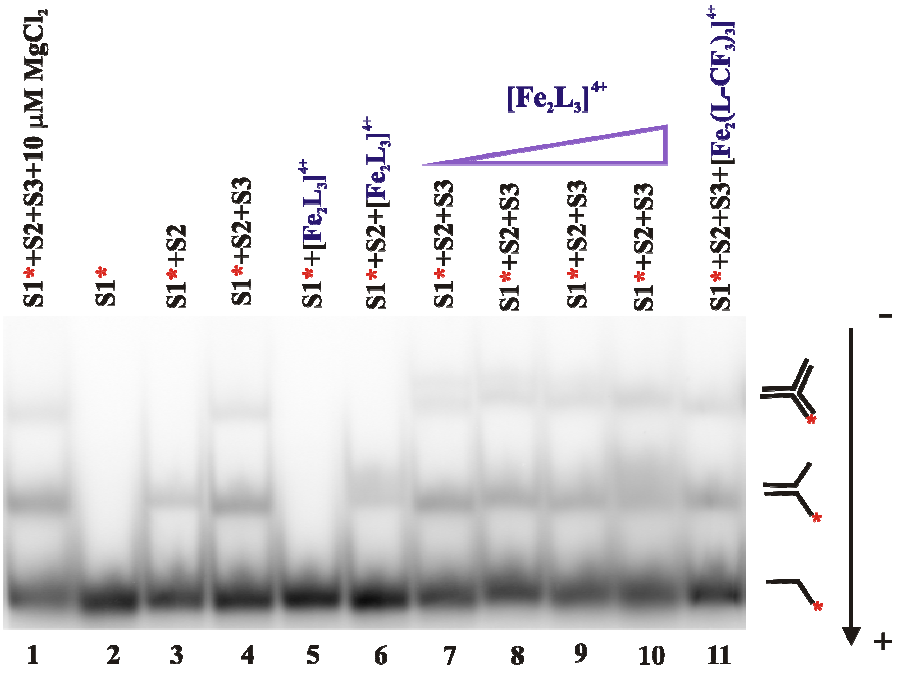

Figure 2.3 Autoradiogram of the gel run on nondenaturing 15% polyacrylamide gel at 4 °C. Lane 1: Positive control consisting of 10 nM of S1, S2 and S3 in TBN buffer with 10 μM $MgCl_2$. Lanes 2-4: Control containing S1, S1+S2 and S1+S2+S3 of RNA in the buffer. Lanes 5-6: Control containing S1 and S1+S2 of RNA in the buffer with $[Fe_2L_3]^{4+}$ ratio 3:1 (RNA strand:cylinder). Lanes 7-10: Sample containing S1, S2 and S3 in the buffer with increasing the concentrations of the cylinder from 3:0.5, 3:1, 3:2 and 3:10 corresponding to 5, 10, 20 and 100 nM, respectively. Lane 11: Negative control containing S1, S2 and S3 of RNA in the buffer with $[Fe_2 (L\text{-}CF_3)_3]^{4+}$ ratio 3:1 (RNA strand:cylinder).

To further explore the importance of the shape and size of the cylinder, a bulky cylinder $[Fe_2(L\text{-}CF_3)_3]^{4+}$ **(Figure 2.4)** was introduced. The bulky cylinder was used as a control since it has the same electrostatic charge but can not bind at centre of a three way junction due to additional CF_3 groups protruding from the carbon in the middle of the parent ligand. Interestingly in the presence of the bulky cylinder, a three way junction was formed. This unexpected band might be due to self formation of the RNA three way junction together with unspecific binding effects at low temperature. Therefore, the experiment was carried out again at 25 °C in order to inhibit self formation of the three way junction and remove any unspecific binding effects.

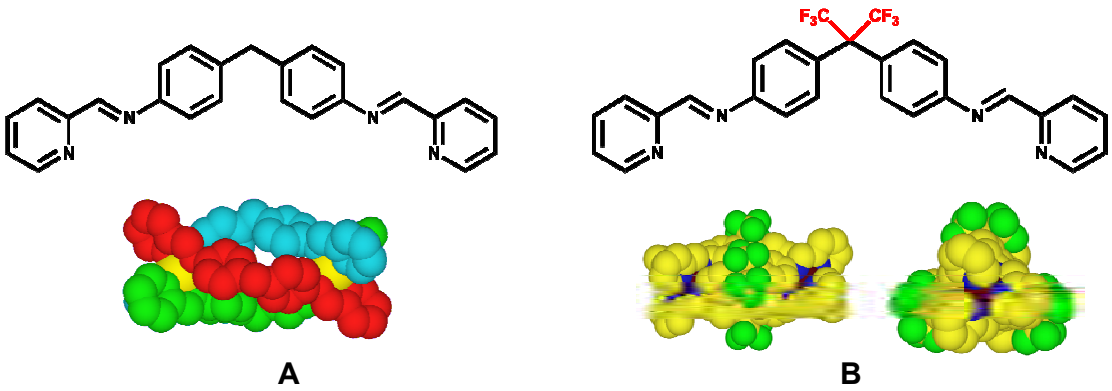

Figure 2.4 Schematic drawing of the ligands (top) and iron metallosupramolecular cylinders (bottom) used in this chapter. **A)** $[Fe_2L_3]Cl_4$, L = $C_{25}H_{20}N_4$. **B)** $[Fe_2 (L\text{-}CF_3)_3]Cl_4$ or bulky cylinder.

The result of the gel experiment performed at 25 °C (**Figure 2.5**) demonstrates that an RNA three way junction alone is inherently less stable. Neither magnesium chloride nor bulky cylinder causes stabilisation of the structure. Note that a band corresponding to a three way junction in the presence of magnesium chloride is a three way junction formed from self assembly of RNA. On the other hand, the three way junction was formed in the presence of the iron cylinder. This implies that the iron cylinder does induce and stabilise the RNA three way junction during electrophoresis. Lane 11 shows the negative control; an RNA three way junction with the bulky cylinder. The result (**Figure 2.5**) shows that there was still a band corresponding to three way junction in the presence of the bulky cylinder, however it was weaker than the PAGE performed at 4 °C. Nevertheless, the quantification indicated that the intensity of the band was similar to the lane containing only three strands of RNA. This demonstrates that the band is not due to the bulky cylinder but rather from self assembly of RNA. The result also shows that no frayed duplex RNA was formed at 25 °C even in the present of divalent salt (10 μM $MgCl_2$) nor the iron cylinder.

It is possible that the stabilisation of the fraying RNA three way junction by the iron cylinder is not as strong as the stabilisation from the perfect three way junction. Therefore, the interaction force stabilising the complex and the junction is not great enough to hold the two strands together during electrophoresis so it dissociates.

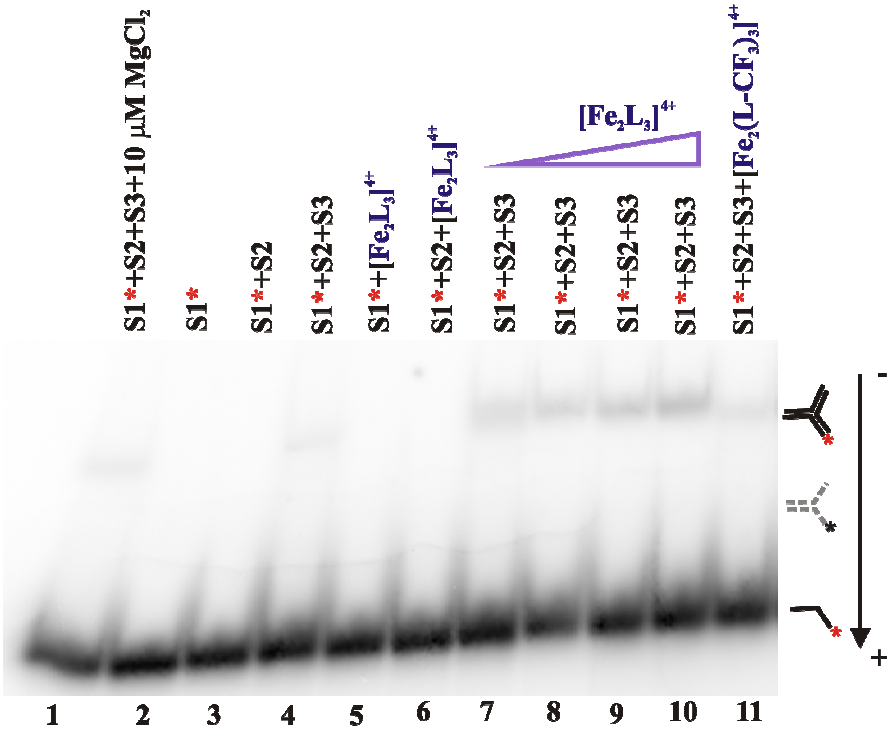

Figure 2.5 Autoradiogram of the gel performed on nondenaturing 15% polyacrylamide gel at 25 °C. Lane 1: Positive control consisting of 10 nM S1, S2 and S3 in TBN buffer with 10 μM $MgCl_2$. Lanes 2-4: Control containing 10 nM S1, S1+S2 and S1+S2+S3 of RNA in the buffer. Lanes 5-6: Control containing S1 and S1+S2 of RNA in the buffer with $[Fe_2L_3]^{4+}$ ratio 3:1 (RNA strand:cylinder). Lanes 7-10: Sample containing S1, S2 and S3 in the buffer with increasing concentration of cylinder from 3:0.5, 3:1, 3:2 and 3:10 corresponding to 5, 10, 20 and 100 nM, respectively. Lane 11: Negative control containing S1, S2 and S3 of RNA in the buffer with $[Fe_2 (L\text{-}CF_3)_3]^{4+}$ ratio 3:1 (RNA strand:cylinder).

It can be seen (**Figure 2.5**) that increasing the iron cylinder concentration does enhance the formation of the RNA three way junction. To investigate this further, the quantification of lanes 7-10 on the gel (**Figure 2.5**) were examined.

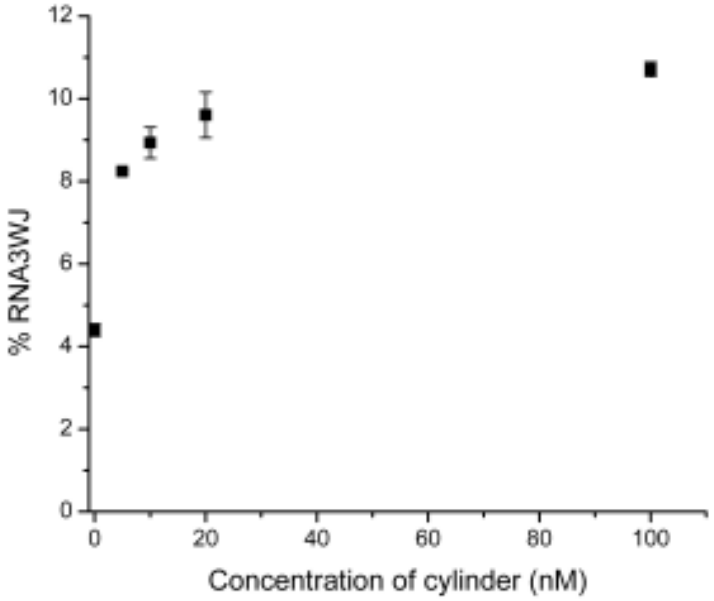

Figure 2.6 Plot of percentage of RNA three-way junction carried out at 25 °C as a function of the iron cylinder concentration. The result represents the mean of three individual experiments ± SD (n = 3).

As shown in **Figure 2.6**, the RNA three way junction remarkably formed when the concentration of the iron cylinder increased. Interestingly, the plot started to level off at 20 nM corresponding to the ratio of RNA to cylinder 3:2 which was more than the expected ratios of RNA strand to cylinder 3:1 corresponding to 10 nM. This implies that at high concentration of the cylinder, the specificity of the iron cylinder to the three way junction decreases as it can bind to the arm of the RNA three way junction.

2.2.3 The RNA three way junction assembled by the ruthenium cylinder $[Ru_2L_3]^{4+}$ ($L=C_{25}H_{20}N_4$)

The previous section has shown that the triple stranded helicate iron cylinder binds to the RNA three way junction. It has also been demonstrated that the size and shape of the cylinder is crucial for molecular recognition. The triple stranded ruthenium cylinder was chosen to compare the stabilisation and recognition of RNA three way junction versus the iron cylinder as it has a similar size and shape but contains a different metal. This ruthenium complex has fluorescence properties and is used for visualising the nuclei in tumor cells and monitoring the changes of tumor cells in real time. Therefore, it is an attractive alternative for future application. Moreover, the ruthenium cylinder exhibits similar DNA binding properties to the iron cylinder, however the cytotoxicity is drastically different. This compound has been indicated to be inactive against an ovarian cancer cell line compared to the parent cylinder.[16, 17] Obviously, the ruthenium cylinder might have a different mode of action from the parent cylinder. To further explore this, experiments were carried out with the RNA three way junction and the ruthenium cylinder.

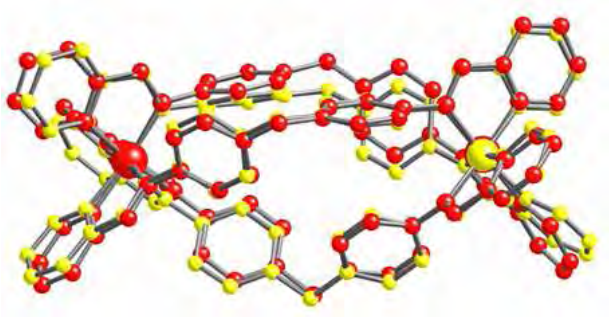

Figure 2.7 An overlay of the crystal structure[16] illustrations of the iron cylinder in red ($[Fe_2L_3]Cl_4$, L = $C_{25}H_{20}N_4$) and ruthenium cylinder in yellow ($[Ru_2L_3]Cl_4$, L= $C_{25}H_{20}N_4$).

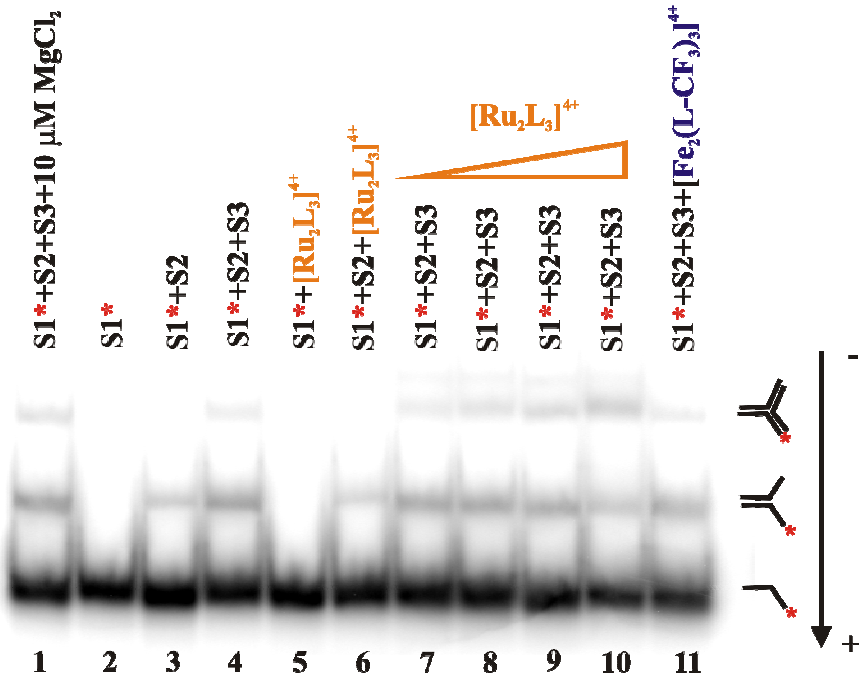

Figure 2.8 Autoradiogram of the gel carried out on nondenaturing 15% polyacrylamide gel at 4 °C. Lane 1: Positive control consisting of S1, S2 and S3 in TBN buffer with 10 μM $MgCl_2$. Lanes 2-4: Control containing 10 nM S1, S1+S2 and S1+S2+S3 of RNA in the buffer. Lanes 5-6: Control containing S1 and S1+S2 of RNA in the buffer with $[Ru_2L_3]^{4+}$ ratio 3:1 (RNA strand:cylinder). Lanes 7-10: Sample containing S1, S2 and S3 in the buffer with increasing the concentration of the cylinder from 3:0.5, 3:1, 3:2 and 3:10 corresponding to 5, 10, 20 and 100 nM, respectively. Lane 11: Negative control containing S1, S2 and S3 of RNA in the buffer with $[Fe_2\ (L\text{-}CF_3)_3]^{4+}$ ratio 3:1 (RNA strand:cylinder).

The results of the autoradiogram at 4 °C show that three way junction was formed in the absence and presence of the ruthenium cylinder i.e. lanes 4, 7, 8, 9 and 10. These bands correspond to the three way junction as they are located at the same position as the positive control (lane 1). Unexpectedly, the three way junction was observed in the negative control containing the bulky cylinder, even though the size and shape of the cylinder is not expected to induce three way junction formation. As has been mentioned in the previous section, these are the effects of non specific binding at low temperature. Therefore, the experiment carried out at 25 °C was undertaken.

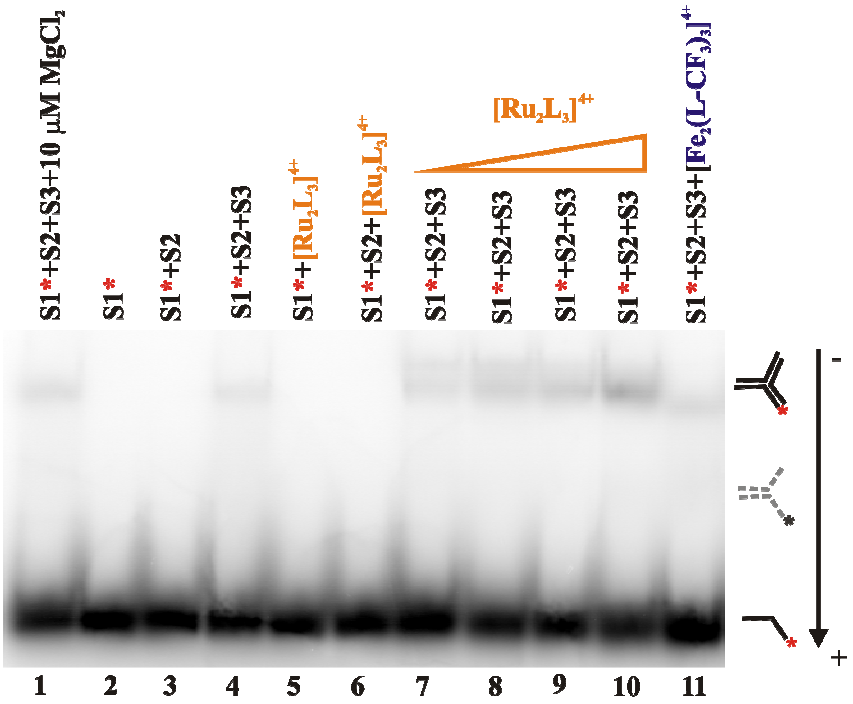

Figure 2.9 Autoradiogram of the gel run on nondenaturing 15% polyacrylamide gel at 25 °C. Lane 1: Positive control consisting of S1, S2 and S3 in TBN buffer with 10 μM $MgCl_2$. Lanes 2-4: Control containing 10 nM S1, S1+S2 and S1+S2+S3 of RNA in the buffer. Lane 5-6: Control containing S1 and S1+S2 of RNA in the buffer with $[Ru_2L_3]^{4+}$ ratio 3:1 (RNA strand:cylinder). Lanes 7-10: Sample containing S1, S2 and S3 in the buffer with increasing the concentration of the cylinder from 3:0.5, 3:1, 3:2 and 3:10 corresponding to 5, 10, 20 and 100 nM, respectively. Lane 11: Negative control containing S1, S2 and S3 of RNA in the buffer with $[Fe_2 (L\text{-}CF_3)_3]^{4+}$ ratio 3:1 (RNA strand:cylinder).

The results of the experiment at 25 °C (**Figure 2.9**) shows that only bands corresponding to single strand RNA and three way junction were detected. As with the iron cylinder, none of the fraying Y-shaped junction and duplex RNA was observed. A possible explanation for this is that the running temperature is higher than the melting temperature of the duplex (11.5 °C), thus the cylinder is not capable of stabilising Y-shaped junction. Eventually, it dissociates and is not detected on the autoradiogram.

The RNA three way junction was observed with various intensities, which increase with increasing concentration of cylinder (from 3:0.5, 3:1, 3:2 to 3:10 (RNA strand:cylinder) corresponding to 5, 10, 20 and 100 nM, respectively). The bands were quantified and a graph was plotted to compare the RNA three way junction induced from the ruthenium cylinder and those from the iron cylinder (**Figure 2.10**).

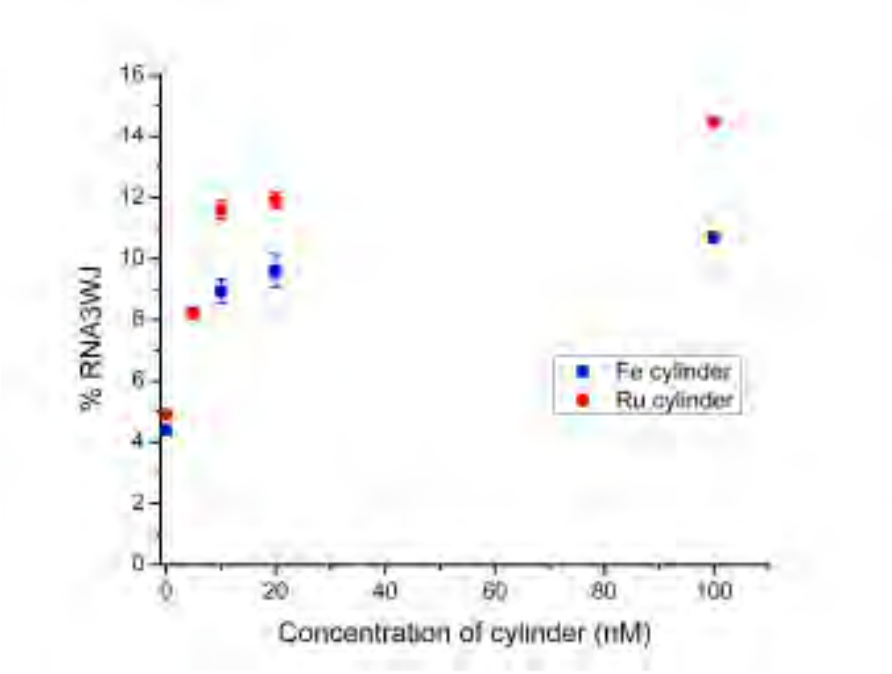

Figure 2.10 Plot of percentage of RNA 3WJ formed at 25 °C versus the concentration of iron and ruthenium cylinder. The result represents the mean of three individual experiments ± SD (n = 3).

The plot shows that the ability of the ruthenium cylinder to induce three way junction formation is greater than the iron cylinder. Considering the size and shape are the same, perhaps the metal plays an important role in the binding and stabilisation of the RNA three way junction. It would be interesting in the future to explore further about the effect of different metals coordinated to the ligand ($C_{25}H_{20}N_4$) on the stabilisation of the RNA three way junction.

2.2.4 The effect of enantiomers of the iron cylinder $[Fe_2L_3]^{4+}$ ($L=C_{25}H_{20}N_4$) on the stabilisation of the RNA three way junction

The iron cylinder is a helical molecule, thus has two enantiomers, termed M and P for the left and the right handed helicate, respectively. Both enantiomers are easily separated by a cellulose column as stationary phase and 20 mM NaCl as eluent.[18] Both enantiomers have different DNA binding properties. The M enantiomer has a stronger binding affinity to DNA than the P enantiomer.[19] Moreover, the crystal structure of the DNA three way junction demonstrates that only the M enantiomer is located in the heart of the DNA three way junction, although the racemic mixture was used in the crystallisation approach.[1] Furthermore, the recent gel electrophoresis studies demonstrate that the M enantiomer has a higher ability to stabilise a DNA three way junction than the P enantiomer.[3]

To further investigate this, the binding of the enantiomerically pure iron cylinder to the RNA three way junction was carried out at 4 °C and 25 °C on a 15% polyacrylamide gel electrophoresis. It should be noted that following experiments and the discussion in this section will mainly focus on the results at 25 °C rather than 4 °C, due to the non-specific binding and self assembly of RNA at 4 °C. (see **Section 2.2.2 and 2.2.3**)

The different effect of the two enantiomers on the gel results at 25 °C (**Figure 2.12B**) were not readily apparent by eye. In addition, the quantification results (**Figure 2.12C**) reveal that there was not significantly different between the binding of M enantiomer and P enantiomer to the RNA three way junction at the range of 0.1 - 0.4 μM. Recently, the crystal structure of the RNA three way junction and the iron cylinder has been achieved by Joachim Schnabl and Dr. Eva Freisinger, our collaborator working with Professor Roland K.O. Sigel from The University of

Zurich, Switzerland (unpublished result). The crystal structure reveals that the M enantiomer is located at the heart of the RNA three way junction as shown in **Figure 2.11**. Interestingly, the crystal was grown from the racemic mixture of the iron cylinder. Unexpectedly, the result achieved from the gels was conflicted to the crystallographic result that M and P enantiomer has no preferent binding to the RNA three way junction. It could be possible that in crystallographic approach, the concentration of the cylinder and RNA are much higher (mM) than that used for gel experiment (nM). This might affect to the recognition in term of thermodynamic. The further results and discussion about the concentration of RNA and cylinder will be discussed in **Section 2.2.6.**

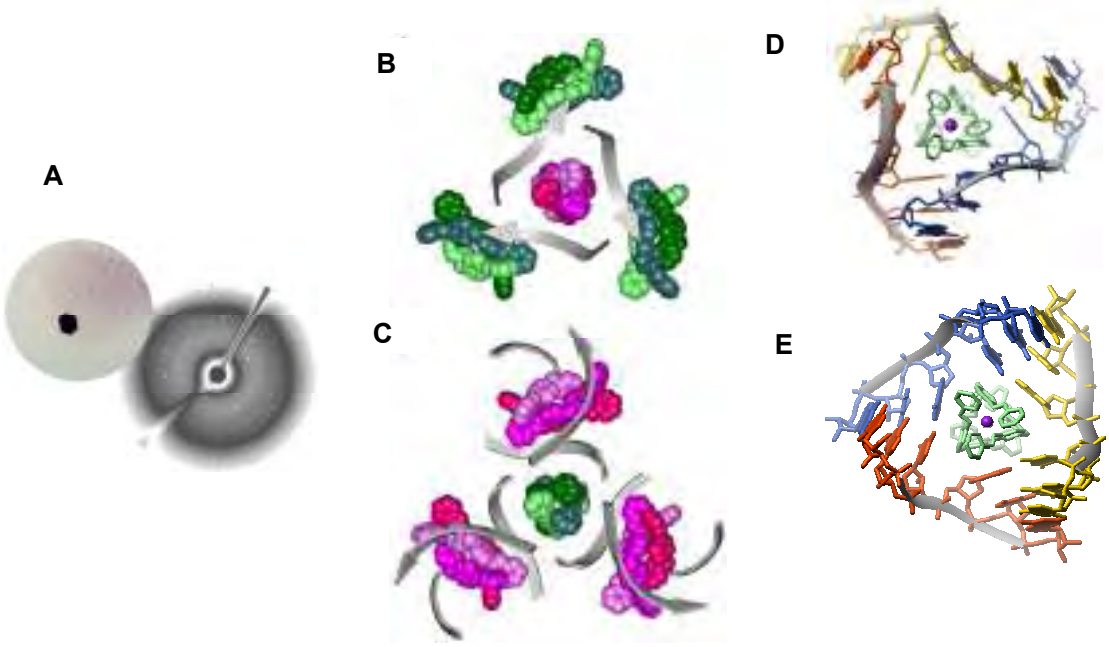

Figure 2.11 Crystal of the RNA-$[Fe_2L_3]^{4+}$ complex. **A)** The diffraction pattern of the RNA three way junction and the iron cylinder complex. **B)** RNA three-way junction (grey ribbon) formed around a $[Fe_2L_3]^{4+}$ cylinder (magenta) with additional terminal cylinder molecules (green). **C)** Three RNA three-way junctions arranged around the additional cylinder molecule (green). **D)** X-ray structure of DNA three way junction with $[Fe_2L_3]^{4+}$. [1] **E)** Crystal structure of RNA three way junction with $[Fe_2L_3]^{4+}$.[20]

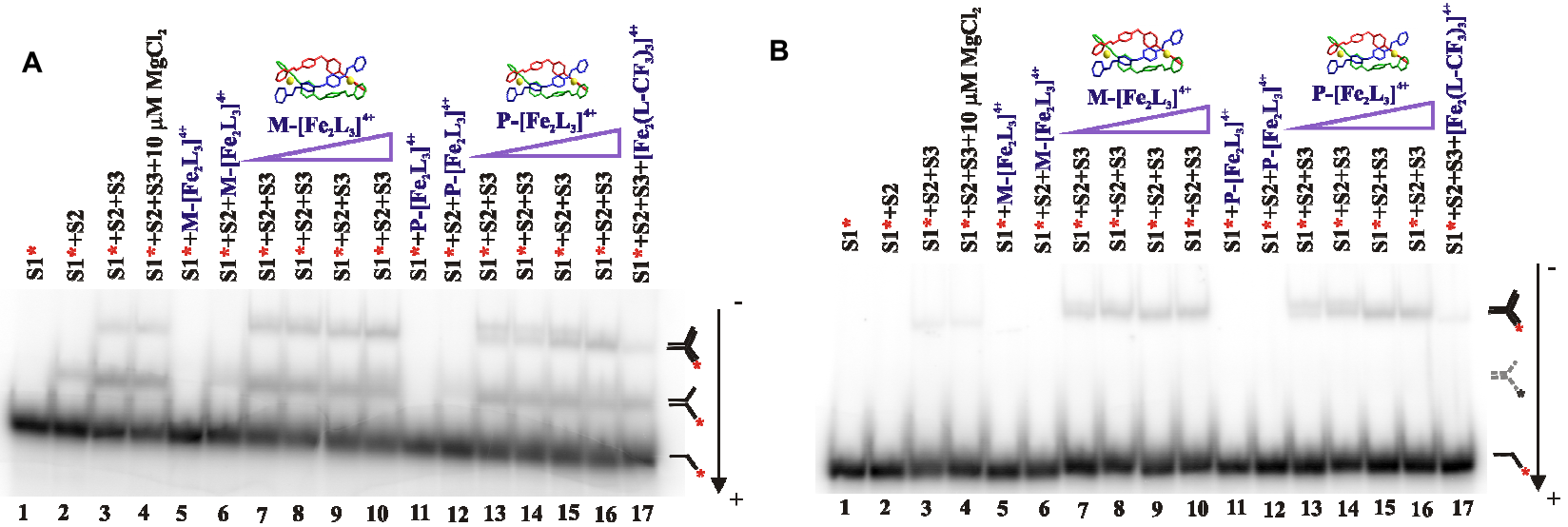

Figure 2.12 Autoradiogram of the RNA three way junctions and enantiomers of the iron cylinder performed on a 15% polyacrylamide gel at 4 °C (**A**) and at 25 °C (**B**), respectively. Lanes 1-3: Control containing S1, S1+S2 and S1+S2+S3 of RNA in TBN buffer. Lane 4: Positive control consisting of 10 nM S1, S2 and S3 in the buffer with 10 μM $MgCl_2$. Lanes 5-6: Control containing S1 and S1+S2 of RNA in the buffer with M enantiomer ratio 3:1 (RNA strand:cylinder). Lanes 7-10: Sample containing S1, S2 and S3 in the buffer with increasing ratios of M enantiomer from 3:0.5, 3:1, 3:2 and 3:10 corresponding to 5, 10, 20 and 100 nM, respectively. Lanes 11-12: Control containing S1 and S1+S2 of RNA in the buffer with P enantiomer ratio 3:1 (RNA strand:cylinder). Lanes 13-16: Sample containing 10 nM S1, S2 and S3 in the buffer with enhancing ratios of P enantiomer from 3:0.5, 3:1, 3:2 and 3:10 corresponding to 5, 10, 20 and 100 nM, respectively. Lane 11: Negative control containing S1, S2 and S3 of RNA in the buffer with $[Fe_2(L\text{-}CF_3)_3]^{4+}$). **C)** Plot of percentage of RNA 3WJ formed at 25 °C versus the concentration of enantiomers. The result represents the mean of three individual experiments ± SD (n = 3).

2.2.5 The iron cylinder $[Fe_2L_3]^{4+}$ ($L=C_{25}H_{20}N_4$) also binds to bulged RNA three way junction

In the previous experiment, the results show that the iron cylinder recognises and binds to the perfect RNA three way junction. This RNA three way junction is not the only possible structure that can be found in nature. Most naturally occurring RNA three way junctions contain unpaired bases, bulges, and internal loops. Interestingly, it has been shown that these types of structure are crucial for specific protein binding such as the binding of the HIV transactivator protein Tat to the three pyrimidine bulge in the trans–activation response elements (TAR).[12, 21, 22] To investigate the recognition ability of the iron cylinder to bulged RNA three way junctions, gel electrophoresis was carried out.

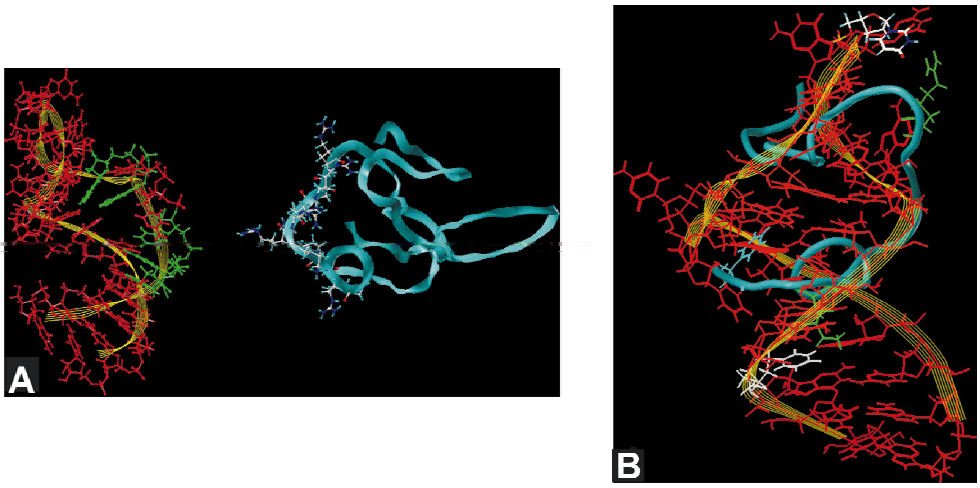

Figure 2.13 A) Structures of the unbound TAR RNA and Tat protein obtained from NMR. Important regions for intermolecular recognition are highlighted. Nucleotides of TAR RNA involved in Tat binding are shown in green. **B)** Proposed model for Tat protein-TAR interactions. The yellow and red are represented the structure of TAR RNA and nucleotide respectively. The structure of the Tat peptide drawn from Tat protein structure is shown in cyan. Taken from ref. [23]

The sequences used to form the bulged RNA three way junctions were designed by adding one or two uracils (U) into the middle of either S2 or S3 (**Figure 2.14**).

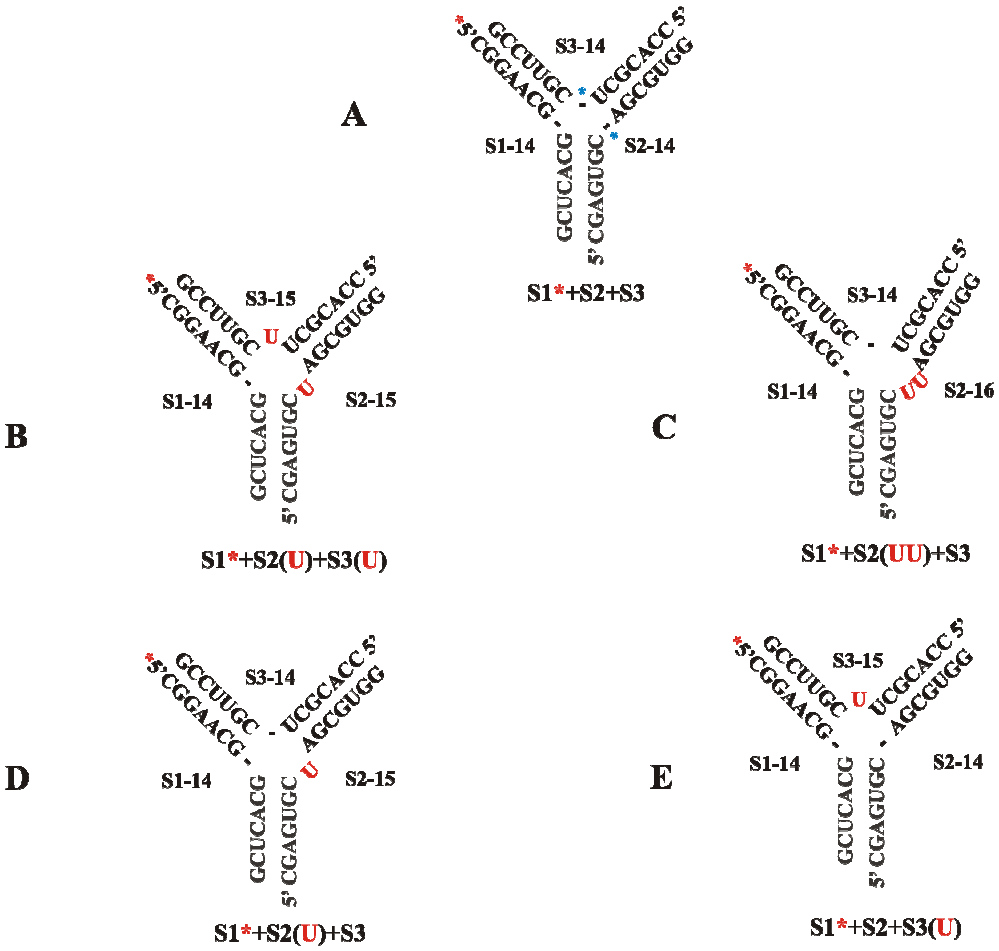

Figure 2.14 Schematic drawing of RNA three way junctions. **A)** A Fully matched RNA three way junction containing seven nucleotides on each arm. **B), C), D)** and **E)** Bulged RNA three way junctions. Additonal uracils were added onto a fully matched RNA in different position at the centre of the RNA three way junction.

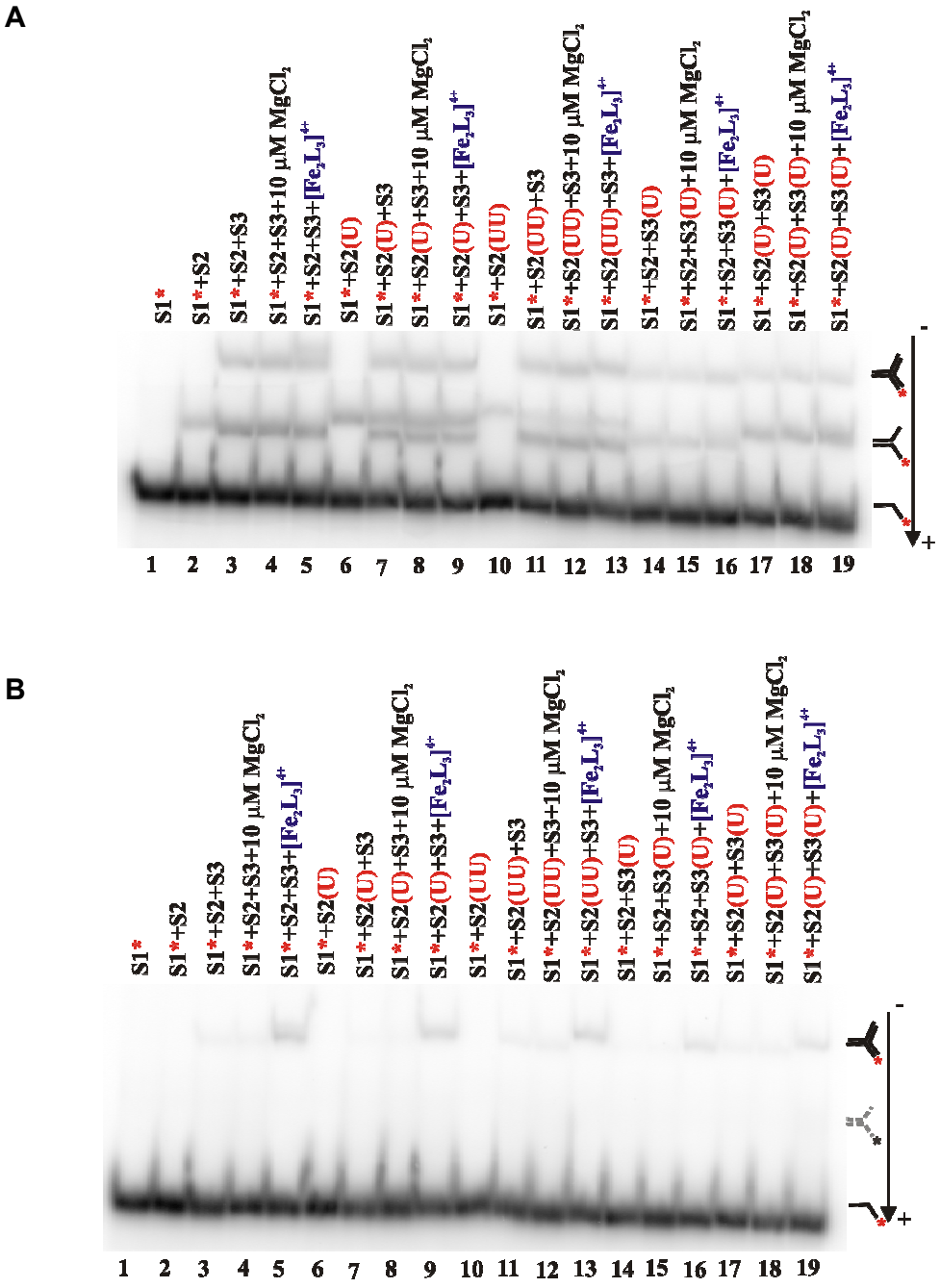

Figure 2.15 Autoradiogram of bulged RNA three way junctions performed on non-denaturing 15% polyacrylamide gel at 4 °C (**A**) and 25 °C (**B**), respectively. Lanes 1-5: Control comprising of the fully matched RNA three way junctions. Lanes 6-9, 10-13, 14-19, 17-19: A set of bulged RNA three way junctions containing additional uracil at the center of three way junction in various RNA strands treated with 10 μM $MgCl_2$ and the iron cylinder at the ratio 3:1 (RNA strand:complex) corresponding to 10 nM.

The results in **Figure 2.15A** show that at 4 °C, all bands were clearly illustrated. Apparently, a self assembly of the fully matched and bulged three way junctions occurred. Interestingly, two bands corresponding to duplex RNA were observed in lanes 7-9 and lanes 11-13. In lanes 7-9, the lower band corresponds to S1*+S3 which has the same molecular weight as S1*+S2. Consequently, both components had the same mobility through the gel electrophoresis. The presence of the upper band corresponding to S1*+S2(U) in lanes 7-9 and S1*+S2(UU) in lanes 11-13 were observed. The gel shows that the increasing molecular weight caused by adding one or two uracil to S2 retarded the mobility of the bulged duplex compared to the original duplex. In lanes 17-19, the duplex formation of S1*+S2(U) and S1*+S3(U) have the same molecular weight thus the migration ability is the same, resulting in only a duplex band.

The gel experiment was carried out again at 25 °C to compare the result with the experiment carried out at 4 °C. **Figure 2.15B** shows that the fully matched and bulged three way junction formation were increased in the presence of the iron cylinder even if self formation occurred. To compare the three way junctions obtained from each sequence, the bands on the gel were quantified by ImageQuant. The quantified analysis is represented in a bar graph (**Figure 2.6**).

The bar graph (**Figure 2.16**) demonstrates that the percentage of three way junctions from both bulged and fully matched sequences was increased in the presence of the iron cylinders even if self formation of the three way junction has occurred. Furthermore, the effect of the iron cylinder on the three way junction stabilisation was greater than the effect of the divalent ion, magnesium chloride.

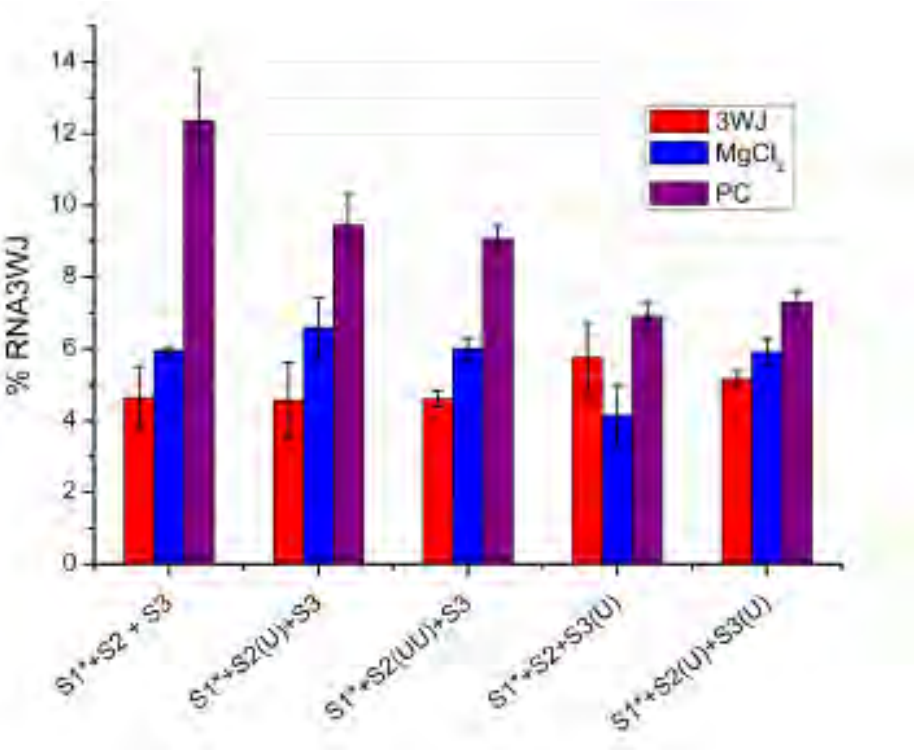

Figure 2.16 Bar graph depicting the percentage of RNA three way junction at 25 °C and the sequences used. The result represents the mean of three individual experiments ± SD (n = 3).

It can be concluded that the iron cylinder is capable of recognising and binding to the bulged junctions, although the stabilisation of the iron cylinder to the bulged three way junction was not greater than the perfect three way junction.

2.2.6 Increasing RNA concentration enhances the formation of the three way junction induced by the iron cylinder

It has been demonstrated from the previous section that the iron cylinder has the ability to bind to the RNA three way junction. However, the concentration of oligoribonucleotide used in the experiments was incredibly low, 10 nM. The low yield from the RNA labelling of S1 was the main reason for using this concentration for the experiments. In addition, the problem of achieving low yield in RNA labelling could be from the use of high concentration of RNA in the labelling step so the radioactivity

is not enough to label all RNA strands in the solution. Practically, the problem could be solved by reducing the stock concentration of RNA from 100 μM to 2.5 μM. The radioactivity in the labelling solution will be excess thus resulting in an increase of the labelling efficiency.

Considering the concentration of RNA used in the section **2.2.2-2.2.5**, it was very low. This will affect the concentration of the cylinder which is depended on the concentration of RNA. Consequently, the amount of the cylinder added into the solution was also low even at excess amount of the cylinder which is at 3:10 corresponding to 100 nM. Apparently, this concentration is much lower than the dissociation constant of the cylinder and DNA (**See Chapter 5**). This is important issue as the concentration of the cylinder used in the experiment should be higher than the dissociation constant. Therefore, the experiments mentioned previously were carried out again under new condition in which the concentration of the RNA three way junction was increased from 10 nM to 0.20 μM by adding the non-labelled S1, called cold strand, to boost the concentration of S1. In addition, it is known that salt in the buffer, NaCl, facilitates the stabilisation of the three way junction by reducing the repulsion of the negative charge from the phosphate backbone. Thus, the concentration of NaCl was increased from 100μM to 100 mM corresponding to the increasing concentration of the RNA three way junctions. Consequently, all the experiments shown above were carried out again using 0.20 μM of the RNA three way junction and TBN buffer containing 100 mM NaCl.

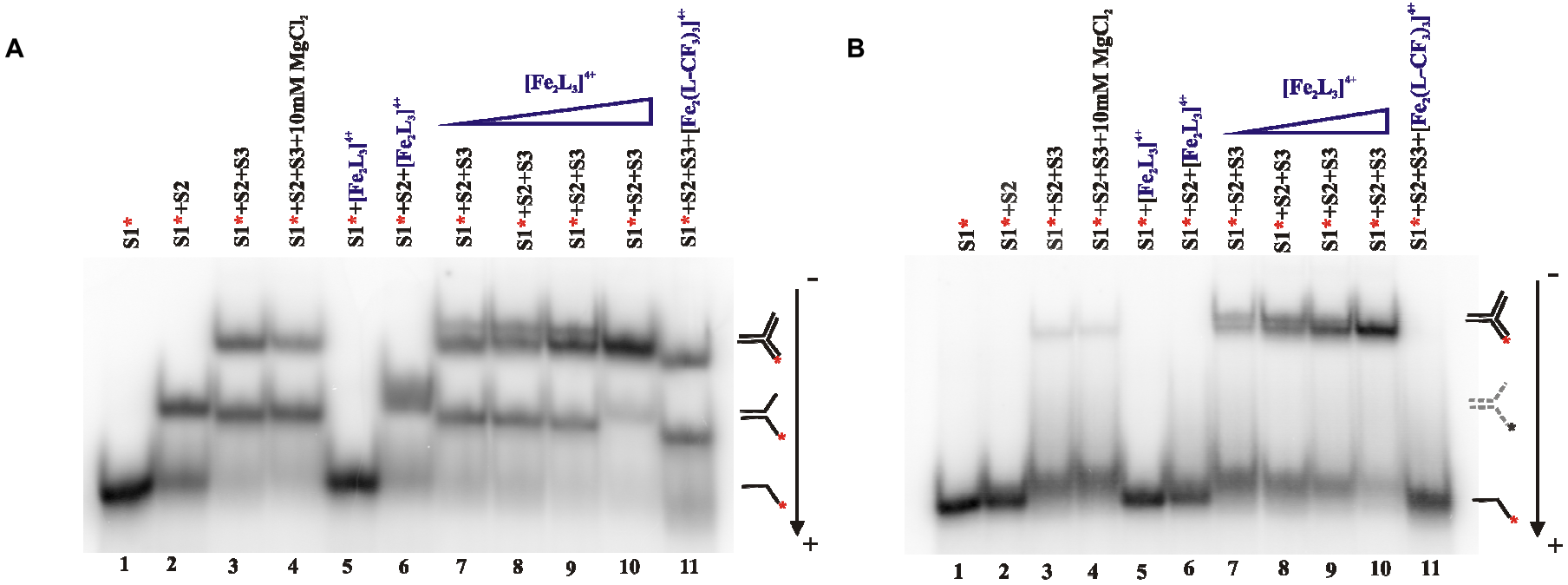

Figure 2.17 Autoradiograms of gels were performed on 15% native polyacrylamide showing the stabilisation and recognition of iron cylinder to the RNA three way junction with the new conditions, high concentration of RNA and high salt concentration at 4 °C (**A**) and 25 °C (**B**). Lanes 1-3: Control containing 0.2 µM S1, S1+S2 and S1+S2+S3 of RNA in the buffer. Lane 4: Positive control consisting of 0.2 µM S1, S2 and S3 in the buffer with 10 mM $MgCl_2$. Lanes 5-6: Control containing 0.2 µM S1 and S1+S2 of RNA in the buffer with $[Fe_2L_3]^{4+}$ ratio 3:1 (RNA strand:cylinder). Lanes 7-10: Sample containing S1, S2 and S3 in the buffer with increasing the concentration of the cylinder from 3:0.5, 3:1, 3:2 and 3:10 corresponding to 0.1, 0.2, 0.4 and 2 µM, respectively. Lane11: Negative control containing S1, S2 and S3 of RNA in the buffer with $[Fe_2(L\text{-}CF_3)_3]^{4+}$ ratio 3:1 (RNA strand:cylinder). 0.2 µM of the RNA three way junction and TBN buffer containing 100 mM NaCl was used for the entire experiment carried out at high RNA and high salt concentration.

The results of the native gel electrophoresis performed at high RNA concentration (**Figure 2.17**) show that the stabilisation and recognition of the iron cylinder to a three way junction is similar to the one performed at low RNA concentration at both temperatures. In addition, in the presence of the iron cylinder at 4 and 25 ºC, doublet bands corresponding to a three way junction band were observed. It could be possible that the top band of the doublet could be a three way junction-cylinder adduct as the migration rate was slower than the bottom doublet which could be a three way junction alone. Furthermore, the quantification information is intriguing. The percentage of three way junction obtained from the gel undertaken at high concentration of RNA is remarkably higher than the one carried out at low RNA concentration. The plot of gel carried out in both conditions is shown below. These results were compared at the same ratio of RNA strand to the complex.

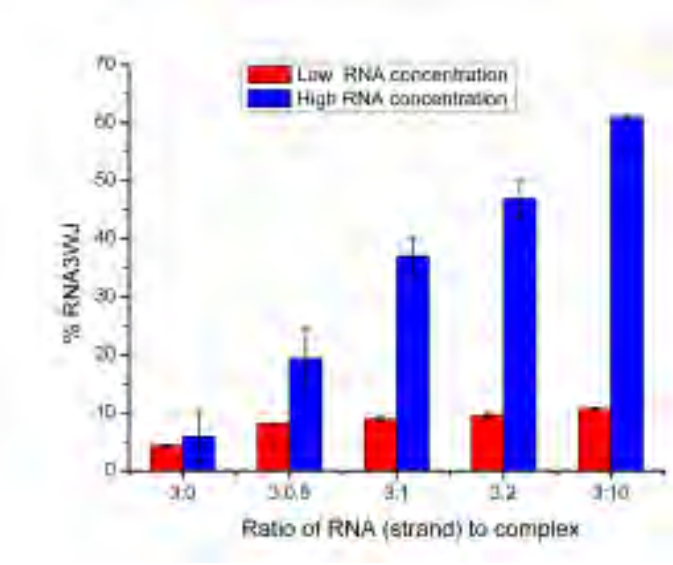

Figure 2.18 Bar graph illustrating the percentage of the RNA three way junction versus the ratios of RNA to complex at 25 °C under low and high RNA concentration conditions. The result represents the mean of three individual experiments ± SD (n = 3).

The plot **(Figure 2.18)** shows that in the absence of the iron cylinder, the starting amount of the RNA three way junction in both conditions, low and high RNA

concentration, was the same. Interestingly, the percentages of the RNA three way junction obtained from high RNA concentration were distinctively more than those at low RNA concentration. This result is interesting as the same percentages of the three way junction was assumed to achieve even if the RNA concentration was increased. The theory of thermodynamic equilibrium may explain this result as illustrated in **Figure 2.19**.

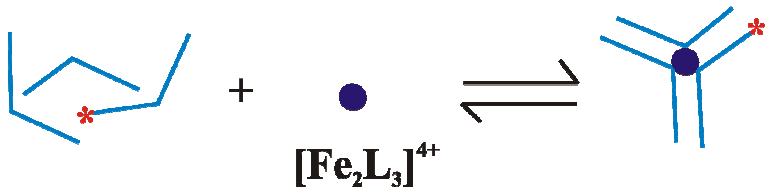

Figure 2.19 Schematic of the formation of the RNA three way junction in the presence of the iron cylinder

In the steady state, the rate of the RNA three way junction formation in the presence of the iron cylinder, forward reaction, is equal to the rate of breakdown of the three way junction, backward reaction. At high RNA concentration, the RNA added disturbs the equilibrium. To remain in equilibrium, the formation of the three way junction induced by the cylinder has to increase.

A gel experiment to probe the preferential binding effect of both enantiomers of the iron cylinder on the RNA three way junction was also performed at 4 °C and 25 °C. The gel results are represented in **Figure 2.20**. The gel quantification at 25 °C is shown in **Figure 2.21**. The results show that the three way junction induced by both enantiomers at high RNA concentration is dramatically increased when compared to the gel experiments carried out at low RNA concentration at both temperatures. In addition, at high RNA concentration, the M enantiomer has a higher binding affinity to the RNA three way junction than the P enantiomer.

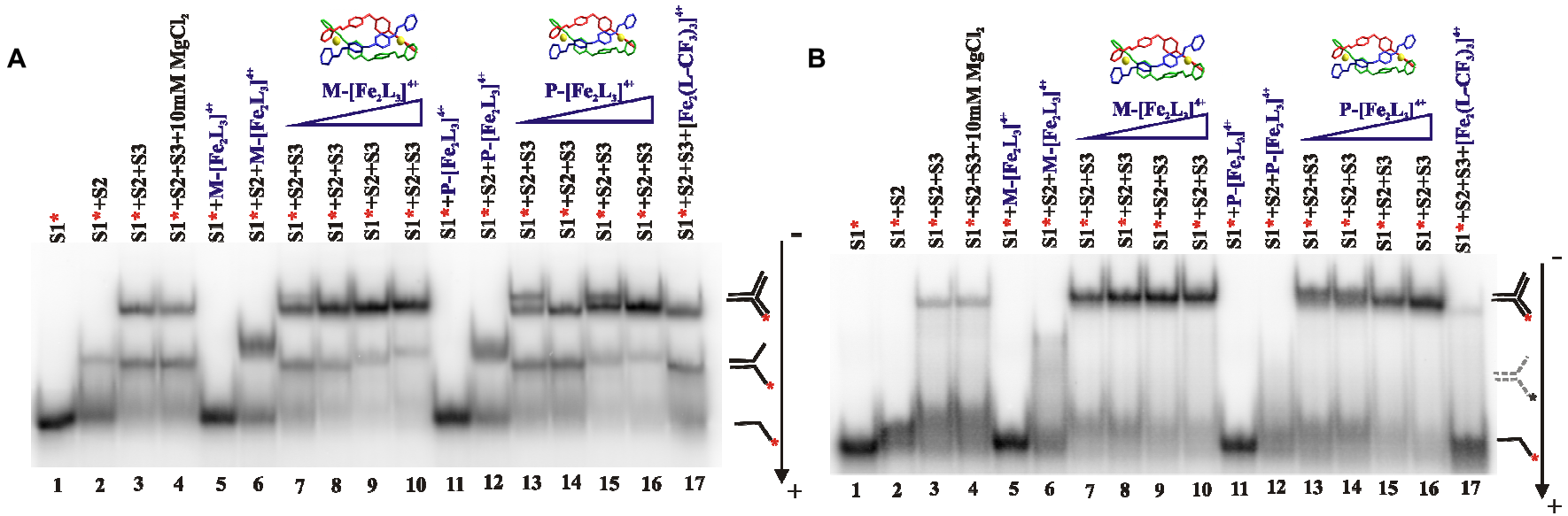

Figure 2.20 Autoradiogram of the RNA three way junction stabilised by enantiomers of the iron cylinder at 4 °C. Autoradiogram of the RNA three way junctions and enantiomers of the iron cylinder performed on a 15% polyacrylamide gel at 4 °C (**A**) and at 25 °C (**B**), respectively. Lanes 1-3: Control containing 0.2 μM S1, S1+S2 and S1+S2+S3 of RNA in TBN buffer. Lane 4: Positive control consisting of 0.2 μM S1, S2 and S3 in the buffer with 10 μM $MgCl_2$. Lanes 5-6: Control containing 0.2 μM S1 and S1+S2 of RNA in the buffer with M enantiomer ratio 3:1 (RNA strand:cylinder). Lanes 7-10: Sample containing 0.2 μM S1, S2 and S3 in the buffer with increasing ratios of M enantiomer from 3:0.5, 3:1, 3:2 and 3:10 corresponding to 0.1, 0.2, 0.4 and 2 μM, respectively. Lanes 11-12: Control containing 0.2 μM S1 and S1+S2 of RNA in the buffer with P enantiomer ratio 3:1 (RNA strand:cylinder). Lanes 13-16: Sample containing 0.2 μM S1, S2 and S3 in the buffer with enhancing ratios of P enantiomer from 3:0.5, 3:1, 3:2 and 3:10 corresponding to 0.1, 0.2, 0.4 and 2 μM, respectively. Lane 11: Negative control containing 0.2 μM S1, S2 and S3 of RNA in the buffer with $[Fe_2(L\text{-}CF_3)_3]^{4+}$).

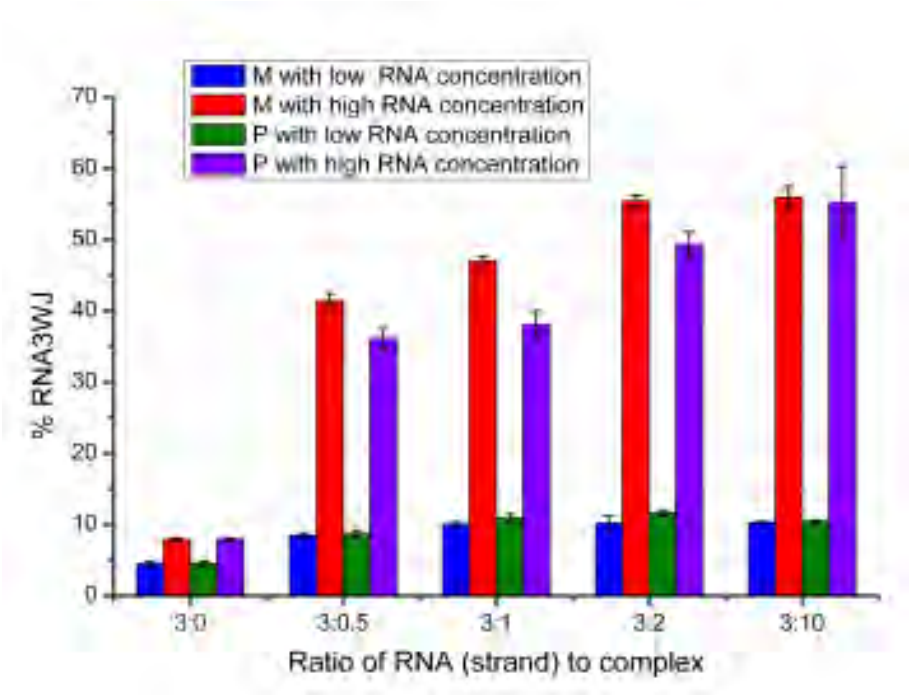

Figure 2.21 Bar graph comparing percentage of RNA three way junction obtained from each enantiomer at low and high RNA concentration versus the ratio of RNA per strand to the complex. The result represents the mean of three individual experiments ± SD (n = 3).

The bulged RNA three way junctions were also treated with high RNA concentration (**Figure 2.22**). The increase of the bulged RNA three way junctions was monitored at 4 °C and 25 °C respectively. Surprisingly, the result at 4 °C at high RNA concentration did not give as good a resolution as the one at low RNA concentration. For example, lane 6 showed two bands of fraying Y-shaped RNA i.e. S1+S2(U) and S1+S3 at low RNA concentration, however only a single band of duplex RNA correlated to S1+S3 was observed at high RNA concentration.

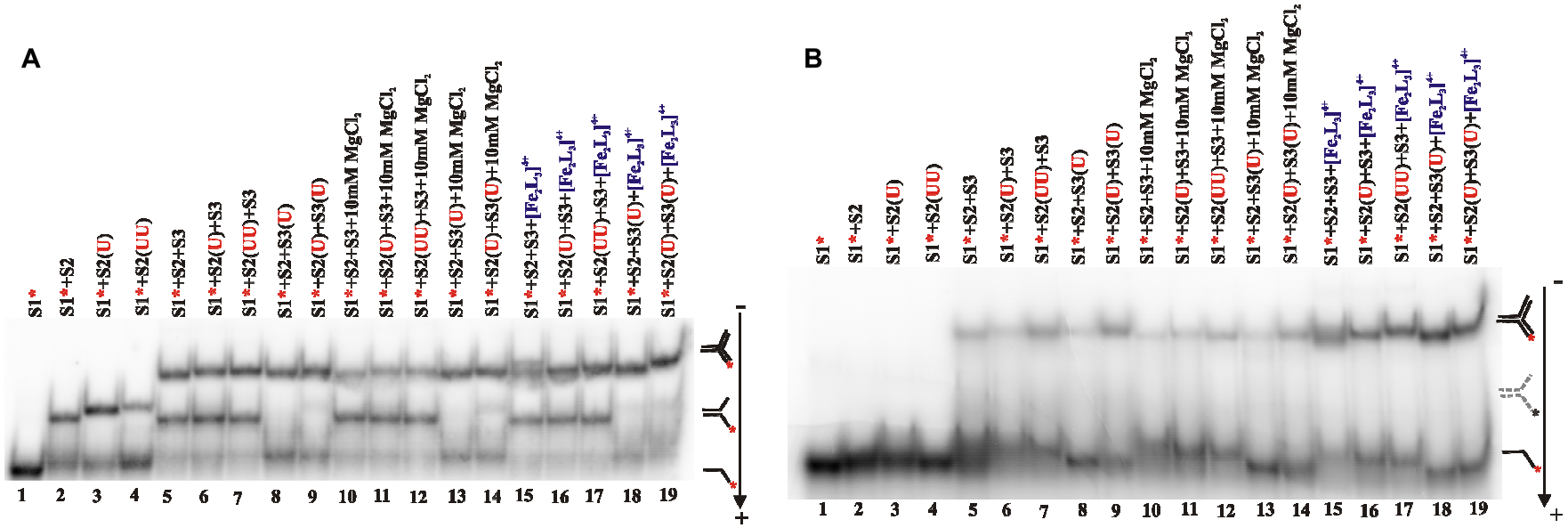

Figure 2.22 Autoradiogram of bulged RNA three way junctions performed on non-denaturing 15% polyacrylamide gel at 4 °C (**A**) and 25 °C (**B**), respectively. Lanes 1-9: Control comprising of 0.2 μM RNA three way junctions in the absence of the iron cylinder. Lanes 10-14: A set of 0.2 μM RNA three way junctions containing fully matched and bulged RNA three way junctions which have additional uracil at the center of the three way junction in various RNA strands treated with 10 mM $MgCl_2$. Lanes 15-19: 0.2 μM fully matched RNA three way junction and bulged RNA three way junctions treated with the iron cylinder at the ratio 3:1 (RNA strand:complex) corresponding to 0.2 μM. All sample solutions were contained TBN buffer.

Quantification reveals that at high RNA concentration, more bulged RNA three way junction is formed than at low RNA concentration as shown in **Figure 2.23**. A bar graph demonstrates that in the absence of the iron cylinder either at low or high RNA concentration, the self formation of bulged RNA three way junctions was always detected. However, the enhancement of the bulged RNA three way junction was observed in the presence of the iron cylinder indicating that the iron cylinder recognises and stabilises to bulged RNA three way junctions.

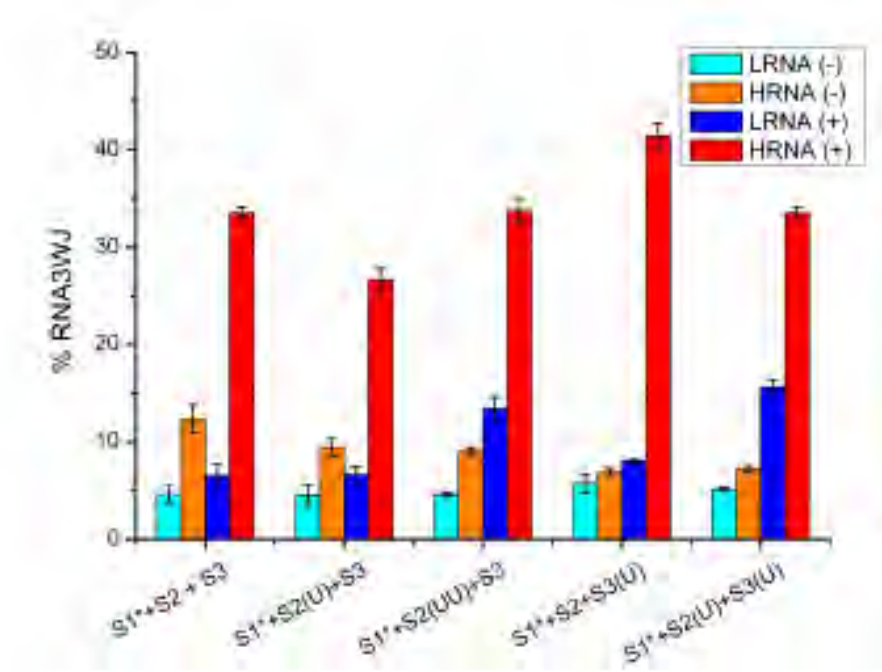

Figure 2.23 Bar graph showing the comparison percentage of each bulged RNA three way junction obtained in the absence and presence of iron cylinder at high and low RNA concentration. LRNA(-), HRNA(-) are low RNA and high RNA concentration, repectively, in the absence of the iron cylinder. LRNA(+), HRNA(+) are low RNA and high RNA concentration, repectively, in the presence of the iron cylinder. The result represents the mean of three individual experiments ± SD (n = 3).

2.2.7 A competition experiment between the DNA and RNA three way junction

Previous studies have elucidated the binding of the iron cylinder to the DNA three way junction by X-ray crystallography[1], gel electrophoresis[3] and NMR spectroscopy[2]. The results above show that the cylinder also binds to the RNA three way junction. The question that arises is that to which nucleic acid junction the iron cylinder preferentially binds. Therefore, an assay was established in which competition between the DNA and the RNA three way junction was induced. Consequently, a preferential binding of the cylinder to a nucleic acid is assumed.

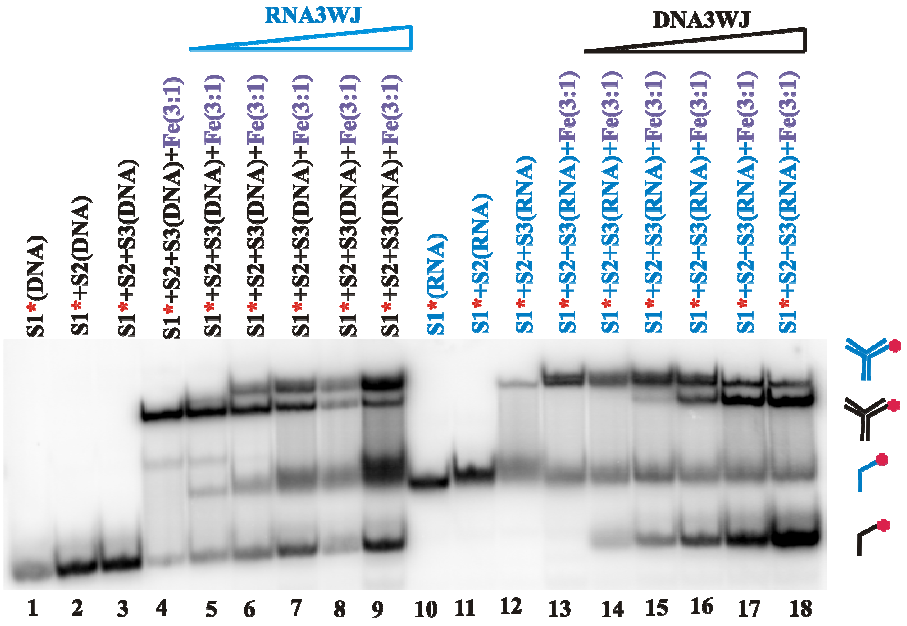

Figure 2.24 The competition assay of the iron cylinder to nucleic acid (DNA and RNA) performed on 20% native polyacrylamide gel electrophoresis at 25 °C. Lanes 1-3 and 10-12: Control containing 0.2 µM S1, S1+S2, S1+S2+S3 of DNA and RNA respectively. Lanes 4, 13: Control containing 0.2 µM S1+S2+S3 of DNA (4) and RNA (13) in the presence of 0.2 µM iron cylinder. Lanes 5-9: 0.2 µM DNA three way junction and 0.2 µM iron cylinder in the presence of increasing RNA three way junction concentration (40, 100, 200, 400 and 1000 nM, respectively). Lanes 14-18: 0.2 µM RNA three way junction and 0.2 µM iron cylinder in the presence of increasing DNA three way junction concentration (40, 100, 200, 400 and 1000 nM, respectively).

It was found that the competition of the nucleic acids with the cylinder could be followed on the same native gel although RNA strands are identical to DNA in

term of length and sequence. However, DNA strands run faster on the gel due to the absence of the hydroxyl group on the pentose ring in the 2′position in DNA which results in a lower molecular weight. Therefore, the DNA three way junction and the RNA three way junction can be distinguished from each other. The assay was performed as follows. To a constant concentration of DNA three way junction and cylinder, increasing amounts of the RNA three way junction were added. A second experiment was performed where the concentration of RNA three way junction and cylinder were fixed and the concentration of DNA three way junction added into the solution was increased.

The results (**Figure 2.24**) show that competition between the nucleic acids for the iron cylinder occurred. An increase of the RNA three way junction results in a decrease of the DNA three way junction and a simultaneous rise of single stranded DNA. The single strand detected on the gel was from the dissociation of the three way junction, caused by the removal of iron cylinder from the three way junction by the competitor. The result demonstrates that the dissociated single stranded DNA from the DNA three way junction when the RNA three way junction was added does increase compare to dissociated single stranded RNA when the DNA three way junction was added. The latter shows the constant intensity of the single strand RNA. This illustrates that the iron cylinder is hardly taken from the RNA three way junction in the other word the iron cylinder prefers to bind to RNA three way junction rather than DNA three way junction. However, care must be taken when interpreting the results, as the equilibrium being studied is not the simple competition between a RNA three way junction and a DNA three way junction that would be most desirable. Rather the equilibrium is between cylinder bound DNA three way junction plus single stranded RNA versus cylinder bound RNA three way junction and single strand DNA

(**Figure 2.25**). It has been known (since some unbound RNA three way junction is present in the absence of cylinder) that the energy required to form an RNA three way junction from a single stranded RNA is lower than that needed to form a DNA three way junction from a single strand of DNA and this will influence the position of the equilibrium.

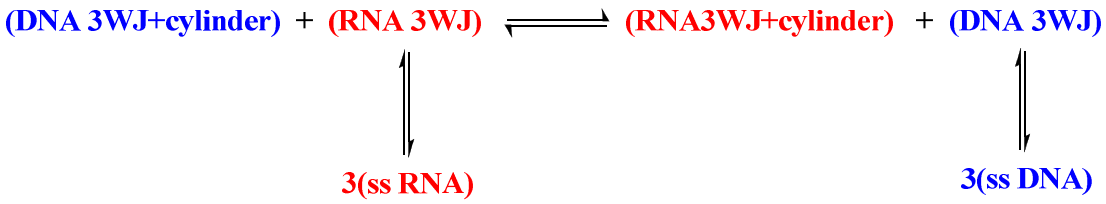

Figure 2.25 Schematic drawing of proposed equilibrium for a competition assay between DNA and RNA three way junction to the iron cylinder.

In addition, the competition assay could alternatively have been performed in by labelling one of nucleic acid three way junction. Then, the non-labelled competitor will be added to a solution containing a constant concentration of labelled nucleic acid and the cylinder. This alternative experiment may aid the interpretation of the experiment by reducing a number of bands on the gel.

2.2.8 DNA-RNA hybrid three way junctions

Targeting nucleic acids using small molecules usually exploits the material involving in the gene expression pathway, for instance DNA, RNA and protein. However, the intermediate processes, DNA-RNA, have not often been considered. The DNA-RNA hybrid formation offers a specific target for manipulating the transfer of genetic information through binding by small molecules. Due to the different conformation of the DNA-RNA hybrid, compared to entirely DNA or RNA, and also

the low occurrence within biological systems, it would be interesting to further explore their therapeutic potential.

The aim of this experiment was to examine the recognition of the iron cylinder to a DNA-RNA hybrid three way junction. A set of DNA-RNA hybrid three way junction combinations was created as shown in **Figure 2.26**. Note that in this experiment strand 3 of DNA and RNA were labelled. In fact, it does not matter which strand is labelled as long as it is one of the three strands. The autoradiogram of the hybridisation experiment is shown in **Figure 2.27**.

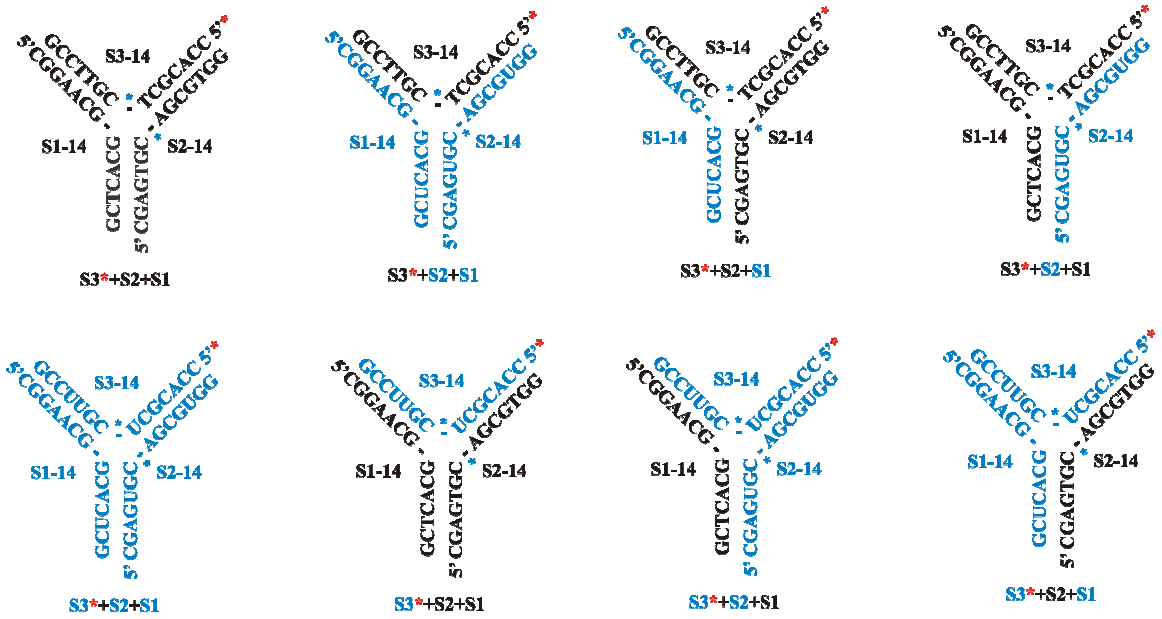

Figure 2.26 Schematic drawing of DNA-RNA hybrid three way junctions. Note that S3 of DNA and RNA were labelled. The black letters represents DNA strand and the blue letters represent RNA strand.

The result (**Figure 2.27**) shows that the formation of the three way junctions was observed only in the presence of the iron cylinder. This indicates that the iron cylinder recognises and binds to the DNA-RNA hybrid three way junctions. The migration distances of the hybrids are different from the three way junctions composed of entire DNA or RNA and even among the hybrids. According to

electrophoresis principles, the nucleic acid will migrate differently depending on its charge, Y-shaped configuration and molecular weight. Since the charge and conformation of the hybrid are assumed to be the same, the difference in migration comes from the component of the hybrid. Note that in the same length of oligonucleotide, RNA has a higher molecular weight than DNA due to the hydroxyl group on C3 position in the ribose sugar. Therefore, the components that have less RNA strands will run faster than the ones that have more RNA strands.

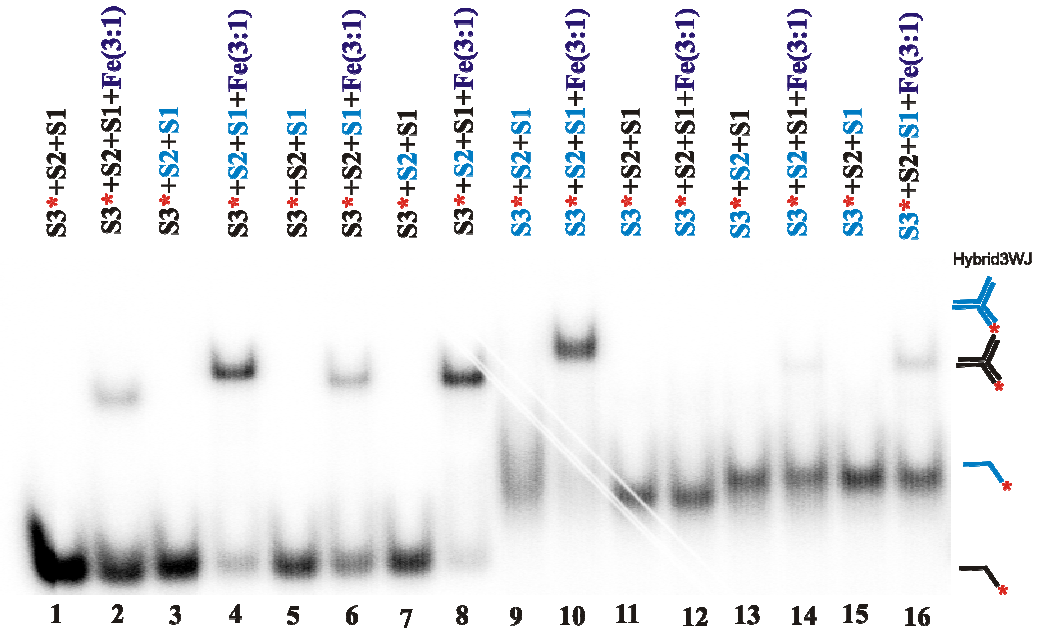

Figure 2.27 The autoradiogram of DNA-RNA hybrid three way junction carried out on 20% native polyacrylamide gel at 25 °C. Lanes 1, 9: Control containing 0.2 μM DNA and RNA three way junction respectively. Lanes 2, 10: Control containing 0.2 μM DNA and RNA three way junction, respectively in the presence of 0.2 μM iron cylinder. Lanes 3, 5, 7: 0.2 μM DNA-RNA hybrid three way junctions consisting of various DNA and RNA components as shown in the figure and S3 of DNA was labelled. Lanes 4, 6, 8: Containing 0.2 μM DNA-RNA hybrid three way junctions in the presence of 0.2 μM iron cylinder. Lanes 11, 13, 15: Sample containing different components of DNA-RNA hybrid three way junctions in which S3 of RNA was labelled. Lanes 12, 14, 16: Sample containing 0.2 μM DNA-RNA hybrid three way junction in the presence of 0.2 μM iron cylinder. The black letters represent DNA strand while the blue one represent RNA strand.

Furthermore, the result indicates that the iron cylinder prefers to bind to each DNA-RNA hybrid three way junction combination differently. Among the hybrid combinations, lane 12, containing S1 (DNA), S2 (DNA), S3 (RNA), was remarkably not stable at all even in the presence of the iron cylinder. Lane 14, consisting of S1 (DNA), S2 (RNA), S3 (RNA) in the presence of the cylinder was less stable but slightly better than lane 12. The two hybrids share a similar feature in which both contain S1 (DNA) and S3 (RNA). This might be a key point for the recognition and stabilisation of the iron cylinder to DNA-RNA hybrid. On the other hand, the great stability of the hybrid achieved in lane 4, 8 containing S1 (RNA), S2 (RNA), S3 (DNA) and S1 (DNA), S2 (RNA), S3 (DNA) respectively in the presence of the iron cylinder. It is noticed that S2 (RNA), S3 (DNA) play important role in the recognition of the cylinder to the DNA-RNA hybrid.

2.3 Conclusions

The results herein demonstrate that the iron cylinder $[Fe_2L_3]^{4+}$ binds and stablilises RNA three way junctions. The results also show that the effect of the iron cylinder on stabilising the three way junction structure is greater than the effect of the divalent cations. The expected interactions underpinning the stabilisation are electrostatic interactions between the highly positively charged (4+) complex and the negatively charged RNA phosphate backbone. Also, the hydrophobic interaction of the aromatic exterior of the iron cylinder which prefers to be accommodated in the hydrophobic cavity of an RNA three way junction. The perfect size and shape of the iron cylinder also plays a major role in the stabilisation, since the bulky cylinder possess the same charge, but is not capable of stabilising the RNA Y-shaped junction. A similar result but with a slightly higher stabilisation efficiency has been achieved

with the ruthenium cylinder, which has the same size and shape as the iron cylinder. The difference in the stabilisation of the two cylinders to the RNA three way junction could be one of the factors involved in the difference in cytotoxicity of the cylinders: the ruthenium cylinder is inactive in ovarian cancer cell lines while the iron cylinder is active.[16, 17] The binding of the iron cylinder to the RNA three way junction without perturbing the A-form structure of the arms is confirmed by circular dichroism. Furthermore, the results indicate that both M and P enantiomers can stabilise the three way junction but the M is apparently more effective than the P at high RNA concentration. This is also confirmed again by crystal structure achieved from Joachim Schnabl and Dr. Eva Freisinger, our collaborator, in Univeristy of Zurich, Switzerland. This crystal structure obtained from the solution of RNA three way junction and the racemic mixture demonstrates that only the M is located at the heart of the RNA three way junction. This result is similar to the binding of the two enantiomers to the DNA three way junction, in which the M enantiomer is more effective than the P enantiomer. Interestingly the iron cylinder also recognises bulged RNA three way junctions. This is important since the majority of RNA three way junctions present in nature consisting of bulged and looped structures, involving the specific protein binding such as HIV protein (Tat) to TAR. By this discovery, the binding of the iron cylinder to the specific region of the bulged RNA is possible to block the binding of the specific protein involving in the gene expression resulting in gene suppression. Beside, RNA conformation, in nature, the DNA-RNA hybrid could occur during transcription and there are only a few studies about this.[24] The iron cylinder shows the preferential binding to a specific combination of the DNA-RNA hybrid three way junction. Thus, RNA three way junctions might be an intriguing alternative target for this kind of supramolecular cylinder drug which is specifically

capable of inhibiting gene expression in translation level. Moreover, the competition assay has revealed that the iron cylinder prefers to bind to RNA three way junctions rather than DNA three way junctions however I am not completely convinced for this as the equilibrium being studied is not the simple competition between a RNA three way junction and a DNA three way junction as shown in **Figure 2.25.** Increasing RNA concentration in all experiments, as shown in this chapter, does lead to more three way junction formation. The studies are continuing in our group and collaborators to confirm the binding of the iron cylinder to RNA three way junctions and characterising by NMR and crystallography.

2.4 Experimental

RNA purification: All synthetic HPLC grade oligonucleotides (DNA; S1: CGGAACGGCACTCG, S2: CGAGTGCAGCGTGG, S3: CCACGCTCGTTCCG) and RNA (S1: CGGAACGGCACUCG, S2: CGAGUGCAGCGUGG, S3: CCACGCUCGUUCCG, S2(U): CGAGUGCUAGCGUGG, S2(UU): CGAGUGC UUAGCGUGG, S3(U): CCACGCUUCGUUCCG) used in this chapter were purchased from Microsynth, Switzerland. The purification is described as following. The oligonucletides were run on 18% denaturing polyacrylamide gel (42g urea, 10 ml of 10x TBE buffer (Geneflow), 45 ml of 40% acrylamide (29:1) (Geneflow)). The gel was run slowly at 5 watts, room temperature until the oligonucleotide had migrated approximately two thirds of the length of the gel. The gel was placed on Saran Wrap. It was then laid on fluorescent thin-layer chromatographic plate where the oligonucleotide is predicted to be. Then, a hand-held UV lamp was used to examine the oligonucleotide by illumination from above at 260 nm. The desired oligonucleotide, which should be the slowest-migrating band, was recovered by cutting the oligonucleotide band with a sharp and clean scalpel. The gel pieces were put in the electroelution machine (Bio-rad) applying 200 volt for 3 hours. 1 ml of solution containing oligonucleotide was collected from the machine every hour. To obtain the DNA pellet, the 3 ml DNA was precipitated with a solution containing 9 ml of absolute ethanol and 125 µl of 5 M NaCl and left at -20°C overnight. The solution was centrifuged at 9,500 rpm at 4 °C for 30 minutes. The supernatant was discarded then the DNA was dried in vacuum centrifuge (eppendorf) at 45 °C for 3 hours.

Radiolabelling RNA at 5´terminus: A reaction mixture of 10 µl in 1.5 ml Eppendorf containing 4.8 µl of MilliQ water, 1 µl of 10x bacteriophage T4 polynucleotide kinase buffer, 1.2 µl of 100 µM oligonucleotide, 1µl of bacteriophage T4 polynucleotide

kinase (Promega, UK) and 2 µl of γ-^{32}P ATP (6000 Ci/mmol, 10 mCi/ml) from Perkin Elmer were well mixed and incubated for 40 min at 37 °C. In addition to the reaction mixture, an excess of radioactivity is usually required for the labelling of nucleic acids. Considering the reaction mixture shown above, it suggests that the reaction mixture may either needs more γ-^{32}P ATP or needs less oligonucleotide by 40 times from the initial reaction mixture. Reducing the concentration of oligonucleotide will be more practical for a new radiolabelling recipe. To purify the labelled oligonucleotide the sample was mixed with 10 µl of formamide loading buffer and loaded into 18 % denaturing polyacrylamide gel running at 15 watts for 2.50 hours. The gel was taken out then wrapped with Saran and exposed to a phosphor imager plate for 10 minutes for visualisation. The band corresponding to labelled RNA was cut and crushed with a spatula in a 1.5 ml eppendorf. After adding 4 times volume of elution buffer (10 mM MOPS pH 6, 1 mM EDTA, 250 mM NaCl) to a volume of cut gel pieces, the eppendorf was placed on a shaker at 4 °C for 2 hours. The mixture was centrifuged at 13,000 rpm for 5 min to separate gel pieces from the solution. To precipitate RNA three volumes of cold ethanol were added to supernant and left at -20°C overnight. The solution was centrifuged at 13,000 rpm for 5 minutes and the supernatant was discarded. The eppendorf was placed under vacuum to dry off the ethanol residual. Finally a pellet was dissolved in 50 µl of milliQ water. The concentration of the labelled strand was measured by a scintillator machine from the mixture of 1 µl of labelled strand and 5 ml of scintillator solution. The calculation is shown in the **Appendix**.

Gel electrophoresis experiment

Polyacrylamide gel preparation: 15% native polyacrylamide gel solution containing 20 ml of 10x TB buffer pH 8.3 (890 mM tris(hydroxymethy) amino methane, 890

mM boric acid), 75 ml of 40% acrylamide (29:1) from Geneflow, 105 ml of milliQ water, 1ml of 10%(w/v) ammonium persulfate and 100 µl TEMED, was poured onto a set of glass plates. The wells of the polymerised gel were thoroughly washed with a running buffer (TB buffer) before use. Note that prerunning of the gel at 200 volts for 5 minutes is required before the experiment is performed.

Gel electrophoresis experiment: 10 µl of the samples in 1.5 ml eppendorf tubes were prepared by mixing equal amounts of three strands of oligonucleotides (10 nM as final concentration for low RNA concentration and 0.2 µM as final concentration for high RNA concentration) with the metal complex in TBN buffer (100 µM or 100 mM NaCl in case of low and high salt concentration respectively.). Ratios of RNA per strand to complex were 3:0.5, 3:1, 3:2 and 3:10 respectively. The samples were then incubated at room temperature for 1 hour and on ice for 20 min. 5 µl of 30% glycerol was added to each sample to increase the density of the sample to be able to sink into a well. All samples then were loaded into 15% native polyacrylamide gel. Note that loading dye (5x GelPilot DNA Loading Dye, QIAGEN) was separately loaded into the first and the last well to mark where the RNA migrates to. The gel was run at 5 watts for 4 hours then the gel was placed in between a sheet of 3MM whatman paper and Saran wrap. The gel was dried on a Maxi gel dryer (Thermo Scientifc) at 85°C for 20 minutes. The dried gel was cooled to room temperature. A phosphorimaging plate (Amersham, GE health care) was exposed to the gel overnight. The bands were visualised by scanning the phosphorimaging plate on typhoon storm (GE healthcare). The ImageQuant TL from Amersham Bioscience was used for the quantification.

Circular Dichroism (CD) Measurements: A spectropolarimeter (JASCO) was used for CD measurements. The experiments were performed at 20 °C with 0.1 and 1 cm path length cuvettes (Strana) for measuring at 200-400 nm and 400-750 nm

respectively. Before the measurement, the RNA samples were heated to 95 °C for 5 min then gently cooled down by thermal block. 30 μM total strand concentration of RNA in buffers of 0.89 mM Na-cacodylate (pH 7.0) and 20 mM NaCl were titrated with stock solution 700 μM complex various from stochiometry of RNA 3WJ and complex from 1:0.5 to 1:10. During the titration UV-Vis spectra (Cary 5000) were recorded.

DNA and RNA three way junction hybridisation: 10 μl of the samples in 1.5 ml eppendorf tubes were prepared by mixing the combination of RNA, DNA and DNA-RNA hybrid three way junctions in equal amounts of three strands of oligonucleotides (0.2 μM as final concentration) with the metal complex in TBN buffer (100 mM). Ratios of nucleic acid three way junction per strand to complex was 3:1. The samples were then incubated at room temperature for 1 hour and on ice for 20 min. 5 μl of 30% glycerol was added into each sample to increase the density of the samples to be able to sink into a well. All samples then were loaded into 15% polyacrylamide gel. Note that loading dye (5x GelPilot DNA Loading Dye, QIAGEN) was separately loaded into the first and the last well to mark where the RNA migrates to. The gel was run at 5 watts for 4 hours then the gel was placed in between a sheet of 3MM whatman paper and Saran wrap. The gel was dried on a Maxi gel dryer (Thermo Scientifc) at 85°C for 20 minutes. The dried gel was cooled to room temperature. A phosphorimaging plate (Amersham, GE health care) was exposed on the gel overnight. The bands were visualised by scanning the phosphorimaging plate on typhoon storm (GE healthcare). The ImageQuant TL from Amersham Bioscience was used for the quantification.

Competition assay between the DNA and RNA three way junction to the iron cylinder: The stock solutions of the DNA and RNA three way junction (0.4, 1.0, 2.0

and 5.0 μM) were prepared by combining equimolar quantities of preformed oligonucleotides (DNA and RNA) in TBN buffer. It should be noted that strand 1 of DNA and RNA were labelled. Five samples containing 0.2 μM of the DNA three way junction as a final concentration and the iron cylinder (0.2 μM) were mixed in each tube. The solutions were incubated at room temperature for an hour. The RNA three way junction from the stock solution was added to obtain the final concentration 40 nM, 100 nM, 200 nM, 400 nM and 1000 nM. The same experiment was carried out again but the DNA three way junction was added to constant concentration of RNA three way junction and the iron cylinder. All samples were incubated again at room temperature for an hour. 5 μl of 30% glycerol was added to each sample. Then, the samples were loaded onto 20% non-denaturing polyacrylamide gel. The gel was run for 4 hours at 5 watts. The gel was dried and exposed on phosphorimaging machine overnight in the film cassette. The autoradiogram was developed by scanning the plate on the scanner. The quantification was performed by ImageQuant.

The triple stranded helicate $[Fe_2(L\text{-}CF_3)_3]Cl_4$ synthesis:[25]

Ligand (L-CF_3; $C_{27}H_{18}N_4F_6$) synthesis: 4, 4′-(Hexafluoroisopropylidene)-dianiline (0.55g, 1.65 mmol) and 2-pyridinecarboxaldehyde (0.35g, 3.28 mmol) were added to methanol (25 cm^3). Then, five drops of acetic acid were added to the solution. The mixture was heated to reflux for 5 hours. The solvent was removed by rotary evaporation to produce green oil (0.71g, 84%) and used without further purification.

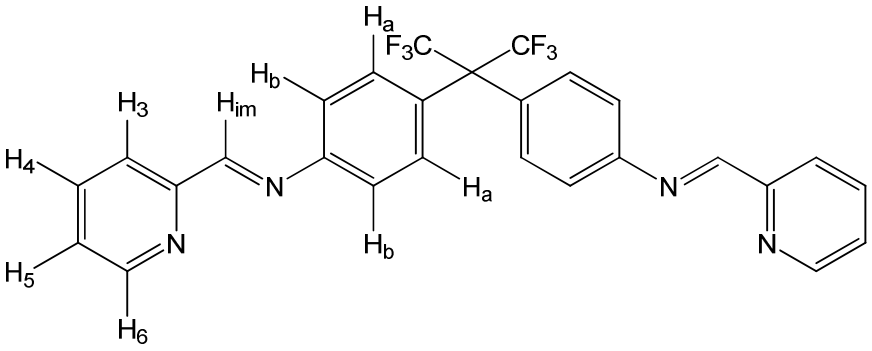

Mass spectrum (ESI): *m/z* 513 {M+H}.

^{1}H NMR (300 MHz, $CDCl_3$, 298K):δ 8.75 (2H, d, J = 3.4 Hz, H_6), δ 8.64 (2H, s, H_{im}), δ 8.23 (2H, dt, J = 7.9,1.2 Hz, H_3), δ 7.86 (2H, td, J = 7.6, 1.7 Hz, H_5), δ 7.50 (4H, d, J = 8.5 Hz, $H_{a/b}$), δ 7.42 (2H, ddd, J = 7.9, 4.9, 1.3 Hz, H_4), δ 7.30 (4H, d, J = 8.5 Hz, $H_{a/b}$).

Coordination of L-CF_3 to iron (II)

The ligand (L-CF_3) (0.60g, 1.17 mmol) and iron (II) chloride tetrahydrate (0.16g, 0.78 mmol) were added to methanol (25 cm^3). After 2 hours of stirring, the deep purple solution was obtained. The iron (II) triple stranded helicate was precipitated upon the addition of diethylether and following with the filtration. Then, it was allowed to dry in a vacuum dessicator. The purple solid was obtained (0.62g, 89%).

Mass spectrum (ESI): *m/z* 561 $\{[Fe_2(L\text{-}CF_3)]Cl\}^{3+}$, 412 $[Fe_2(L\text{-}CF_3)]^{4+}$

^{1}H NMR (300 MHz, CD_3OD, 298K): δ 9.21 (2H, s, H_{im}), δ 8.72 (2H, d, J = 6.8 Hz, H_3), δ 8.52 (2H, t, J = 6.8 Hz, H_4), δ 7.90 (4H, m, $H_{a/b\ \&\ 5}$), δ 7.44 (2H, d, J = 4.5 Hz, H_6), δ 6.83 (4H, d, J = 8.2 Hz, $H_{a/b}$), δ 6.05 (4H, d, J = 7.7 Hz, $H_{a/b}$), δ 5.11 (4H, d, CH_2, J = 7.9 Hz, $H_{a/b}$)

Elemental analysis calculated (%) for $[Fe_2(L\text{-}CF_3)_3]Cl_4.9.5H_2O$: C: 49.61, H: 3.76, N: 8.58; found: C: 49.58, H: 3.74, N: 8.58.

The triple stranded helicate $[Fe_2L_3]Cl_4$ synthesis[25]:

Ligand (L; $C_{25}H_{20}N_4$) synthesis: 4, 4'–Methylenedianiline (1.0g, 5.04 mmol) was combined with 2-pyridinecarboxaldehyde (1.08g, 10.08 mmol) in ethanol (50 cm^3) and the solution was allowed to stir overnight. The yellow precipitate was filtered off and dried in *vacuo* (1.57g, 82.6 %).

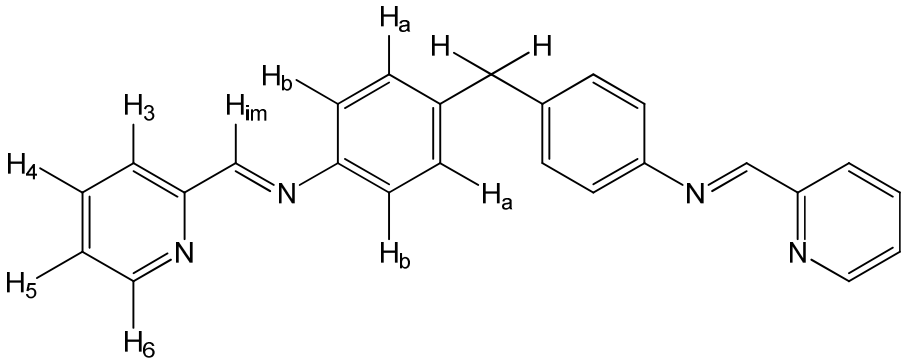

Mass spectrum (ESI): *m/z* 377 {M+H}.

^{1}H NMR (300 MHz, $CDCl_3$, 298K): δ 8.72 (2H, d, J = 3.9 Hz, H_6), δ 8.62 (2H, s, H_{im}), δ 8.23 (2H, d, J = 7.0 Hz, H_3), δ 7.83 (2H, td, J = 8.3, 1.9, 0.6 Hz, H_4), δ 7.41 (2H, ddd, J = 7.6, 4.9, 1.2 Hz, H_5), δ 7.30 (8H, m, $H_{a/b}$), δ 4.09 (2H, s, CH_2)

Coordination of L to Iron (II)

The iron triple helicate $[Fe_2L_3]Cl_4$ was synthesised by simply mixing of the ligand (L; 0.3 g, 0.797 mmol) with iron(II) chloride tetrahydrate (0.106 g, 0.533 mmol) in methanol (25 cm^3) at room temperature. The purple solution, characteristic of iron(II) tris-pyridylimine compounds, was stirred for 3 hours. The purple compound was precipitated by diethylether. The purple precipitate was filtered off and dried *in vacuo* (0.33 g, 87 %).

Mass spectrum (ESI): *m/z* = 425 $\{[Fe_2L_3]Cl_3\}^+$, 310 $[Fe_2L_3]^{4+}$

^{1}H NMR (300 MHz, CD_3OD, 298K): δ 9.17 (2H, s, H_{im}), δ 8.70 (2H, d, J = 7.2 Hz, H_3), δ 8.49 (2H, td, J = 7.7, 1.1 Hz, H_4), δ 7.86 (2H, ddd, J = 5.6, 1.1 Hz, H_5), δ 7.46 (2H, d, J = 5.2 Hz, H_6), δ 7.04 (4H, broad, $H_{a/b}$), δ 5.61 (4H, broad, $H_{a/b}$), δ 4.07 (2H, s, CH_2)

Elemental analysis calculated (%) for $[Fe_2L_3]Cl_4.7H_2O$: C: 59.74, H: 4.95, N: 11.16; found: C: 59.22, H: 4.95, N: 11.05.

Separation of the iron cylinder $[Fe_2L_3]Cl_4$ enantiomers

A cellulose column was prepared by pouring a suspension containing 6 g of cellulose and 40 ml of 20 mM aqueous sodium chloride into a 2 x 30 cm sintered column. 25 mg of $Fe_2L_3Cl_4$ diluted in 100 µl of 20 mM sodium chloride was loaded onto the column (approximately 5 mg/ml). The fractions were collected by visual separation of two bands, one from each purple band. Each fraction was desalted by using Sephadex G10: Sephadex G10 was swelled in methanol for 3 hours and was packed into a 1 x 30 cm sintered column by pouring the slurry into the column taking care not to trap air bubbles. The compound was loaded and eluted with methanol. The purple fraction was collected and dried using a freeze dryer. The UV-Vis absorbance and CD of each fraction were recorded to check the purity of obtained enantiomers.

2.5 References

1. A. Oleksi, A. G. Blanco, R. Boer, I. Uson, J. Aymami, A. Rodger, M. J. Hannon and M. Coll, *Angew. Chem. Int. Ed.*, 2006, **45**, 1227-1231.
2. L. Cerasino, M. J. Hannon and E. Sletten, *Inorg. Chem.*, 2007, **46**, 6245-6251.
3. J. Malina, M. J. Hannon and V. Brabec, *Chem. Eur. J.*, 2007, **13**, 3871-3877.
4. T. Hermann, *Angew. Chem. Int. Ed.*, 2000, **39**, 1891-1905.
5. N. D. Pearson and C. D. Prescott, *Chem. Biol.*, 1997, **4**, 409-414.
6. S. J. Sucheck and C. H. Wong, *Curr. Opin. Chem. Biol.*, 2000, **4**, 678-686.
7. Y. Tor, *Angew. Chem. Int. Ed.*, 1999, **38**, 1579-1582.
8. C. S. Chow and F. M. Bogdan, *Chem. Rev.*, 1997, **97**, 1489-1513.
9. R. Schroeder and U. Von Ahsen, in *Nucleic Acids & Molecular Biology*, Eds. F. Eckstein and D. M. J. Lilley, Springer Verlag, Berlin, Edn., 1996, vol. 10, pp. 53-74.
10. T. Hermann and E. Westhof, *J. Med. Chem.* , 1999, **42**, 1250-1261.
11. W. Saenger, *Principle of nucleic acid structure*, Springer, New York, 1984.
12. D. M. J. Lilley, *Biopolymers*, 1998, **48**, 101-112.
13. M. Eriksson, B. Nordén and M. J. W. Jonathan B. Chaires, in *Methods in Enzymology*, Academic Press, Edn, 2001, vol. Volume 340, pp. 68-98.
14. N. B. Leontis, W. Kwok and J. S. Newman, *Nucleic Acids Res.* , 1991, **19**, 759-766.
15. J. L. Kadrmas, A. J. Ravin and N. B. Leontis, *Nucleic Acids Res.* , 1995, **23**, 2212-2222.
16. G. I. Pascu, A. C. G. Hotze, C. Sanchez-Cano, B. M. Kariuki and M. J. Hannon, *Angew. Chem. Int. Ed.*, 2007, **46**, 4374-4378.

17. A. C. G. Hotze, N. J. Hodges, R. E. Hayden, C. Sanchez-Cano, C. Paines, N. Male, M. K. Tse, C. M. Bunce, J. K. Chipman and M. J. Hannon, *Chem. Biol.*, 2008, **15**, 1258-1267.

18. J. M. C. A. Kerckhoffs, J. C. Peberdy, I. Meistermann, L. J. Childs, C. J. Isaac, C. R. Pearmund, V. Reudegger, S. Khalid, N. W. Alcock, M. J. Hannon and A. Rodger, *Dalton Trans.*, 2007, 734-742.

19. I. Meistermann, V. Moreno, M. J. Prieto, E. Moldrheim, E. Sletten, S. Khalid, P. M. Rodger, J. C. Peberdy, C. J. Isaac, A. Rodger and M. J. Hannon, *Proc. Natl. Acad. Sci. USA*, 2002, **99**, 5069-5074.

20. J. Schnabl, S. Paulus, S. Phongtongpasuk, M. J. Hannon, B. Spingler, E. Freisinger and R. K. O. Sigel, in *RNA versus DNA: Three-way junctions induced by the same molecular cylinder, but being distinctly different*, Unpublished work, edn., 2009.

21. C. Dingwall, I. Ernberg, M. J. Gait, S. M. Green, S. Heaphy, J. Karn, A. D. Lowe, M. Singh and M. A. Skinner, *EMBO J.*, 1990, **9**, 4145-4153.

22. K. M. Weeks, C. Ampe, S. C. Schultz, T. A. Steitz and D. M. Crothers, *Science*, 1990, **249**, 1281-1285.

23. T. M. Rana and K.-T. Jeang, *Archives of Biochemistry and Biophysics*, 1999, **365**, 175-185.

24. N. N. Shaw and D. P. Arya, *Biochimie*, 2008, **90**, 1026-1039.

25. M. J. Hannon, C. L. Painting, A. Jackson, J. Hamblin and W. Errington, *Chem. Commun.*, 1997, 1807-1808.

Chapter 3

The recognition and stabilisation of a DNA three way junction by a metallosupramolecular cylinder

3.1 Introduction

In the postgenomic era, more information about how DNA sequence is responsible for gene function has been unveiled. This information is useful in many aspects. One example is that gene expression, which can cause disease either from over expression or decreased expression, can now start to be controlled. This can be achieved by creating a synthetic agent which can recognise either the sequences or the structure of DNA and bind selectively to DNA. In principle, this might be used to normalise the gene expression, stopping the disease.[1]

One strategy for designing these agents is to imitate the traits, such as size or shape, of a natural DNA recognition protein i.e. alpha helix or zinc finger protein. The synthetic agent designed may be able to interact in a similar way to natural DNA recognising biomolecules. By exploiting supramolecular chemistry as an approach to design and synthesise a DNA binding agent, Hannon *et al*. created a tetracationic triple stranded helicate ($[Fe_2L_3]^{4+}$, L = $C_{25}H_{20}N_4$). The synthesis involves only one step, offering a high yield with cheap starting materials.[2] This helicate, a iron cylinder, has a cylindrical shape. The dimensions of this cylinder, obtained from its crystal structure, are ~1.8 nm in length and ~1 nm in diameter. DNA binding studies of the helicate show that it binds to natural polymeric DNA like ct-DNA in the DNA major groove and causes dramatic intramolecular DNA coiling. This effect is reminiscent of DNA coiling induced by histones in the nucleus of living cells.[3] Biological testing with several cancer cell lines indicates that the iron cylinder has cytotoxicity to cancer cells without exhibiting genotoxicity.[4] Interestingly, an unprecedented DNA binding mode for the iron cylinder was revealed when a palindromic hexaoligonucleotide sequence of DNA was used in a

crystallographic approach. Surprisingly, rather than duplex DNA binding, the three strands of palindromic DNA formed a Y-shaped DNA three way junction with the iron cylinder sitting in the middle as shown in **Figure 3.1**.[5] Although this is mentioned in **Section 1.1.4.6**, it is worth considering this structure in more detail since it is the key to the work in this chapter.

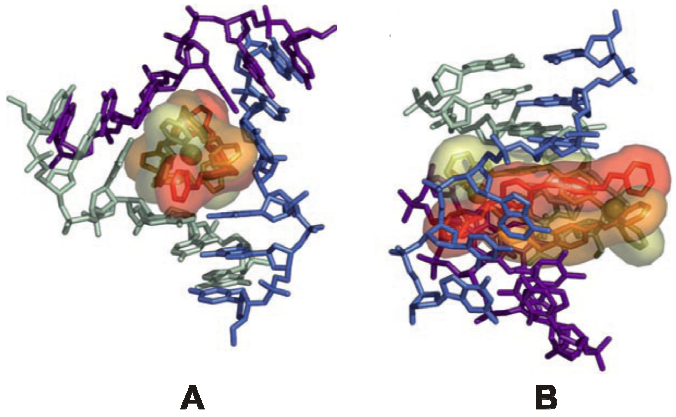

Figure 3.1 The crystal structure of $[Fe_2L_3]^{4+}$ and palindromic hexaoligonucleotide. **A)** Top view of $[Fe_2L_3]^{4+}$ binding to DNA major groove. **B)** Lateral view of the iron cylinder interacting with DNA three way junction. Taken from ref.[5]

This unprecedented DNA structure, in which the supramolecular helicate $[Fe_2L_3]^{4+}$ located at the heart of a DNA Y-shaped junction, is supported by several non covalent interactions.[5] The cylinder has a high positive charge (4+) and interacts with the negatively charged phosphate backbone of DNA through electrostatic interactions (**Figure 3.2A**). Moreover, the three bis-pyridylimine ligands provide a large hydrophobic surface allowing the helicate to be accommodated in the hollow hydrophobic cavity of the DNA three way junction. The information gained from the crystal structure shows

that the spacer unit of the ligand, consisting of two phenyl rings, can form π-π stacking interaction with the thymine and adenine bases of the junction (**Figure 3.2B**).

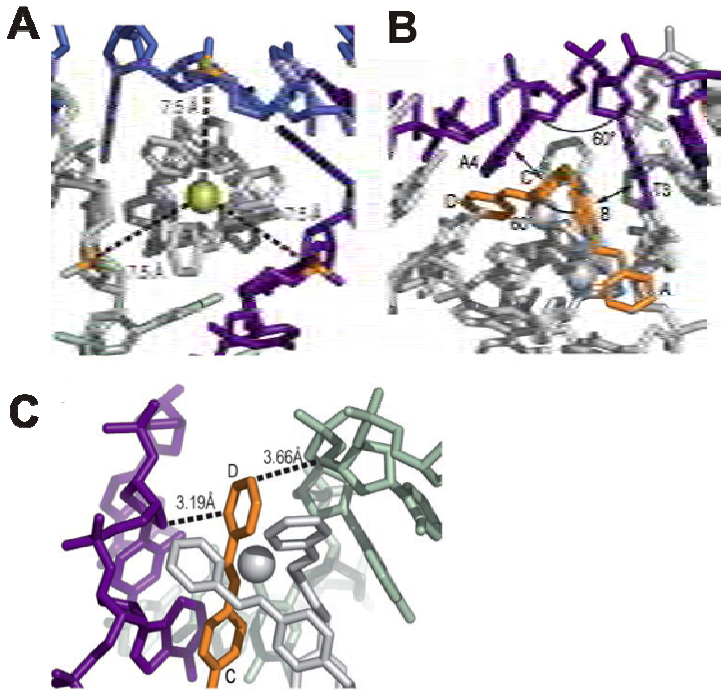

Figure 3.2 A) View from the minor groove illustrating threefold axis of the iron interacting with the phosphate backbone of DNA via electrostatic interactions. **B)** π-π stacking interaction between the phenyl ring (labeled as C and B) and base A and T. **C)** Interaction between terminal phenyl ring of the cylinder and the minor groove DNA. Taken from ref.[5]

Sandwiching interactions in the minor grooves from the pyridine rings at the end of the cylinder were also observed (**Figure 3.2C**). In addition, hydrogen bonding was also detected from the imine hydrogen adjacent to the minor groove end of the cylinder forming a C-H···X hydrogen bond with N3 nitrogen of adenine. The interactions mentioned above allow such a structure to be formed and eventually stabilised. Further studies were carried out by NMR[6] and radioactive polyacrylamide gel electrophoresis.[7]

These studies confirm this unprecedented binding mode is not solely an artifact from the crystal structure but rather a real structure seen in both the solid state and solution.

Three way junction and related structures are involved in many biological functions in both RNA and DNA. The splicing process[8] and translation[9-11] are examples of the function of RNA three way junctions while a DNA three way junction known as a replication fork is present as the intermediate structure during DNA replication.[9] The DNA three way junction is also believed to be associated with several human genetic diseases such as myotonic dystrophy type1 and Huntingtons disease.[10] The relevance to the replication fork means that the DNA three way junction can be proposed as a new target for anticancer agents. Binding to a replication fork should inhibit cancer cell's growth and eventually lead to apoptosis, programmed cell death. The crystallographic studies show that the dimensions of the cylinder are crucial to the DNA recognition. Changing the dimensions of the cylinder will alter the DNA binding properties: Uerpmann *et al.* probed the effect of dimensional change on the dimetallo supramolecular cylinder by inserting a ketimine spacer unit between the pyridylimime and diphenyl methane of the parent ligand, the bispyrimidylimine ligand (**Figure 3.3B**).[11] The new tetracationic supramolecular helicate was longer and wider than the parent cylinder (**Figure 3.3E**) but the cylindrical shape was retained. DNA binding studies of the complex with ct-DNA showed that the modified cylinder retained its DNA binding. However, the DNA coiling effect of the new cylinder was much less than the parent cylinder. Peberdy *et al.* have introduced a methyl group on the parent ligand at the 3 and 5 positions on the pyridyl ring adjacent to the metal binding site unit as shown in **Figure 3.3C; L^3 and L^5**, repectively.[12] The 3 methyl group points directly out of the sides of the

cylinder (**Figure 3.3F**) while the 5 methyl group is located at the ends of the cylinders and does not dramatically affect the cylindrical surface itself (**Figure 3.3G**). Investigation of the DNA binding behavior of the two compounds showed that the DNA binding of the position 3 methyl substituted cylinder was weaker than the parent cylinder, as was the coiling effect. For the position 5 methyl substituted cylinder, the DNA binding was found to be comparable to that of the parent compound. These previous two studies indicate that the dimensions of the tetracationic dimetallo supramolecular iron cylinder are the key feature of its DNA binding ability to the major groove of ct-DNA.

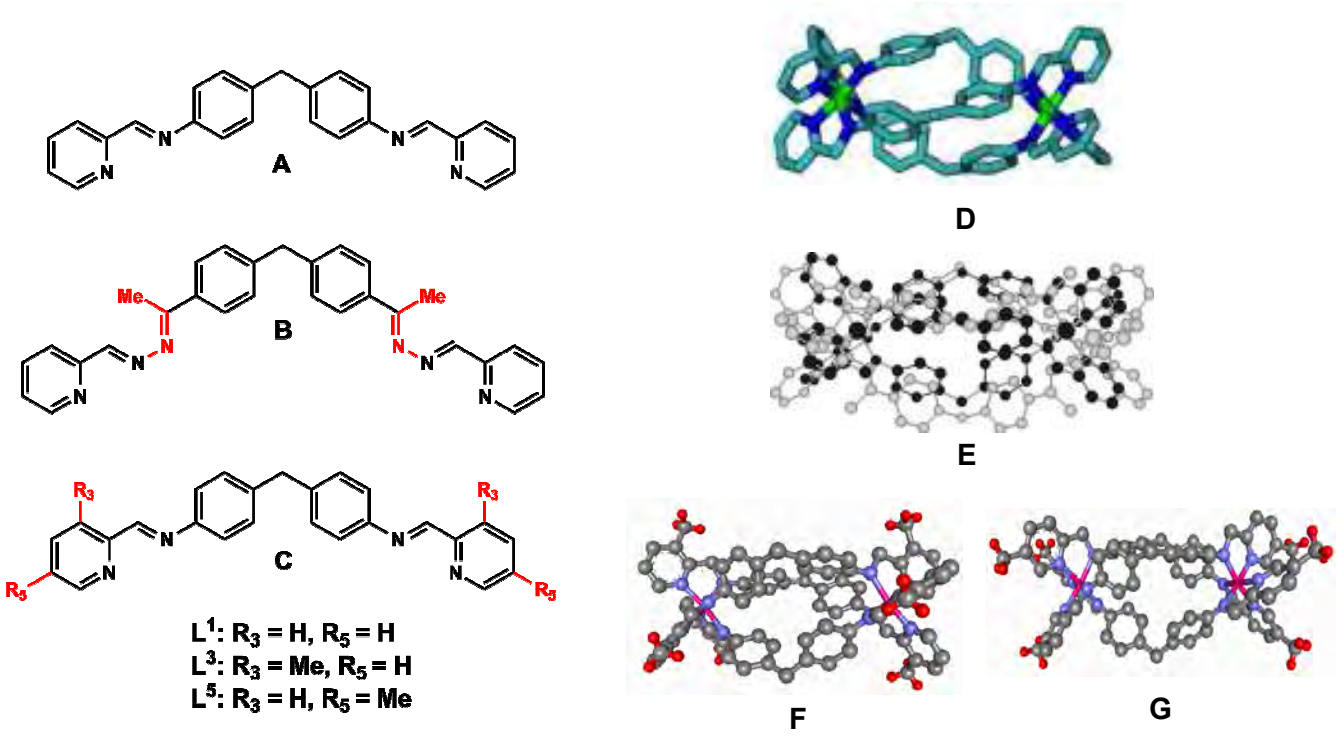

Figure 3.3 The chemical structures of ligand modification to form tetracationic supramolecular iron cylinders. **A)** Parent ligand. **B)** Uerpmann's ligand.[11] The ketimine group (labled as red letter) was inserted between the diphenylmethane spacer and pyridylimine metal binding site units. **C)** Peberdy's ligand.[12] The methyl group is substituted at the position as labelled. **D)** Crystal structure of the parent cylinder. **E)** Overlay of crystal structure of parent cylinder (black) and Uerpmann's cylinder (grey). **F), G)** Crystal structure of Peberdy's iron cylinder with L^3 and L^5 ligand, repectively. Taken from ref.[11, 12]

The focus of this chapter is to explore the effect of the size, shape and coordinated metal centre of the cylinders on the recognition of a DNA three way junction. Gel electrophoresis proves to be a powerful way to probe this and a competition assay of the DNA three way junction and other DNA structures is also presented.

3.2 Results and discussion

3.2.1 Overview

In order to achieve more information about this unprecedented DNA binding mode, the recognition of three way junction by metallo-supramolecular cylinders are investigated with the aid of polyacrylamide gel electrophoresis (PAGE). The sensitivity of this technique can be increased by the use of radioactivity labeling on a DNA strand instead of ethidium bromide staining. In this technique, it requires very low concentration of the cylinders and DNA (in μM concentration) compared to that used for crystallographic approach (in mM concentration). Therefore, an artifact arising from crystal packing from X-ray study can be excluded from the experiment.

DNA sequences used in this experiment were designed to employ a 14-mer nonpalindromic oligonucleotide (**Figure 3.4A**) as it has been shown in literature to be the minimum length of DNA required for a three way junction lacking unpaired bases to stay stable during electrophoresis on a native gel at 5 °C but not stable at higher temperature i.e. at room temperature.[13] The idea of this experiment is that in the absence of the cylinder, the pre-formed single stranded DNAs will appear as single stranded DNAs at room temperature since the DNA three way junction can not form.

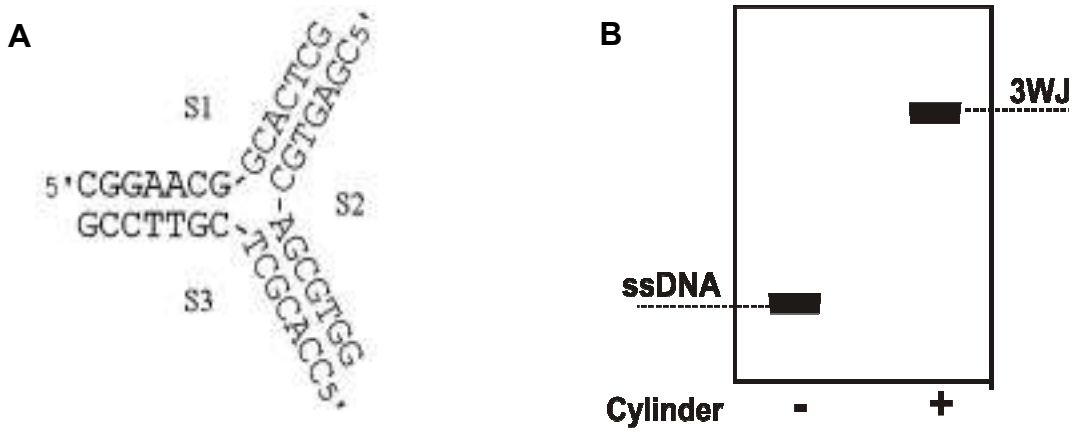

Figure 3.4 **A)** Sequences used to form fully paired DNA three way junction.[7] **B)** Idea of PAGE experiment to probe the recognition and stabilisation of three way junction DNA by the cylinder.

However in the presence of the iron cylinder, the formation of three way junction DNA will be observed as the result of the recognition and stabilisation of the DNA by the complex (**Figure 3.4B**). It should be noted that this study was carried out in the lab of Professor Viktor Brabec at Institute of Biophysics Academy of Sciences, Brno, Czech Republic.[7] The conditions and apparatus used to perform the experiments, mentioned in the publication, were however different from what we have in Birmingham therefore the gel experiments were established again in the group of Professor Kevin Chipman, School of Bioscience, University of Birmingham.

3.2.2 Establishing purity of labelled strand

When using radioactive polyacrylamide gel electrophoresis the labelling of a DNA strand is required. In this experiment, oligonucleotide (strand 3) was labelled with γ-phosphate of ATP at the 5' terminus by catalysing of bacteriophage T4 polynucleotide kinase.[14] The forward reaction in which the γ-phosphate is transferred to the 5' terminus of dephosphorylated DNA is employed. As the electrophoresis experiment to be conducted is a high sensitivity method, the purity of the labelled strand must be determined. This is because any contamination from oligonucleotide (n-1) will be detected and subsequently will affect the experiment. Therefore, it is important to check the purity of the labelled strand and this is achieved by running the labelled oligonucleotide on denaturing polyacrylamide gel.

Figure 3.5 The autoradiogram of labelled oligonucleotide run on 18% denaturing polyacrylamide gel electrophoresis.

The result (**Figure 3.5**) shows that the labelled oligonucleotide produces a single band indicating that the oligonucleotide is pure. Therefore this labelled oligonucleotide (strand 3) was used for further experiments.

3.2.3 Recognition and stabilisation of the iron cylinder $[Fe_2L_3]^{4+}$to DNA three way junction

As mentioned in **Section 3.2.1,** these PAGE studies were carried out and published in the lab of Professor Brabec.[7] To establish the same experiment in the lab of Professor Chipman, our collaboration from School of Bioscience, University of Birmingham, a control experiment is needed to carry out to ensure that the changed condition of the experiment will produce the same result.

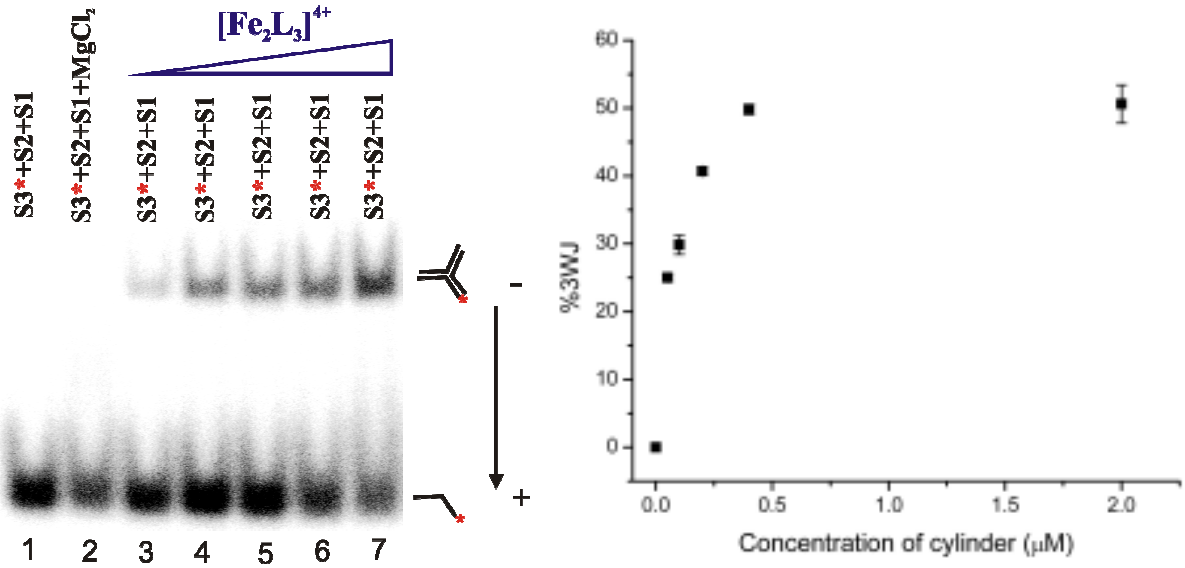

Figure 3.6 Left: The autoradiogram of 15% PAGE running at room temperature. Lane 1: S3*+S2+S1 in TBN buffer. The concentration of oligonucleotide was 0.2 μM per strand. Lane 2: S3*+S2+S1 with 10 mM $MgCl_2$. Lane 3-7: S3*+S2+S1 with $[Fe_2L_3]^{4+}$ increasing the ratio of DNA per strand to complex from 3:0.25, 3:0.5, 3:1, 3:2 and 3:10, corresponding to 0.05, 0.1, 0.2, 0.4 and 2 μM of the complex, respectively. **Right:** the graphical plot of concentration of iron cylinder (μM) as a function of % DNA three way junction. The red asterisk represents labeled strand. The plot represents the means of three individual experiments ± SD (n = 3).

The results (**Figure 3.6**) shows that a band corresponding to the DNA three way junction was observed in the presence of the iron cylinder and three oligonucleotides (lane 3-7) while the control containing three oligonucleotides and no cylinder produced

only a band corresponding to single stranded DNA (lane 1). This indicates that three way junction formation can occur only in the presence of the iron cylinder. The iron cylinder not only binds to the DNA three way junction but also stabilises the structure. Surprisingly, the three way junction band was not formed in the presence of magnesium chloride which was used as a positive control at room temperature (**Lane 2**). It could be possible that the stabilisation of magnesium chloride to DNA three way junction was less than that of the iron cylinder therefore only a band corresponding to single strand was detected. However, it has been shown that magnesium chloride can promote three way junction formation at 5°C.[7] Furthermore, increasing the concentration of iron cylinder results in enhanced formation of DNA three way junction. At the point where the iron cylinder is in excess, the graph levels off. In addition, this PAGE experiment for investigating the recognition and stabilisation of three way junction DNA by the iron cylinder was successfully established as achieved results are similar to the publication.[7]

3.2.4 Recognition and stabilisation of the ruthenium cylinder $[Ru_2L_3]^{4+}$ and its enantiomers to DNA three way junction: effect of the metal on three way junction formation

Next, the effect of changing the metal in the cylinder on three way junction stabilisation was probed using a ruthenium cylinder. Ruthenium has been highlighted as an advantageous metal for metal based anticancer drugs due to several attractive features. The advantages of utilising ruthenium are described as follows.[15-18] First, ruthenium provides a variety of oxidation states e.g. Ru^{II}, Ru^{III} and Ru^{IV} which can be accessed under physiological conditions resulting in remarkably good anticancer activity. Second,

ruthenium compounds are less toxic when compared to platinum compounds due to the ability of ruthenium to mimic iron in the binding to the significant biological molecules such as serum, transferrin and other proteins. In addition, the novel mechanism of ruthenium based anticancer drug is obtained from the octahedral coordination geometry of the metal, which is completely different from the square planar geometry of platinum (II). This is also believed to overcome drug resistance which was one of the main disadvantages of platinum based drug.

To combine the intriguing features of ruthenium and the unprecendent DNA binding mode of the iron cylinder, a dinuclear ruthenium(II) triple stranded helicate $[Ru_2L_3]^{4+}$ was synthesised.[19] The size and shape of the ruthenium complex (**Figure 3.7**), $[Ru_2L_3]^{4+}$, is similar to the iron cylinder, $[Fe_2L_3]^{4+}$, with a cylindrical shape with ~1.8 nm in length and ~1 nm in width.

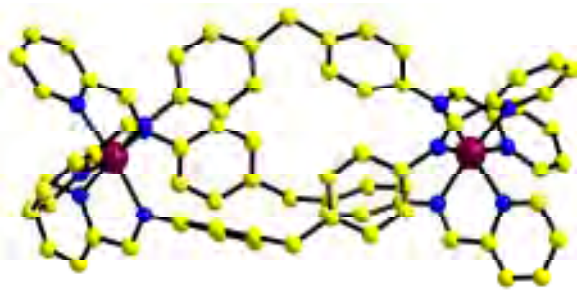

Figure 3.7 X-ray crystal structure of $[Ru_2L_3]^{4+}$. The red, blue and yellow spheres represent Ru, N and C, respectively. [19]

Interestingly, this ruthenium cylinder is fluorescent which may enable its application as a probe. The visualisation of the DNA binding of this compound in the nuclei of tumor cells and the proliferation of these tumor cells in real time could be achieved. Moreover, the ruthenium triple stranded helicate it is shown to bind to DNA and coil DNA in a

similar way to the parent cylinder.[20] However, the cytotoxicity of the ruthenium cylinder is different from that of the iron cylinder. The iron cylinder is active against an ovarian cancer cell line while the ruthenium cylinder is not.[4, 22] This indicates that the mechanism of action of the ruthenium cylinder interaction with DNA could be different from that of the iron cylinder. One interesting DNA binding property of the iron cylinder is the unprecedented DNA three way junction binding mode. However, the three way junction binding ability of the ruthenium cylinder has not yet to be explored. To investigate this unusual DNA binding mode with the ruthenium cylinder, a radioactive gel experiment was carried out. The ruthenium cylinder was kindly provided by Anna Leczkowska from our group.

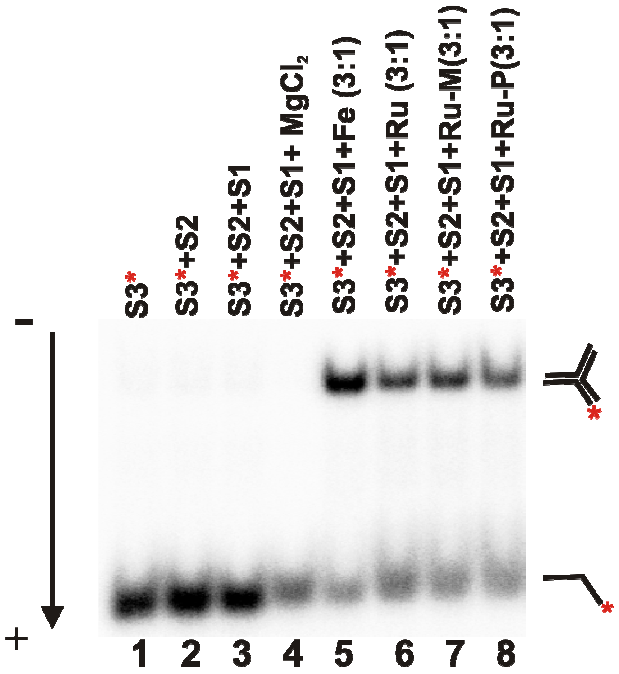

Figure 3.8 Autoradiogram of ruthenium triple stranded helicate binding to DNA. Lane 1-4: control containing S3*, S3*+S2, S3*+S2+S1 and S3*+S2+S1 with 50 mM $MgCl_2$ respectively in Tris-borate containing 100 mM NaCl buffer. The concentration of the oligonucleotide is 0.2 μM per strand. Lane 5-8: containing S3*+S2+S1 with $[Fe_2L_3]^{4+}$, $[Ru_2L_3]^{4+}$and their enantiomers e.g. M and P enantiomers at ratio 3 to 1 (DNA per strand : complex).

The results (**Figure 3.8**) demonstrate that in the presence of the ruthenium triple stranded helicate, the three way junction was formed. This reveals that the ruthenium cylinder and its enantiomers can recognise and stabilise the DNA three way junction.

The $[Ru_2L_3]^{4+}$ helicate has two enantiomers, which are the M enantiomer or left handed helicate and the P enantiomer or right handed helicate. Both enantiomers were separated easily using a cellulose column and NaCl solution as eluent (work of Anna Leczkowska). This separation method is again similar to that of the iron cylinder.[21] To probe the stabilisation ability of the enantiomers of the ruthenium cylinder with a DNA three way junction, a gel experiment was carried out. The experiment was performed by treating a constant concentration of oligonucleotide (S1, S2 and S3) with increasing ratio of DNA (per strand) and ruthenium complex from 3:0, 3:0.5, 3;1 to 3:2 corresponding to 0, 0.2, 0.4 and 0.8 μM of the complex. The effect of each enantiomer on the stabilisation of DNA three way junction is compared by plotting the percentage of three way junction obtained as a function of complex concentration.

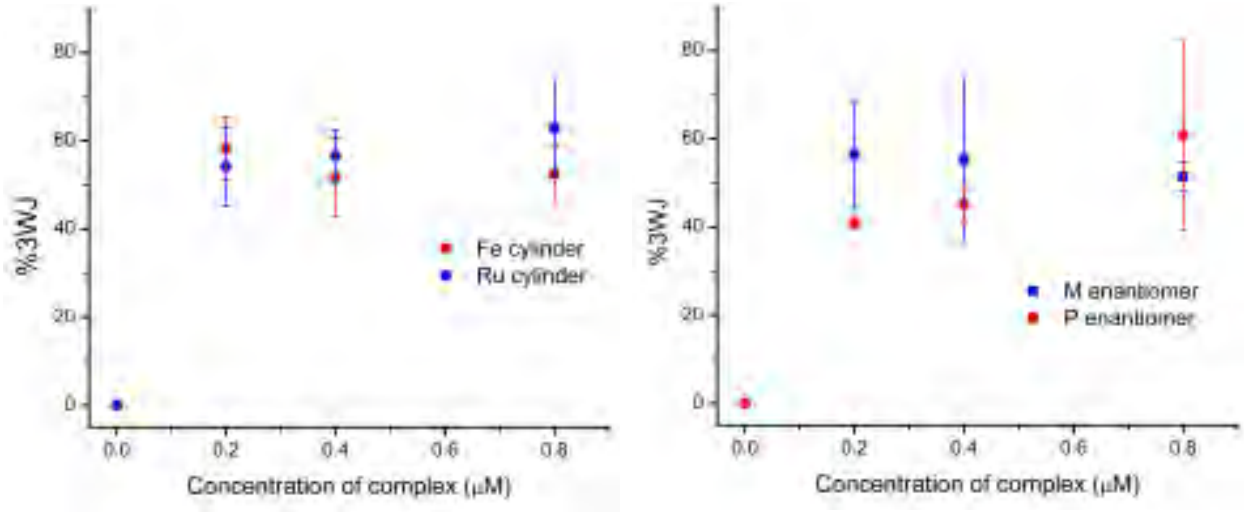

Figure 3.9 Plot of percentage of DNA three way junction formation as a function of concentration of complex. **Left:** comparison of $[Fe_2L_3]^{4+}$ and $[Ru_2L_3]^{4+}$. **Right:** comparison of M and P enantiomer of $[Ru_2L_3]^{4+}$. The plot represents the means of three individual experiments ± SD (n = 3).

The results (**Figure 3.9, Left**) demonstrate that the amount of DNA three way junction formed in the presence of the iron cylinder was not significantly different from that in the presence of the ruthenium cylinder. Considering the similarity in the size, shape and structure of the ligand of both the ruthenium and iron cylinders, ($[Ru_2L_3]^{4+}$) and ($[Fe_2L_3]^{4+}$), it is not surprising that the amount of DNA three way junction formed is the same. This is because the main interaction forces; electrostatic, hydrophobic and sandwiching in minor groove between the cylinder and DNA three way junction are similar for both the iron and ruthenium cylinders.

The effect of the enantiomers of the ruthenium cylinder ($[Ru_2L_3]^{4+}$) on DNA three way junction formation and stabilisation was also investigated. The results (**Figure 3.9, Right**) show that the affinity of M and P enantiomers of the ruthenium cylinder to DNA three way junction was not dramatically different.

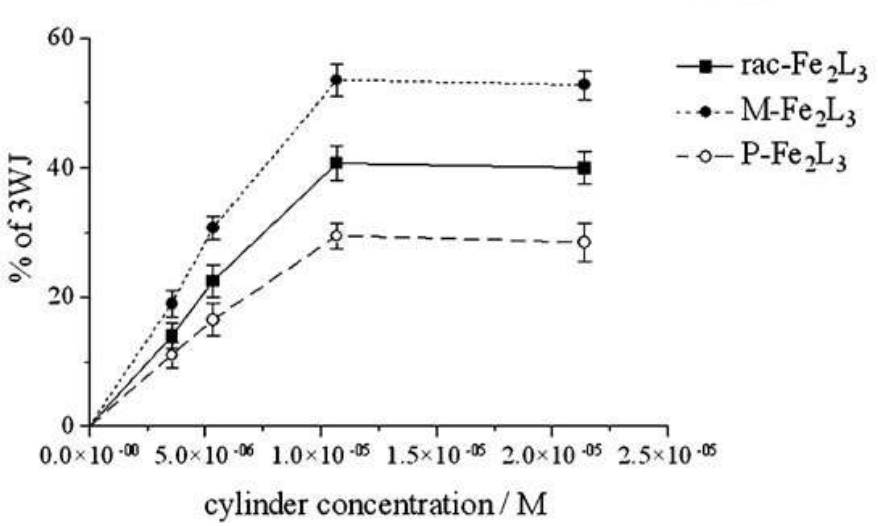

Figure 3.10 Plots of the formation of DNA three way junction by the iron cylinder and its enantiomers as a function of cylinder concentrations. Taken from ref.[7]

It could be possible that the twist from the helicate does not have much effect as the same amount of DNA three way junction was formed for both enantiomers. Interestingly, the three way junction formation in the presence of the P enantiomer of the ruthenium cylinder ($[Ru_2L_3]^{4+}$) was remarkably greater than that for the P enantiomer of the iron cylinder ($[Fe_2L_3]^{4+}$) (**Figure 3.10**).[7] However, a direct comparison between two experiments would be difficult because these results came from different sets of experiment. To gain more understanding of the effect of $[Ru_2L_3]^{4+}$ on the DNA three way junction, study of the crystal structure may be needed in the future. Perhaps, if the crystal structure of the DNA three way junction with both enantiomers of $[Ru_2L_3]^{4+}$ is obtained it may shed light on the gel electrophoresis results.

3.2.5 Effect of size and shape of the metallosupramolecular cylinder on a DNA three way junction formation

There are several factors contributing to the binding of the iron cylinder $[Fe_2L_3]^{4+}$ to the DNA three way junction. The size and shape of the metallosupramolecular cylinder are crucial for the binding of the complex to the cavity of the three way junction. Malina *et al*. demonstrated that a bulkier cylinder $[Fe_2(L\text{-}CF_3)_3]^{4+}$ (**Figure 3.11**) does not stabilise the three way junction formation.[7] This compound is identical to the parent cylinder $[Fe_2L_3]^{4+}$ apart from an additional CF_3 group attached to the carbon in the middle of the ligand, resulting in a huge enlargement of the diameter of the cylinder. Therefore, it is unlikely to fit into the core cavity of the junction.

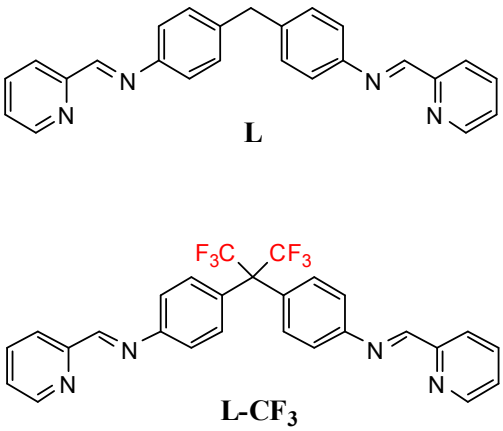

Figure 3.11 Schematic drawing of ligands. **Top:** Parent ligand ($C_{25}H_{20}N_4$). **Bottom:** Ligand to form bulky cylinder ($C_{27}H_{18}N_4F_6$).

To further explore the importance of the size and shape of the cylinder, gel electrophoresis on a range of substituted cylinder, with phenyl and pyridine substituents, peptide conjugates and a triangular platinum compound were carried out.

3.2.5.1 The effect of a substitution adjacent to imine bond on three way junction formation

It has been shown that the spacer unit is important for the helicate to bind to the core cavity of the three way junction. To probe the effect of the substitution group of the ligand on the DNA binding, it was decided that the substitution position to be investigated would be the imine bond, which is adjacent to the metal coordination site. The substitutions performed on the parent ligand are shown in **Figure 3.12**.

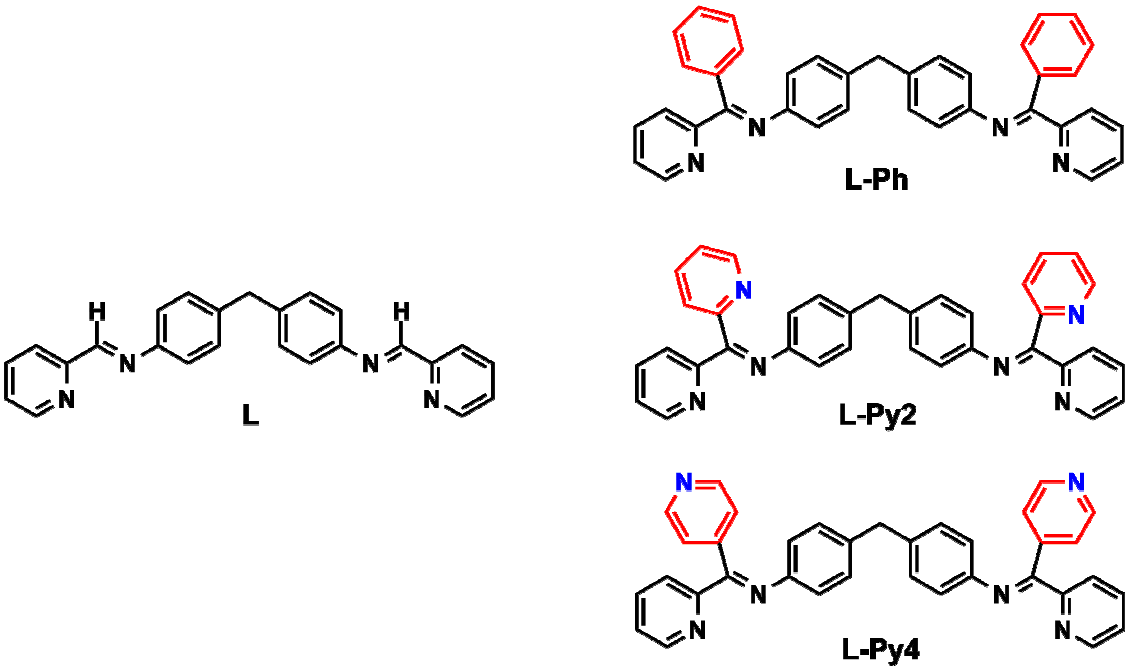

Figure 3.12 Left: The chemical structure of a parental ligand (L). **Right:** The substitution on imine bond on the hydrogen position with phenyl ring (L-Ph), on the second position of pyridine ring (L-Py2) and on the fourth position of pyridine ring (L-Py4) respectively.

A CD experiment investigating the binding of the compounds (chloride form) to calf thymus DNA was carried out by Natalia Calle Alonso from the Hannon group. The results show that the substituted compounds ($[Fe_2(L\text{-}Ph)_3]^{4+}$, $Fe_2(L\text{-}Py2)_3]^{4+}$ and $Fe_2(L\text{-}Py4)_3]^{4+}$) bind and coil polymeric ct-DNA, however the coiling effect is far less than for that of the parent cylinder, $[Fe_2L_3]^{4+}$. To probe the effect of the substitution group on DNA three way junction formation, PAGE was carried out. The substituted iron compounds, as the chloride salt, were synthesised and kindly provided by Natalia Calle Alonso from Hannon group.

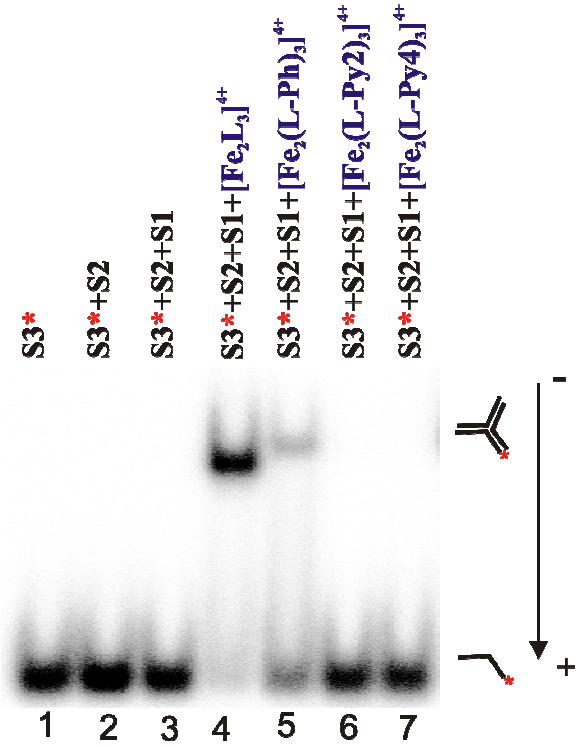

Figure 3.13 Autoradiogram of a substituted helicate and the three strands of oligonucleotides. Lane 1-3: the controls; S3*, S3*+S2, S3*+S2+S1 respectively. Lane 4-7: S3*+S2+S1 in presence of parent cylinder ,$[Fe_2(L)_3]^{4+}$, which used as a control (4), $[Fe_2(L\text{-}Ph)_3]^{4+}$ (5), $[Fe_2(L\text{-}Py2)_3]^{4+}$ (6), $[Fe_2(L\text{-}Py4)_3]^{4+}$ (7). All the loaded samples contained 0.4 μM of oligonucleotide to have a DNA:complex ratio of 3:1.

The results (**Figure 3.13**) show that the three way junction was prominently observed in the presence of the parent cylinder (lane 4). Out of the three substituted cylinders tested, the phenyl substituted was the only compound which allowed formation of three way junction, obtained in lane 5, containing $[Fe_2(L\text{-}Ph)_3]^{4+}$. However, it was much less effective at stabilising three way junction than the parent complex. The mobility of this band is less than that of the parent cylinder due to its higher molecular weight. This is an interesting result as an analogous carried out by Malina *et al*. (2007) testing the three way junction formation of the phenyl substituted compound ([Fe_2(L-

$Ph)_3]^{4+}$) to a *palindromic* DNA sequence, showed that no DNA three way junction was detected.[7] It is unclear whether this is a difference between the relative ease of stabilising a nonpalindromic three way junction versus a palindromic three way junction or whether $[Fe_2(L\text{-}Ph)_3]^{4+}$ has some preference for the DNA sequence at the junction point. The difference in three way junction forming ability of the three substituted compounds gives evidence that the substitution group on the parent ligand does influence three way junction formation.

3.2.5.2 The effect of non metallo helicate on the recognition and stabilisation of DNA three way junction

It has previously been mentioned that the size and shape of the cylinder is crucial for the recognition and stabilisation of the DNA three way junction. Beside these helicates, the other structures e.g. non helicate, having the potential to stabilise DNA three way junction were also investigated[7] to elucidate the best structure of metal based compound for DNA three way junction recognition in order to design a novel metallosupramolecular complex for targeting selectively to higher order DNA structure, DNA three way junction. One interesting compound is a trinuclear Pt (II) complex containing 2, 2'-bipyrazine ligands (bpz) as shown in **Figure 3.14**.

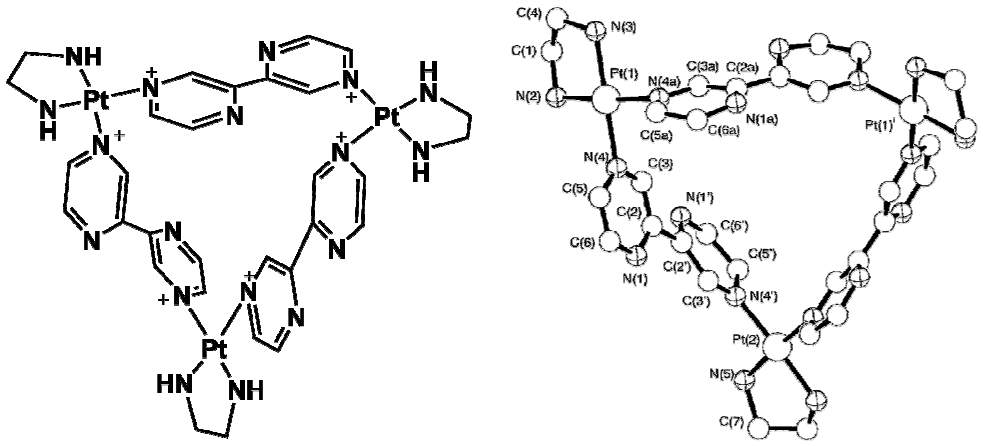

Figure 3.14 Schematic drawing (left) and crystal structure[22] (right) of $[\{(en)Pt(bpz)\}_3]^{6+}$ where en = ethylenediamine.

Unlike the helicates investigated**,** this compound has a cyclic structure containing three platinum atoms bridged by a pyrazine ligand thus resulting in an approximate equilateral triangle formation. Considering this compound in terms of DNA three way junction recognition, it posses several advantages. It has a high positive charge (6+) and a triangular shape, which should allow good recognition. Moreover, the length between Pt-Pt is approximately 1 nm[22] which is comparable to that of the iron cylinder (1 nm in width). Therefore, a gel experiment was carried out to probe the DNA three way junction recognition of this triangular platinum compound. This compound, which has a nitrate ($NO3^-$) counter ion, was kindly provided by Philipp von Grebe, a PhD student working with Professor Bernhard Lippert at the University of Dortmund.

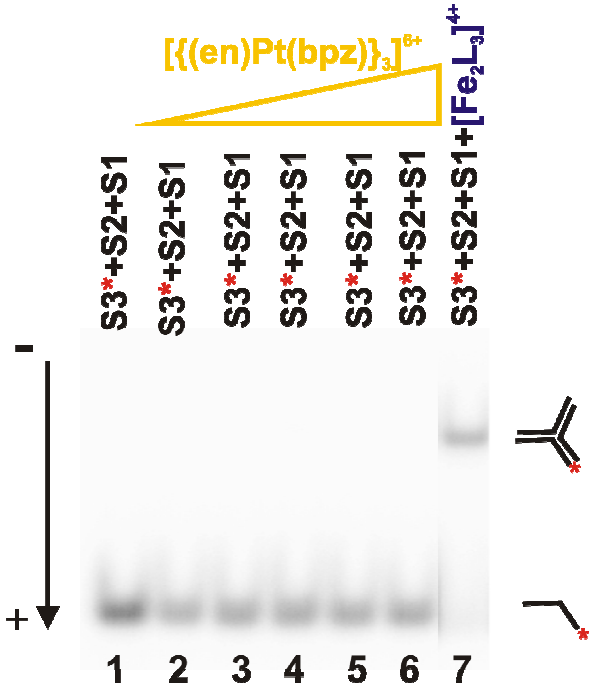

Figure 3.15 Autoradiogram of the recognition and stabilisation of $[\{(en)Pt(bpz)\}_3]^{6+}$ to DNA three way junction. Lane 1: S3*+S2+S1. The concentration of DNA per strand was 0.4 μM. Lane 2-6: S3*+S2+S1 with $[\{(en)Pt(bpz)\}_3]^{6+}$. The ratios of DNA (strand) to complex increased from 3:0.25, 3:0.5, 3:1, 3:2 to 3:10. Lane 7: control containing S3*+S2+S1 with $[Fe_2L_3]^{4+}$ at 3:1 ratio. The samples were incubated for 24 hours.

Initially, the experiment was carried out following the protocol in which the solution containing DNA and the complex were incubated for an hour before PAGE was run. However, the band corresponding to DNA three way junction was not observed. Since increasing the time the compound and DNA were able to interact could possibly promote the formation of the DNA three way junction therefore the experiment was repeated with an increased incubation time of 24 hours. The result shown in **Figure 3.15** demonstrates that the platinum compound ($[\{(en)Pt(bpz)\}_3]^{6+}$) was not able to recognise and stabilise DNA three way junction. This could be due to the molecule. It could be

possible that the ethylenediamine coordinated to platinum is not in the right orientation. Also the ligand contains a rigid bond between the two pyrazines which may not be as flexible as the CH_2 spacer of $[Fe_2L_3]^{4+}$ therefore the π-π stacking of the complex to the bases at the core cavity may be absent.

This result again confirms that the complex's size and shape are the key features for the recognition of a DNA three way junction. Interestingly, the higher positive charge (6+) from the platinum complex (4+ for the iron cylinder) did not simply electrostatically aid the three way junction formation confirming that the size and shape of the complex are a key requirement of binding in the junction.

3.2.5.3 The effect of the peptide conjugated iron cylinder on the recognition and stabilisation of a DNA three way junction

Recently, many researchers have focused on enhancing the specificity of metal complexes to DNA sequences by conjugating short amino acids to these metal complexes. This is because amino acids play a crucial role in the recognition of specific DNA base sequences in natural systems.[23-25] Therefore, combining the DNA binding properties of the iron cylinder and specificity from short amino acids would be the most promising strategy to create cylinders with unprecedented DNA binding properties that selectively recognise DNA sequences. Based on this concept, the iron cylinder-peptide conjugates (**Figure 3.16**) were synthesised by Lucia Cardo, colleague from the Hannon group.[26] In order to retain the efficiency of their DNA recognition properties, the peptides were designed to attach at the end of the cylinder at the 5-position of the pyridine ring. This attachment site was thought to be the best site for conjugation as the peptides are

kept far away from the key DNA binding motif of the cylinder. They should not interfere with the coordination sphere of the octahedral metal ions of the complex.

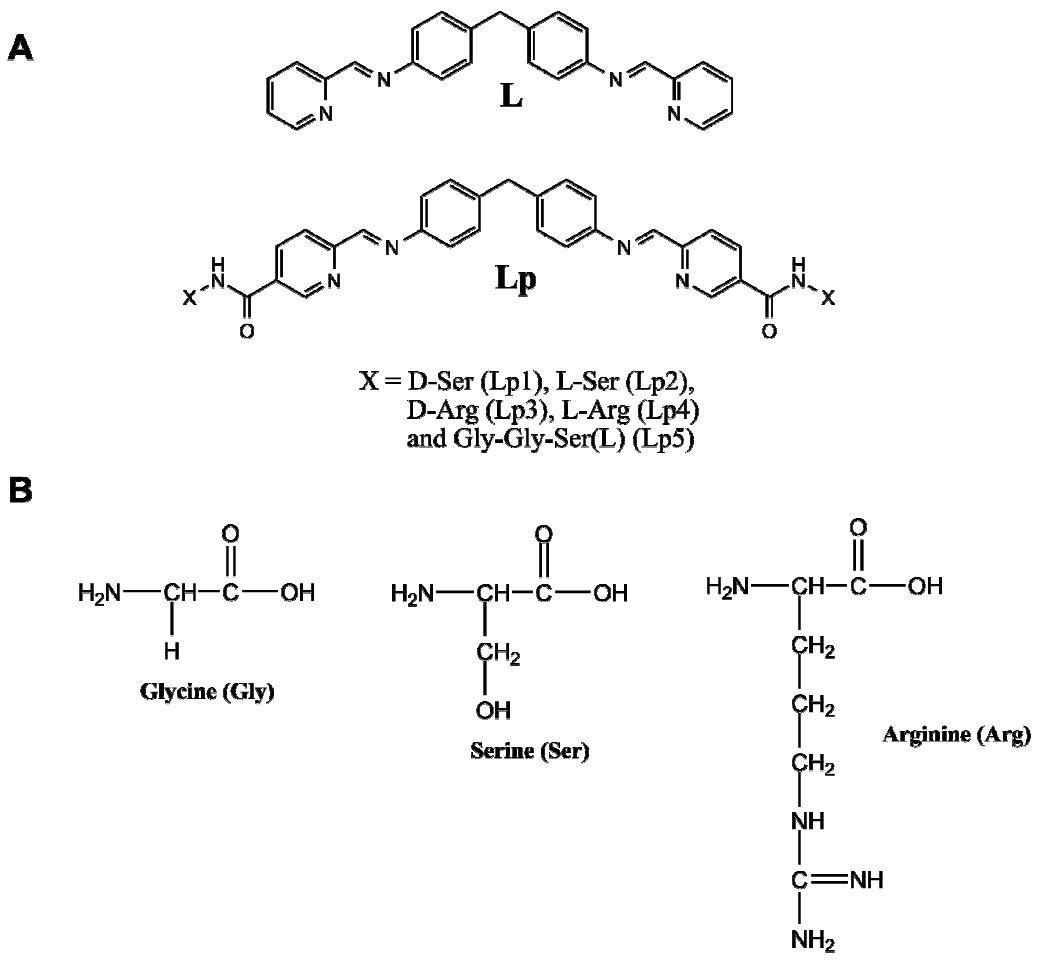

Figure 3.16 A) Illustrating the chemical structure of the parent ligand (L) and the ligand-peptide conjugated used to form the iron triple stranded helicate. Note that X is the amino acids that conjugate to the ligand (Lp). It consists of D-Serine (Lp1), L-Serine(Lp2), D-Arginine(Lp3), L-Arginine(Lp4) and tripeptide, Glycine-Glycine-Serine (Lp5). **B)** Amino acids used to attach to the iron cylinder.

DNA binding experiments using circular and linear dichroism techniques confirm the binding and reveal that all conjugated cylinders are capable of coiling and bending ct-DNA differently.[26] However, the binding of the conjugated cylinder to a DNA three way junction has not yet been investigated. An experiment to explore the effect of the

conjugated amino acid on the recognition of a DNA three way junction, compared to the parent cylinder, was carried out. In this experiment all the conjugated iron cylinders, with chloride counter ions, were kindly provided by Lucia Cardo (Hannon group) who designed and synthesised the conjugated cylinders.

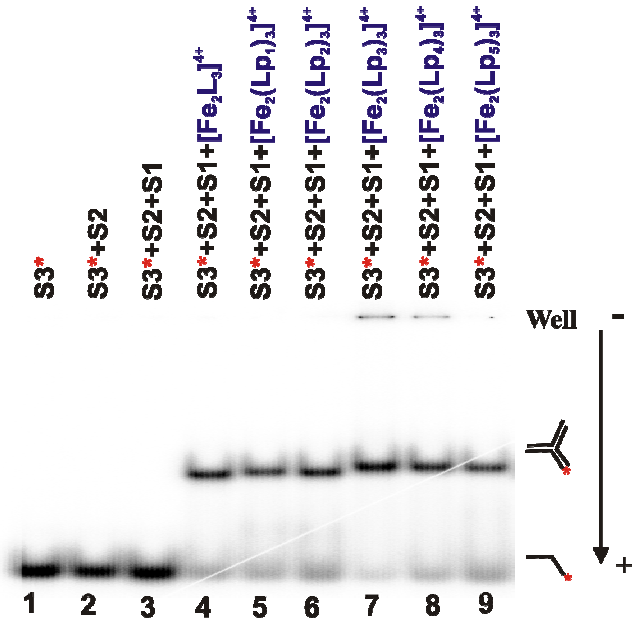

Figure 3.17 The autoradiogram shown the recognition of the conjugated iron cylinder to a DNA three way junction on 15% PAGE at room temperature. Lane 1-3: Controls including S3*, S3*+S2, S3*+S2+S1 respectively. Lane 4-9: S3*+S2+S3 in the presence of the parent cylinder, $[Fe_2L_3]^{4+}$, $[Fe_2(Lp1)_3]^{4+}$, $[Fe_2(Lp2)_3]^{4+}$, $[Fe_2(Lp3)_3]^{4+}$, $[Fe_2(Lp4)_3]^{4+}$ and $[Fe_2(Lp5)_3]^{4+}$, respectively where Lp1, Lp2, Lp3, Lp4 and Lp5 are D-serine, L-serine, D-arginine, L-arginine and tripeptide (glycine-glycine-L-serine). The concentration of DNA (per stand) was 0.4 μM and the ratio of DNA (per strand) to complex was 3:1 corresponding to 0.4 μM of the complexes.

The result shown in **Figure 3.17** demonstrates that all conjugated iron cylinders, $[Fe_2(Lp1)_3]^{4+}$, $[Fe_2(Lp2)_3]^{4+}$, $[Fe_2(Lp3)_3]^{n+}$, $[Fe_2(Lp4)_3]^{n+}$ and $[Fe_2(Lp5)_3]^{4+}$ in lane 5, 6, 7, 8 and 9 respectively, show the ability to promote DNA three way junction formation. Furthermore, the different migration distances among the conjugated iron cylinders and a DNA three way junction adduct were observed. The gel reveals that the D and L serine

(lanes 5 and 6) conjugates migrated slightly slower than the iron cylinder due to the increased molecular weight from the serine attachment. Moreover, the migration of the D and L arginine conjugates (lanes 7 and 8) was the slowest among all of the conjugated helicates. This is because the D and L-arginine conjugated cylinder ($[Fe_2(Lp3)_3]^{n+}$ and $[Fe_2(Lp4)_3]^{n+}$) adducts have a high positive charge so they run slower than the adducts that are less positively charged, i.e. $[Fe_2L_3]^{4+}$ (lane 4), $[Fe_2(Lp1)_3]^{4+}$ (lane 5), $[Fe_2(Lp2)_3]^{4+}$ (lane 6) and $[Fe_2(Lp5)_3]^{4+}$ (lane 9). Precipitation of DNA on the well was observed in lane 7 and 8 containing D and L- arginine due to the high positive charge (10+) arising from the metal and amino acid. The tripeptide conjugated iron cylinder adduct ($[Fe_2(Lp5)_3]^{4+}$) in lane 9 migrated slower than the D and L-serine conjugates due to its the higher molecular weight. However, the tripeptide conjugate ran faster than the D and L arginine conjugated cylinders. This is because the effect of the charge (potentially as high as 10+) from the D and L arginine is greater on the migration than the molecular weight of the tripeptide conjugate. Although the mobility shift of each compound-three way junction adduct was different, the result will be more obvious if the gel electrophoresis is run longer than 4 hours or the concentration of polyacrylamide gel is increased up to 20%. In addition, the quantification of the distance migration of each adduct could be used to calculate a R_f value (distance of 3WJ over distance of ssDNA) and therefore the migration of each adduct could be accurately compared.

To compare DNA three way junction formation due to each conjugated complex, quantification of the band intensity from **Figure 3.17** was performed. It should be noted that the experiments were carried out only in duplicate as in the other experiments herein as the amount of each compound was limited.

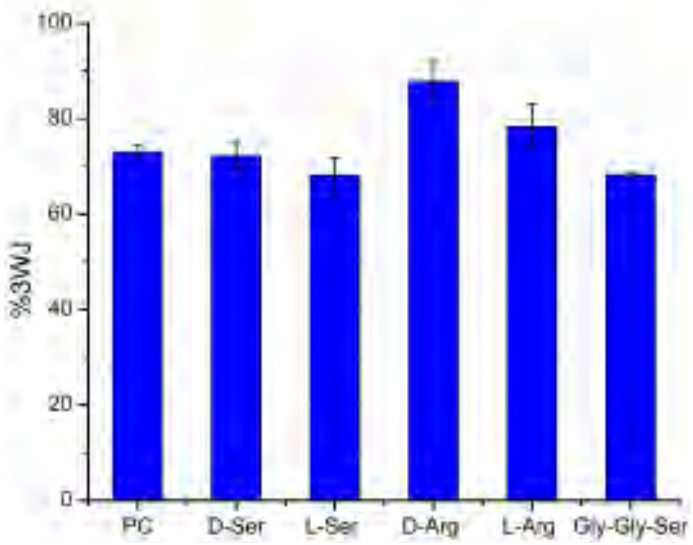

Figure 3.18 A Bar graph depicting the comparison percentage of 3WJ treated with the peptide conjugated iron cylinders. Each conjugating units of the complex has been labelled in x-axis. PC = parent cylinder ($[Fe_2L_3]^{4+}$). The graph represents the means of two individual experiments ± SD (n = 2).

The percentage of DNA three way junction formed, illustrated in the graph **Figure 3.18,** shows that the arginine conjugates, both D and L configurations, cause the highest three way junction formation among all conjugates. In addition, the D-arginine conjugate has a higher ability to induce three way junction formation than the L-arginine conjugate. This indicates that the chirality of the conjugated compounds contributes to the recognition of a DNA three way junction. Interestingly, DNA binding studies by CD showed that the M enantiomer conformation of the triple stranded helicate, remarkably induced by the anchored D-arginine, is more effective in DNA recognition than the P enantiomer promoted by the anchored L-arginine.[27] The parent cylinder (PC), the serine conjugates, in D and L configuration, and the tripeptide conjugate show a comparable activity to promote DNA three way junction formation. This experiment shows that

conjugation of an appropriate amino acid to the iron cylinder does enhance DNA three way junction formation.

3.2.6 Competitive assay of DNA three way junction and the other DNA structures to $[Fe_2L_3]^{4+}$

It is known that cisplatin and its analogs have great efficacy in the treatment of certain types of cancers such as testicular, ovarian, bladder, cervical, head, neck and lung cancer.[28] This anticancer drug binds all along the DNA to a guanine base at the N7 position and kinks the DNA. One result of this widespread DNA platination is unpleasant side effects.[29] One strategy for drug design is to focus on a very specific DNA sequence. However to explore the effective sequence selectivity, many bases have to be recognised and high throughput screening is required. Recently, an alternative approach to anticancer drug design has been to seek to recognise higher order DNA structures such as targeting DNA three way junctions or G-quadruplex DNA.[33, 34]

It has been shown that the iron cylinder $[Fe_2L_3]^{4+}$ binds in the DNA major groove and causes dramatic intramolecular coiling. Additionally, it also recognises and promotes DNA three way junction formation. Recently, Yu *et al.* reported results from several biophysical experiment.[30] It was proposed that the P enantiomer of the iron cylinder $[Fe_2L_3]^{4+}$ selectively recognised and stabilised human telomeric G-quadruplex DNA with a stronger efficiency than the M enantiomer. Corresponding results from several biological tests, including telomerase inhibition, telomere shortening, β-galactosidase activity and up-regulation of CDK inhibitors p16 and p21, appeared to confirm that the P

enantiomer exhibited a stronger preference to G-quadruplex DNA than the M enantiomer.[31]

The preference of the iron cylinder for different DNA structures was therefore investigated. A competition assay between several DNA structures and the iron cylinder ($[Fe_2L_3]^{4+}$) was established.

The experiment, herein, was designed around an S1, S2 and S3 three way junction in which only the S3* strand is labelled. Increasing concentrations of the iron cylinder were added to the solution in the presence of different competitor DNAs. The competitor DNAs were selected to have the same charge (number of bases) as the three way junction to minimise electrostatic effects. Alternatively, the experiment could be designed to add increased concentrations of competitor into a fixed concentration of complex and DNA three way junction.

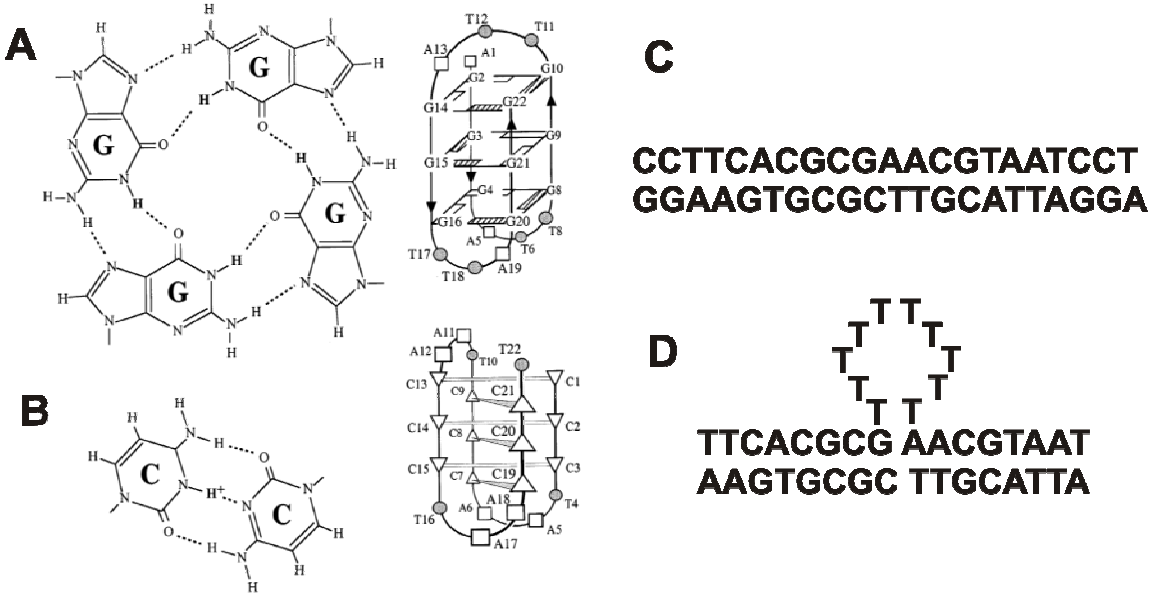

Figure 3.19 Sequences of competitors. **A)** G-quartet (left) and its G-quadruplex scaffold (right). **B)** C-C base pair (left) and its i-motif structure (right). Taken from the ref.[32] **C)** Double stranded DNA. **D)** Double stranded with a loop containing ten thymines.

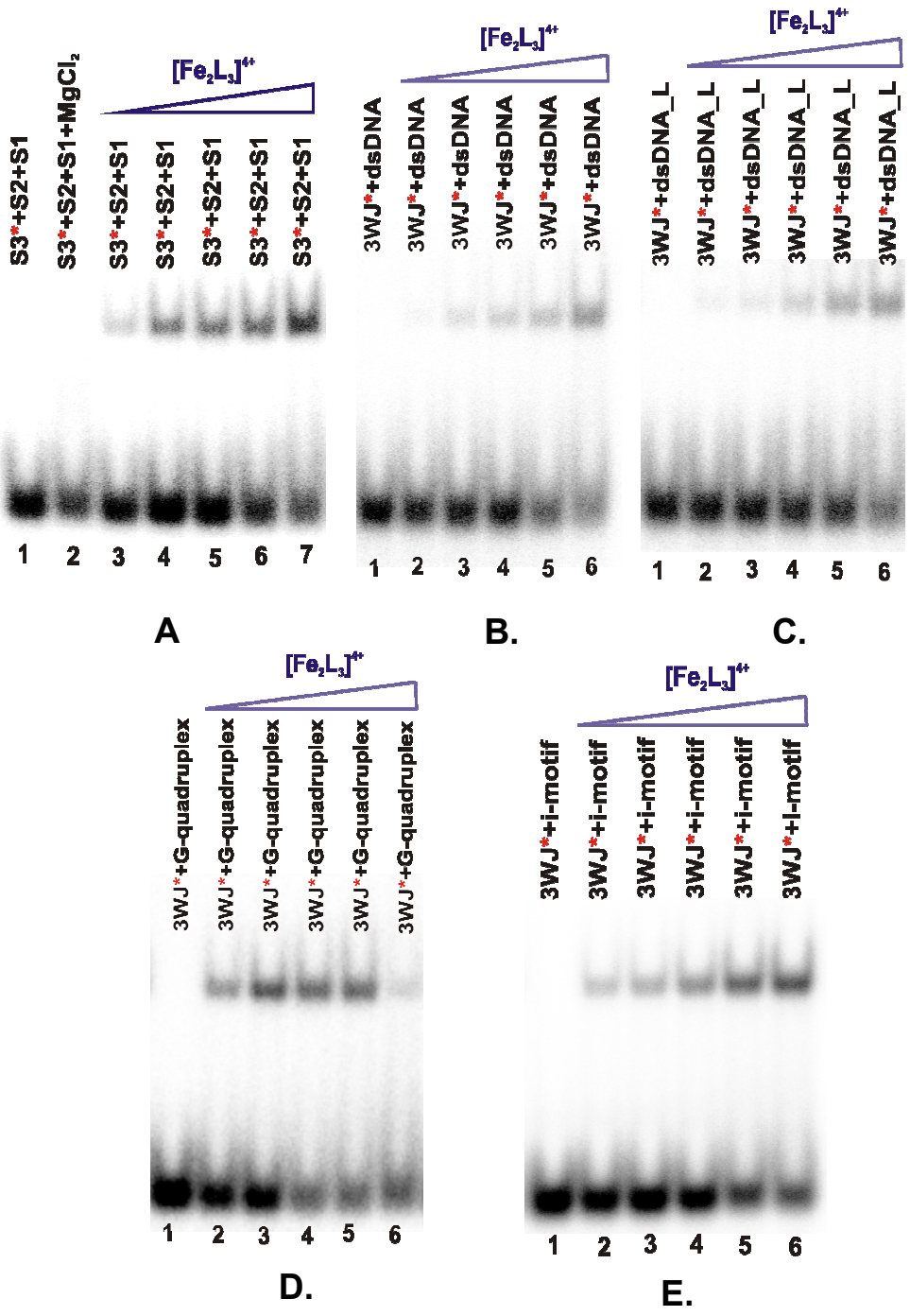

Figure 3.20 Autoradiogram of a competitive assay of a DNA three way junction and the other DNA structures to the iron cylinder $[Fe_2L_3]^{4+}$. The competitiors used for this experiments were double stranded DNA (dsDNA, B), double strand with loop (dsDNA_L, C), G-quadruplex (D) and i-motif (E). The concentration of a DNA three way junction and competitor were constant at 0.2 μM. The ratio of complex to DNA three way junction to competitor increased from 0.25:1:1, 0.5:1:1, 1:1:1, 2:1:1 to 10:1:1, corresponding to 0.05, 0.1, 0.2, 0.4 and 2 μM of complex.

Our assumption is that the competitors bind preferentially to the iron cylinder then less three way junction will be stabilised when the cylinder is added. The competitors used in this experiment were a double strand DNA (dsDNA), a double strand DNA with 10 loops (dsDNA_L), a G-quadruplex structure and an i-motif structure as shown in **Figure 3.19**.

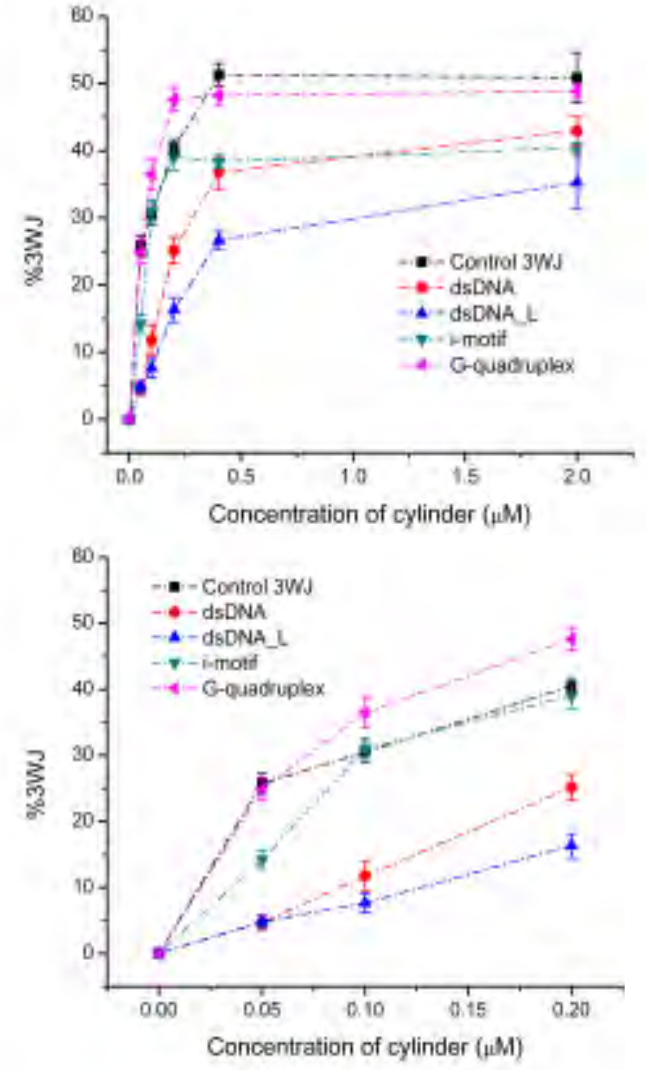

Figure 3.21 Top: A plot illustrating percentage of three way junction versus concentration of iron cylinder (μM) in the presence of competitors. The ratio of complex: DNA three way junction: competitor increased from 0.25:1:1, 0.5:1:1, 1:1:1, 2:1:1 to 10:1:1, respectively. **Bottom:** A plot the top graph focusing the ratio of complex: DNA three way junction: competitor increased from 0.25: 1: 1, 0.5: 1: 1, 1: 1: 1, respectively corresponding to 0.05, 0.1, 0.2, 0.4 and 2 μM of complex. The trend lines were drawn for clarity. The experiments were conducted in triplicate and the error bars representing SD value.

The gel electrophoresis results shown in **Figure 3.20** were later evaluated and compared among the DNA structures.

The gel quantification represented as a graph in **Figure 3.21** shows that if we consider low concentration of the cylinder (0 – 0.2 μM) it shows that double stranded DNA and double stranded DNA with loop are good competitors.

G-quadruplex and i-motif DNA structures do not seem to compete for binding. These two structures are pre-formed in the solution so the fact that the cylinder can assemble the three way junction structure in their presence indicates a much stronger binding constant to the three way junction. This finding raises question marks over the validity of Yu's recent report.[30] Yu's experiments based on DNA melting experiments conducted at temperature above the stability of the cylinder and may therefore be reporting on a cylinder component (such as the iron centre) rather than the cylinder. It should be aware that the i-motif structure probably did not form because pH, used in the experiment, was not low enough (required ~ 5.5) for the protonation of cytosine bases in the i-motif structure.

The double stranded and double stranded with loop DNAs are clearly competitors though the precise preference is hard to quantify in the experiment as both the double stranded and double stranded with loop DNAs will be preformed in solution while with three way junction is only formed in presence of the cylinder. The loop point represents a Y-shaped junction and the double stranded DNA is likely to denature at the ends (providing Y-shaped forks).

From studies with a palindromic DNA, it is known that cylinder binds to three way junction over double stranded DNA, with a strong preference, with no double

stranded DNA observed in these experiments either at low or high cylinder loading. The sensitivity of this competition binding assay is shown by the fact that at 1:1:1 ratio of cylinder: three way junction: double stranded DNA, ~60% is bound to the three way junction and 40% to the double stranded DNA. This reinforces just how great the preference for three way junction over G-quadruplex is.

The looped DNA, which contains the form at loop point, is bound in preference to double stranded DNA. This may indicate that the competition comes not from major groove binding but from Y-shaped junction binding.

However, to elucidate the recognition of the iron cylinder to the DNA structures, i.e. DNA three way junction, G-quadruplex and i-motif structure, further experiments will be required to support this preliminary testing experiment. The binding constant of the iron cylinder to the DNA three way junction, G-quadruplex and i-motif DNA structure must be determined and the mechanism of the iron cylinder exhibiting cell growth and leading to apoptosis elucidated by cell testing.

3.3 Conclusions

In summary, gel electrophoresis with radiolabelling is a powerful technique offering high sensitivity in the study of the recognition of the metallo supramolecular cylinder to a DNA three way junction. In the rational drug design of new analogues, consideration of the size, shape, metal centre, the conjugation of functional groups are crucial in retaining the DNA recognition of the parent drug. The results herein show that only an iron cylinder with a certain size and shape allows three way junction formation. Results also show that changing the metal ion centre of the metallo cylinder from iron to

ruthenium does not alter the recognition of the complex to DNA three way junction. The selectivity and recognition of the iron cylinder to the DNA three way junction can be increased by conjugating amino acids to the ligand. Moreover, the competition assay of several DNA structures shows that the iron cylinder binds to three way junction preferentially over G-quadruplex structure but binding to other Y-shaped junctions is a possible competition.

3.4 Experimental

All chemicals were purchased from Fisher, Sigma-Aldrich and Fluka otherwise the source will be specified.

Radioactive labelling: A reaction mixture of 10 µl in 1.5 ml eppendrof containing 4.8 µl of MilliQ water, 1 µl of 10x bacteriophage T4 polynucleotide kinase buffer, 1.2 µl of 100 µM oligonucleotide (S3), 1µl of bacteriophage T4 polynucleotide kinase (New England Biolab) 2 µl of γ-^{32}P ATP (6000 Ci/mmol) from Perkin Elmer were well mixed and incubated for 40 min at 37 °C. Then the mixture was heated at 80 °C for 3 minutes to inactivate the polynucleotide kinase. For cleanup of radioactive DNA fragments from unincorporated ATP A QIAquick nucleotide removal kit (QIAGEN) was used. Briefly, 10 volumes of Buffer PN were added to 1 volume of the reaction sample. Then the mixture was transferred onto spin column and centrifuged column at 6000 rpm for 1 minute. The supernatant was discarded. The column was transferred into a new elution tube and buffer PE was added 500 µl. The flow-through was discarded and the wash was repeated with another 500 µl of Buffer PE. The column was centrifuged again at 13,000 rpm for 1 minute to discard the residual buffer. The column was transferred into a 1.5 ml eppendrof. 30 µl of milliQ water was added to the column and allowed to stand for 5 minutes before being centrifuged at 13,000 rpm for 2 minutes to obtain 8 µM of stock radiolabeled DNA.

Polyacrylamide gel preparation: 15% native polyacrylamide gel solution containing 10 ml of 10x TB buffer pH 8.3 (890 mM tris(hydroxymethy) amino methane, 890 mM boric acid), 37.5 ml of 40% acrylamide (29:1) from Geneflow, 52.5 ml of milliQ water, 500µl of 10%(w/v) ammonium persulfate and 75 µl TEMED, was poured onto a set of glass

plates. The wells of the polymerised gel were thoroughly washed with a running buffer (TB buffer) before use. Note that pre-running of the gel at 200 volts for 5 minutes is required before the experiment is performed.

Purity checking by 18% denaturing polyacrylamide gel electrophoresis: 18% denaturing polyacrylamide gel solution containing 10 ml of 10x TBE buffer pH 8.3 (890 mM tris(hydroxymethy) amino methane, 890 mM boric acid and 2 mM Na_2EDTA) from National Diagnostics, 45 ml of 40% acrylamide (29:1) from Geneflow, 42 g of urea, top the milli Q water up to 100 ml. The solution was mixed very well until all components became a homogenous solution. Then 500µl of 10%(w/v) ammonium persulfate and 75 µl TEMED were added to the solution. Subsequently, the solution was poured onto a set of glass plates. The wells of the polymerised gel were thoroughly washed with a running buffer (TB buffer) before use. Note that prerunning of the gel at 200 volts for 5 minutes is required before the experiment is performed. The labelled strand was loaded onto the well and run for 2 hours. The gel was then taken out from the glass plate and exposed to the phosphorimager for 10 min, then the image was developed.

Gel electrophoresis experiment: The highly pure oligonucleotides (S1:CGGAACGGCACTCG, S2: CGAGTGCAGCGTGG, S3: CCACGCTCGTTCCG) were bought from Eurofins, Germany. Stoichiometric amounts of the oligonucleotides (0.4 µM, related to strand) were mixed with complexes in the TBN buffer pH 8.3 containing 89 mM tris(hydroxymethy) amino methane, 89 mM boric acid and 100 µM NaCl. The solutions were incubated at room temperature for 1 hour and on ice for 15 minutes. The samples were loaded onto 15% polyacrylamide gel electrophoresis and run for 4 hours at 120 volts using Gel System (Thermo Scientific, UK). Then, the gel was

exposed on a phosphor plate for an hour. The image was obtained from Molecular imager FX (Bio-Rad). The quantification was operated by Quantity one (Bio-Rad).

Competition assay of DNA 3WJ and other DNA structures: the solution of labelled DNA 3WJ (0.2 μM) in TBN buffer was incubated with the iron cylinder for an hour at room temperature. DNA (per strand):complex ratios 3:0.25, 3:0.5, 3:1, 3:2 and 3:10. The concentration of the cylinder, corresponded to those ratios are 0.05, 0.1, 0.2, 0.4 and 2 μM. Then the same amount of a solution of non-labelled competitor (0.2 μM) was added in to each ratio. The solutions were incubated for 1 hour at room temperature. The samples were loaded, run and quantified using the same method as described previously. The sequences of competitor are shown below.

Competitor	Abbreviation	Sequences (5'-3')
G-quadruplex[30]	G-quadruplex	AGG GTT AGG GTT AGG GTT AGG G
i-motif DNA[30]	i-motif	CCC TAA CCC TAA CCC TAA CCC T
Double stranded DNA	dsDNA	CCT TCA CGC GAA CGT AAT CCT, AGG ATT ACG TTC GCG TGA AGG
Double strand DNA with loop	dsDNA_L	TTC ACG CGT TTT TTT TTT AAC GTA AT, ATT ACG TTC GCG TGA A

3.5 References

1. M. J. Hannon, *Chem. Soc. Rev.*, 2007, **36**, 280-295.
2. M. J. Hannon, C. L. Painting, A. Jackson, J. Hamblin and W. Errington, *Chem. Commun.*, 1997, 1807-1808.
3. M. J. Hannon, V. Moreno, M. J. Prieto, E. Moldrheim, E. Sletten, I. Meistermann, C. J. Isaac, K. J. Sanders and A. Rodger, *Angew. Chem. Int. Ed.*, 2001, **40**, 880-884.
4. A. C. G. Hotze, N. J. Hodges, R. E. Hayden, C. Sanchez-Cano, C. Paines, N. Male, M. K. Tse, C. M. Bunce, J. K. Chipman and M. J. Hannon, *Chem. Biol.*, 2008, **15**, 1258-1267.
5. A. Oleksi, A. G. Blanco, R. Boer, I. Uson, J. Aymami, A. Rodger, M. J. Hannon and M. Coll, *Angew. Chem. Int. Ed.*, 2006, **45**, 1227-1231.
6. L. Cerasino, M. J. Hannon and E. Sletten, *Inorg. Chem.*, 2007, **46**, 6245-6251.
7. J. Malina, M. J. Hannon and V. Brabec, *Chem. Eur. J.*, 2007, **13**, 3871-3877.
8. C. Guthrie and B. Patterson, *Annu. Rev. Genet.*, 1988, **22**, 387-419.
9. M. R. Singleton, S. Scaife and D. B. Wigley, *Cell*, 2001, **107**, 79-89.
10. R. R. Sinden, *Nature*, 2001, **411**, 757-758.
11. C. Uerpmann, J. Malina, M. Pascu, G. J. Clarkson, V. Moreno, A. Rodger, A. Grandas and M. J. Hannon, *Chem. Eur. J.*, 2005, **11**, 1750-1756.
12. J. C. Peberdy, J. Malina, S. Khalid, M. J. Hannon and A. Rodger, *J. Inorg. Biochem.*, 2007, **101**, 1937-1945.
13. J. L. Kadrmas, A. J. Ravin and N. B. Leontis, *Nucleic Acids Res.*, 1995, **23**, 2212-2222.

14. C. C. Richardson, in *Procedure in nucleic acid research*, eds. G. L. Cantoni and D. R. Davies, Harper and Row, New York, Edn., 1971, Vol. 2, pp. 815-828.

15. W. H. Ang and P. J. Dyson, *Eur. J. Inorg. Chem.*, 2006, 4003-4018.

16. V. Brabec and O. Nováková, *Drug Resistance Updates*, 2006, **9**, 111-122.

17. M. A. Jakupec, M. Galanski, V. B. Arion, C. G. Hartinger and B. K. Keppler, *Dalton Trans.*, 2008, 183-194.

18. J. Reedijk, *Platin. Met. Rev.*, 2008, **52**, 2-11.

19. G. I. Pascu, A. C. G. Hotze, C. Sanchez-Cano, B. M. Kariuki and M. J. Hannon, *Angew. Chem. Int. Ed.*, 2007, **46**, 4374-4378.

20. J. Malina, M. J. Hannon and V. Brabec, *Chem. Eur. J.*, 2008, **14**, 10408-10414.

21. M. J. Hannon, I. Meistermann, C. J. Isaac, C. Blomme, J. R. Aldrich-Wright and A. Rodger, *Chem. Commun.*, 2001, 1078-1079.

22. R. D. Schnebeck, L. Randaccio, E. Zangrando and B. Lippert, *Angew. Chem. Int. Ed.*, 1998, **37**, 119-121.

23. C. A. Hastings and J. K. Barton, *Biochemistry*, 1999, **38**, 10042-10051.

24. K. Karidi, A. Garoufis, N. Hadjiliadis and J. Reedijk, *Dalton Trans.*, 2005, 728-734.

25. N. Y. Sardesai, K. Zimmermann and J. K. Barton, *J. Am. Chem. Soc.*, 1994, **116**, 7502-7508.

26. L. Cardo and M. J. Hannon, *Inorg. Chim. Acta* 2009, **362**, 784-792.

27. L. Cardo, PhD thesis, University of Birmingham, 2010.

28. B. Rosenberg, in *Chemistry and Biochemistry of a Leading Anticancer Drug*, Ed. B. Lippert, Wiley-VCH, Basel, Edn., 1999, pp. 3–27.

29. V. M. Gonzalez, M. A. Fuertes, C. Alonso and J. M. Perez, *Mol. Pharmacol.*, 2001, **59**, 657-663.

30. H. J. Yu, X. H. Wang, M. L. Fu, J. S. Ren and X. G. Qu, *Nucleic Acids Res.*, 2008, **36**, 5695-5703.

31. H. J. Yu, C. Q. Zhao, Y. Chen, M. L. Fu, J. S. Ren and X. G. Qu, *J. Med. Chem.*, 2010, **53**, 492-498.

32. A. T. Phan and J. L. Mergny, *Nucleic Acids Res.*, 2002, **30**, 4618-4625.

Chapter 4

The application of the metallosupramolecular cylinder to DNA nanotechnology

4.1 Introduction

DNA polyhedra are prepared for a wide range of applications such as for the encapsulation and release of drugs, regulation of protein folding and activity, and the assembly of 3D networks for catalysis and biomolecule crystallisation.[1-3] The first DNA nanostructure, the cube-like DNA, was constructed by Nadrian Seeman and co-workers.[4] In the procedure described, two quadrilaterals were annealed to form a belt-like object that was then purified, reconstituted, cylised and ligated to produce an assembly of six interconnected cyclic DNA strands as a cube like object, in less than 1% yield. The synthetic route is shown in **Figure 4.1**.

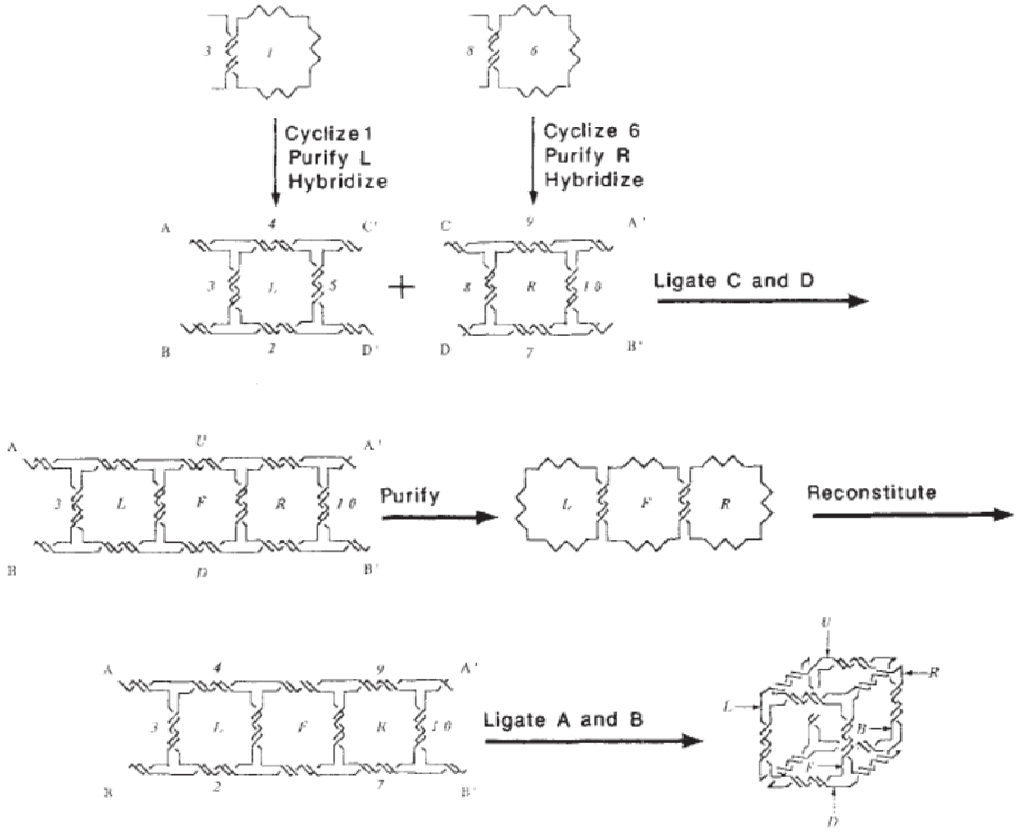

Figure 4.1 Synthetic scheme[4] for cube-like DNA nanostructure.

Later, the same group modified the method by utilising a solid-phase synthesis to combine individual polygons and polygonal clusters into a truncated DNA octahedron[5] containing 14 faces (six squares and eight hexagons), 24 vertices, and 36 edges. The DNA octahedron[6] was later constructed from a mixture of a 1,669 base nucleotides, defined as the heavy chain, and five 40 base nucleotides, the light chains, by a simple denaturation–renaturation procedure. These constructions were complicated and required several sequences for the construction. However, Turberfield and co-workers subsequently synthesised a DNA tetrahedron designed from a single step synthesis.[7, 8] The tetrahedron was assembled from four strands each comprising a 55 base oligonucleotides. Each strand contains three 17 base sub-sequences, separated by two-base hinges. The unhybrided hinges are designed to ensure that the structure has sufficient flexibility to achieve an angle of 60° between adjacent edges. The ease of the synthesis and the rigidity make this DNA nanostructure promising as a DNA cargo vessel. The application of this design was then demonstrated by the same group. Turberfield and co-workers encapsulated the protein, cytochrome c, into a DNA tetrahedron by conjugating it to the inner surface of the DNA tetrahedron.[9] Moreover, the rigidity of the DNA tetrahedron is beneficial for the binding of fluorescent dyes to the nanostructure. Armitage *et al*. showed that the DNA tetrahedron provides a protective medium for the fluorophores, YOYO-1 (**Figure 4.2**), resulting in their improved photostability and increased resistance to nuclease digestion.[10] This is an example of ultilising the DNA tetrahedron to enhance the stability of the intercalating dye.

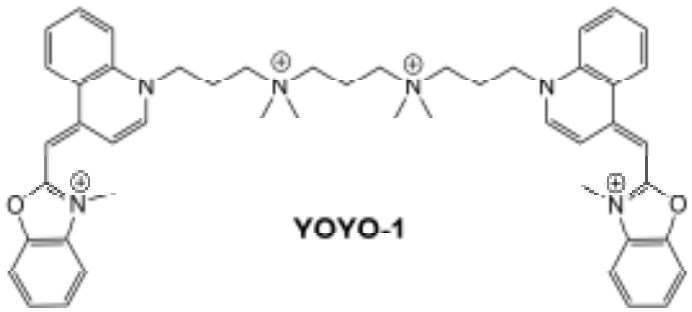

Figure 4.2 Chemical structure of YOYO-1.

The triple stranded supramolecular cylinder, $[Fe_2L_3]^{4+}$, is formed from three bis-pyridylimine ligands wrapped around two iron metal centres[11] and is cylindrical in shape. This cylinder has been shown to bind in the major groove of DNA and causes remarkable intramolecular coiling of DNA.[12, 13] It can also bind to DNA three way junction.[14] However, the interaction between this cylinder and a three dimensional DNA construct has never been established.

Herein, the interaction between the iron cylinder and the DNA tetradron was demonstrated by CD and gel electrophoresis. The change in topology was illustrated by AFM, and later the stability of the iron cylinder and the DNA structure was probed by melting temperature experiment.

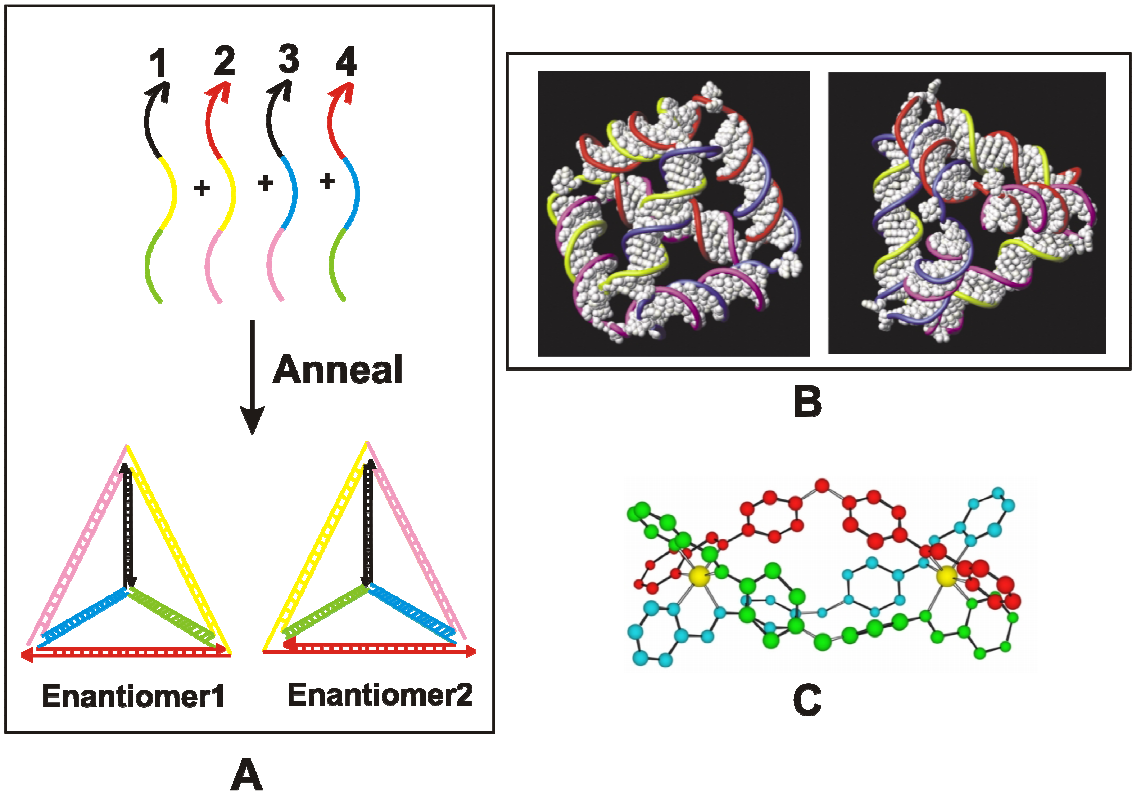

Figure 4.3 A) Synthetic scheme of DNA tetrahedron. **B)** A side view (left) and top view (right) of a spacefilling representation[8] of tetrahedron. Each face of tetrahedron is illustrated by a single color. **C)** The structure of the iron cylinder[12] $[Fe_2L_3]^{4+}$ which has ~2 nm in length and ~1 nm in diameter.

4.2 Results and discussion

4.2.1 CD binding study of the iron cylinder and the DNA tetrahedron

CD spectroscopy is a useful technique to analyze changes in DNA morphology by the interaction of DNA with small molecules. The changes in CD signal of DNA observed on interaction with drugs may often be assigned to the corresponding changes in DNA structure. To confirm that the iron cylinder interacts with the DNA tetrahedron, circular dichroism (CD) was utilised to probe the interaction. The iron cylinder was titrated into the DNA tetrahedron solution in cacodylate buffer. In addition, the concentration of the DNA tetrahedron was kept constant during the titration. The ratio of

the DNA tetrahedron (bases) to the cylinder started from 60:1, 30:1, 15:1, 8:1, 6:1 to 4:1. The concentrations of the iron cylinder corresponding to these ratios are 0.17, 0.33, 0.67, 1.25, 1.67 and 2.5 μM, respectively.

The results (**Figure 4.4**) show that the B-form DNA was still retained, due to a characteristic pattern from 220 nm to 300 nm. The unique pattern remained during the titration, revealing that the iron cylinder does not perturb the conformation of the DNA. Also the recorded UV-Vis spectra during the titration indicate that the iron cylinder retained its structure. Interestingly, an induced CD (ICD) was not observed during the titration. It is possible that the DNA tetrahedron contains two enantiomers[7] as does the iron cylinder[15, 16]. Therefore, any ICDs cancelled each other out and no signal was detected.

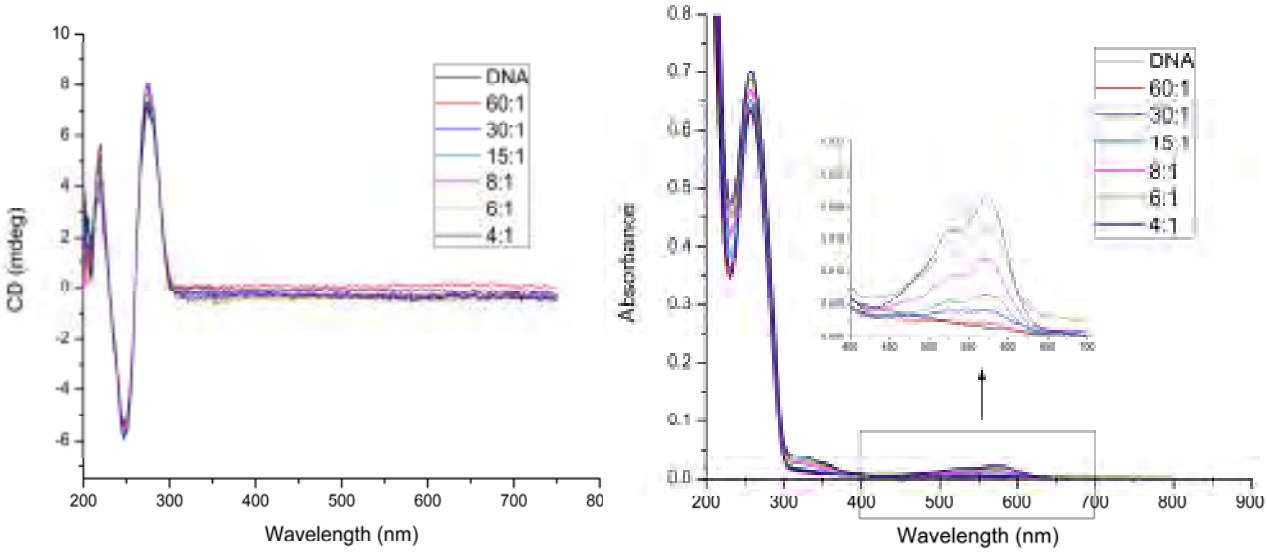

Figure 4.4 CD spectra (left) and UV-Vis spectra (right) from 1 cm pathlength cuvette containing 10 μM DNA tetrahedron in 20 mM NaCl and 1 mM cacodylate buffer with increasing concentration of $[Fe_2L_3]^{4+}$. The DNA in bases:$[Fe_2L_3]^{4+}$ ratios are 60:1, 30:1, 15:1, 8:1, 6:1 and 4:1. The concentration of the cylinder corresponding to these ratios are 0.17, 0.33, 0.67, 1.25, 1.67 and 2.5 μM, respectively.

4.2.2 Gel electrophoresis studies

To probe any potential binding in more detail, gel electrophoresis was introduced to investigate the effect of the iron cylinder on the DNA nanostructure. The experiment was designed to have a control, the DNA tetrahedron synthesised by hybridising four strands of DNA as mentioned in the literature.[7] Then, the DNA tetrahedron was treated with the iron cylinder at increasing ratios (DNA tetrahedron:cylinder) from 1:0.5, 1:1, 1:2, 1:4, 1:8 to 1:16. The concentration of the cylinder corresponding to these ratios are 0.5, 1, 2, 4, 8, 16 μM.

The results (**Figure 4.5**) show that the DNA nanostructure was formed with migration of the hybridised four strands, the DNA tetrahedron, being slower than the three strands, double strands and a single strand ,respectively (on 10% PAGE). In the presence of the iron cylinder, $[Fe_2L_3]^{4+}$, the migration of the DNA nanostructure was accelerated starting from 1:1. In addition, the migration was significantly accelerated at higher concentration of the cylinder. A possible explanation for this observation is that the iron cylinder binds to the DNA nanostructure and causes DNA bending, thus the DNA nanostructure becomes more compact and migrates though the gel network faster than the one of that has less cylinder. A trace of precipitation, shown as a band on the well, was detected at 1:4 ratio and more dramatically observed at 1:8 and 1:16

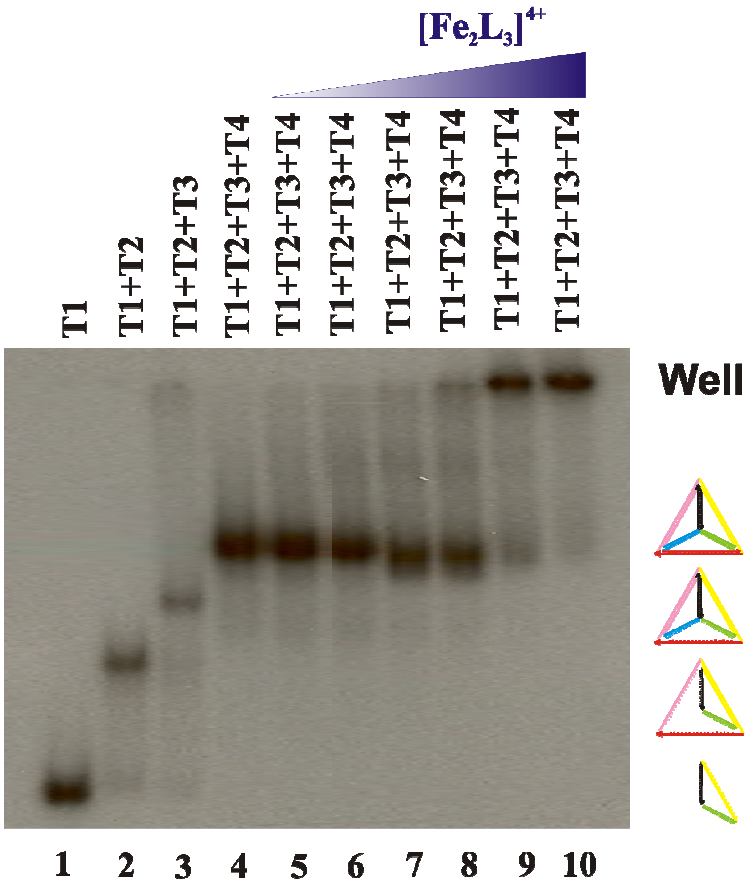

Figure 4.5 Autoradiogram illustrating the interaction between the DNA tetrahedron and the iron cylinder on 10% non-denaturing polyacrylamide gel electrophoresis. Lanes 1-3: Control containing T1, T1+T2, T1+T2+T3. Lane 4: Control consisting of strand 1, 2, 3 and 4, (T1+T2+T3+T4), forming DNA tetrahedron (1 μM). Lanes 5-10: Sample containing a DNA tetrahedron in the presence of the iron cylinder, $[Fe_2L_3]^{4+}$. The ratio of DNA tetrahedron to the iron cylinder started from 1:0.5, 1:1, 1:2, 1:4, 1:8 to 1:16 respectively. The concentrations of the cylinder corresponding to these ratios are 0.5, 1, 2 ,4, 8, 16 μM. All the samples were carried out in TM buffer (10 mM Tris, 1 mM 20 mM $MgCl_2$, pH 8.0).

It is known that the DNA tetrahedron has a rigid structure. However, the iron cylinder appears to have a high affinity for interacting with the structure and in fact alters the structure, however the B-DNA configuration is retained. To study this further, ethidium bromide, a representative intercalator was used to compare its interaction and effects with these of the iron cylinder.

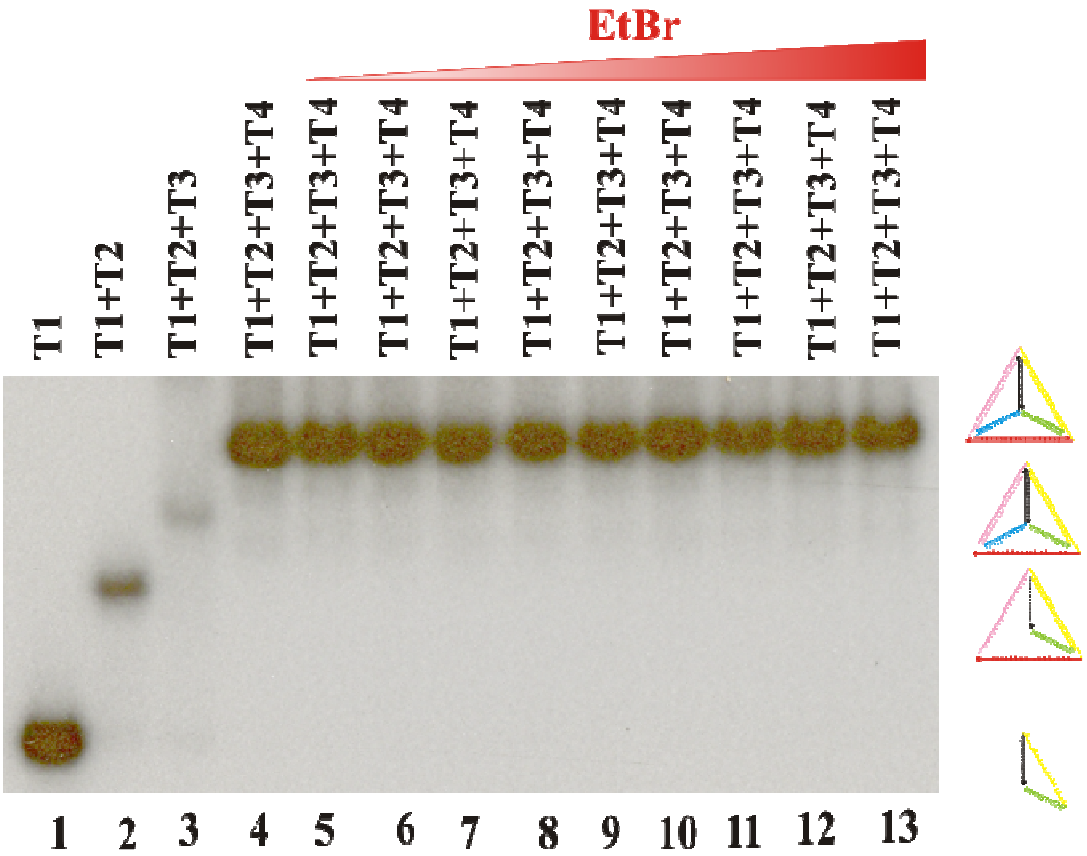

Figure 4.6 Autoradiogram illustrating the interaction between DNA tetrahedron and ethidium bromide on 10% non-denaturing polyacrylamide gel electrophoresis. Lanes 1-3: Control containing T1, T1+T2 and T1+T2+T3 respectively. Lane 4: Control containing strand 1, 2, 3 and 4, (T1+T2+T3+T4), forming a control, DNA tetrahedron (1 µM). Lanes 5-10: Sample containing a DNA tetrahedron in the presence of ethidium bromide. The ratio of DNA tetrahedron in base pairs to ethidium bromide started from 220:1, 220:2, 220:4, 220:8, 220:16, 220:32, 220:55, 220:110 to 220:220 respectively. The concentrations of ethidium bromide corresponding to these ratios are 1, 2, 4, 8, 16, 32, 55, 110 and 220 µM. All the samples were carried out in TM buffer (10 mM Tris, 1 mM 20 mM $MgCl_2$, pH 8.0)

The results (**Figure 4.6**) demonstrate that increasing the concentration of ethidium bromide causes a slight retardation of the migration of the DNA tetrahedron. This result is the converse of what we observed using the iron cylinder. It is possible that ethidium bromide intercalated between base pairs will stiffen the DNA arms leading to a more rigid slower moving tetrahedron. Alternatively, this nanostructure could be unwinded and stiffened by ethidium bromide resulting in the twisting away of the DNA nanostructure.

Moreover, in the presence of ethidium bromide, the band has shifted only a small amount compared to shifts observed with the iron cylinder. This implies that the DNA bending effect of the iron cylinder on the DNA tetrahedron is more powerful than the stiffening effect of ethidium bromide. Nevertheless, both clearly interact differently with the DNA nanostructure.

4.2.3 Atomic Force Microscopy (AFM)

Gel electrophoresis experiments show the change of DNA nanostructure resulting in the accelerated migration. However, imaging and measuring the dimensions of the tetrahedron would be intriguing for monitoring the interaction of the iron cylinder with the DNA nanostructure. Herein, AFM was carried out to image the effect of the iron cylinder on the DNA tetrahedron. In addition, the dimensions of the tetrahedron in the presence and absence of the iron cylinder will be presented. This work was performed in the laboratories of Professor Richard E. Palmer, School of Physics, The University of Birmingham.

The DNA tetrahedron was designed to have six of 17 base pair (bp) edges meeting at one vertex. Consequently, only one orientation giving a height of ~ 6.2 nm is expected on the surface.[8] The three dimensional plot reveals that the height of the DNA tetrahedron is ~ 6-8 nm, corresponding to that observed in the literature. However, the images were not well resolved due to the tip radius. The radius of the tip was 6 nm which is bigger than the nanostructure (~ 6.2 nm) thus resulting in the image appearing as a dot (**Figure 4.7**).

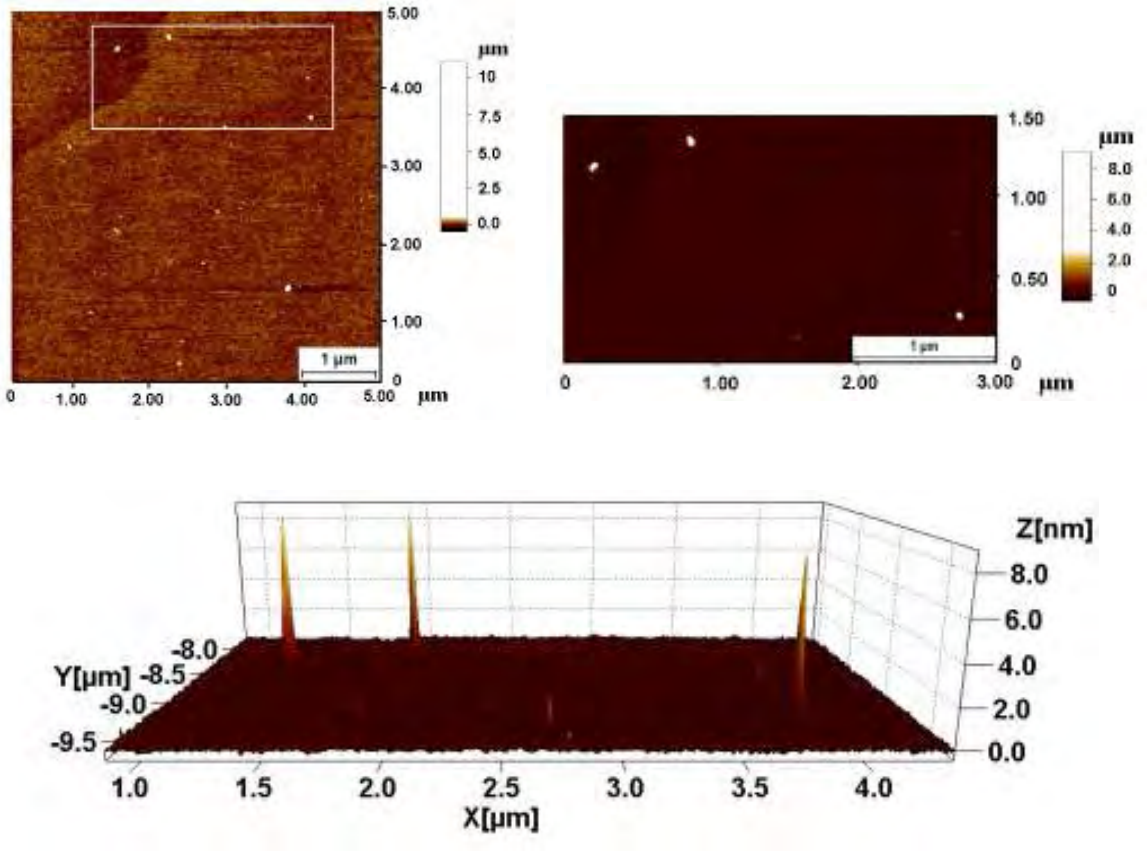

Figure 4.7 AFM images of the DNA tetrahedron. **Top left:** AFM image showing the DNA tetrahedron deposited on a mica surface. **Top right:** Enlargement of the top left image. **Bottom:** A three dimensional plot of the top right image showing the height of the DNA tetrahedron and the scanning area.

In the presence of the iron cylinder (**Figure 4.8**), the plot reveals that the dimension of the DNA tetrahedron was altered. The height of the structure was reduced from ~ 6.2 nm to 2 nm i.e. to a collapsed structure from the bending which corresponds to the gel electrophoresis results. This plot confirms that the iron cylinder interacts with the DNA tetrahedron resulting in a structural change.

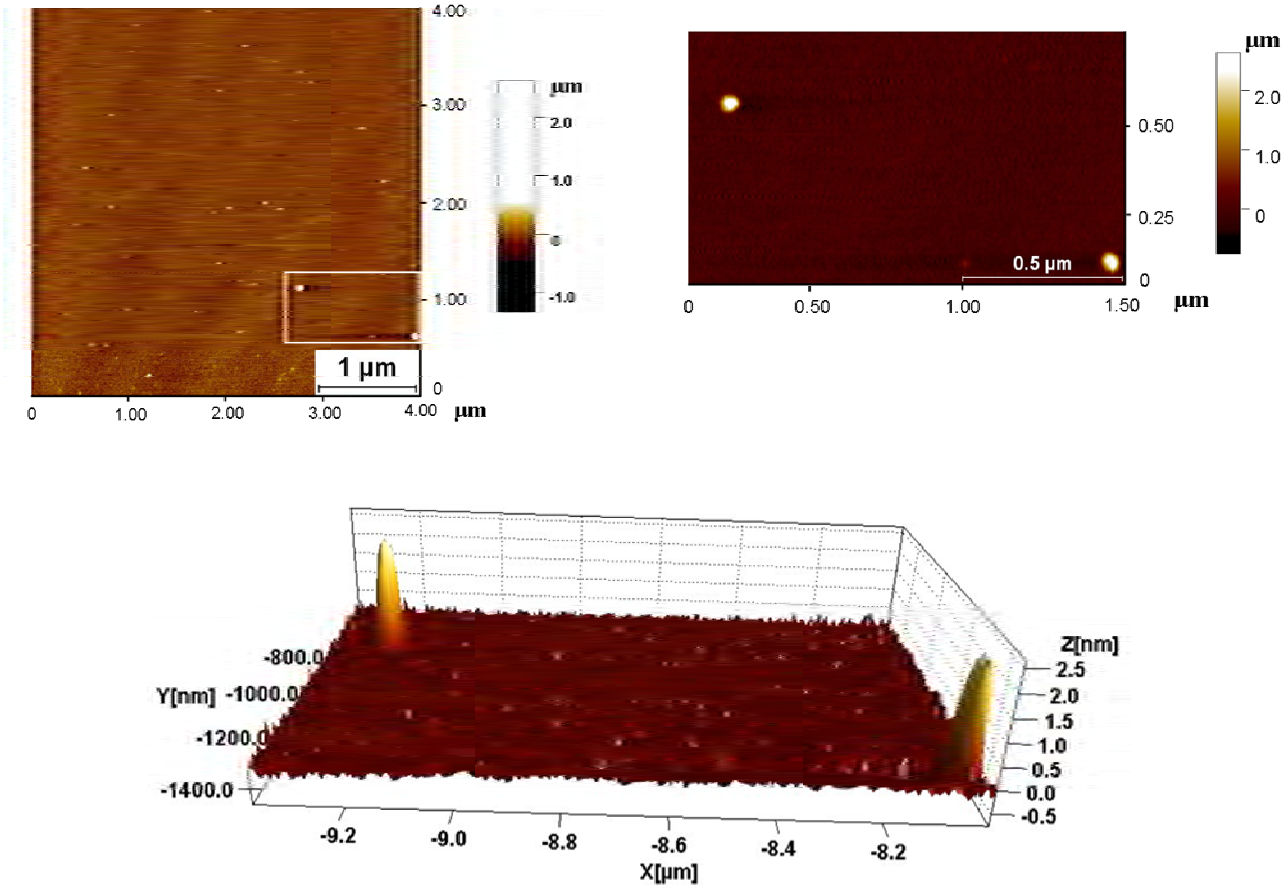

Figure 4.8 AFM images of the DNA tetrahedron treated with iron cylinder. **Top left:** AFM image showing the DNA tetrahedron treated with iron cylinder. **Top right:** Enlargement of the top left image. **Bottom:** Three dimensional plot of the top right image showing the height of the DNA tetrahedron and scanning area. The ratio of tetrahedron:iron cylinder is 1:2.

4.2.4 DNA thermal denaturation studies

It is known that when a solution of DNA is heated enough, the non covalent forces that hold the two strands together are not sufficiently strong enough and the bonds will break. When this happens, the two strands come apart in a process known as DNA melting or DNA denaturation. The temperature at which the DNA strands are half denatured is called the melting temperature or T_m. Plotting absorbance, at 260 nm, against temperature is known as a melting curve.[17] T_m is usually used to indicate the stability of the double helix DNA. The interaction of synthetic agent and DNA may alter T_m by

stabilising (increase of T_m) or destabilising (decrease of T_m) effect. Therefore, the melting curve experiment was established to monitor the stability of the iron cylinder and DNA tetrahedron adduct.

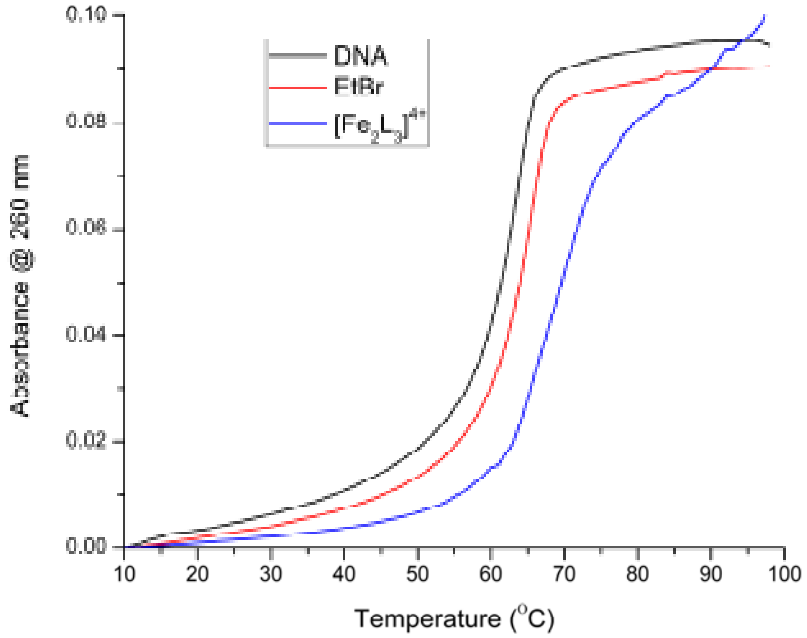

Figure 4.9 Melting curve of the DNA tetrahedron (10 μM) in the presence of the iron cylinder ($[Fe_2L_3]^{4+}$; 10 μM)) at ratio 1:1 (DNA tetrahedron:complex) and ethidium bromide (EtBr; 1.1 mM) at ratio 2:1 (DNA(bases):ethidium bromide). All samples were carried out in TM buffer (10 mM Tris, 5 mM $MgCl_2$, pH 8.0)

On the addition of ethidium bromide to the DNA solution, the DNA melting temperature was found to increase from 64 °C to 66 °C at the ratio of DNA tetrahedron base pair:ethidium bromide of 2:1. This shows that the stability of the DNA tetrahedron is increased by ethidium bromide. Note that at lower ratios (less than 2:1) no change in the melting temperature was observed. Monitoring at higher ratios of the DNA base pair to ethidium bromide was not achievable due to the overlap of absorbance, from ethidium

bromide, with the DNA at 260 nm. Interestingly, the melting temperature significantly increased from 64 °C to 69 °C in the presence of $[Fe_2L_3]^{4+}$ at a ratio of DNA tetrahedron:$[Fe_2L_3]^{4+}$, 1:1. Just as for ethidium bromide, at higher concentration of the cylinder, overlapping spectroscopy was an issue and at lower concentration, no change was found. These results show that the iron cylinder ($[Fe_2L_3]^{4+}$) has a greater ability in stabilising the DNA tetrahedron than ethidium bromide, used as a control.

4.3 Conclusions

Herein, it is shown that the iron cylinder interacts with the DNA tetrahedron, known to have a rigid structure confirmed by a number of techniques. Firstly the CD experiment suggests that the cylinder and DNA B-structure are not affected by their interactions. Gel electrophoresis demonstrates that the structure of the DNA tetrahedron changes in the presence of the iron cylinder, shown by the migration of the bands. The topological information obtained from AFM demonstrates that the dimensions of the structure are altered. Additionally, the dimensional measurements carried out support the topological change. AFM images reveal that the height of the tetrahedron in the presence of the iron cylinder is reduced from 6.2 nm to 2 nm. Finally, a thermal denaturation experiment indicates that the stability of the DNA tetrahedron treated with the iron cylinder is greater than the one without the iron cylinder. The studies in this chapter were mainly focused on how the iron cylinder and ethidium bromide interact with the nanostructure. It would be interesting to carry out the experiment in which the nanostructure was assembled in the presence of ligand e.g. T1+ligand, T1+T2+ligand,

T1+T2+T3+ligand and T1+T2+T3+T4+ligand. It could be possible that the binding of the ligand to the preformed DNA may change the topology of the final nanostructure.

4.4 Experimental

Assembly of Tetrahedra.[7] To form the tetrahedral, equimolar quantities (10 μM) of oligonucleotides 1 to 4 were combined in TM buffer (10 mM Tris, 5 mM $MgCl_2$, pH 8.0), heated to 95°C for 2 minutes and then cooled to 4°C over 30 seconds using a PCR machine (Eppendorf Mastercycler). All oligonucleotides were supplied by MWG Eurofin (Germany). Strand T1: ACA TTC CTA AGT CTG AAA CAT TAC AGC TTG CTA CAC GAG AAG AGC CGC CAT AGT A. Strand T2: TAT CAC CAG GCA GTT GAC AGT GTA GCA AGC TGT AAT AGA TGC GAG GGT CCA ATA C. Strand T3: TCA ACT GCC TGG TGA TAA AAC GAC ACT ACG TGG GAA TCT ACT ATG GCG GCT CTT C. Strand T4: TTC AGA CTT AGG AAT GTG CTT CCC ACG TAG TGT CGT TTG TAT TGG ACC CTC GCA T

Circular Dichroism (CD): A spectropolarimeter (JASCO) was used for CD measurements. The parameters used are as follows; 100 mdeg; data pitch, 0.5 nm; scanning mode, continuous; scanning speed, 200 nm per min; response, 0.1 seconds; bandwidth, 1.0; accumulation, 12. The experiments were performed at 25 °C with 1 cm path length cuvette (Strana) for measuring at 200-750 nm. Before the measurement, the DNA tetrahedron was formed as described above. 250 μl of the DNA tetrahedron (10 μM) in buffers of 0.89 mM Na-cacodylate (pH 7.0) and 20 mM NaCl were titrated with complex (250 μM). The concentration of the DNA tetrahedron (bases):complex ratios are 60:1, 30:1, 15:1, 8:1, 6:1 and 4:1. During the titration UV-Vis spectra (Cary 5000) were recorded.

Gel electrophoresis:

Polyacrylamide gel preparation: 10% native polyacrylamide gel solution containing 20 ml of 10x TB buffer pH 8.3 (890 mM tris(hydroxymethy) amino methane, 890 mM boric acid), 50 ml of 40% acrylamide (29:1) from Geneflow, 130 ml of milliQ water, 1ml of 10%(w/v) ammonium persulfate and 100 µl TEMED, was poured onto a set of glass plates. The wells of the polymerised gel were thoroughly washed with a running buffer (TB buffer) before use. Note that prerunning of the gel at 200 volts for 5 minutes is required before the experiment is performed.

Gel electrophoresis experiment: 20 µl of the samples in 1.5 ml Eppendorf tubes were prepared by mixing the tetrahedra assembled (1 µM as final concentration) with the iron cylinder $[Fe_2L_3]^{4+}$ in TM buffer. Ratios of the DNA tetrahedron (bases) to complex were 220:0.5, 220:1, 220:2, 220:4, 220:8 and 220:16 respectively while ratios of the DNA tetrahedron (bases) to ethidium bromide were 220:1, 220:2, 220:4, 220:8, 220:16, 220:32, 220:55, 220:110 and 220:220. The samples were incubated at room temperature for 1 hour and then on ice for 20 min. 10 µl of 30% glycerol was added to each sample to increase the density of the sample to be able to sink into a well. All samples then were loaded into 10% polyacrylamide gel. Note that loading dye (5x GelPilot DNA Loading Dye, QIAGEN) was separately loaded into the first and the last well to mark where the DNA migrates to. The gel was run at 120 volt for 2.50 hours then the gel was placed in between a sheet of 3MM whatman paper and Saran wrap. The film (Kodak, Sigma-aldrich) was exposed on the gel overnight at -80°C. The film was developed by Curix60 processor (AGFA).

AFM imaging: samples were prepared for AFM by placing a drop containing 10 µl of 10 nM tetrahedron or tetrahedron treated with metal complex (ratio tetrahedron :

complex ; 1:2) in TM buffer (10 mM Tris, 15 mM $MgCl_2$, pH 8.0) and 2 µl of 10 mM $NiCl_2$[18] on freshly cleaved mica (1 cm × 1 cm) by the adhesive tape. After incubating for 30 minutes, the samples were rinsed for 5 seconds in a jet of deionised water directed onto the surface with a squeeze bottle. The samples were blow dried with compressed nitrogen gas and imaged using a Dimension 3100 scanning probe microscope and Nanoscope IIIa controller (Veeco, California), operation in tapping mode in air at a scan rate of 1-2 Hz. The AFM probes were 125 µm-long cantilever made of single crystal silicon with pyramidal shaped Si tips (VISTAprobes), with an average resonance frequency of 300 kHz and spring constant K = 40 N/m. The tip radius given by the supplier (Vistaprobes T300) is <10 nm. The images were obtained at room temperature (T = 23 ± 2 °C). The samples were imaged in several places and many times

DNA melting curve: The experiment was run simultaneously in the cuvettes of 1.2 mL volume using a thermostatic cell-changer UV-Vis spectrophotometer on a Cary 5000 spectrophotometer. Solution of a DNA tetrahedron, a DNA tetrahedron-metal complex consisting of DNA (bases):complex in a ratio of 220:1 and a DNA tetrahedron-ethidium bromide solution of DNA (base):ethidium bromide; 220:110 were prepared. The solutions were prepared independently and all contained the same DNA nanostructure concentration (10 µM) as well as buffer (TM buffer; 10 mM Tris, 5 mM $MgCl_2$, pH 8.0). Before and after running the melting curves, UV spectra of the solutions were recorded. Cary 5000 UV-Visible Parameters: wavelength: 260 nm; signal band width: 1.0 nm; average time: 10.0s; data interval: 0.2°C; temperature scan: 10–95°C; ramp rate: 0.2°C/min; hold time: 10.0.

4.5 References

1. N. C. Seeman, *J. Biomol. Struct. Dyn.*, 1985, **3**, 11-34.
2. N. C. Seeman, *Annu. Rev. Biophys. Biomolec. Struct.*, 1998, **27**, 225-248.
3. N. C. Seeman, *J. Theor. Biol.* , 1982, **99**, 237-247.
4. J. Chen and N. C. Seeman, *Nature*, 1991, **350**, 631-633.
5. Y. W. Zhang and N. C. Seeman, *J. Am. Chem. Soc.*, 1994, **116**, 1661-1669.
6. W. M. Shih, J. D. Quispe and G. F. Joyce, *Nature*, 2004, **427**, 618-621.
7. R. P. Goodman, R. M. Berry and A. J. Turberfield, *Chem. Commun.*, 2004, 1372-1373.
8. R. P. Goodman, I. A. T. Schaap, C. F. Tardin, C. M. Erben, R. M. Berry, C. F. Schmidt and A. J. Turberfield, *Science*, 2005, **310**, 1661-1665.
9. C. M. Erben, R. P. Goodman and A. J. Turberfield, *Angew. Chem. Int. Ed.*, 2006, **45**, 7414-7417.
10. H. Ozhalici-Unal and B. A. Armitage, *ACS Nano*, 2009, **3**, 425-433.
11. M. J. Hannon, C. L. Painting, A. Jackson, J. Hamblin and W. Errington, *Chem. Commun.*, 1997, 1807-1808.
12. M. J. Hannon, V. Moreno, M. J. Prieto, E. Moldrheim, E. Sletten, I. Meistermann, C. J. Isaac, K. J. Sanders and A. Rodger, *Angew. Chem. Int. Ed.*, 2001, **40**, 880-884.
13. I. Meistermann, V. Moreno, M. J. Prieto, E. Moldrheim, E. Sletten, S. Khalid, P. M. Rodger, J. C. Peberdy, C. J. Isaac, A. Rodger and M. J. Hannon, *Proc. Natl. Acad. Sci. U. S. A.*, 2002, **99**, 5069-5074.

14. A. Oleksi, A. G. Blanco, R. Boer, I. Uson, J. Aymami, A. Rodger, M. J. Hannon and M. Coll, *Angew. Chem. Int. Ed.*, 2006, **45**, 1227-1231.

15. M. J. Hannon, I. Meistermann, C. J. Isaac, C. Blomme, J. R. Aldrich-Wright and A. Rodger, *Chem. Commun.*, 2001, 1078-1079.

16. J. M. C. A. Kerckhoffs, J. C. Peberdy, I. Meistermann, L. J. Childs, C. J. Isaac, C. R. Pearmund, V. Reudegger, S. Khalid, N. W. Alcock, M. J. Hannon and A. Rodger, *Dalton Trans.*, 2007, 734-742.

17. Y.-J. Liu, H. Chao, L.-F. Tan, Y.-X. Yuan, W. Wei and L.-N. Ji, *J. Inorg. Biochem.*, 2005, **99**, 530-537.

18. H. G. Hansma and D. E. Laney, *Biophys. J.*, 1996, **70**, 1933-1939.

Chapter 5

The determination of the binding constant of the iron cylinder to oligonucleotide by Surface Plasmon Resonance (SPR)

5.1 Introduction

The determination of a binding constant from an experiment is important for investigating interaction of a drug and its target. There are several methods facilitating calculation of the binding constant between the DNA binding drug and target DNA such as UV-Vis absorption spectroscopy[1-3] DNA footprinting[4], circular dichroism (CD)[5] and fluorescence quenching[6]. However, these techniques can have drawbacks, for example absorption spectroscopy requires hypochromism of absorption band while radiolabelling is desired for DNA footprinting. CD experiments can be time consuming. Quenching in fluorescence by ethidium bromide displacement is an indirect approach to determine the binding constant, defined as apparent binding constant. Therefore, the alternative techniques for the determination of the binding constant which are reliable, detect the interaction in real time and do not involve labelling are desirable.

Surface plasmon resonance (SPR) potentially fulfills all these requirements. This biosensor technology has recently become an established method of measuring a variety of biomolecular interactions (principally involving proteins), e.g. kinetics and equilibrium constants, in real time and characterising binding reactions in the absence of any labelling requirements.[7-13] The principle of SPR-based instruments (**Figure 5.1**) is to measure the refractive index near a sensor surface. In order to detect an interaction, the receptor which might be either DNA or protein is immobilised onto the sensor surface. The analyte (molecule of interest) is injected in aqueous solution through the flow cell, under continuous flow.

When the analyte and the receptor interact to form a complex, the SPR detector records changes in refractive index near the sensor surface in real time. These changes are proportional to the mass of molecules binding to the surface. The result, plotted as response in resonance unit (RU) versus time (second), is known as a sensorgram.

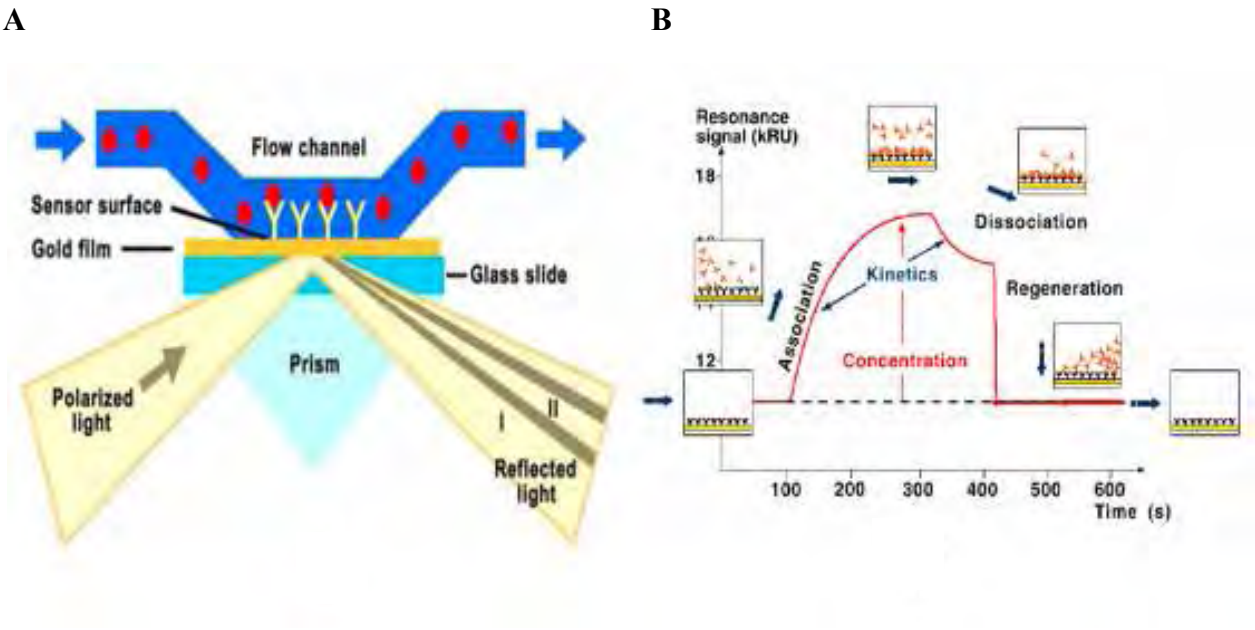

Figure 5.1 A) Schematic diagram of basic components for SPR biosensor: Light passes through the prism and slide, reflects off the gold film and passes back through the prism to a detector. Changes in reflectivity versus angle give a signal that is proportional to the amount of complex bound near the surface. **B)** Schematic sensogram, showing association, dissociation and regeneration phases: (1) Association of analyte with DNA during sample injection; (2) Dissociation of analyte from the surface during the buffer flow; (3) Regeneration of the complex to allow surface to be re-used many times. Taken from ref. [14]

SPR based biosensor technology is widely exploited to determinate the binding constant and stoichiometry of binding as shown in **Table 5.1**

Table 5.1 Studies of the interaction between DNA-binding drugs and target DNA sequences facilitated by SPR technique. Taken from ref. [15]

Analyte (DNA-binding drug)	Ligand (target DNA)	K_b (M^{-1})[a]	K_b (M^{-1})[b]	n[c]
Sandramycin	5'-d(GCATGCTTTTGCATGC) 5'-d(GCGCGCTTTTGCGCGC) 5'-d(GCCGGCTTTTGCCGGC) 5'-d(GCTAGCTTTTGCTAGC)	9.0×10^7 3.8×10^7 2.5×10^7 2.3×10^7	7.8×10^7 4.0×10^7 1.5×10^7 1.8×10^7	1.0 1.0 0.83 0.83
Actinomycin	47 bp DNA sequence including five G-C sites		1.9×10^6	
Mithramycin	HIV-1 Sp1 DNA			6
Distamycin	HIV-1NF-kB DNA			5
Carbazole dication derivatives	DNA hairpin oligomer with stem sequences CGAATTCG		K_1= 1.2~6.1x10^6, K_2= 2.5~4.2x10^5	1.4
DB293 (aromatic dication)	Oligo2-1 hairpin duplex		K_1= 2.8×10^6, K_2= 7.3×10^7	2
DB293 derivative	CTATGAC-containing Oligo2-1		K_1=1.38×10^7, K_2=6.20×10^7	2
DB293 derivative	AATT- containing Oligo1		K_1=3.11×10^7, K_2=1.22×10^4	1
DB358 (trithiophene derivates of furimidazoline)	AT, AATT, and GC-containing hairpin loop DNA sequence		1.7×10^6, 1.4×10^6, 0.6×10^6, respectively	3
Acridine derivative 1, 2, 3, 4	d($AG_3[T_2AG_3]_3$) duplex sequence	1.1×10^6, 2×10^5, 4×10^5, 5×10^5		
Acridine derivative 1, 2, 3, 4	d($AG_3[T_2AG_3]_3$) quadruplex sequence	1.3×10^6, 8.3×10^5, 1.6×10^7, 1.6×10^7		
2,7 bis-amidine carbazole	d(CATATATATCCCCATATATATG) d(CGCGCGCGTTTTCGCGCGCG)		K_1=11.5×10^6; K_2= 0.9×10^6 K_1=2.5×10^5; K_2= 0.8×10^5	
3,6 bis-amidine carbazole	d(CATATATATCCCCATATATATG) d(CGCGCGCGTTTTCGCGCGCG)		K_1=2.3×10^6; K_2= 0.3×10^6 K_1=4.7×10^5; K_2= 1.1×10^5	
DB293(aromatic dication)	Various 13-bp sequences including ATGA motif		K_1=0.3~1.8×10^6; K_2= 4.1~9.5×10^7	2
Ditercalinium	d(CGAATTCGTCTCCGAATTCG) d(CGCGCGCGTTTTCGCGCGCG) d([AG_3[$TTAG_3$]$_3$]	0.9×10^7 1.0×10^7 3.0×10^7		2 2 2
AT2433-B1 (indolocarbazole aglycone compound)	AT-rich DNA sequence GC-rich DNA sequence		13×10^3 (25°C), 15×10^3 (4°C) 89×10^3 (25°C), 76×10^3 (4°C)	4-5 3
DB75-related diphenylfuran dications	5'-biotin-CATATATATCCCCATATATATG-3' 5'-biotin-CGCGCGCGTTTTCGCGCGCG-3'			

(Table 1. Contd....)

Analyte (DNA-binding drug)	Ligand (target DNA)	K_b (M^{-1})[a]	K_b (M^{-1})[b]	n[c]
Macrocyclic compound BOQ1	d(CGAATTCGTCTCCGAATTCG) d(CGCGCGCGTTTTCGCGCGCG) d([AG_3($TTAG_3$)$_3$]		$1.1x10^6$ $1.5x10^6$ $1.2x10^7$	2 2 2
Macrocyclic monomer MOQ2	d(CGAATTCGTCTCCGAATTCG) d(CGCGCGCGTTTTCGCGCGCG) d([AG_3($TTAG_3$)$_3$]		$1.1x10^6$ $1.9x10^6$ $1.4x10^6$	1 1-2 2
Macrocyclic monomer MMQ1	d(CGAATTCGTCTCCGAATTCG) d(CGCGCGCGTTTTCGCGCGCG) d([AG_3($TTAG_3$)$_3$]		$4.7x10^5$ $4.1x10^5$ $8.6x10^5$	3 4-5 4

[a] Binding constant calculated as $K_b = k_a / k_d$

[b] Steady state Binding constant calculated as $R/C = K_b R_{max} - K_b R$

[c] Stoichiometry of binding

It is know that the triple stranded iron cylinder interacts with DNA by binding in the major groove and causes intramolecular coiling and also binds to the hollow cavity of a DNA three way junction.[16, 17] As mentioned above, the binding constant of the DNA and DNA binding drug is important for the design of new anticancer drugs in terms of preferential binding of the drug to a particular DNA site. Pebedery *et al.* initially determined the binding constant of the iron cylinder and calf thymus DNA by ethidium bromide displacement assay.[6] The principle of this technique is based on fluorescent quenching. The experiment is carried out by adding iron cylinder $[Fe_2L_3]^{4+}$ to a solution of DNA with sufficient ethidium bromide. The fluorescence dramatically increases when ethidium bromide binds to DNA. The principle of ethidium bromide displacement is based on the fact that the iron cylinder which has a high positive charge (4+), serving as a stronger binder, will displace ethidium bromide bound DNA resulting in decreasing fluorescent intensity due to the displacement. The binding constants determined from the ethidium bromide displacement experiment are 6 x 10^7, $7x10^7$ and $7x10^7$ M^{-1} for the iron cylinder in racemic mixture and the M and the P enantiomers, respectively, to calf thymus DNA. However, two criteria are needed to be considered: 1) the quenching of

fluorescence could either originate from the displacement of ethidium bromide, bound to DNA, by the cylinder or the cylinder interacting with the ethidium bromide without displacement occurring. 2) the binding mode of ethidium bromide and the cylinder is different. Ethidium bromide is known as an intercalator while the cylinder is a major groove binder.[16] These criteria show that this technique should be used with caution for determining the binding constant of the iron cylinder to DNA.

To try to more accurately determine the binding constant and the kinetic behaviour of the iron cylinder, and its enantiomers, with DNA. SPR based technique is explored herein.

5.2 Results and discussion

5.2.1 Streptavidin immobilisation

To introduce the SPR technique, an overview of the principle steps of a SPR experiment are described as follows (**Figure 5.2**).

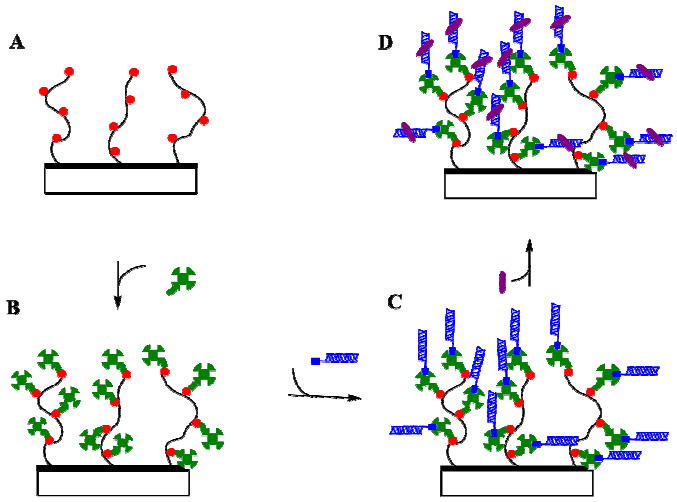

Figure 5.2 Overview of SPR experiment. **A)** Sensor surface. **B)** Carboxyl group (red spheres) conjugated with streptavidin (green). **C)** The binding of biotinylated oligonucleotide (blue) to streptavidin. **D)** The binding of the iron cylinder (purple) to oligonucleotide.

Firstly, the correct sensor chip is chosen for the experiment. Secondly, the functional group on the sensor surface needs to be activated to be able to conjugate a ligand (DNA) to the chip surface. Then, analyte (the iron cylinder) is injected over the flow cells containing immobilised ligands. Finally, the binding constant is calculated from the results of the experiment using a mathematical equation.

In our studies, a CM5 sensor chip was chosen for the experiment due to its versatility and popularity for the direct immobilisation of the ligand (oligonucleotide). The CM5 surface is shown in **Figure 5.3**.

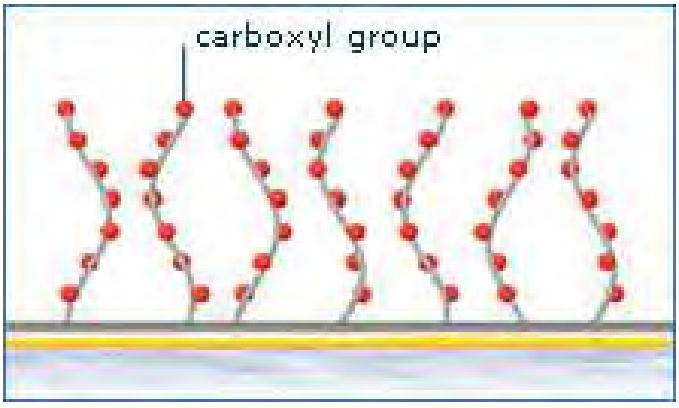

Figure 5.3 Schematic drawing illustrating the carboxymethylated dextran covalently attached to the gold surface of CM5 chip. Taken from ref.[18]

To immobilise the oligonucleotide to the sensor surface, the chip was treated with streptavidin providing a functional group to bind to the biotinylated oligonucleotide via the streptavidin-biotin interaction. The sensorgram of streptavidin immobilisation over four flow cells is shown in **Figure 5.4**.

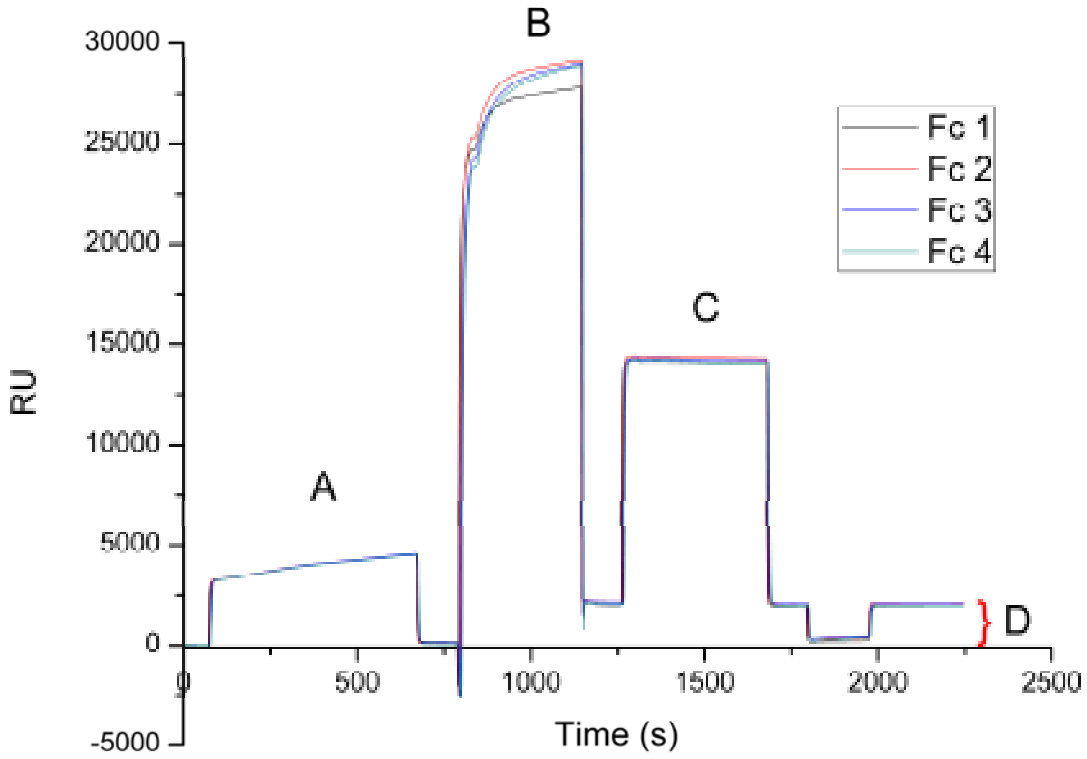

Figure 5.4 Sensorgram for streptavidin immobilisation on the CM5 chip.

The sensorgram in **Figure 5.4** is a plot between response (RU) in Y axis and time (s) in X axis. The outstanding three peaks, marked A, B and C on the sensorgram are the result of the refractive index changing due to the binding of injected chemicals to the surface. The matrix of this CM5 chip is carboxymethylated dextran covalently attached to a gold surface; this group is suitable for covalently coupling target molecules to the sensor surface via amine, thiol, aldehyde or carboxyl groups. The first peak (peak A) corresponds to injection of an EDC-NHS mixture. The NHS (N-hydroxysuccinimide) activates the carboxymethyl groups on the surface, thus creating a highly reactive succinimide ester which will react with an amine group on streptavidin in the next step. The second peak (peak B) corresponds to the streptavidin immobilisation on the surface.

To block the remaining activated carboxymethyl groups, ethanolamine was injected to quench and elute a non-covalent bound material as shown in peak C. The amine coupling via reactive esters is demonstrated in **Figure 5.5**. The amount of streptavidin immobilised on the surface was calculated by subtracting response (RU) at the end of injection from response (RU) at the beginning of injection as labelled D in **Figure 5.4**. The streptavidin was immobilised at similar loading (1895.9, 2002.1, 1986.4 and 1896.4 response unit in flow cell 1, 2, 3 and 4 respectively).

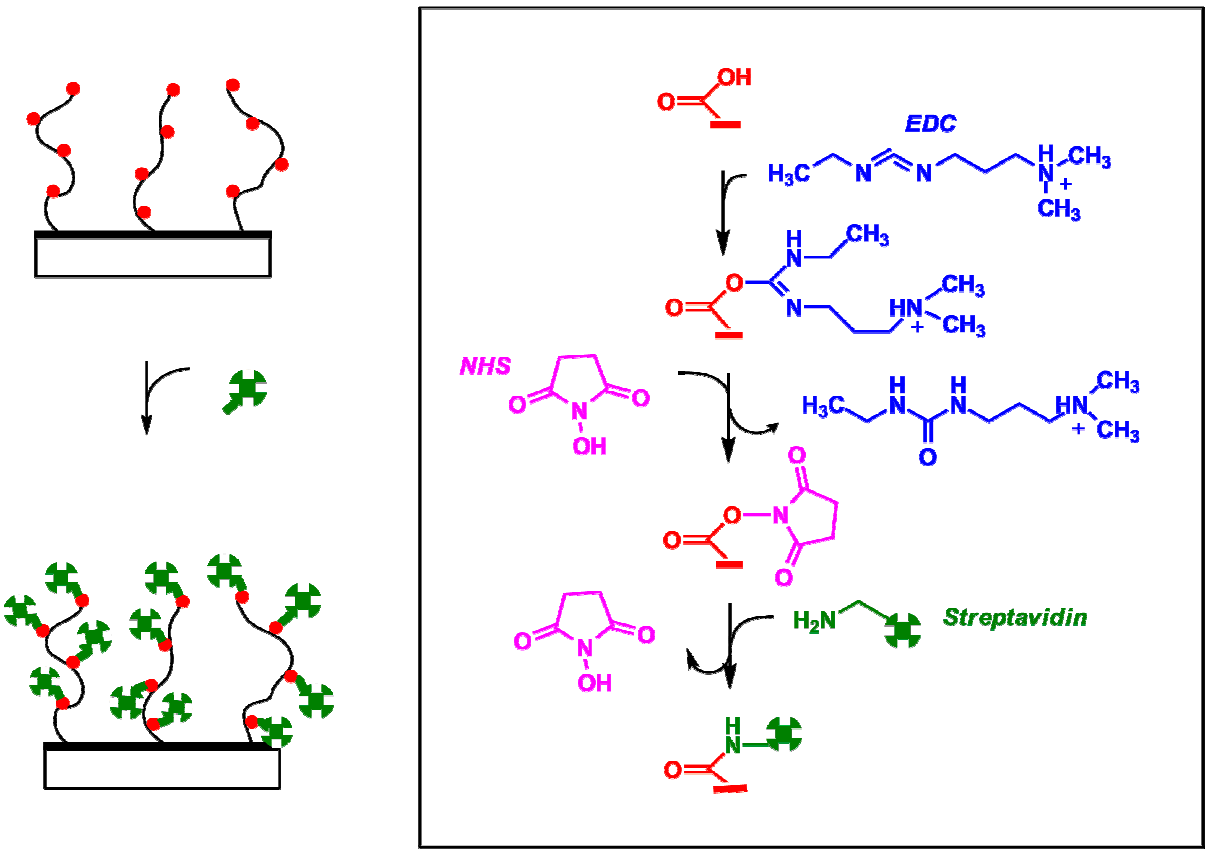

Figure 5.5 Streptavidin immobilisation. **Left:** A simple schematic drawing of streptavidin immobilisation. The red spheres represent carboxyl group on dextran (black line). The green cartoons illustrate streptavidin **Right:** Reaction scheme of carboxyl (COOH) activation with EDC/NHS.

5.2.2 Oligonucleotide immobilisation

The hairpin oligonucleotide labelled with biotin at 5′end (5′ 5GC ATC GTT TTC GAT GC 3′; 5 is biotin) was injected over three flow cells (1, 2 and 3) with streptavidin coated surfaces. Flow cell 4 was left as a control. A time-dependent, stable immobilisation of DNA was observed (**Figure 5.5**) on the streptavidin surface.

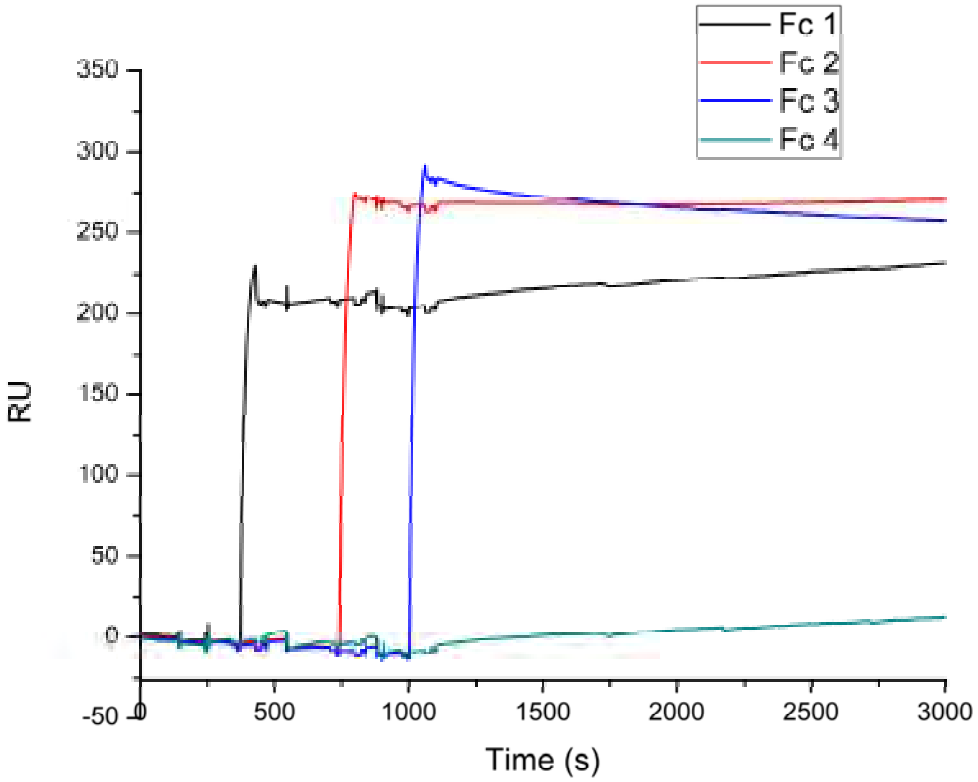

Figure 5.5 Sensorgram of the biotinylated oligonucleotide bound to surface treated with streptavidin.

The sensorgram in **Figure 5.5** shows the large change in refractive index during immobilisation due to the binding of biotinylated oligonucleotide and streptavidin immobilised on the surface. The response (RU) of oligonucleotide immobilisation were 214.2, 280.4, 293.6 RU in flow cell 1, 2 and 3 respectively. Flow cell 4 was a reference cell so the response (RU) was zero.

5.2.3 Affinity binding study of the iron cylinder to the oligonucleotide

The binding of the iron cylinder to the oligonucleotide was carried out in cacodylate buffer containing 150 mM NaCl, pH 7.95. These conditions were established to give reproducible results and minimise the non specific binding of the cylinder to the sensor surface. Different concentrations of the iron cylinder, $[Fe_2L_3]^{4+}$, increasing from 0.117 to 15 µM were injected across the four flow cells. The sensorgram of $[Fe_2L_3]^{4+}$ binding to immobilised oligonucleotide is shown in **Figure 5.6.**

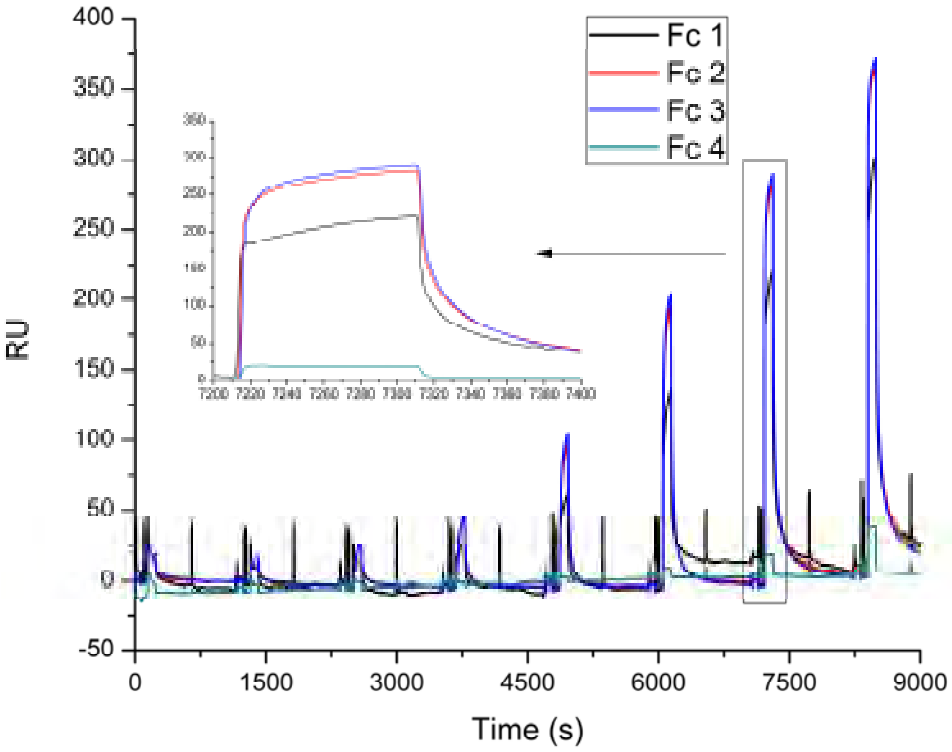

Figure 5.6 Overlay plot sensorgrams of the iron cylinder $[Fe_2L_3]^{4+}$ binding to oligonucleotide of flow cell 1, 2 and 3 in 150mM NaCl and 100 mM cacodylate buffer, pH 7.95.

Each peak in the sensorgram represents the binding of $[Fe_2L_3]^{4+}$ to the oligonucleotide in each injection carried out from low to high concentration of $[Fe_2L_3]^{4+}$. The sensorgram in **Figure 5.6** demonstrates that each peak corresponding to refractive index increases

rapidly and then levels off to an equilibrium in a short time (approximately 105 seconds). This indicates that $[Fe_2L_3]^{4+}$ binds strongly to the immobilised oligonucleotide. Although most of the iron cylinder ($[Fe_2L_3]^{4+}$) was dramatically dissociated from oligonucleotide in 15 min, some small quantities of $[Fe_2L_3]^{4+}$ remained on the chip, as the level of sensorgram before and after the injection was not at the same level. In addition the remaining iron cylinder on the surface was apparently increased at high concentration of the injected iron cylinder. However, the remaining $[Fe_2L_3]^{4+}$ on the sensor chip was not significant compared to the huge binding signal achieved. The sharp spikes in flow cell 1 suggest that air bubbles blocked the flow cell during injection. Therefore, this flow cell was not taken into account for the binding constant determination. Surprisingly, there were small signals in flow cell 4 which was a control, presumably indicating some weak adhesions of the cylinder to streptavidin. However, these signals are considerably smaller than the responses in the other three cells. Nevertheless, the response from flow cell 4, reference cell, will be subtracted from flow cells 2 and 3 to obtain the corrected equilibrium response. The overlay of the concentrations in flow cell 2 and 3 is illustrated in **Figure 5.7**. It can be seen that the dissociation of the iron cylinder from the oligonucleotide, started from ~ 235 seconds, was rapidly decreased (in few second) then it took long time (~ 400 seconds) to be completely dissociated. This clearly suggests that the iron cylinder exhibits biphasic dissociation kinetics to oligonucleotide.

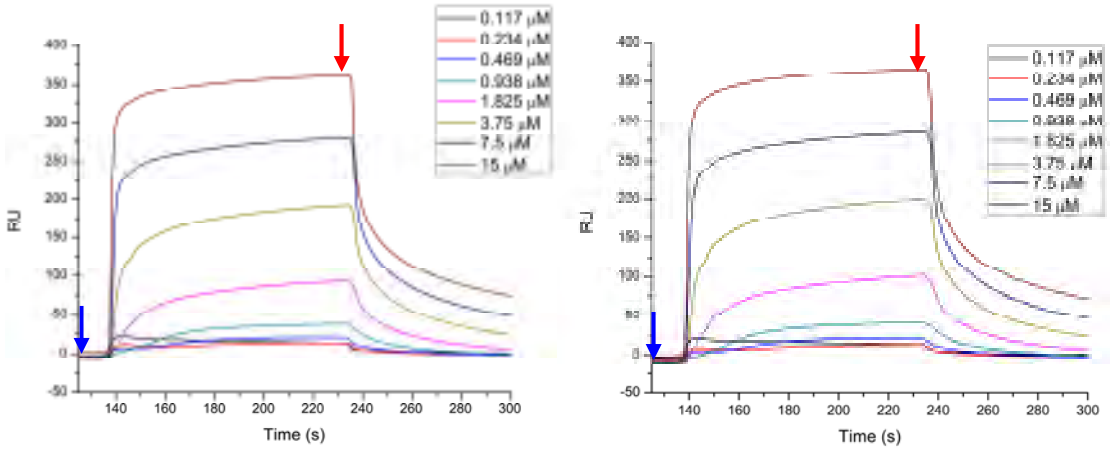

Figure 5.7 Overlay plot sensorgrams of the iron cylinder $[Fe_2L_3]^{4+}$ binding to the oligonucleotide. The concentration of the cylinder was increased from 0.117 µM (bottom curve) to 15 µM (top curve). **Left:** Flow cell 2. **Right:** Flow cell 3. The blue arrow represents the initial RU value before the iron cylinder is injected onto the surface while the red arrow marks the point that DNA-$[Fe_2L_3]^{4+}$complex is in the equilibrium phase.

5.2.3.1 Equilibrium analysis

The formation of the analyte-ligand complex (AB) can be defined as shown in **Equation 1.**

$$A + B \underset{k_d}{\overset{k_a}{\rightleftharpoons}} AB \qquad (1)$$

Where k_a and k_d are the rate constants for the association and dissociation respectively of DNA-drug complex. A is analyte, $[Fe_2L_3]^{4+}$. B is the ligand, DNA. Therefore, the rate of complex formation is demonstrated below.

$$\frac{d[AB]}{dt} = k_a[A]([B]_0 - [AB]) - k_d[AB] \qquad (2)$$

where [AB] is the amount of bound analyte, [A] is the amount of a free analyte ,$[B]_0$ is the total amount of ligand on the sensor surface. The binding constant can be calculated by the method as described below.

If the total amount of ligand $[B]_0$ is represented in terms of the maximum analyte binding capacity of the surface ,i.e., the total amount of DNA binding sites on the sensor surface, then the concentration term is equal to and can be changed to SPR response signal, R. The binding can be expressed as shown below.

$$\frac{dR}{dt} = k_a C(R_{\max} - R) - k_d R \qquad (3)$$

where dR/dt is the rate of change of the SPR response signal. R is the response signal directly measured from the binding. R_{max} is the maximum response signal at the saturation surface binding site. This can be determined as described below. C is the injected concentration of the drug analyte (M). k_a is the association rate constant ($M^{-1}s^{-1}$) and k_d is the dissociation rate constant (s^{-1}). The binding constant, i.e., association constant, K_A, may be calculated as $K_A = k_a / k_d$ (M^{-1}). At equilibrium, dR/dt = 0 and **Equation 3** can be rewritten.

$$\frac{R_{eq}}{C} = K_A R_{\max} - K_A R_{eq} \qquad (4)$$

Therefore, the steady state association constant K_A can be obtained from the slope of a plot of R_{eq} /C versus R_{eq} and the dissociation constant K_D can be calculated as $1/K_A$ as illustrated in **Figure 5.8**. This plot is called a Scatchard plot.[19] Although the data is frequently represented in a Scatchard plot (R_{eq}/C vs R_{eq}) as a straight line, large errors can occur in the plot, especially at low concentration.[20] Therefore a non-linear regression shown in **Equation 5** is selected for the binding constant calculation.

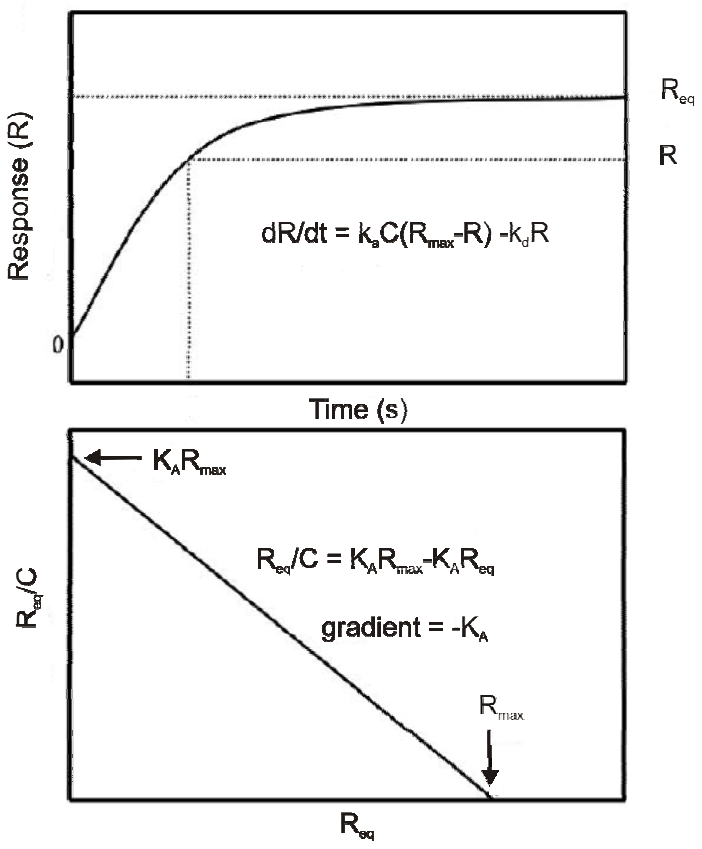

Figure 5.8 Top: Simulated sensorgram illustrating affinity and kinetic measurement of DNA-drug interaction according to Equation (3). **Bottom:** A plot of R_{eq}/C against R_{eq} at different drug concentration according to Equation (4) thus giving a straight line from which R_{max} and K_A can be calculated. Taken from ref.[15]

From **Equation 3**, at equilibrium, dR/dt = 0,

$$0 = k_aC\,(R_{max}-R_{eq}) - k_dR_{eq} \quad (5)$$

$$k_dR_{eq} = R_{max}k_aC - R_{eq}k_aC \quad (6)$$

Divided by k_d on both side and $K_A = k_a / k_d$

$$R_{eq} = R_{max}K_AC - R_{eq}K_AC \quad (7)$$

$$R_{eq} + R_{eq}K_AC = R_{max}K_AC \quad (8)$$

$$R_{eq}(1 + K_AC) = R_{max}K_AC \quad (9)$$

$$R_{eq} = \frac{R_{max} K_A C}{(1 + K_A C)} \qquad (10)$$

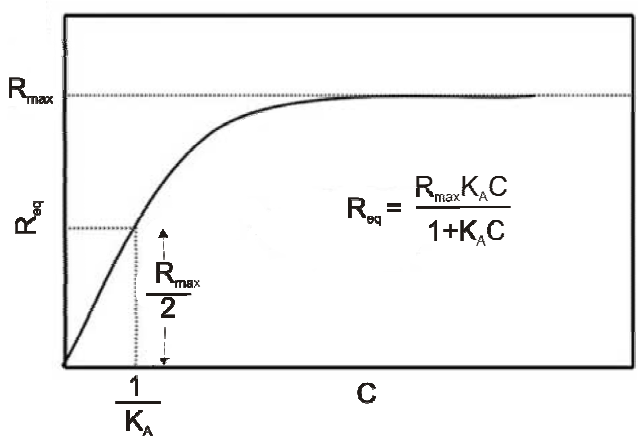

Figure 5.9 A binding curve of the steady state binding response R_{eq} versus drug concentration C according to Equation (10). Taken from ref.[15]

The maximum response (R_{max}) can be obtained from the plot of SPR response in resonance units (RU) against the concentration of the analyte. Furthermore, the equilibrium binding constant can be obtained from the inverted concentration of the analyte ($1/K_A$) corresponding to half of the maximum binding response ($R_{max}/2$) as shown in **Figure 5.9.** It should be noted that binding constants in this chapter are calculated by non linear regression. All curves are fitted by using "Origin Pro8".

To calculate the equilibrium binding constant of the iron cylinder to the oligonucleotide, the response (RU) of each iron cylinder concentration, shown in **Figure 5.7,** were plotted against the concentration of $[Fe_2L_3]^{4+}$ in order to obtain a non-linear curve. In addition, binding of the iron cylinder to DNA was background subtracted using a blank flow cell i.e. flow cell 4. In addition flow cell 4 was treated in the same way as flow cells 1, 2 and 3 apart from oligonucleotide immobilisation step omitted.

The "Origin Pro8" software was used to determined R_{max} and K_A by fitting the data to the model (**Equation 10**). Note that K_A and K_{eq} are the same which is the equilibrium binding constant. K_{eq} will be used for this entire chapter.

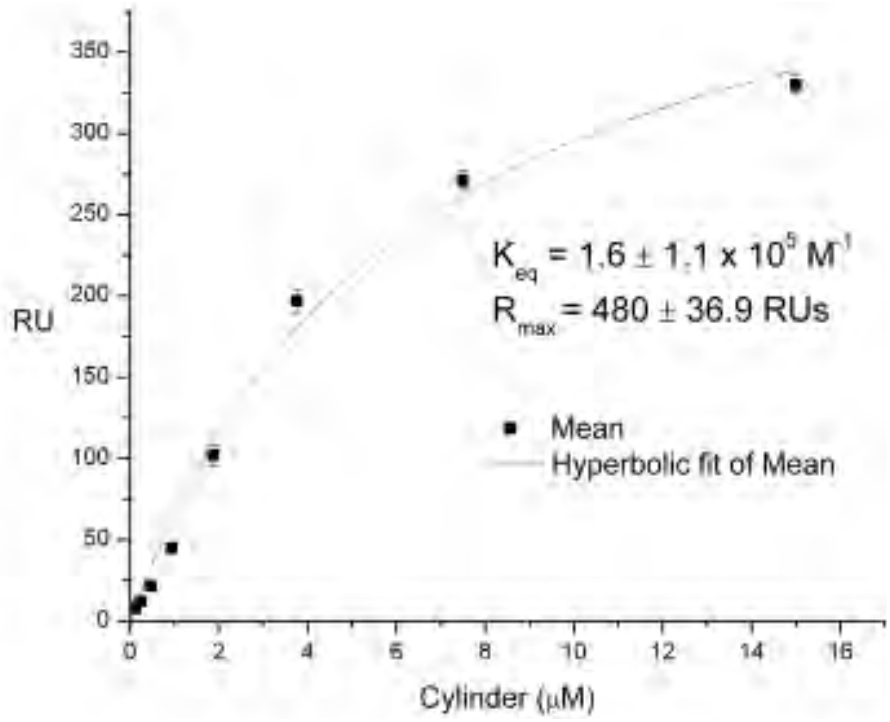

Figure 5.9 Response (RU) at equilibrium versus concentration of the iron cylinder binding to 16 bp DNA surface. The concentration of the iron cylinder ranged from 0.12 to 15 μM. Graph representing non-linear fitting by hyperbolic equation of the mean of three individual experiments ± SD (n = 3)

The results show that the equilibrium binding constant (K_{eq}) calculated from the fitting of the non linear regression is 1.6 ± 1.1 x 10^5 M^{-1} and the maximum response at saturation surface binding (R_{max}) is 480 ± 36.9 RUs.

5.2.3.2 Maximum binding ratio (mbr)

Beside the binding constant (K_{eq}) and the maximum binding response (R_{max}), a maximum binding ratio (mbr) can be determined from the experiment. The correlation of the measured SPR response in resonance units (RUs) to the surface concentration of immobilised target DNA and drug bound is assumed by using the estimate 1 RU ≈ 1 pg.mm^{-2}. This value has been used for proteins and oligonucleotides.[11] Therefore, the R_{max} value calculated from the previous section can be used to calculate a maximum binding ratio (mbr) (mol drug bound/ mol DNA immobilised), assuming one set of independent non-interacting binding sites, using the following equation[21]:

$$Maximum\ binding\ ratio\ (mbr) \quad = \quad \frac{R_{\max}}{R_{DNA}} x \frac{MW\ DNA}{MW\ drug} x \frac{1}{n} \qquad (11)$$

Where R_{DNA} is the amount of surface immobilised DNA (RUs) and n is the number of bases of the target DNA. MW DNA and MW drug are the molecular weight of the immobilised DNA and of the drug respectively. R_{max} is the maximum response at the saturation of surface binding sites and can be determined by the method described above. To determine the maximum binding ratio of the iron cylinder to DNA, all the parameters shown in **Equation 11** must be known. The maximum binding response was obtained from **section 5.2.3.1** and is 480 RUs, as well as the immobilised DNA on the surface **(section 5.2.2)** which is 574 RUs. The molecular weight of DNA and drug are 4863.2 and 1382.86 RU respectively. In addition, the number of bases of the oligonucleotide is 16.

$$Maximum\ \ binding\ \ ratio\,(mbr) \;=\; \frac{480}{574}\,x\,\frac{4863\cdot 2}{1382\cdot 86}\,x\,\frac{1}{16}$$

Consequently, the maximum binding ratio (mbr) of the iron cylinder $[Fe_2L_3]^{4+}$ to the oligonucleotide was 0.18 ≈ 1 drug/ 5 bp. This value corresponds to expected ratio of 0.2 ≈ 1 drug/ 5 bp as it has been shown that the iron cylinder binds to DNA in the major groove across 5 bp.[22, 23]

5.2.4 Affinity binding study of the enantiomers of the iron cylinder ($[Fe_2L_3]^{4+}$) to the oligonucleotide

The supramolecular cylinder, $[Fe_2L_3]^{4+}$, is a helical molecule and comprises of two enantiomeric forms defined as M and P for left and right handed helicates, respectively.[24, 25] Both enantiomers interact differently with DNA; M has a stronger binding affinity to DNA than the P enantiomer.[26-28] Moreover, the binding mode for the enantiomers is believed to be different; the M enantiomer binds to the DNA major groove while phosphate backbone binding is expected for the P.[27] However, the binding constant of the enantiomers to DNA has never been determined. To achieve these values, SPR experiments were introduced.

5.2.4.1 M enantiomer

The two fold dilution of the M enantiomer starting from 15 µM to 0.117 µM was dissolved in cacodyate buffer containing 150 mM NaCl, pH 7.95 and injected over four flow cells containing immobilised oligonucleotide. The sensorgrams of the M enantiomer binding to the oligonucleotide are depicted in **Figure 5.10**. Interestingly, the biphasic dissociation kinetics was also observed in the M enantiomer to the oligonucleotide.

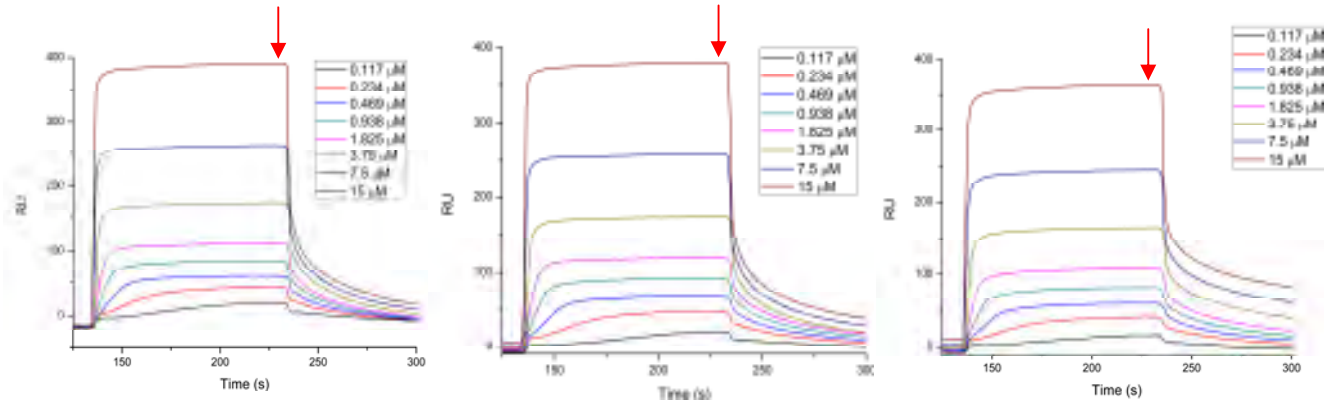

Figure 5.10 Overlay plot of sensorgram of M enantiomer binding to oligonucleotide. The concentrations of M enantiomer range from 0.117 µM in the lowest curve to the 15 µM in the top curve. Cacodylate buffer pH 7.95 with 150 mM NaCl was used in the SPR experiment. The red arrow marks the points in which the sensorgram reaches a steady state.

To determine the binding constant (K_{eq}) for the M enantiomer to the oligonucleotide the plot of response (RU) from the steady-state region of the SPR sensorgrams versus the concentration of the enantiomer was plotted. The graph is shown in **Figure 5.11**.

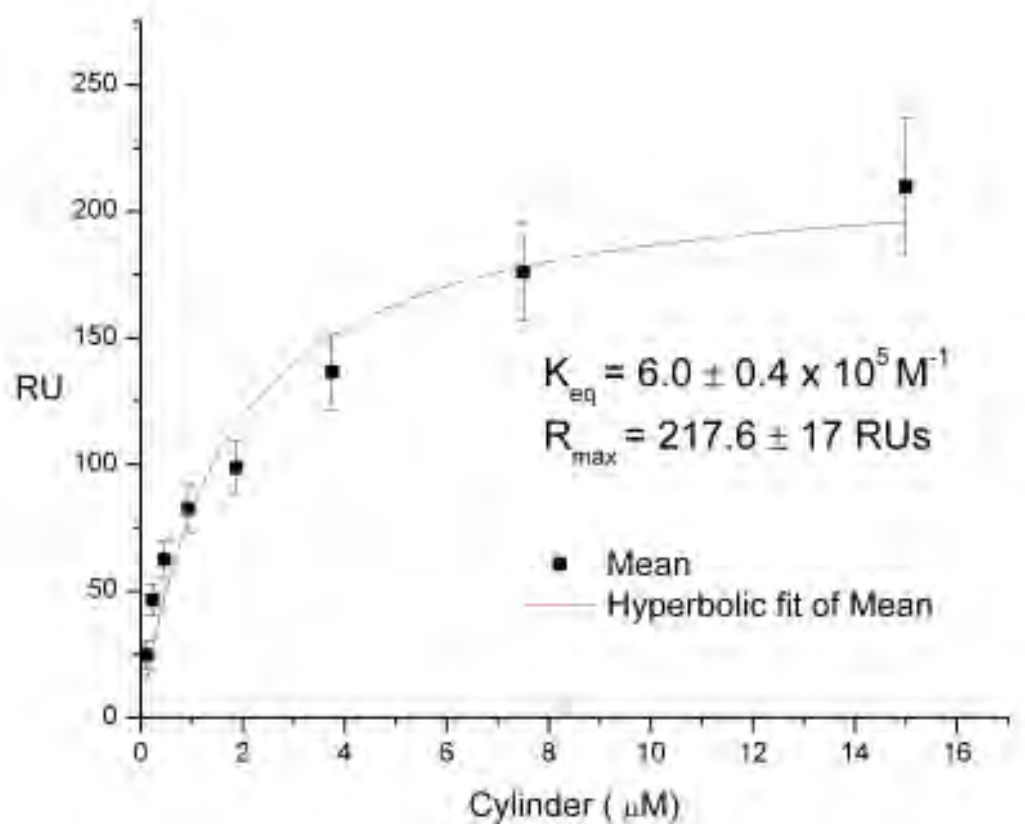

Figure 5.11 Equilibrium binding response versus concentration of M enantiomer binding to 16 bp DNA surface. The concentrations of M enantiomer ranged from 0.117 to 15 μM. The DNA surface immobilisation level of three flowcells (1, 2, 3) were 158, 150.5 and 145 RUs, respectively. Graph representing non-linear fitting by hyperbolic equation of the mean of three individual experiments ± SD (n = 3)

The non linear regression function from Origin Pro8 was employed to fit the curve in **Figure 5.11.** The maximum binding response (R_{max}) was 217.6 ± 17 RUs and the binding constant (K_{eq}) was 6.0 ± 0.4 x 10^5 M^{-1}.

5.2.4.2 P enantiomer

To compare the kinetic values, i.e. R_{max} and K_{eq}, with the M enantiomer, the SPR experiment with the P enantiomer was carried out. The same procedure was repeated in which two folded dilution of the P enantiomer from 15 µM to 0.117 µM dissolved in cacodylate buffer containing 150 mM NaCl pH 7.95 was injected over four flowcells containing 16 bases immobilised oligonucleotide. The sensorgrams of the P enantiomer binding to the oligonucleotide are illustrated in **Figure 5.12**. The plot of sensorgrams of the P enantiomer binding to oligonucleotide reveals that the dissociation of the P enantiomer from the oligonucleotide is biphasic kinetics. The first phase can be seen in few seconds after dissociation as the graph is rapidly decreased. The slow dissociation of the P enantiomer from oligonucleotide is demonstrated in the second phase.

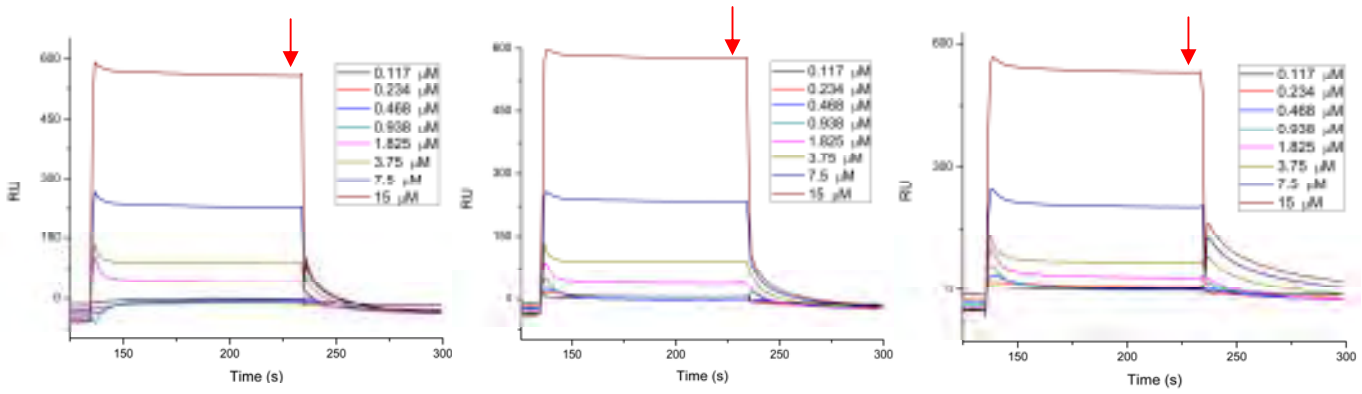

Figure 5.12 Overlay plot sensorgrams of P enantiomer binding to oligonucleotide of flow cells 1, 2 and 3 from left to right respectively. The concentrations of P enantiomer in cacodylate buffer with 150 mM NaCl range from 0.117 µM in the lowest curve to 15 µM in the top curve. The red arrows mark the points in which the sensorgram reaches to an equilibrium phase.

To calculate the binding constant (K_{eq}) for the P enantiomer to the oligonucleotide, the plot of RU values from the steady-state region of the SPR sensorgrams versus the concentration of the P enantiomer was required. The graph is shown in **Figure 5.13**.

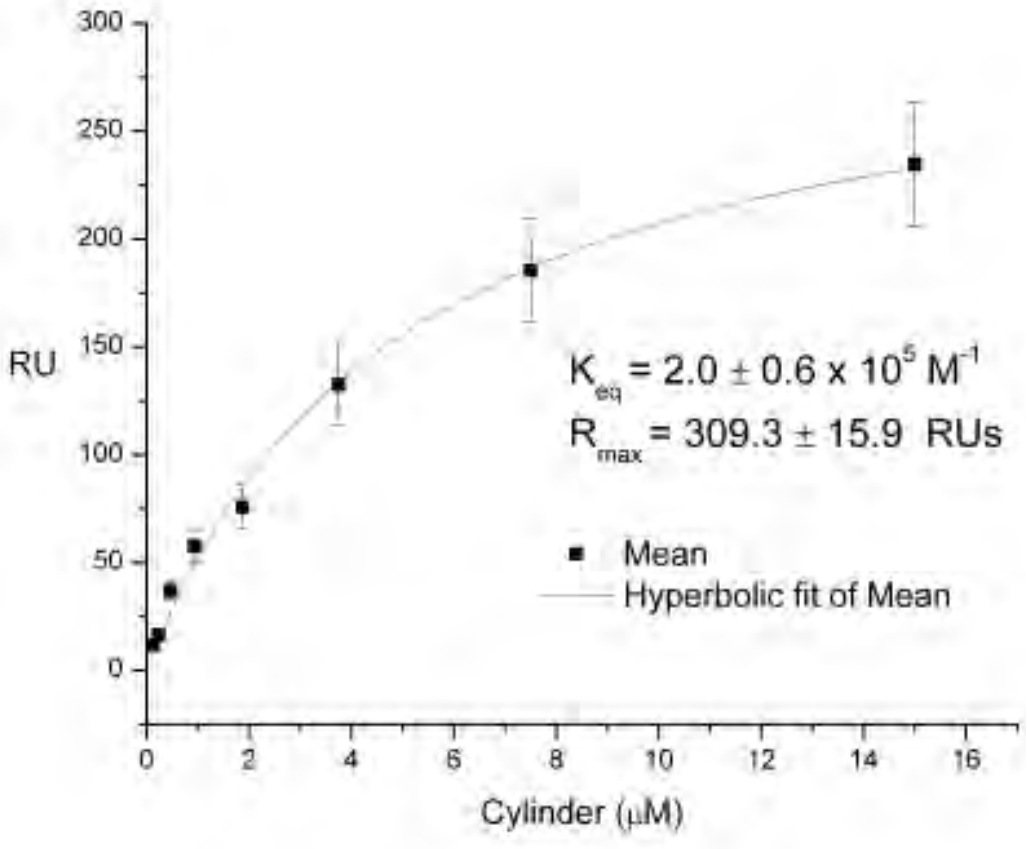

Figure 5.13 Equilibrium binding response (RU) versus concentration for P enantiomer binding to the 16 bases DNA surface. The concentrations of P enantiomer ranged from 0.117 to 15 μM. The DNA surface immobilisation level among three flow cells (1, 2 and 3) were 196.2, 176.1 and 221.7 RUs respectively. Graph representing non-linear fitting by hyperbolic equation of the mean of three individual experiments ± SD (n = 3)

The data (**Figure 5.13**) was curve fitted by non linear regression function using Origin Pro8. The maximum binding response (R_{max}) was 309.3 ± 15.9 RUs and the binding constant (K_{eq}) was 2.0 ± 0.6 x 10^5 M^{-1}. Regarding the previous **section 5.2.4.1** the R_{max} and K_{max} of the M enantiomer were 217.6 ± 17 RUs and 6.0 ± 0.4 x 10^5 M^{-1}. The results show that the binding constant (K_{eq}) of the M enantiomer (6.0 ± 0.4 x 10^5 M^{-1}) is higher than that of the P enantiomer (2.0 ± 0.6 x 10^5 M^{-1}). This implies that the binding affinity of the M enantiomer to the oligonucleotide is higher than that of the P enantiomer. Surprisingly the iron cylinder $[Fe_2L_3]^{4+}$ was found to have the same maximum binding ratio, which was 5 bases per drug as shown in the literature.[23] The summary of R_{max} of $[Fe_2L_3]^{4+}$, the M enantiomer and the P enantiomer is shown in **Table 5.2**.

Table 5.2 Summary of equilibrium parameters obtained from the SPR experiments.

	K_{eq} (M^{-1})	R_{max} (RUs)
$[Fe_2L_3]^{4+}$	1.6 ± 1.1 x 10^5	480 ± 36.9
M enantiomer	6.0 ± 0.4 x 10^5	217.6 ± 17
P enantiomer	2.0 ± 0.6 x 10^5	309.3 ± 15.9

5.3 Conclusions

SPR is a powerful technique for the investigation of small molecule binding to DNA due to its high sensitivity which can detect a small refractive index change in the range of 10-100 RUs. Herein, the results demonstrate that SPR can detect and quantify binding of the iron cylinder $[Fe_2L_3]^{4+}$ to DNA as well as its enantiomers. It reveals that the M enantiomer has a higher binding affinity ($K_{eq} = 6.0 \pm 0.4 \times 10^5\ M^{-1}$) than the P enantiomer ($K_{eq} = 2.0 \pm 0.6 \times 10^5\ M^{-1}$). In addition, the dissociation of the iron cylinder and its enantiomers from oligonucleotide is a biphasic kinetics which consists of an initial rapid dissociation and follows by a slow dissociation. Moreover, the maximum binding ratio of the $[Fe_2L_3]^{4+}$ cylinder is 5 bases per drug. This methodology is very useful for determining novel quantitative kinetic data and the equilibrium constant.

5.4 Experimental

The machine setup procedure. The CM5 chip (Biacore, GE Healthcare) was inserted into the appropriate socket. Then, HBS-EP (0.01 HEPES pH 7.4, 0.15 M NaCl, 3 mM EDTA, 0.005% v/v Surfactant P20, Biacore) was placed on the machine. To prime the machine, 0.5 ml of BIAnormalising solution (Biacore) was injected over the chip's surface. 150 mM NaCl, 100mM cacodylate buffer pH 7.95 was placed on the machine.

Streptavidin immobilisation. To immobilise streptavidin on the surface, the following reagents were employed: 150 µl of EDC (0.4 M) mixed 1:1 with NHS (0.1 M) made up before coupling, 120 µl of 0.5mg/ml streptavidin in 10mM Na Acetate pH 5.5, 120 µl of 1.0 M ethanolamine-HCl pH 8.5 and 500 µl of 10 mM glycine-HCl pH 2.5. Each reagent separately contained in a plastic tube, was placed on the right position in the machine in which the reagents were injected in order. The buffer used during the immobilisation was HBS-EP as it was used for the machine setup.

Oligonucleotide immobilisation. Biotinylated oligonucleotide (5´ 5GC ATC GTT TTC GAT GC 3´; 5 is biotin) which can form a hairpin was supplied by AltaBioscience. The machine was firstly primed with 100 mM cacodylate buffer pH 7.95 containing 150 mM NaCl before the oligonucleotide was immobilised to get rid of the negative signal caused from changing buffer. Then the oligonucleotide was diluted to 1 µg/ml in 150 mM NaCl, 100 mM cacodylate buffer pH 7.95 and separately injected over flow cells 1, 2 and 3 at the rate of injection 5 µl/min by using quick injection mode. Flow cell 4 was left as control.

Affinity binding of the iron cylinder $[Fe_2L_3]^{4+}$ to immobilised oligonucleotide. Two-fold dilution of $[Fe_2L_3]^{4+}$ in 150mM NaCl and 100 mM cacodylate buffer pH 7.95 carried

out from 15 μM to 0.117 μM were injected over four flow cells from low to high concentration with kinject injection mode.

Affinity binding of the enantiomers of the iron cylinder $[Fe_2L_3]^{4+}$ to immobilised oligonucleotide. Two-fold dilution of M and P enantiomers in 150mM NaCl and 100 mM cacodylate buffer pH 7.95 carried out from 15 μM to 0.117 μM were injected over four flow cells from low to high concentration with kinject injection mode.

5.5 References

1. A. Wolfe, G. H. Shimer and T. Meehan, *Biochemistry*, 1987, **26**, 6392-6396.
2. T. Urathamakul, D. J. Waller, J. L. Beck, J. R. Aldrich-Wright and S. F. Ralph, *Inorg. Chem.*, 2008, **47**, 6621-6632.
3. G. Barone, N. Gambino, A. Ruggirello, A. Silvestri, A. Terenzi and V. T. Liveri, *J. Inorg. Biochem.*, 2009, **103**, 731-737.
4. B. Ward, R. Rehfuss, J. Goodisman and J. C. Dabrowiak, *Biochemistry*, 1988, **27**, 1198-1205.
5. F. H. Stootman, D. M. Fisher, A. Rodger and J. R. Aldrich-Wright, *Analyst*, 2006, **131**, 1145-1151.
6. J. C. Peberdy, J. Malina, S. Khalid, M. J. Hannon and A. Rodger, *J. Inorg. Biochem.*, 2007, **101**, 1937-1945.
7. G. Bischoff, R. Bischoff, E. Birch-Hirschfeld, U. Gromann, S. Lindau, W. V. Meister, S. D. Bambirra, C. Bohley and S. Hoffmann, *J. Biomol. Struct. Dyn.*, 1998, **16**, 187-203.
8. T. M. Davis, W. David Wilson and M. J. W. Jonathan B. Chaires, in *Methods in Enzymology*, Academic Press, Edn., 2001, Vol. 340, pp. 22-51.
9. M.-H. Hou and A. H. J. Wang, *Nucleic Acids Res.*, 2005, **33**, 1352-1361.
10. U. Jonsson, L. Fagerstam, B. Ivarsson, B. Johnsson, R. Karlsson, K. Lundh, S. Lofas, B. Persson, H. Roos, I. Ronnberg, S. Sjolander, E. Stenberg, R. Stahlberg, C. Urbaniczky, H. Ostlin and M. Malmqvist, *Biotechniques*, 1991, **11**, 620-626.
11. B. Persson, K. Stenhag, P. Nilsson, A. Larsson, M. Uhlen and P. A. Nygren, *Anal. Biochem.*, 1997, **246**, 34-44.

12. M.-P. Teulade-Fichou, C. Carrasco, L. Guittat, C. Bailly, P. Alberti, J.-L. Mergny, A. David, J.-M. Lehn and W. D. Wilson, *J. Am. Chem. Soc.* , 2003, **125**, 4732-4740.

13. L. Wang, C. Bailly, A. Kumar, D. Ding, M. Bajic, D. W. Boykin and W. D. Wilson, *Proc. Natl. Acad. Sci. U. S. A.*, 2000, **97**, 12-16.

14. C. T. Campbell, *Surface plasmon resonance (SPR) biosensor development*, http://depts.washington.edu/campbelc/projects/plasmon.pdf.

15. L.-P. Lin, L.-S. Huang, C.-W. Lin, C.-K. Lee, J.-L. Chen, S.-M. Hsu and S. Lin, *Curr. Drug Targets - Immune Endocr. Metab. Disord.*, 2005, **5**, 61-72.

16. M. J. Hannon, V. Moreno, M. J. Prieto, E. Moldrheim, E. Sletten, I. Meistermann, C. J. Isaac, K. J. Sanders and A. Rodger, *Angew. Chem. Int. Ed.*, 2001, **40**, 880-884.

17. A. Oleksi, A. G. Blanco, R. Boer, I. Uson, J. Aymami, A. Rodger, M. J. Hannon and M. Coll, *Angew. Chem. Int. Ed.*, 2006, **45**, 1227-1231.

18. http://www.biacore.com/lifesciences/products/Consumables/guide/cm5/index.html.

19. G. Scatchard, *Ann. NY Acad. Sci.*, 1949, **51**, 660-672.

20. K. Zierler, *Trends Biochem. Sci.*, 1989, **14**, 314-317.

21. M. L. Ciolkowski, M. M. Fang and M. E. Lund, *J. Pharm. Biomed. Anal.*, 2000, **22**, 1037-1045.

22. I. Meistermann, University of Warwick, 2001.

23. S. Khalid, M. J. Hannon, A. Rodger and P. M. Rodger, *Chem. Eur. J.*, 2006, **12**, 3493-3506.

24. M. J. Hannon, I. Meistermann, C. J. Isaac, C. Blomme, J. R. Aldrich-Wright and A. Rodger, *Chem. Commun.*, 2001, 1078-1079.

25. J. M. C. A. Kerckhoffs, J. C. Peberdy, I. Meistermann, L. J. Childs, C. J. Isaac, C. R. Pearmund, V. Reudegger, S. Khalid, N. W. Alcock, M. J. Hannon and A. Rodger, *Dalton Trans.*, 2007, 734-742.

26. J. Malina, M. J. Hannon and V. Brabec, *Chem. Eur. J.*, 2007, **13**, 3871-3877.

27. I. Meistermann, V. Moreno, M. J. Prieto, E. Moldrheim, E. Sletten, S. Khalid, P. M. Rodger, J. C. Peberdy, C. J. Isaac, A. Rodger and M. J. Hannon, *Proc. Natl. Acad. Sci. U. S. A.*, 2002, **99**, 5069-5074.

28. J. Malina, M. J. Hannon and V. Brabec, *Nucleic Acids Res.* , 2008, **36**, 3630-3638.

Chapter 6

Conclusions and future work

6.1 Conclusions

The majority of the work described in this thesis has shown how well a metallosupramolecular cylinder can recognize and interact specifically with a range of nucleic acids. The biophysical experiments herein were performed to elucidate the preferential interaction of the cylinder to nucleic acids including DNA, RNA and a three dimensional DNA nanostructure.

In Chapters 2 and 3, gel electrophoresis was the main technique employed to investigate the recognition and stabilisation of three way junction nucleic acids by a metallosupramolecular cylinder.

Chapter 2 focused on the recognition and stabilisation of RNA three way junctions by a metallosupramolecular triple stranded helicate. This experiment was designed to answer the question that also arises for cisplatin, a well known anticancer drug, since that drug can potentially also bind not only DNA but also RNA. The polyacrylamide gel electrophoresis studies demonstrated that the iron cylinder can recognise and stabilise RNA three way junctions with both perfect base pairing and mismatched base pairing. Additionally, this binding does not perturb the A-form structure of the RNA arms as confirmed by circular dichroism. Moreover, the specific combination of the DNA-RNA hybrid was shown to be preferentially recognized by the iron cylinder.

The effect of enantiomers of the iron cylinder on the recognition of RNA three way junction was examined. The result revealed that the M is obviously more effective than the P enantiomer for the binding at high RNA concentration. The corresponding result from the recent crystal structure, grown from the solution of RNA three way junction and the racemic mixture of the iron cylinder, shows that only the M is sitting at

the core cavity of the RNA three way junction. Interestingly, the M is also more effective than the P in the recognition of DNA three way junction.

Besides the iron cylinder, the ruthenium cylinder which has an identical size and shape but different metal centre was investigated for the recognition of RNA three way junction. Slightly higher stabilisation efficiency was observed with the ruthenium cylinder. It might be possible that the difference in the stabilisation of the two cylinders to the RNA three way junction could be related to the difference in cytotoxicity of the cylinders: the iron cylinder is active against ovarian cancer cell lines while the ruthenium cylinder is not.

The competition assay of nucleic acids to the cylinder revealed that the iron cylinder may preferentially bind to RNA three way junction rather than the DNA. However, this is not certain because the equilibrium being studied is not the simple competition but rather more complicated as shown in **Figure 2.25**. It is worth noting that increasing RNA concentration in all experiments can promote three way junction formation.

In Chapter 3, the size and shape of metallosupramolecular cylinder were shown to be the key factors for the recognition and stabilisation of the DNA three way junction by the cylinder. Several cylinder derivatives were tested for the recogniton. Among those complexes, the iron cylinder conjugated a peptide showed the highest promotion of three way junction (compared to the parent cylinder) due to a high positive charge of the compound from the amino acid attached. Moreover, the preferential binding of the iron cylinder to the other DNA structures was examined. The result shows that the three way junction structure is the most favourite structure for the binding of the cylinder compared

to G-quadruplex and i-motif structures but other Y-shaped junctions i.e. a double stranded DNA and a double stranded DNA with loop can compete for binding.

The recent emergence of DNA nanotechnology initiated the idea of combining concept of supramolecular chemistry and DNA nanotechnology by utilising the supramolecular chemistry as an approach to synthesise the metallosupramolecular cylinder that enables to recognise and control the three dimensional DNA nanostructure. To demonstrate the powerful methodology, supramolecular chemistry, for modulating a DNA nanostructure, the experiments in Chapter 4 were undertaken. Gel electrophoresis, AFM and thermal denaturation indicated that the iron cylinder can bind and alter a very rigid DNA nanostructure, DNA tetrahedron. The ability to recognise and (reversibly) modify the morphology of a DNA nanostructure could be a very powerful tool indeed and opens up new possibilities in the field of DNA nanotechnology.

In Chapter 2, 3 and 4, it has been shown that the cylinder recognises and binds to nucleic acids. To have a closer quantitative look, SPR was established and exploited to determine the binding affinity of the iron cylinder to DNA. Detection in real time and precisely providing kinetic parameters are the advantages of this method.

This thesis has established that the cylinder can bind to a range of nucleic acids. This takes the work beyond the original DNA binding of the cylinder, recognized at the outset, and shows that its biological targets may be wider than envisaged and that its applications may also extend into nanotechnology. Within the binding to DNA, the thesis has demonstrated that the three way junction is the preferred DNA structural target over a range of other DNA motifs, but that other Y-shaped DNA structures can also be bound. The apparent preferential recognition of DNA-RNA hybrid structure demonstrated in this

thesis is intriguing and was not predicted. This could be exciting as DNA-RNA Y-shaped hybrids are present when DNA is transcribed. It is also noteworthy that siRNA are a current area of research and powerful application involving DNA-RNA hybrid structure. The thesis has also confirmed the importance of the size, shape and chirality of the cylinder in its nucleic acid recognition.

6.2 Future work

The work herein provides much information about the recognition of nucleic acids by the cylinder and it enables and indicates exciting work that can be developed in the future.

As described in the thesis, the technique exploited to probe the recognition of the stabilisation of RNA three way junction by a metallosupramolecular cylinder was mainly polyacrylamide gel electrophoresis (PAGE). The other techniques should be now introduced for probing this such as an NMR study of the interaction of RNA three way junction with the cylinder. This technique will provide more detail about how exactly the cylinder interacts with the RNA three way junction in the solution. The information gained from this study will be useful for the design of the novel metallosupramolecular cylinders which might selectively recognise RNA recognitions. In addition, the competition assay of DNA three way junction and other DNA structures shown in this thesis would need further experiments to confirm the apparent results. Possible experiments would be to exploit SPR technique (mentioned in Chapter 5) to determine the binding constant of the iron cylinder to the other DNA structures then compare the binding constant among the structures. The result from this experiment would support the

result from the competition assay from the gel experiment. Another exciting future experiment is a synthesis of the iron cylinder conjugated with a gold nanoparticle for investigating the preferential binding of DNA three way junction over double stranded DNA. The idea is to conjugate the gold nanoparticle to a capped iron cylinder which will allow only a particle to be anchored at the end of the cylinder instead of six as seen with the peptides. The different size of gold nanoparticle from the cylinder will be positioned on the arms of the junction or its heart depending on the location of the cylinder. In addition, each DNA strand can be labelled with a different size of metal particle for example gold nanoparticle. The result of the binding will be shown by Transmission Electron Microscopy (TEM). In TEM, if the cylinder prefers to bind to the heart of the three way junction it will show the arrangement of the dots representing gold nanoparticle labeling on the three way junction in a triangle shape with a single dot in the middle of triangle. However, if the single dot is not in the middle it means that the iron cylinder prefers to bind to the double stranded DNA as it binds to the arm of the three way junction. The schematic drawing is shown in **Figure 6.1**.

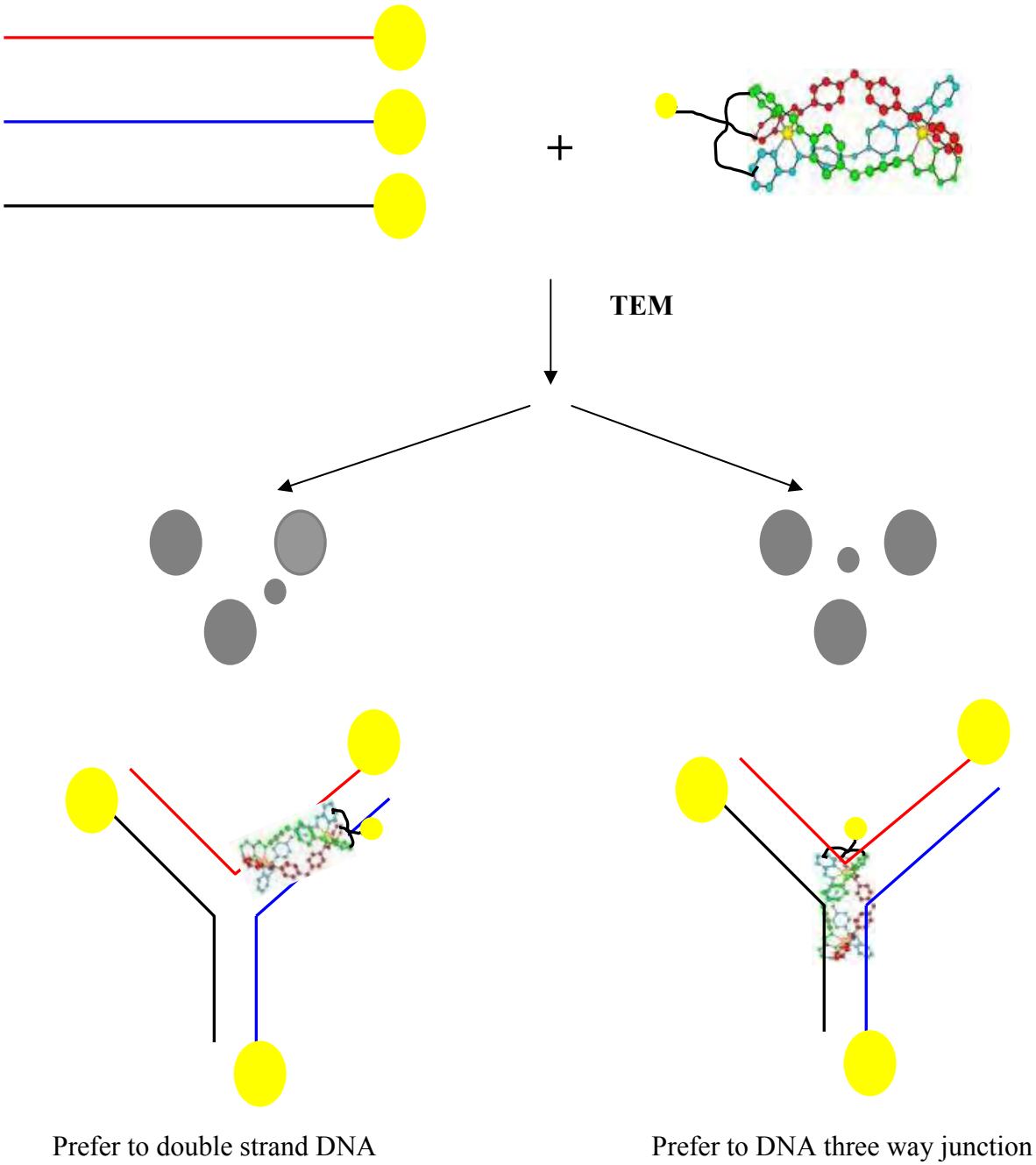

Figure 6.1 Schematic drawing depicted the idea of using conjugated gold nanoparticle cylinder to probe the preferential binding of the cylinder to the double stranded DNA and the three way junction.

Besides biophysical investigations, molecular biology and biological experiment are required to monitor the effect of the cylinder on the biological function of a cell line in order to find the specific gene that response to the iron cylinder treatment and whether the regulation of that specific gene in response to the iron cylinder treatment is crucial to the antitumor activity. This would be an exciting experiment which should be done in the future. The experiment that mentioned in the future work will drive the research going and it might be a quick driving force to launch the cylinder in the clinical trial.

Appendix

Scintillator Counting

The specific activity is specified as of the calibration date. This must be taken into consideration when calculating concentration in mass-dependent applications. The specific activity on any day prior to the calibration date can be calculated using the formula:

$$SA = \frac{SA\,cal.}{D_F + \frac{SA\ cal.(1 - D_F)}{(SATheo)}}$$

The specific activity on any day after the calibration date can be calculated using the formula:

$$SA = \frac{D_F}{\frac{1}{SAcal.} + \frac{(1 - D_F)}{(SATheo)}}$$

where:

SA = Specific Activity expressed as Ci/mmol

SA cal. = Specific Activity on the calibration date.

D_F = Fraction of current radioactivity that will remain on the calibration date (from the decay table) For example, for a date 8 days prior to the calibration date $D_F = 0.678$.

SA Theo = 9120 Ci/mmol for the theoretical specific activity of carrier free ^{32}P.

Table A.1 The decay table of phosphorus 32

days	0	1	2	3	4	5	6	7	8	9
0	1.000	0.953	0.906	0.865	0.824	0.785	0.748	0.712	0.678	0.646
10	0.616	0.587	0.559	0.532	0.507	0.483	0.460	0.436	0.418	0.396
20	0.379	0.361	0.344	0.328	0.312	0.297	0.283	0.270	0.257	0.245
30	0.233	0.222	0.212	0.202	0.192	0.183	0.174	0.166	0.158	0.151
40	0.144	0.137	0.130	0.124	0.118	0.113	0.107	0.102	0.096	0.093
50	0.088	0.084	0.080	0.077	0.073	0.069	0.066	0.063	0.060	0.057
60	0.054	0.052	0.049	0.047	0.045	0.043	0.041	0.039	0.037	0.035

To use the decay table above, find the number of days in the top and left hand columns of the chart, then find the corresponding decay factor. To obtain a precalibration number, divide by the decay factor. For a postcalibration number, multiply by the decay factor.